An investigation into the potential cardioprotective effects of ghrelin in a rat model of chronic Doxorubicin-induced cardiotoxicity

by
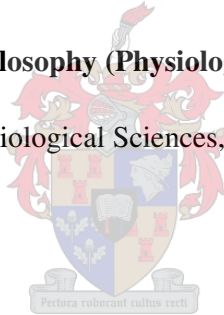
Toni L Goldswain

Dissertation presented for the Degree of

Doctor of Philosophy (Physiological Sciences)

in the Department of Physiological Sciences, at Stellenbosch University

Promoter: Dr Balindiwe JN Sishi

Faculty of Science

December 2017

DECLARATION OF ORIGINALITY

By submitting this dissertation electronically, I declare that the entirety of the work contained therein is my own, original work, that I am the sole author thereof (save to the extent explicitly otherwise stated), that reproduction and publication thereof by Stellenbosch University will not infringe any third party rights and that I have not previously in its entirety or in part submitted it for obtaining any qualification.

December 2017

i

Abstract

Introduction

Doxorubicin (DOX) is an anthracycline that has significantly improved the outcome of cancer patients since its discovery. However, its clinical success remains limited due to the dose-dependent cardiotoxic side effects associated with its use. While the mechanisms responsible for this condition are still not well defined, oxidative stress alongside apoptosis, remain the classical but major contributors. Ghrelin, an endogenous brain-gut peptide, most well-known for its effects on appetite and growth hormone release, has been shown to exert anti-apoptotic, antioxidative, anti-inflammatory and anti-fibrotic effects in several models of cardiovascular disease. These cardioprotective effects offered by ghrelin have been indicated to occur through the activation of the pro-survival proteins, ERK1/2, Akt/PKB and STAT3. This study therefore investigated the protective effects of ghrelin in a chronic model of DOX-induced cardiotoxicity.

Methods

Male Sprague-Dawley rats were acclimatized and divided into five experimental groups. While the control group remained untreated, the ghrelin group received 300 µg/kg ghrelin per week, the DOX group received 2.5 mg/kg per week, the combination group received both DOX and ghrelin at the previously mentioned doses and the vehicle group received saline. All injections were performed via intraperitoneal injection for eight weeks. One week after the last injection, the rats were euthanized, blood was collected and the hearts were subjected to a 40-minute working heart perfusion protocol to obtain functional data. The hearts were weighed and then cut transversely into two sections, where one half was snap frozen for biochemical analysis and the other half was preserved in formalin for histological analysis. Cardiovascular markers of damage and pro-inflammatory cytokines were measured in serum using a luminex assay, and fibrosis and general morphology were assessed using the Masson's Trichrome and H&E stains, respectively. Cytochrome c expression was evaluated by immunohistochemistry, while oxidative stress was assessed using the TBARS, conjugated diene, ORAC, SOD and glutathione assays. Apoptosis was determined using the Caspase Glo® assay and the expression of pro-survival proteins was measured using Western blot analysis.

ii

Results

During the eight weeks of treatment, DOX significantly reduced weight gain and food consumption, whereas ghrelin maintained normal body weight and stimulated appetite. As expected, DOX induced significant oxidative stress when compared to the control, as demonstrated by the formation of conjugated dienes (1.64 ± 0.11 vs 0.55 ± 0.12 µmol/gram, $p = 0.0003$) and a reduction in the GSH:GSSG ratio (2.10 ± 0.47 vs 9.66 ± 1.08 arbitrary units, $p < 0.05$), whereas ghrelin attenuated these effects. Apoptotic cell death was also induced, as evident by an increase in cytochrome c staining, caspase activity (67877 ± 15686 vs 13421 ± 1871 relative light units, $p < 0.0001$) and PARP cleavage (2.11 ± 0.24 vs 1.00 ± 0.09 fold change, $p = 0.0081$). The decrease in cell death and oxidative stress in this scenario was associated with a reduction in TNF-α and an improvement in cardiac function, which was otherwise worsened in the DOX group due to the decline cardiac output, coronary flow, rate-pressure product, left ventricular developed pressure and total work. Even though ghrelin treatment in the presence of DOX did not induce noteworthy changes in the protein expression of ERK1/2 and Akt/PKB, the phosphorylation of STAT3 was improved with ghrelin administration.

Discussion and Conclusion

The observations presented in this study indicate that while DOX is a known effective chemotherapeutic agent, it produces cardiotoxic effects through the induction of oxidative stress and consequently apoptosis, possibly due to the downregulation of ERK1/2 and Akt/PKB. The co-administration of ghrelin with DOX significantly decreased the detrimental effects associated with DOX treatment alone. The effects of ghrelin were not only beneficial at organ level, but also at the organism level, as a result of improved general well-being of the experimental animals and through the maintenance of cardiac function, a decline in myocardial TNF-α production and the stimulation of the STAT3 signaling pathway. The fact that ghrelin alone did not exert any detrimental effects makes this peptide an appealing cardioprotective agent and may therefore have the potential to improve the high morbidity and mortality rates of cancer survivors. While ghrelin in this context may possess anti-cardiotoxic effects, further research is required to determine the effects of ghrelin on cancer cell proliferation.

Uittreksel

Inleiding

Doksorubisien (DOX) is 'n antrasiklien wat die uitkoms vir kankerpasiënte betekenisvol verbeter het sedert die ontdekking daarvan. Die kliniese sukses is steeds beperk as gevolg van die dosis-afhangklike kardiotoksiese newe-effekte wat verband hou met die gebruik daarvan. Terwyl die meganismes wat verantwoordelik is vir hierdie toestand steeds nie bekend is nie, is oksidatiewe stres, tesame met apoptose, die klassieke bydraers. Ghrelien,'n endogene brein-derm peptied wat wel bekend is vir sy effekte op aptyt en vrystelling van groeihormoon, vertoon anti-apoptotiese, antioksidatiewe, anti-inflammatoriese en anti-fibrotiese effekte in verskeie kardiovaskulêre siekte modelle. Hierdie kardio-beskermende effekte van ghrelien is te wyte aan die aktivering van die pro-oorlewingsproteïene, ERK1/2, Akt/PKB en STAT3. Hierdie studie het die beskermende effekte van ghrelien in 'n chroniese model van DOX-geïnduseerde kardiotoksisiteit ondersoek.

Metodes

Manlike Sprague-Dawley rotte is geaklimatiseer en in vyf eksperimentele groepe verdeel. Terwyl die kontrole groep onbehandel is, het die ghrelien groep weekliks 300 µg/kg ghrelien, die DOX groep 2.5 mg/kg per week, die kombinasie groep beide DOX en ghrelien by dieselfde vorige dossisse, en die draer groep 'n soutoplossing ontvang. Alle toedienings is *via* intraperitoneale inspuiting vir agt weke gedoen. Een week voor die laaste inspuiting, is die rotte doodgemaak, bloed is versamel, en die harte is blootgestel aan 'n 40-minute werkende hartperfusie protokol om funksionele data te versamel. Die harte is geweeg en transversaal in twee dele gedissekteer, waar die een helfte geklampvries is vir biochemiese analises, en die ander helfte is in formalien gepreserveer vir histologiese analises. Kardiovaskulêre merkers, vir skade en pro-inflammatoriese sitokiene is in serum bepaal deur 'n Luminex platvorm, terwyl fibrose en algemene morfologiese ondersoeke deur Masson se Trichrome en H&E kleuringstegniek onderskeidelik van gebruik te maak. Sitochroom-c uitdrukking is deur middel van immune-histochemie bepaal, en oksidatiewe stres deur van TBARS, gekonjugeerde diëne, ORAC, SOD en glutatioon toetse. Apoptose is deur middel die Caspase Glo® getoets, en uitdrukking van die pro-oorlewingsproteïene is bepaal deur Westerse kladtegniek.

Resultate

Gedurende die agt weke behandeling het DOX toename in gewig. asook voedselinname betekenigsvol verlaag, terwyl ghrelien normale liggaamsgewig en aptyt gestimuleer. Soos verwag, het DOX oksidatiewe stres betekenisvol geïnduseer vergeleke met die kontrole groep soos waargeneem deur die vorming van gekonjugeerde diëne (1.64 ± 0.11 *vs* 0.55 ± 0.12 µmol/gram, $p = 0.0003$), en 'n verlaging in die GSH:GSSG verhouding (2.10 ± 0.47 *vs* 9.66 ± 1.08 AU, $p < 0.05$), terwyl ghrelien hierdie effekte verlaag het. Apoptotiese seldood is ook geïnduseer soos waargeneem deur die toename in sitochroom-c kleuring, kaspase aktiwiteit (67877 ± 15686 *vs* 13421 ± 1871 RLU, $p < 0.0001$) en PARP klowing (2.11 ± 0.24 *vs* 1.00 ± 0.09 voudige verandering, $p = 0.0081$). Die verlaging in seldood en oksidatiewe stres in hierdie scenario is met 'n verlaging in TNF-α vorming en verbeterde kardiale funksionering geassosiëer, wat nie in die DOX groep waargeneem is nie weens verlaagde kardiale omset. koronêre vloei, tempo-druk produk, linker ventrikulêre-ontwikkelde druk en totale arbeid. Hoewel ghrelien behandeling in die teenwoordigheid van DOX behandeling geen waarneembare veranderinge in die proteïenuitdrukking van ERK1/2 en Akt/PKB vertoon het nie, het ghrelien toediening wel die fosforilering van STAT3 verbeter.

Bespreking en gevolgtrekking

Die waarnemings wat in hierdie studie rapporteur word wys daarop dat terwyl DOX 'n welbekende effektiewe chemoterapeutiese middel is, veroorsaak dit kardiotoksiese effekte deur die induksie van oksidatiewe stres, en gevolglik apoptose, moontlik deur die afregulering van ERK1/2 en Akt/PKB. Die toediening van ghrelien met DOX verlaag die skadelike effekte betekenisvol vergeleke met enkel behandeling van DOX. Die effek van ghrelien is beide voordelig op orgaanvlak sowel organisme vlak, weens verbeterde algemene welstand van die eksperimentele diere en deur die handhawing van kardiale funksie, 'n afname in miokardiale TNF-α vorming, en die stimulering van die STAT3 seinweg. Die feit dat ghrelien as 'n enkel middel geen skadelike effekte vertoon het nie, maak van hierdie peptied 'n gepaste kardiobeskermende middel en kan dus daarom die potensiaal hê om die hoë morbiditeit en mortaliteit van kanker pasiente te verbeter. Alhoewel ghrelien in hierdie konteks anti-kardiotoksiese effekte vertoon het, daar word voorgestel dat die effek van ghrelien op kankerselle eers ondersoek word alvorens enige behandelingsvoorstelle toegepas kan word.

Acknowledgements

Mom and dad, where do I start? Thank you! Without you I would never have completed this degree, and the many before it. Thank you for your support, both financial and emotional, for your encouragement, and for always showing an interest in my life. Craig, sometimes I feel like you're the older sibling. Thank you for your advice, patience, wisdom and knowledge about all things. Thank you for always being there for me. I love you all.

Dr Bali Sishi, my amazing supervisor. Taking on my PhD was a journey for both of us. You have been the most incredible support system and mentor over the last few years. I would never have made it without you. Thank you for always being excited about my project and for keeping me grounded when I became flustered. Thank you for being a leader, a mother, a sister and a friend. I will be forever grateful for having you as my supervisor.

Morne Mortimer, thank you for the years of love and support. I am sure that if you hadn't been such a good Biochemistry demi all those years ago I would never have pursued my academic career. Thank you for your patience and advice. Thank you for staying in Stellenbosch for me. I am so grateful for all that you are.

Nev, thank you for your wisdom and advice from afar. Although I hardly see you, your words of encouragement played in my mind whenever I felt overwhelmed. You are the reason I took on a PhD and persevered when things felt impossible. I can see why you were chosen to be my godparent. Thank you.

Dr Lydia Lacerda, thank you for literally always having an open door. No matter what time of day, you never hesitated to help. Thank you for sharing your advice and knowledge on all aspects of the lab and life. Your warm presence made the department a happy place to be.

My department friends, Megs, Zil, Ash, Lyne, Tash, Tanja and Jason. Thank you for the years of friendship – you made the lab a fun place to be. I will miss you all.

Tope, where do I begin? Without you I would still be trying to inject my rats. Thank you for always encouraging me, supporting me and reassuring me in my animal study. Thank you for sharing your precious time when you had your own things to do. Thank you for being a friend and allowing me to vent at times. Thank you for laughing with me every day. I will miss you, but I know we will keep in touch.

List of Conference Proceedings

National

- Goldswain, T.L., Bester, D. & Sishi, B.J.N. Can ghrelin satisfy our hunger to protect the heart? 44th meeting of the Physiology Society of Southern Africa (PSSA). 28th – 31st August 2016. University of Cape Town, South Africa. Abstract accepted for poster presentation (winner of the best general poster award).

- Goldswain, T.L., Lacerda, L. & Sishi, B.J.N. The RISK(y) and (un)SAFE sides of Doxorubicin-induced Cardiotoxicity. 42nd meeting of the Physiology Society of Southern Africa (PSSA). 14th – 17th September 2014. University of Kwa-Zulu Natal, South Africa. Abstract accepted for oral presentation.

- Goldswain, T.L., Krygsman, A., Makunga, N. & Engelbrecht, AM. Elucidation of the cytotoxicity of natural extracts from plants in cancer cells. 40th meeting of the Physiology Society of Southern Africa (PSSA). 10 – 13 September 2012. University of Stellenbosch, South Africa. Abstract accepted for poster presentation.

International

- Goldswain, T.L., Bester, D. & Sishi, B.J.N. Ghrelin: A multifunctional hunger hormone that 'satisfies' several conditions associated with Doxorubicin-induced cardiotoxicity. 38th World Congress of the International Union of Physiological Sciences – Rhythms of Life. 1 – 5 August 2017. Rio de Janeiro, Brazil. Abstract accepted for poster presentation.

- Goldswain, T.L., Lacerda, L. & Sishi, B.J.N. The RISK(y) and (un)SAFE sides of Doxorubicin-induced Cardiotoxicity. International Cell Death Society. 8 – 10 May 2014. Stellenbosch, South Africa. Abstract accepted for poster presentation (winner of second prize).

List of Collaborative Publications

- Rautenbach, A., Goldswain, T., Davis, T., Krygsman, A., Engelbrecht, A & Makunga, N.P. 2015. Investigating the potential of a traditional medicinal plant as an adjuvant remedy in the treatment of breast cancer. *South African Journal of Botany* 98: 198 – 199. (Published abstract)

List of Figures

List of Tables

List of Abbreviations

6-HD   6-hydroxydopamine

AAPH   2,2'-Azobis (2-methylpropionamidine) dihydrochloride

ACE   Angiotensin-converting enzyme

Acetyl CoA   Acetyl coenzyme A

ADP   Adenosine diphosphate

AgRP   Agouti-related protein

AIDS   Acquired immunodeficiency syndrome

ANOVA   Analysis of variance

Apaf-1   Apoptotic protease activating factor 1

ATP   Adenosine triphosphate

AU   Arbitrary units

AUC   Area under the curve

Bcl-2   B-cell lymphoma 2

Bcl-XL   B-cell lymphoma extra large

BHT   Butylated hydroxytoluene

BNP   Brain natriuretic peptide

BP   Blood pressure

BSA   Bovine serum albumin

cAMP   Cyclic adenosine monophosphate

CHF   Congestive heart failure

cIAP   Cellular inhibitor of apoptosis protein 1

CK-MB	Creatine kinase myocardial band
CTGF	Connective tissue growth factor
cTnI	Cardiac troponin inhibitory
cTnT	Cardiac troponin tropomyosin
CuZn	Copper zinc
DAB	3,3'-Diaminobenzidine
DAG	Diacylglycerol
DETAPAC	Diethylenetriaminepentaacetic acid
DNA	Deoxyribonucleic acid
DOX	Doxorubicin
DTNB	5,5'-dithio-bis(2-nitrobenzoic acid
DXZ	Dexrazoxane
EDTA	Ethylenediaminetetraacetic acid
ERK	Extracellular-signal regulated kinase
GH	Growth hormone
GHRH	Growth hormone-releasing hormone
GHSR-1α	Growth hormone secretagogue receptor 1 alpha
GR	Glutathione reductase
GSH	Glutathione
GSH-Px1	Glutathione peroxidase 1
GSSG	Glutathione disulphide
H&E	Hematoxylin and Eosin
HCL	Hydrochloric acid

HIV	Human immunodeficiency virus
HR	Heart rate
HRP	Horseradish peroxidase
i.p	Intraperitoneal
IGF-1	Insulin-like growth factor 1
IHC	Immunohistochemistry
IL-6	Interleukin 6
IL-8	Interleukin 8
IP$_3$	Inositol trisphosphate
IRI	Ischemia reperfusion injury
JAK2	Janus kinase 2
KHB	Krebs-Henseleit buffer
LVDP	Left ventricular developed pressure
M2VP	1-methyl-2-vinyl-pyridium trifluoromethane sulfonate
MAFbx	Muscle atrophy F-box
MAPK	Mitogen-activated protein kinase
MDA	Malondialdehyde
MEK	Mitogen-activated protein kinase kinase
MnSOD	Manganese/mitochondrial SOD (SOD2)
mPTP	Mitochondrial permeability transition pore
mRNA	messenger ribonucleic acid
MTT	3-[4, 5-dimethylthiazol-2-yl]-2, 5-diphenyl tetrazolium bromide
MuRF-1	Muscle ring finger 1

NAC	N-acetyl cysteine
NaCl	Sodium chloride
NADH	Nicotinamide adenine dinucleotide + hydrogen
NADPH	Nicotinamide adenine dinucleotide phosphate + hydrogen
NaF	Sodium fluoride
NFκB	Nuclear factor kappa-light-chain-enhancer of activated B cells
NPY	Neuropeptide Y
ORAC	Oxygen radical absorbance capacity
PARP	Poly (ADP-ribose) polymerase
PBS	Phosphate buffered saline
PDK1	Protein 3-phosphoinositide-dependent protein kinase 1
PI3K	Phosphatidylinositol-4,5-bisphosphate 3-kinase
PIP$_2$	Phosphatidylinositol 4,5-bisphosphate
PKA	Protein kinase A
PKC	Protein kinase C
PLC	Phospholipase C
PMSF	Phenylmethylsulfonyl fluoride
PVDF	Polyvinylidene fluoride
RIPA	Radioimmunoprecipitation assay
RISK	Reperfusion injury salvage kinase
RLU	Relative light units
ROS	Reactive oxygen species
RPM	Revolutions per minute

RPP	Rate-pressure product
RTK	Receptor tyrosine kinase
SAFE	Survivor activating factor enhancement
SEM	Standard error of the mean
Ser727	Serine 727
SOD	Superoxide dismutase
STAT3	Signal transducer and activator of transcription 3
TBA	Thiobarbituric acid
TBARS	Thiobarbituric acid reacting substances
TBS-T	Tris-buffered saline with Tween
TGF-β	Transforming growth factor beta
TNFR1	Tumor necrosis factor receptor 1
TNFR2	Tumor necrosis factor receptor 2
TNF-α	Tumour necrosis factor alpha
TRADD	Tumor necrosis factor receptor type 1-associated death domain
TUNEL	Terminal deoxynucleotidyl transferase dUTP nick end labeling
Tyr705	Tyrosine 705
U	Unit
UPP	Ubiquitin proteasome pathway

Units

%	Percentage
°C	Degree Celsius
μg	Microgram
μL	Microlitre
μm	Micrometre
μm^2	Micrometre squared
μmol/g	Micromol per gram
μmol/L	Micromol per litre
cm	Centrimetre
fM	Fentomolar
fmol/mL	Fentomol per milliliter
g	Gram
Hz	Hertz
kDa	Kilo Dalton
M	Molar
mA	Milli-ampere
mg	Milligram
Mg/kg	Milligram per kilogram
mg/m2	Milligram per metre squared
mL	Millilitre
mL/minute	Millilitre per minute
mM	Millimolar

mWatt	Milliwatt
nm	Nanometre
pg/mL	Picogram per milliliter
V	Volt
x g	Multiply by gravity

Symbols

Ca^{2+}	Calcium
CO_2	Carbon dioxide
Fe^{2+}	Ferrous iron
H_2O_2	Hydrogen peroxide
$O_2^{\bullet-}$	Superoxide
$OH^{\bullet}$	Hydroxyl radical
α	Alpha
β	Beta
γ	Gamma
ξ	Extinction co-efficient

Table of Contents

Chapter 1

Literature Review

1.1 Introduction

It is predicted that by the year 2020, the world's population will increase to 7.5 billion people. Cancer continues to be a worldwide disease burden (Anand *et al*., 2008) with an incidence of 17 million cases. By 2050 it is predicted that two thirds of these cases will occur in the developing regions of the world (Bray & Møller, 2006). This is exacerbated by the growing concern for communicable diseases such as human immunodeficiency virus (HIV)/acquired immunodeficiency syndrome (AIDS) and tuberculosis in African countries (Jemal *et al*., 2012). Fortunately, the discovery of anthracyclines has aided a steadily increasing population of cancer survivors (Lipshultz *et al*., 2008). Doxorubicin (DOX) is an anthracycline antibiotic, previously isolated as a natural product of *Streptomyces peucetius* in the late 1960s (Arcamone *et al*., 1969). It has a broad spectrum of therapeutic activities and is thus the most effective and widely used drug for the treatment of cancers such as leukemias, lymphomas and solid tumours (Barrett-Lee *et al*., 2009; Blum & Carter, 1974; Bonadonna *et al*., 1970; Weiss, 1992). The chemical structure of DOX (Figure 1.1) consists of aglyconic and sugar moieties (Minotti *et al*., 2004). Doxorubicinone, the aglycone, is made up of tetracyclic rings (A – D) that contain adjacent quinone-hydroquinone moieties in rings B and C. Daunosamine, the sugar moiety, attaches to carbon number 7 by glycosidic bonds (Arcamone *et al*., 1969). These structural features are important for its topoisomerase-targeting and DNA-intercalating abilities (Minotti *et al*., 2004), the mechanisms by which DOX kills cancer cells.
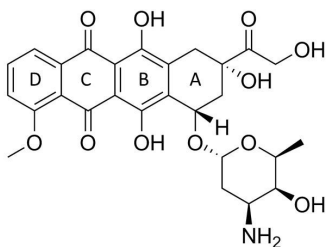
Figure 1.1: The chemical structure of DOX.

DOX consists of quinone and hydroquinone moieties in rings B and C and a sugar moiety attached to carbon number 7 of ring A. Adapted from Carvalho *et al*., (2014), with permission from Wiley.

The heart is a truly remarkable organ with the ability to meet the demands of the body during exercise, and withstand lifetime stressors such as hypertension (Ewer & Ewer, 2010). However, various toxic substances can cause irreversible damage to this otherwise robust pump. One of the measures of the success of DOX is the fact that cancer survivors have an increased lifespan, however, the side effects associated with DOX treatment have become a significant clinical problem. Even though the survival rate is now approximately 80% (Vander Heide & L'Ecuyer, 2007), the use of DOX is limited by several toxic side effects, with dose-dependent cardiotoxicity being the most prominent and the most feared (Swain *et al*., 2003; Lefrak *et al*., 1973; Von Hoff *et al*., 1979). The progressive myocardial damage of this condition can lead to heart failure, a reduced quality of life, and eventually death (Lefrak *et al*., 1973). Although there is no single accepted definition for cardiotoxicity, it can be defined as a "broad range of adverse effects on heart function induced by chemotherapeutic molecules" (Montaigne *et al*., 2012). Cardiotoxicity was not initially detected during pre-clinical animal studies and was only reported during early clinical trials (Lefrak *et al*., 1973). Late into the 1970s, clinical studies identified that the observed cardiac abnormalities that occurred during DOX treatment were directly proportional to the dose of the drug received. DOX-induced cardiotoxicity has also been demonstrated in cell culture (Das *et al*., 2011), in isolated heart studies (Rajagopalan *et al*., 1988), in *in vivo* studies (Arola *et al*., 2000) and in humans (Von Hoff *et al*., 1979). In all instances, the magnitude of DOX-induced cardiac damage was directly proportional to the cumulative dose of the drug received.

Since treatment with DOX has been met with a significant fall in cancer-related mortality rates, the cardiotoxicity that accompanies its use, and the impact thereof, has now emerged as a noticeable problem. It is estimated that the incidence of DOX-induced cardiotoxicity ranges from 4% to more than 36% (Figure 1.2), with these estimates being directly proportional to the dose of drug received (Lefrak *et al*., 1973). Indeed, Hudson *et al*., (2013) showed that 56.4% of childhood cancer survivors treated with anthracyclines showed signs of cardiac dysfunction 10 – 47 years after diagnosis. Various other risk factors for the development of cardiotoxicity also exist, including a cumulative lifetime dose of 450 – 600 mg/m^2 (Minotti *et al*., 2004), previous or concurrent radiation treatment (Bristow *et al*., 1978), young or old age at the time of diagnosis (Mulrooney *et al*., 2016; Bowles *et al*., 2012) and a history of other

cardiovascular disease (Bovelli *et al*., 2010). In addition, lifestyle factors such as smoking, inactivity and excess body weight may contribute to the development of DOX-induced cardiotoxicity, however, further evidence is needed to support these claims (Lipshultz *et al*., 2015).
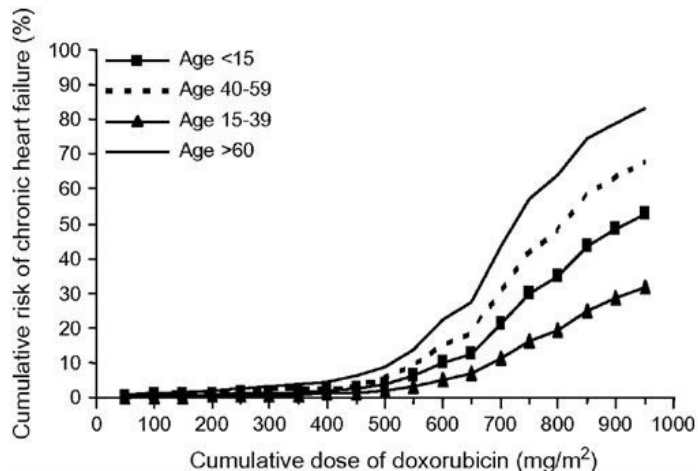
Figure 1.2: Cumulative risk of developing DOX-induced heart failure.
The risk of developing DOX-induced heart failure increases with the cumulative dose of drug received, as well as with young or old age. Taken from Barrett-Lee *et al*., (2009), by permission of Oxford University Press.

There are four types of cardiomyopathies: dilative, hypertrophic, restrictive and arthymogenic right ventricular cardiomyopathy (Olsen, 1975; Marcus *et al*., 2010). However, an additional type known has secondary cardiomyopathy has now been recognized as a consequence of conditions such as inflammation or toxic agents (Sisakian, 2014). Patients diagnosed with DOX-induced cardiotoxicity may be classified into three groups: **i)** acute cardiotoxicity, which usually presents as reversible cardiac dysfunction during or within one week after treatment with an incidence of less than 1%, **ii)** early chronic, which occurs within the first year at an incidence of 1.6 – 2.1 % and **iii)** late onset chronic cardiotoxicity, which can occur between 1 and 30 years after treatment at an incidence of 16 – 20%, presenting as dilated cardiomyopathy and heart failure (Bovelli *et al*., 2010; Carvalho *et al*., 2014; Scully & Lipshultz, 2007). The major morphological characteristics of cardiotoxicity include myofibrillar loss, dilatation of the sarcoplasmic reticulum and swelling of the mitochondria (Tokarska-Schlattner *et al*., 2006). Acute cardiotoxicity is not a clinical concern as it usually resolves on its own shortly after treatment, whereas chronic cardiotoxicity drastically affects the morbidity and survival outcome of patients requiring long-term therapy (Šimùnek *et al*.,

2009). Signs of cardiomyopathy show a prevalence of 7.4% in cancer survivors exposed to DOX at least 20 years earlier (Mulrooney *et al*., 2016), however, a much larger cardiovascular morbidity rate of 19% was reported in a cohort of cancer survivors (Toro-Salazar *et al*., 2015). It has also been reported that childhood cancer survivors face a 5.8-fold greater chance of death due to cardiac disease than the general population (Tukenova *et al*., 2010), emphasizing the serious clinical implications of DOX-induced cardiotoxicity. The unanticipated complication of DOX use brings with it a poor prognosis for cancer survivors, as cardiotoxicity has proven to be fatal in at least 50% of cases (Bristow *et al*., 1978; Von Hoff *et al*., 1979). The discipline of cardio-oncology is thus essential for the survival of cancer patients, as a cancer survivor should not have to become a patient with heart failure. This emphasizes the need for novel adjuvant therapies that can remain effective against cancer but carry minimal cardiotoxic side effects.

1.2 Mechanisms and treatment strategies

Over the years, researchers have invested their time and research funds to investigate the targets and molecular mechanisms involved in the pathogenesis of DOX-induced cardiotoxicity, however, based on the long list of potential, yet controversial mechanisms, it is clear that the development of cardiotoxicity is a complex and multifactorial process. Amongst others, increased systemic and cardiac cholesterol levels have been newly identified as contributors to the development of cardiotoxicity (Monzel et al., 2017), however, one of the mostly wide accepted and commonly quoted mechanisms is the generation of oxygen-derived free radicals, with cardiomyocyte apoptosis being the resultant terminal downstream event (Minotti *et al*., 2004; Olson *et al*., 1981; Kalyanaraman *et al*., 2002; Alderton *et al*., 1992). Oxygen radicals can induce cellular damage to lipid membranes, mitochondria, DNA and proteins once they overwhelm the hearts natural antioxidant defense systems (Doroshow, 1983). This coalition of events all contribute to the ultimate death of the cardiomyocyte (Sinha, 1989; Valko *et al*., 2007). DOX generates free radicals in two ways: **i)** via the mitochondrial respiratory chain and **ii)** via a non-enzymatic pathway involving iron (Olson & Mushlin, 1990). Only a few years after its discovery, various studies reported that DOX was involved in reduction-oxidation reactions by cycling between its quinone and semiquinone form (Goodman & Hochstein, 1977; Bachur *et al*., 1978). Several oxidoreductases within mitochondria convert DOX into a semiquinone through the reduction of ring C (Figure 1.3). In the presence of oxygen, superoxide ($O_2^{\bullet-}$) and hydrogen peroxide (H_2O_2) radicals are

produced (Olson *et al*., 1981; Olson & Mushlin, 1990). Electrons are then donated back to DOX and the parent compound is regenerated. Since no net consumption of DOX takes place, the process of "redox cycling" is endless and generates many molecules of free radicals (Keizer *et al*., 1990).
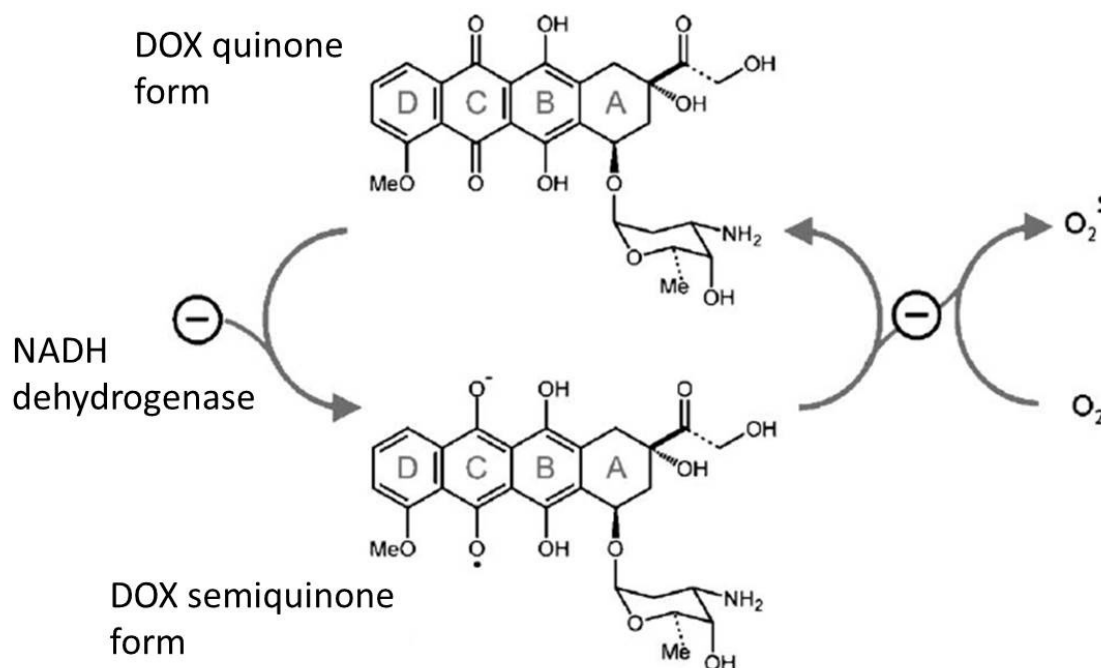
Figure 1.3: The process of redox cycling.

During redox cycling, the reduction of ring C converts DOX into a semiquinone form and produces various oxygen radicals. The parent compound of DOX is regenerated. Adapted from Tokarska-Schlattner *et al*., (2006), with permission from Elsevier.

Alternatively, free radicals can be generated through enzyme-independent mechanisms, as DOX has the ability to chelate iron (Zweier, 1984). Fe^{3+} reacts with the ketone and hydroxy groups of carbon-11 and -12 (rings B and C) of DOX. In this redox reaction, Fe^{3+} accepts an electron and an Fe^{2+}-DOX complex is generated (Olson & Mushlin, 1990). This complex then reduces oxygen into superoxide radicals, after which an electron flows from Fe^{2+} to DOX, producing a Fe^{3+}-DOX complex free radical. The Fe^{3+}DOX complex can induce the peroxidation of lipids and the destruction of the respiratory chain enzymes (Demant & Jensen, 1983). Although there is very little freely available iron within cardiomyocytes, it is believed that DOX is able to release iron from cytosolic ferritin stores (Thomas & Aust, 1986).

Mitochondria are the most extensively damaged organelles affected by DOX-induced cardiotoxicity (Hasinoff *et al.*, 2003; El-Mehy *et al.*, 2008). One of the major reasons for this is due to the high affinity that DOX has for cardiolipin, an abundant phospholipid embedded in the inner mitochondrial membrane (Schlame *et al.*, 2000), allowing DOX to accumulate in the mitochondrion (Goormaghtigh *et al.*, 1980). Cardiolipin is almost exclusively associated with membranes involved in ATP production and may therefore play a role in mitochondrial bioenergetics. The fact that the heart is densely populated with mitochondria, which are both a source and target of free radical production, leaves it vulnerable to oxidative stress-induced damage and sensitive to oxidative stress due to the highly oxidative environment and limited antioxidant defense compared to other organs. Compared to other metabolic organs such as the liver and kidneys, the heart contains reduced levels of intracellular superoxide dismutase (SOD), glutathione (GSH) and catalase, increasing the chances of cardiovascular damage (Doroshow *et al.*, 1980; Quiles *et al.*, 2002). It is therefore plausible that DOX-induced cardiotoxicity could be reduced if these defense systems were upregulated. SOD is an enzyme responsible for the dismutation of $O_2^{\bullet-}$ radicals into H_2O_2 or molecular oxygen (Scandalios, 1993; Perry *et al.*, 2010). H_2O_2 is then scavenged into water and molecular oxygen by catalase. H_2O_2 can also be reduced to water by GSH, which donates a reducing equivalent in a reaction catalyzed by glutathione peroxidase 1 (GSH-Px1). During this reaction, GSH is converted to the oxidized form, glutathione disulphide (GSSG). Once oxidized, GSSG can be regenerated into GSH by glutathione reductase (GR), using electrons donated by NADPH (Figure 1.4).
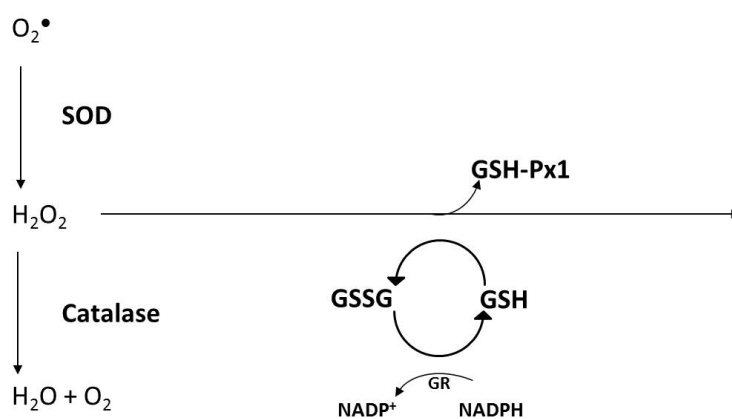
Figure 1.4: The pathways involved in free radical scavenging.

SOD is responsible for converting superoxide radicals into hydrogen peroxide. Hydrogen peroxide can then be reduced to water and oxygen by catalase or glutathione. Abbreviations: $O_2^{\bullet-}$, superoxide; SOD, superoxide dismutase; H_2O_2, hydrogen peroxide; H_2O, water; O_2, oxygen; GSH-Px1, glutathione peroxidase 1; GSH, glutathione; GSSG, glutathione disulphide; GR, glutathione reductase.

One of the earliest antioxidants investigated was vitamin E (Myers *et al*., 1977), which was shown to protect against DOX-induced cardiomyopathy by enhancing the activity of GSH-Px1 in the rat myocardium (Siveski-Iliskovic *et al*., 1994; Kumral *et al*., 2016). Unfortunately, research then showed that vitamin E treatment is only effective in acute studies and does not offer protection from the chronic forms of this condition (Mimnaugh *et al*., 1979). Similarly, N-acetylcysteine (NAC) was highly effective in acute studies (Doroshow *et al*., 1981), but failed to show protection in the chronic setting (Herman *et al*., 1985). The positive results observed in animal studies after treatment with various antioxidants were not echoed in clinical trials, suggesting that the experimental models studied and the type and dose of antioxidants utilized may affect their efficacy (Singal *et al*., 1997).

After several decades of intensive research, Dexrazoxane (DXZ/ICRF-187) is the only drug that has been approved for clinical use as a pharmacological cardioprotective agent. This drug has repeatedly been shown to protect the myocardium from anthracyclines in experimental models and clinical trials (Lipshultz *et al*., 2004; Xiang *et al*., 2009; Asselin *et al*., 2016). DXZ has the ability to chelate iron, which then decreases the DOX-induced damage to DNA and the mitochondria (Lebrecht *et al*., 2007), without jeopardizing its anti-cancer efficacy (Speyer *et al*., 1992). DXZ enters the cell where it undergoes rapid hydrolysis into ADR-925, its metal ion-binding form. By chelating free iron and displacing the iron associated with DOX-iron complexes, DXZ limits the production of reactive species and ultimately reduces mitochondrial dysfunction (Hasinoff *et al*., 2003). In phase III clinical trials, the incidence of cardiac events associated with DOX use was less than 15% in women receiving DXZ, compared to 16 – 50% in women who did not receive it (Swain *et al*., 1997b). The incidence of congestive heart failure (CHF) was also significantly reduced from almost 30% in women not receiving DXZ, to 0 – 3% in women who were (Swain *et al*., 1997a). However, the success of DXZ is hampered by the development of severe myelosuppression (Curran *et al*., 1991), thus limiting its use as a cardioprotective agent.

The severity of cardiotoxicity has highlighted the clinical importance and awareness of this condition, such that it has prompted the development of several experimental models. However, one of the reasons that the mechanisms of chronic cardiotoxicity remain unclear is due to the selection of inappropriate models. Many studies aiming to identify the molecular pathogenesis of cardiotoxicity evaluate the effects of DOX *in vitro* or *in vivo*. These studies usually employ high drug concentrations and examine effects within hours or days, ultimately only simulating the reversible, acute form of cardiotoxicity. The *in vivo* effects of chronic cardiotoxicity require weeks to appear and are associated with lower, but cumulative drug concentrations. Such studies require large sample sizes that need to be monitored over extended periods of time, increasing experimental costs. Still, to realistically simulate the clinical setting, studies of chronic cardiotoxicity should be a high priority. Long-term studies of chronic cardiotoxicity are also important to accurately evaluate the cardioprotective potential of adjuvant therapies so that clinically relevant routes of administration and doses of drugs can be evaluated (Gianni *et al*., 2008). The current strategy for treatment of this condition is aimed at maintaining the efficiency of the weakening myocardium, and a few of the treatment options are outline in Table 1, however, none of these have proven to be ideal.

Table 1: Current treatment strategies for cardiotoxicity.

Drug	Function	Model	Authors
Digoxin/digitalis	Improve contractility	Humans	Guthrie and Gibson, (1977)
Diuretics	Reduce fluid retention	Humans	Antman *et al*., (1984)
ACE-inhibitors	Reduce workload of the heart	Rat	Sacco *et al*., (2001)
β-blockers	Prevent arrhythmias	Human	Kalay *et al*., (2006)

Abbreviations: ACE, angiotensin-converting enzyme

Considering that there is no consensus on an effective strategy to prevent or even treat DOX-induced cardiotoxicity other than a heart transplant (Thomas *et al*., 2002), the best approach is early detection of cardiomyopathies (Pereira *et al*., 2011), however, cardiac damage is usually only detected after the functional impairment has already occurred. An ideal marker of cardiac damage should **i)** be found at high concentrations in the myocardium but low concentrations in other organs, **ii)** be released rapidly after myocardial injury, **iii)** be released at concentrations that are directly proportional to the extent of myocardial injury and **iv)** remain in the blood long enough to provide a diagnostic window (Adams *et al*., 1993a). The elevation of cardiac markers such as cardiac troponin tropomyosin (cTnT), cardiac troponin

inhibitory (cTnI) and creatine kinase–myocardial band (CK-MB) are pivotal for correct diagnosis, as they correlate with the extent of myocardial injury and the subsequent risk of adverse events (Chin *et al*., 2012). The troponins are myofibrillar proteins that form a complex that controls the interaction of actin and myosin. They are the most cardiac-specific markers of all the currently available markers for myocardial damage (Rottbauer *et al*., 1996; Adams *et al*., 1993b). cTnI is not expressed by injured skeletal muscle and is therefore uniquely specific to cardiac injury. Due to their specificity and the very low concentrations in the serum of healthy individuals (Wallace *et al*., 2006), the troponins are incredibly sensitive to even mild myocardial injury. Indeed, Cardinale *et al*., (2002) reported that cTnI is a risk marker for the development of left ventricular dysfunction after chemotherapy. Since it can take several months for the full cardiotoxic side effects of DOX to impact on cardiac function, it is usually too late to make use of conventional heart failure therapy (Kantrowitz & Bristow, 1984). The current approach to reduce DOX-induced cardiotoxicity is to minimize oxidative stress through the use of various antioxidants. However, the positive results of only some antioxidants against DOX-induced cardiotoxicity *in vivo* indicate that oxidative stress may not be the primary culprit for the development of cardiotoxicity. This suggests that several mechanisms are at play, and highlights the need for a cardioprotective agent with mechanisms of action that can target multiple steps of this complex process.

Ghrelin, an orexigenic hunger hormone discovered in 1999, has whet the appetites of many researchers through its diverse array of biological functions. The beneficial effects of ghrelin have been attributed to its ability to stimulate appetite and positive energy balance, affect glucose metabolism, modulate cell proliferation and survival, and influence cardiovascular performance (Van Der Lely *et al*., 2004). It is therefore not surprising that ghrelin has clinical and therapeutic potential in the fields of cardiology and oncology. This review explores the role of ghrelin in the context of chronic DOX-induced toxicity, including its effects on oxidative stress and cell death, the fundamental mechanisms responsible for cardiovascular dysfunction in this condition. Furthermore, this review will investigate the link between ghrelin and two well-known pro-survival pathways, the RISK and SAFE, to not only delineate its influence on these pathways, but to also assess its potential beneficial effects in relation to cardioprotection.

1.3 Identifying a role for ghrelin

Ghrelin, a 28-amino acid acyl peptide, is most well-known for inducing the release of growth hormone (GH) from the pituitary gland and stimulating food intake and adiposity (Tschöp *et al*., 2000; Kishimoto *et al*., 2012; Kojima *et al*., 2001). However, numerous studies (García & Korbonits, 2006; Granata *et al*., 2011) are now highlighting just how multifunctional this peptide hormone is (Figure 1.5). Ghrelin and its messenger RNA (mRNA) are mainly synthesized in X/A-like cells in the oxyntic mucosa of the stomach (Date *et al*., 2000), where the 28-amino acid mature form is cleaved off the pre-cursor, pre-proghrelin. Circulating ghrelin levels exhibit a pre-prandial (fasting) increase, suggesting a role in meal initiation, and a post-prandial (feeding) decrease (Cummings *et al*., 2001), which are directly proportional to the calories ingested. From the submucosal layer of the stomach, ghrelin is then secreted into the blood stream where it acts on the anterior pituitary gland (Kojima *et al*., 1999). In healthy humans, plasma ghrelin circulates at a concentration of 117.2 ± 37.2 fmol/mL (Kojima *et al*., 1999).
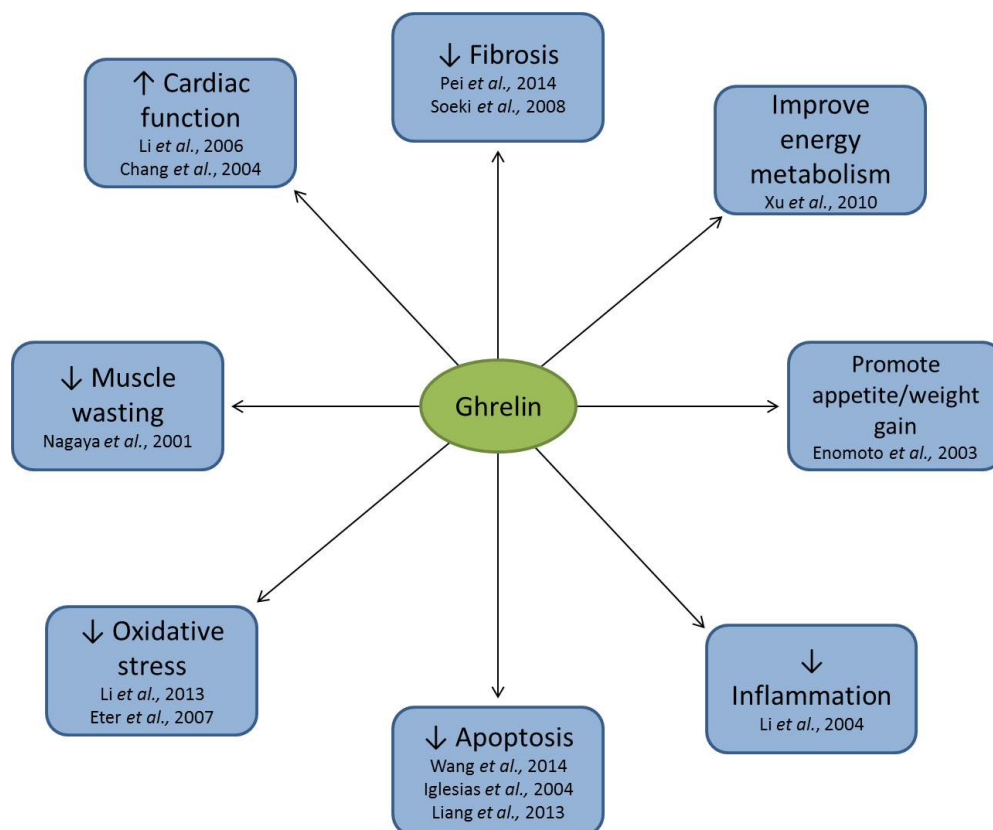
Figure 1.5: A summary of the known biological actions of ghrelin.

Ghrelin exerts various beneficial effects which may also extend to DOX-induced cardiotoxicity.

Ghrelin mediates its endocrine activities via the growth hormone secretagogue receptor 1α (GHSR-1α), a G-protein coupled receptor mainly located in the pituitary gland and the hypothalamus. Acylation of ghrelin with octanoic acid on Serine 3 (**Figure** 1**.**6) is essential for receptor binding (Kojima *et al*., 1999), and the fact that this modification site is evolutionarily conserved emphasizes its importance for ghrelin activity (Kojima *et al*., 2001). In circulation, des-acyl (unacylated) ghrelin also exists. Although des-acyl ghrelin is far more abundant within the cell (3 - 4: 1), it does not bind to GHSR-1α and exerts functions which are currently unknown (Kojima & Kangawa, 2005; Nagaya & Kangawa, 2003; Tong *et al*., 2013). However, it has been reported that both ghrelin and des-acyl ghrelin recognize a common binding site that is distinct from GHSR-1α (Baldanzi *et al*., 2002; Yu *et al*., 2014).

The action of ghrelin is regulated by several mechanisms, including **i)** the transcriptional and translational regulation of the ghrelin gene, **ii)** the enzymatic activity of ghrelin O-acyl transferase that is responsible for the octanoylation on Serine 3, **iii)** the secretion rate of active ghrelin, **iv)** enzymatic processes involved in deactivating ghrelin, **v)** the influence of ghrelin binding proteins on its bioactivity, **vi)** the accessibility of a target tissue, **vii)** clearance and degradation of ghrelin by the kidneys or liver, **viii)** the concentrations of additional circulating endogenous ligands, **ix)** the level of ghrelin receptor expression and **x)** the sensitivity of these receptors to ghrelin (Van Der Lely *et al*., 2004).

- 11 -
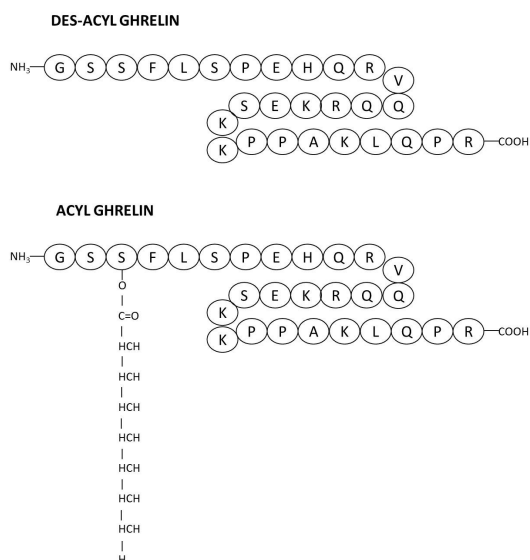
Figure 1.6: Structure of acyl-ghrelin (left) and des-acyl ghrelin (right).

Adapted from Orbetzova, (2012). © Published in *Insulin Resistance* under CC BY 3.0 license. Available from: http://dx.doi.org/10.5772/50977.

1.4 Ghrelin and the heart – an adjuvant therapy for heart failure

Although ghrelin is predominantly produced in the stomach, both ghrelin and its various receptors have been detected in other tissues (lungs, pancreas, kidney, brain) including the heart, albeit at lower levels (Gnanapavan *et al*., 2002; Kojima *et al*., 1999). In addition, Iglesias *et al*., (2004) have reported the presence of ghrelin receptors within cardiomyocytes and that these cultured cells can actually synthesize ghrelin, supporting a role for ghrelin in the cardiovascular system. The fact that ghrelin mRNA and its receptors are abundantly expressed in rat ventricles, atria, aorta, coronary arteries, carotid arteries and vena cava confirms that the heart is also a target for ghrelin (Gnanapavan *et al*., 2002; Zhang *et al*., 2010). Accumulating evidence indicates that ghrelin exerts several functions on the cardiovascular system, including protection against myocardial infarction and ischemia-reperfusion injury (IRI). In *in* vivo models of heart failure, induced as a result of the previously mentioned conditions, treatment with ghrelin resulted in improved systolic dysfunction and reduced systemic vascular resistance and arterial pressure (Chang *et al*., 2004a; Nagaya *et al*., 2001c). In patients with CHF, twice daily treatment with ghrelin caused a significant increase in left ventricular ejection fraction, from 27% to 31% (Nagaya *et al*., 2004). Ghrelin has further been shown to increase posterior wall thickness, inhibit progressive left ventricular enlargement associated with heart failure, and thereby reduced left ventricular wall stress (Wang *et al*., 2014). In ghrelin knock-out mice with heart failure, ghrelin administration substantially improved survival, myocardial remodeling and dysfunction. Interestingly, heart failure deteriorated in knock-out control mice (Mao *et al*., 2013). In the context of DOX-induced cardiotoxicity, the survival rate after five weeks of treatment with DOX was a mere 37.5%, versus 87.5% in mice that received co-treatment with ghrelin (Wang *et al*., 2014). Furthermore, ghrelin treatment increased ejection fraction and heart rate, both of which were negatively affected during DOX treatment. These findings thus emphasize an important role for ghrelin in improving cardiovascular function and reducing mortality during pathological conditions.

It is a well-known phenomenon that individuals who suffer from diseases such as heart failure and cancer experience significant weight loss (Fearon *et al*., 2011; Fülster *et al*., 2013), therefore in addition to its potential cardioprotective effects, ghrelin's appetite-inducing effects may prove beneficial in this context. Indeed, previous studies have shown that ghrelin not only increases appetite in healthy individuals (Enomoto *et al*., 2003), but also in patients with CHF (Nagaya *et al*., 2004). In healthy individuals, ghrelin decreases mean arterial pressure without affecting heart rate, decreases vascular resistance and increases stroke volume (Nagaya *et al*., 2001a). These effects suggest that ghrelin may inhibit the activation of the sympathetic nervous system (Mao *et al*., 2013). The GH-releasing effect of ghrelin appears to occur as a result of ghrelin binding to the GHSR-1α in the anterior pituitary gland, whereafter ghrelin activates growth hormone releasing hormone (GHRH)-containing neurons (Popovic *et al*., 2003). Interestingly, ghrelin can trigger GH production through the phospholipase C (PLC) pathway, where PLC catalyzes the hydrolysis of phosphatidylinositol-4,5-bisphosphate (PIP_2), yielding inositol 1,4,5-trisphosphate (IP_3) and diacyl glycerol (DAG) (Lopez *et al*., 2001). IP_3 and DAG are crucial intercellular second messengers that regulate several cellular processes, as well as serving as substrates for the synthesis of other signaling molecules. When IP_3 binds to its receptors on calcium (Ca^{2+}) channels, it initiates a surge in cytosolic Ca^{2+} from intracellular stores. Ca^{2+} then facilitates GH release from the somatotrophic cells by docking GH secretory granules to the plasma membrane (Smith *et al*., 1997), or by stimulating GHRH on hypothalamic neurons (Lall *et al*., 2004). Ca^{2+} is a second messenger that is involved in processes such as muscle contraction (Berridge *et al*., 2000). Considering that one of the symptoms associated with DOX-induced cardiotoxicity is a decline in cardiac output and contractility (Wang *et al*., 2014; Xiong *et al*., 2006), it is likely that treatment with ghrelin could be of potential benefit by counteracting this decline through enhanced up-regulation of Ca^{2+} ATPase (Tajima *et al*., 1999). Ghrelin may also exert a protective effect on the cardiovascular system through the anabolic effects of GH and its mediator, insulin-like growth factor-1 (IGF-1), both of which are necessary for myocardial growth and metabolic homeostasis (Kishimoto *et al*., 2012; Ledderose *et al*., 2011).

As mentioned previously, ghrelin has been reported to increase appetite and consequently food intake, amongst other functions. Its use was demonstrated to be particularly advantageous in patients suffering from CHF with complications of cachexia, a commonly

observed wasting syndrome associated with this disease. These patients displayed signs of improved weight gain, muscle mass and muscle strength, as well as a positive energy balance (Nagaya *et al*., 2004). In patients undergoing a combined treatment of Cisplatin and DOX, plasma glucose levels were transiently decreased, whilst exogenous administration of ghrelin caused a significant increase in food intake and appetite, preventing the adverse side effects associated with chemotherapy (Hiura *et al*., 2012). During cachexia, ghrelin increases both lean and fat mass in order to re-establish physiological body composition and weight (Strassburg *et al*., 2008). Additionally, body fat is lost more rapidly than lean mass during cancer cachexia, and as such, it is a predictor of survival (Fouladiun *et al*., 2005). Ghrelin promotes food intake either by stimulating vagal afferent nerve fibers (Date *et al*., 2002) or through the blood stream (Banks *et al*., 2002), where after the signal reaches the arcuate nucleus of the hypothalamus. Here, ghrelin-containing neurons send efferent fibers to the neurons that contain the appetite stimulating (orexigenic) peptides neuropeptide Y (NPY) and agouti-related protein (AgRP), subsequently activating these neurons (Chen *et al*., 2004). This results in an increase in NPY and AgRP mRNA expression (Shintani *et al*., 2001; Kamegai *et al*., 2001) and subsequently stimulates food intake (Figure 1.7). However, the exact mechanism by which these neurons stimulate food intake is still unknown. Cardiomyocyte size is reduced during DOX treatment *in vitro* and *in vivo*, indicating a cachectic state (Wang *et al*., 2014). Ghrelin restored cardiomyocyte size, inducing a parallel increase in body weight, suggesting that ghrelin is able to exert a potent anti-cachectic effect during cardiotoxicity. Since the ultimate fate of patients with DOX-induced cardiotoxicity is also heart failure, ghrelin may exert cardioprotective and anti-cachectic effects in the same manner as it does during conventional heart failure, substantiating the merit in further exploring this multifaceted peptide.
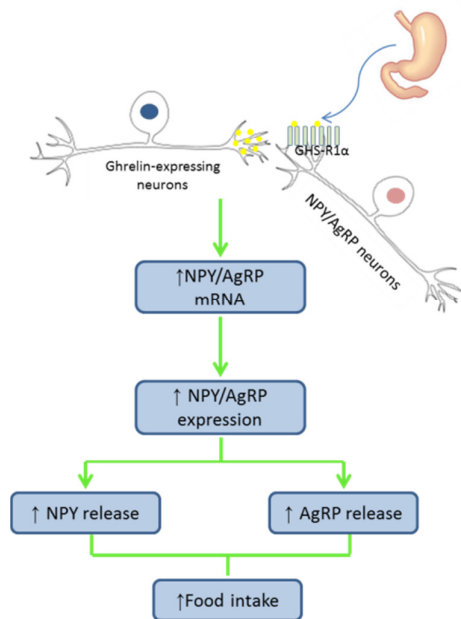
Figure 1.7: Ghrelin regulates energy balance and appetite by at least two mechanisms.
Ghrelin can act as a peripheral hormone from the stomach that sends signals via the vagus nerve or crosses the blood-brain barrier and ii) as a neuropeptide in the arcuate nucleus of the hypothalamus that sends efferent nerve fibers to NPY/AgRP neurons. NPY, neuropeptide Y; AgRP, agouti-related protein.

Since evidence does exist that ghrelin can exert its effects on cardiovascular function, it is likely that the expression of ghrelin and its receptors may be abnormal in certain pathologies. In healthy human myocardial specimens, strong immunoreactivity for ghrelin was demonstrated, as opposed to weak immunoreactions in samples taken from patients with CHF (Beiras-Fernandez *et al*., 2010). This data suggests that myocardial function is directly proportional to ghrelin expression, as a failing heart appears to be associated with impairment in ghrelin production. Contrasting reports show that ghrelin is increased in cachectic patients with CHF, as evident by elevated plasma ghrelin levels of 237 fM (Nagaya *et al*., 2001b) as opposed to approximately 100 fM in healthy subjects (Kojima *et al*., 1999). Likewise, the level of ghrelin mRNA and GHSR-1α were elevated in an isoproterenol-induced model of heart failure (Li *et al*., 2006b). The protein and mRNA levels of ghrelin may therefore be upregulated or down-regulated depending on the severity and stage of the disease model being studied.

1.5 The role of ghrelin in myocardial energy homeostasis

Metabolism is essential for the normal contractility of the heart, which in turn necessitates large amounts of mitochondrial ATP production. Once glucose and free fatty acids are taken up by the cell, they are broken down in the mitochondria into acetyl CoA, which then enters the citric acid cycle. The next process is oxidative phosphorylation in which mitochondria produce ATP from ADP molecules. ATP then leaves the mitochondrion and is available for contraction. In the fed-state, circulating glucose and insulin levels are high, whilst ghrelin levels remain low (Cummings *et al*., 2001) and the level of circulating fatty acids are suppressed. The uptake of fatty acids by the heart therefore falls, allowing glucose oxidation to increase. In contrast, in the fasted state when glucose and insulin levels are low, ghrelin levels are high, and circulating free fatty acid levels are elevated, the high rate of free fatty acid uptake by the heart results in their preferential use in metabolism (Willis *et al*., 2014). Des-acyl ghrelin, but not acylated ghrelin, increases the uptake of medium length fatty acids in cardiomyocytes, which are necessary for the acylation of ghrelin by ghrelin O-acyl transferase (Lear *et al*., 2010). This suggests that des-acyl ghrelin has the ability to indirectly promote the acylation of ghrelin by increasing the uptake of the fatty acids that are used in the process. However, ghrelin is known to decrease fat utilization and increase glucose utilization (Tschöp *et al*., 2000), thereby increasing fat mass and overall body weight (Strassburg *et al*., 2008). This finding suggests that ghrelin signals to the hypothalamus when an increase in metabolic efficiency is needed, as a positive energy balance is necessary to maximize the anabolic effect of GH. Furthermore, the increased use of glucose during fasting (when ghrelin levels are high), suggests a shift towards a more energy efficient form of metabolism during times of starvation or fasting. Interestingly, in the failing myocardium, the heart's ability to supply sufficient energy to meet its demands significantly deteriorates (Sharov *et al*., 2000). Although fatty acids are the heart's substrate of choice for ATP production under aerobic conditions, the heart is often forced to metabolize less optimal substrates. While the use of fatty acids generates more ATP than glucose (Lopaschuk *et al*., 2010), it comes at the expense of a greater requirement for oxygen. It is thus more energy efficient for the heart to metabolize glucose rather than fatty acids during pathological conditions or energy deficits (Tokarska-Schlattner *et al*., 2006). Therefore, shifting the heart's substrate preference away from fatty acids can improve heart function and slow the progression of heart failure (Chandler *et al*., 2002; Bristow, 2000; Bersin & Stacpoole, 1997).

DOX has been reported to reduce cardiac energy reserves by reducing ATP and phosphocreatine (Jeyaseelan *et al*., 1997; Xu *et al*., 2007), while ghrelin administration has been shown to inhibit the decrease in the intracellular ATP : ADP ratio induced by DOX (Xu *et al*., 2008). In addition, treatment with DOX has been shown to impair both glucose and fatty acid metabolism in the heart, ultimately causing the heart to fail (Wakasugi *et al*., 1993). Therefore, since ghrelin has the ability to reduce fatty acid utilization and elevate glucose utilization, it is plausible that ghrelin may protect the myocardium from unnecessary energy expenditure and excess ROS production, preserving contractile function and metabolic efficiency. Considering that the mitochondria are responsible for the production of approximately 90% of the energy used by the heart (Mootha *et al*., 1997), it comes as no surprise that impaired mitochondria results in an inability of the heart to perform work (Pereira *et al*., 2011). Moreover, it is generally accepted that the mitochondria are a primary source of ROS (Vanden Hoek *et al*., 1997), which then cause oxidative damage to the mitochondria and trigger cell death modalities (Cocco *et al*., 2002).

1.6 The role of ghrelin during DOX-induced oxidative stress

The term "oxidative stress" refers to a state of elevated ROS levels, and is associated with a decline in antioxidant defenses (Suzuki *et al*., 2011). Although the mechanisms for the development of cardiotoxicity are still under debate, one of the widely accepted hypotheses is that DOX generates free radicals which damage the myocardium through oxidation of cell membranes and various cytosolic components (Olson *et al*., 1981). Free radical scavengers such as vitamins E, A and C (Myers *et al*., 1977; Ravi *et al*., 2013; Shimpo *et al*., 1991; El-Mehy *et al*., 2008), which provide protection from DOX *in vivo,* support the oxidative stress theory. In addition, the overexpression of the antioxidant enzyme, glutathione peroxidase, protects mice hearts against acute DOX-induced cardiotoxicity and prevents the dysfunction of mitochondrial respiration (Xiong *et al*., 2006). Furthermore, an increase in mitochondrial ROS after DOX treatment has also been deemed responsible for the catabolism of C2C12 myotubes, via the upregulation of the redox-sensitive E3 ubiquitin ligases, muscle atrophy F-box (MAFbx) and muscle ring finger 1 (MuRF1), and caspase-3 activation (Gilliam *et al*., 2012). Taken together, these studies suggest the involvement of ROS in the development of DOX-induced cardiotoxicity. However, the inconsistent and often negative results of such studies suggests that alternative, non-oxidative mechanisms may also be at play (D'Andrea, 2005). It is also difficult to maintain high plasma antioxidant levels due to inactivation of the

antioxidants by organs such as the liver, and antioxidants of high molecular weights, including SOD and catalase, may be unable to enter intracellular compartments to carry out their functions (Kang *et al*., 1996).

With the above in mind, several researchers have investigated the antioxidant properties of ghrelin in various models of disease (Eter *et al*., 2007; Li *et al*., 2013; Wang *et al*., 2014). Ghrelin administration was associated with a dose-dependent reduction in malondialdehyde (MDA) and an increase in GSH content and GSH-Px1 activity *in vivo* and *in vitro*. In models of IRI (Chang *et al*., 2004a) and isoproterenol-induced-injury (Chang *et al*., 2004b), myocardial MDA was substantially increased, whereas administration of ghrelin reduced this by-product of lipid peroxidation. Ghrelin significantly increased catalase activity by 79.9% and 184.3%, while SOD activity was elevated by 64.1% and 373.3% in plasma and cell lysates, respectively, when compared to DOX-treated groups. These findings were further echoed when mRNA expression was studied, indicating that ghrelin upregulates the expression of various antioxidants at both a transcriptional and translational level during DOX treatment. An increase in the intrinsic activity of SOD and catalase by ghrelin in primary cardiomyocytes may be a mechanism by which ghrelin counteracts DOX-induced oxidative stress (Xu *et al*., 2008). Together, these data suggest that ghrelin inhibits oxidative stress by augmenting endogenous antioxidants, although it is possible that ghrelin itself may exert a direct antioxidant effect.

1.7 The effect of ghrelin on DOX-induced cardiomyocyte death

Heart failure is the end result for a number of heart diseases and, over the years, extensive research from human and animal studies has highlighted evidence that suggests that cardiomyocyte apoptosis may be a key modulator in the pathogenesis of heart failure (Takemura & Fujiwara, 2006; Gustafsson *et al*., 2003). Moreover, since DOX-induced cardiotoxicity only manifests itself years to decades after treatment, it is reasonable to think that the chronic loss of terminally differentiated cardiomyocytes with a limited regenerative capacity (Tokarska-Schlattner *et al*., 2006) will drastically affect myocardial function and eventually lead to heart failure. Therefore, a common endpoint is apoptosis, although this is likely to be the final response to a variety of upstream events, such as oxidative stress.

Apoptosis, first described by Kerr *et al*., (1972), is a form of programmed cell death during which the nucleus and cytoplasm condense, DNA fragments and the cell shrinks. These

fragments are enclosed by the plasma membrane so that the contents of the cell can be phagocytosed in its entirety. Apoptosis therefore occurs swiftly and unnoticed and as a result, is not accompanied by an inflammatory response. Research over the last decade has brought to life the various signaling pathways involved in cellular apoptosis. The intrinsic apoptotic pathway is activated when intracellular homeostasis is disturbed by death signals such as DNA damage and oxidative stress. At any given time, the fate of a cell depends on the expression levels of the B-cell lymphoma 2 (Bcl-2) family, which can be both pro- and anti-apoptotic. The anti-apoptotic proteins, Bcl-2 and Bcl-X_L, function to antagonize the pro-apoptotic proteins such as Bax and Bad.

An apoptotic signal such as oxidative stress or treatment with a cytotoxic agent like DOX, causes Bax to translocate to the mitochondrial membrane where it facilitates the opening of the mitochondrial permeability transition pore (mPTP) (Jiang *et al*., 2014). The subsequent collapse in mitochondrial membrane potential results in cytochrome c release (Childs *et al*., 2002). Bcl-2 is able to prevent the activation of apoptosis through an interaction with Bax (Marie Hardwick & Soane, 2013). Free radicals produced during redox cycling, particularly H_2O_2, are actively involved in facilitating cytochrome c release through the mPTP (Green & Leeuwenburgh, 2002). After its release, cytochrome c forms a complex with pro-caspase-9, an adaptor protein known as apoptosis protease activator protein-1 (Apaf-1) and ATP, forming an apoptosome. Pro-caspase-3 is cleaved by active caspase-9 into active caspase-3 which, together with caspases-6 and -7 are known as executioner caspases. These caspases cleave and inactivate poly (ADP-ribose) polymerase (PARP), preventing it from responding to and repairing DNA strand breaks (Cohen, 1997). The caspases also activate DNase, which is responsible for the fragmentation of DNA (Zhang *et al*., 2011). This sequence of events forms part of the intrinsic (Figure 1.8), mitochondrial apoptotic pathway (Zhang *et al*., 2009). In the context of cardiotoxicity, DOX has been shown to induce apoptosis through caspase-3 activation both *in vitro* (Wu *et al*., 2002) and *in vivo* (Ueno *et al*., 2006). Apoptosis was associated with a substantial decline in left ventricular function, suggesting an important role for apoptosis in myocardial dysfunction induced by DOX therapy. Interestingly, Arola *et al*., (2000) reported that apoptosis peaked on the first day after a single DOX injection and declined thereafter, implying that apoptosis may not be a major contributor to the development of heart failure, at least in the acute stages. Moreover, cardiomyocytes may die

via necrosis due to depleted energy stores as a result of repeated exposure to DOX (Zhang *et al*., 2009).
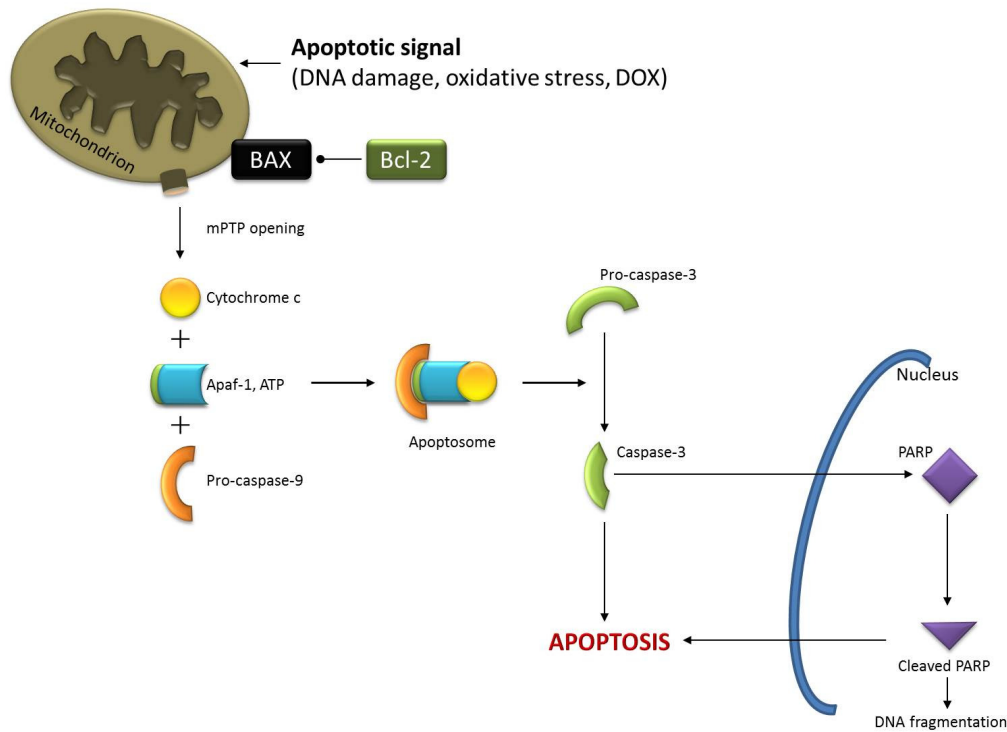
Figure 1.8: The intrinsic apoptotic pathway.

DOX induces oxidative stress that triggers the release of cytochrome c from the mitochondria. Through the formation of an apoptosome, caspase-9 activates the executioner caspases which in turn initiate DNA fragmentation.

Ghrelin has previously been shown to possess anti-apoptotic properties. When cardiomyocytes are treated with high concentrations of glucose, caspase-3 and hence apoptosis, was elevated. However, this observation was reversed after ghrelin administration (Kui *et al*., 2009). A similar phenomenon was observed when the TUNEL index was increased to 467% in the ventricles of DOX-treated mice, but reduced in the mice that received ghrelin (Pei *et al*., 2014). Hexarelin, a synthetic GH secretagogue, prevents DOX-induced cell death in H9c2 cells (Filigheddu *et al*., 2001). Similarly, des-acyl ghrelin and acylated ghrelin are effective at reducing DOX-induced apoptosis (Baldanzi *et al*., 2002). Not only is cell viability improved under these conditions, but H9c2 cellular morphology is maintained (Wang *et al*., 2014). Considering that H9c2 cells are devoid of GHSR-1α, it is

believed that an unknown receptor, that binds to both forms of ghrelin, can act directly on these cells to prevent cell death by activating pro-survival pathways.

The death of cardiomyocytes by apoptosis causes the loss of myofibres and a substantial increase in fibrosis, contributing to the development of cardiovascular dysfunction during cardiotoxicity (Takemura & Fujiwara, 2006; Miyata *et al*., 2010). Collagen accumulation was reduced by ghrelin in a model of DOX-induced cardiotoxicity (Pei *et al*., 2014). This finding extends previous reports on the ability of ghrelin to reduce collagen formation in models of myocardial infarction (Soeki *et al*., 2008), isoproterenol-induced myocardial injury (Li *et al*., 2006b) and diabetic cardiomyopathy (Pei *et al*., 2015). However, the underlying mechanisms by which ghrelin reduces fibrosis are still unclear and remain to be elucidated. Collectively, this data demonstrates that ghrelin can significantly modulate the cardiotoxic effects of DOX, including apoptotic cell death and fibrosis. However, it is important to note that these studies generated data using acute models of cardiotoxicity. Further research is therefore warranted to investigate these effects after prolonged exposure to DOX and whether ghrelin can be used as an adjuvant therapy to mitigate chronic DOX-induced cardiotoxicity. As ghrelin alone does not appear to be toxic in control samples, (Wang *et al*., 2014; Baldanzi *et al*., 2002), it exhibits an appealing property when compared to many other adjuvant therapies. Considering the aforementioned anti-apoptotic effects of ghrelin, a critical aspect that should be considered in this context is the timing of ghrelin administration. Despite the many beneficial effects on the myocardium, the effects of ghrelin on different cancer types is rather contradictory (see Chopin *et al*., (2011) for review). Further research is therefore needed to determine **i)** the effects of ghrelin on cancer progression and tumour growth and **ii)** whether simultaneous administration or administration after chemotherapy reduces cardiovascular damage.

1.8 Ghrelin: a novel RISK pathway activator?

The contribution of oxidative stress during DOX-induced cardiotoxicity has already been discussed, however, during IRI, the restoration of blood flow and reoxygenation of the ischemic myocardium causes a burst of ROS in a phenomenon known as the "oxygen paradox" (Zweier, 1988; Hearse *et al*., 1973; Kalogeris *et al*., 2014). Since ischemia-reperfusion is paradoxical in nature, strategies such as pre- and post-conditioning have been developed to protect the heart (Murry *et al*., 1986; Zhao *et al*., 2003). Both pre- and post-conditioning have been shown to provide protection through the activation of pro-survival

kinases Akt/PKB (protein kinase B) and ERK1/2 (extracellular regulated kinase) (Hausenloy & Yellon, 2004). These kinases also form part of the well-known reperfusion injury salvage kinase (RISK) pathway. Literature has demonstrated that the activation of these kinases by pre- and post-conditioning reduces infarct size by 40 – 50% (Hausenloy, 2009). Furthermore, the activation of this pathway down-regulates pro-apoptotic proteins and promotes mitochondrial integrity (Xiang *et al.*, 2009).

ERK1/2 forms part of the mitogen activated protein kinase (MAPK) cascade which, in cardiomyocytes, is initiated by stress stimuli, G-protein coupled receptors and receptor tyrosine kinases (Sugden & Clerk, 1998). This pathway has been implicated in cell survival in response to IRI, oxidative stress and exposure to anthracyclines. Inhibition of ERK1/2 signaling was shown to exacerbate Daunomycin-induced apoptosis in cardiomyocytes (Zhu *et al.*, 1999), whereas ERK1/2 activation in a model of IRI attenuated the apoptosis associated with this condition (Yue *et al.*, 2000). However, although these reports do suggest that ERK1/2 activation is protective, little is known about how ERK1/2 signaling promotes protection. Akt is a serine/threonine protein kinase that exerts a wide variety of functions including the promotion of cell survival by regulating apoptosis within the cell (Cross *et al.*, 2000). This is evident in studies that have demonstrated a reduction in DOX-induced apoptosis via Akt activation (Chen *et al.*, 2012; Fukazawa *et al.*, 2003). Furthermore, the heart was protected against DOX-induced cardiomyopathy when constitutively active Akt was delivered to the heart through the use of an adenovirus (Taniyama & Walsh, 2002).

Considering that ghrelin administration protects the heart against IRI by maintaining cardiac function and ATP levels (Chang *et al.*, 2004a), ghrelin may exert its effects against DOX by activating the RISK pathway. In advanced glycation end product (AGE)-induced apoptosis of human umbilical vein endothelial cells, ERK1/2 and Akt/PKB phosphorylation are thought to be responsible for the anti-apoptotic effects of ghrelin, as indicated by reduced caspase-3 activation (Xiang *et al.*, 2011). When ERK1/2 and Akt inhibitors were employed, the effects of ghrelin were attenuated and the levels of caspase-3 increased. Similarly, ghrelin prevented apoptotic cell death in serum-starved osteoblasts through ERK1/2 and Akt/PKB activation (Liang *et al.*, 2013). Western blot analysis also showed that the activation of ERK1/2 and Akt/PKB by ghrelin occurred in a time- and dose-dependent manner in serum-starved pancreatic cells (Zhang *et al.*, 2007). In the presence of inhibitors, however, the

cytoprotective effects of ghrelin were abolished, indicating that ghrelin inhibits cell death by activating these pro-survival kinases. Literature on the effects of ghrelin on ERK1/2 and Akt/PKB expression in the context of chronic DOX-induced cardiotoxicity is limited (Baldanzi *et al*., 2002; Pei *et al*., 2014; Kui *et al*., 2009). While it is known that DOX reduces pro-survival activation (Das *et al*., 2011; Xiang *et al*., 2009; Lou *et al*., 2005), others have shown that ghrelin reverses these effects in acute models of cardiotoxicity (Pei *et al*., 2014; Mousseaux *et al*., 2006). However, the fact that endogenous ghrelin is increased during the progression of DOX-induced heart failure (Xu *et al*., 2007) suggests that ghrelin contributes to a protective, compensatory mechanism by exerting anti-apoptotic and antioxidative effects to maintain cardiac morphology and function.

The signaling pathways involved in ghrelin-mediated ERK1/2 activation are still unclear, however, the signaling events can be classified into various pathways including **i)** the Ras-dependent activation of ERK1/2 via receptor tyrosine kinases (RTKs), **ii)** the Ras-independent ERK1/2 activation via the protein kinase C (PKC) family that converges with the RTK signaling at the Raf level and **iii)** the modulation of ERK1/2 activation via the cAMP/protein kinase A (PKA) pathway. Binding of ghrelin to the GHSR-1α has also been shown to transactivate the tyrosine kinase receptor via the β and γ subunits, leading to activation of ERK1/2 via the Ras–Raf–MEK pathway (Nanzer *et al*., 2004). IP_3 and DAG result from the hydrolysis of PIP_2 by PLC. While IP_3 induces Ca^{2+} release from the endoplasmic reticulum, DAG activates PKC (Lopez *et al*., 2001), shown to be critical for ERK1/2 activation during ghrelin treatment (Mousseaux *et al*., 2006). Through the α-subunit of the GHSR-1α, ghrelin induces the activation of the PLC-PKC-Raf-MEK pathway, thereby mediating ERK1/2 activation. Finally, ghrelin and des-acylated ghrelin have been shown to exert their effects through stimulation of cyclic adenosine monophosphate (cAMP)/ protein kinase A (PKA) pathway (Rossi *et al*., 2009; Granata *et al*., 2007). cAMP is an important second messenger which, together with PKA exerts a wide variety of functions (Insel *et al*., 2012). PKA indirectly activates Ras, subsequently activating the Raf-MEK-ERK1/2 cascade (Bos, 2003). As mentioned previously, ghrelin induces the activation of PIP_2 after binding to its receptor. PIP_2 is not only involved in the hydrolysis reaction of the PLC pathway, but also acts as a substrate for the synthesis of phosphatidylinositol 3,4,5-trisphosphate (PIP_3). The catalytic domain of phosphoinositide-3-kinase (PI3K) converts PIP_2 to PIP_3 (Hemmings & Restuccia, 2012). Akt then binds to PIP_3, allowing phosphoinositide-dependent protein kinase

(PDK1) to phosphorylate Akt on threonine 308, inducing partial activation. Phosphorylation of Akt at serine 473 is required for full activation (Alessi *et al.*, 1997). It is highly possible that ghrelin may activate AKT/PKB directly, via an unknown receptor, since Baldanzi *et al.*, (2002) illustrated AKT activation in H9c2 cells which lack GHSR-1α (Figure 1.9). The anti-apoptotic downstream events of these pro-survival kinases include inhibiting the release of cytochrome c from the mitochondria and inhibiting the activation of caspases (Zhou *et al.*, 2000; Xia *et al.*, 2016).
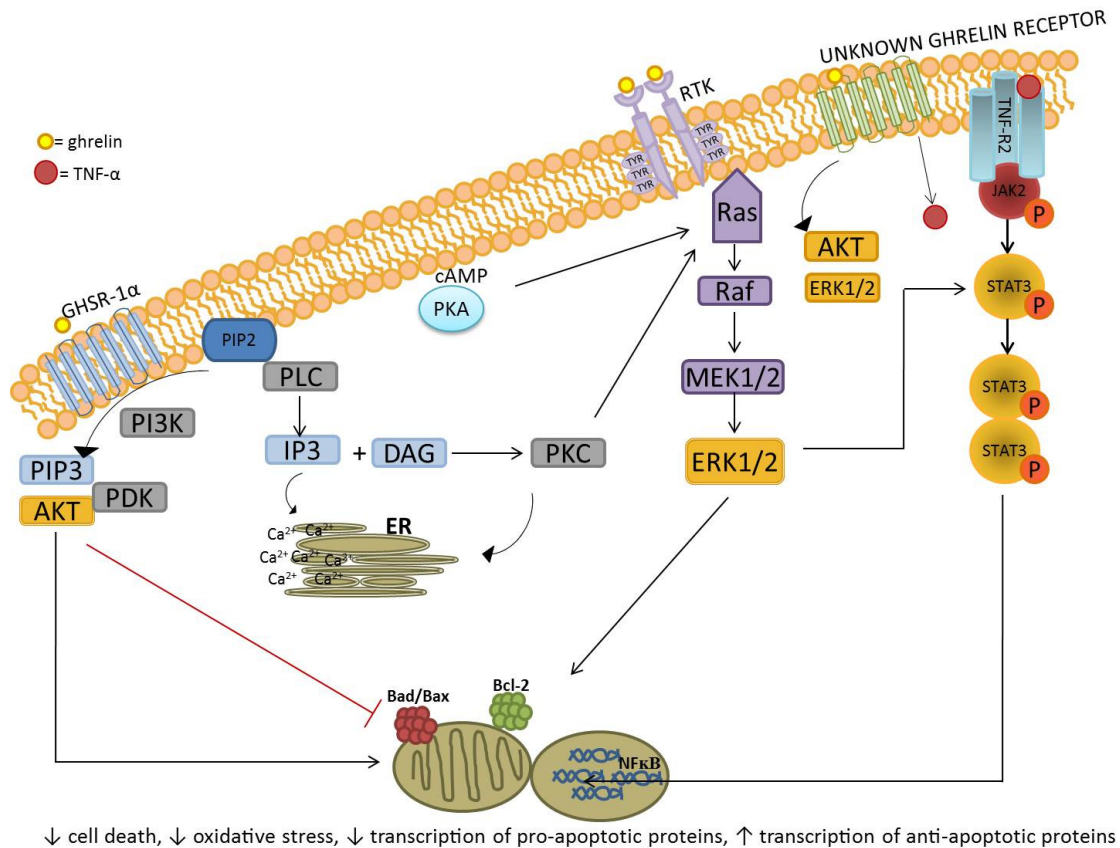
Figure 1.9: The potential signaling pathways induced by ghrelin.

Ghrelin (yellow circles) binds to its receptor (GHSR-1α), inducing the hydrolysis of PIP_2 to IP_3 and DAG. Cytosolic Ca^{2+} increases, resulting in growth hormone release. PIP_2 is also converted into PIP_3, activating Akt. DAG activates PKC which stimulates the Ras-Raf-MEK-ERK1/2 cascade, also activated by PKA. Ghrelin can also activate ERK1/2 and Akt via an unknown receptor. The SAFE pathway (JAK2/STAT3) could potentially be activated through PI3K, ERK1/2 or TNF-α. All of these pathways ultimately reduce cell death and oxidative stress. GHSR-1α, growth hormone secretagogue receptor 1 alpha; PIP_2, Phosphatidylinositol 4,5-bisphosphate; IP_3, Inositol trisphosphate; DAG, diacyl glycerol; Ca^{2+}, calcium; PIP_3, Phosphatidylinositol (3,4,5)-trisphosphate; PKC, protein kinase C; PKA, protein kinase A; JAK2, janus kinase 2; STAT3, signal transducer and activator of transcription 3; TNF-α, tumor necrosis factor alpha; ER, endoplasmic reticulum; PI3K, Phosphatidylinositol-4,5-bisphosphate 3-kinase; PDK, pyruvate dehydrogenase kinase; RTK, receptor tyrosine kinase.

1.9 Can ghrelin keep the heart 'SAFE'?

In addition to the RISK pathway, pre- and post-conditioning activate another intrinsic pro-survival pathway known as the survivor activating factor enhancement (SAFE) pathway (Lecour, 2009b, 2009a). This pathway is activated when a ligand such as interleukin-6 (IL-6) or tumor necrosis factor (TNF-α) binds to and induces dimerization of the receptor, activating various Janus kinases (JAKs) (Figure 1.9). JAKs induce phosphorylation of the receptor, thereby creating docking sites for signal transducer and activator of transcription proteins (STATs). STATs are phosphorylated on tyrosine 705 by the activated JAKs, where after they dimerize and then translocate to the nucleus to upregulate the transcription of various genes (Boengler *et al*., 2008). Phosphorylation on a specific serine residue (serine 727) enhances the transcriptional activity of STAT. Whilst several JAKs and STATs have been identified in the heart (see Kiu & Nicholson, (2012) for review), it is JAK2 and STAT3 that are specifically involved in the SAFE pathway (Lecour, 2009a). This pathway, and the subsequent cellular protection that it offers, is activated by TNF-α (Lacerda *et al*., 2009). TNF-α is a pro-inflammatory cytokine that is mainly produced by macrophages (Bradley, 2008; Chu, 2013), however, TNF-α and the tumor necrosis factor receptors 1 and 2 (TNFR1 and TNFR2) have been identified in virtually all cell types (Vandenabeele *et al*., 1995).

The role of this cytokine is complex and multifunctional, since TNF-α can exert both protective and harmful effects depending on the context of its activation (Monden *et al*., 2007). TNF-α is involved in apoptotic cell death through the death receptor pathway (Gustafsson *et al*., 2003). The death receptors in this pathway form part of the TNF-α superfamily which, upon ligand binding, activate the apoptotic machinery of the cell. Subsequent to this, the TNFR-associated death domain (TRADD) adaptor protein is recruited which leads to the activation of caspase-8 (Hsu *et al*., 1995). Caspase-8 then activates the downstream caspases, ultimately resulting in cell death. Neither TNF-α protein nor mRNA appear to be expressed in the heart under normal conditions, however, both are expressed in the failing human heart (Torre-Amione *et al*., 1996) and have therefore been implicated in the pathophysiology of this disease. Evidently, TNF-α is upregulated in patients with CHF, particularly in those with cardiac cachexia (Nagaya *et al*., 2001b). Ghrelin has been shown to exert anti-inflammatory effects *in vivo* and *in vitro* by suppressing the production of pro-inflammatory cytokines (Eter *et al*., 2007; Dixit *et al*., 2004; Huang *et al*., 2009; Li *et al*., 2013). Even at very low concentrations of ghrelin, both basal and TNF-α-induced IL-8

- 26 -

production is inhibited (Li *et al*., 2004). Furthermore, ghrelin administration reduces both the production and mRNA of several pro-inflammatory cytokines including TNF-α and IL-6. Ghrelin also inhibits nuclear factor κB (NFκB) activation (Waseem *et al*., 2008), a transcriptional regulator of pro-inflammatory cytokine gene expression, suggesting that ghrelin plays an important role in the transcriptional regulation of pro-inflammatory cytokine production. Since many cardiovascular diseases, including cardiotoxicity (Teng *et al*., 2010), are accompanied by an amplified inflammatory response, ghrelin may promote cardioprotection through its anti-inflammatory actions.

Whilst high levels of TNF-α are toxic to the heart (Kubota *et al*., 1997), low levels may actually protect cardiomyocytes from subsequent exposure to IRI, a form of preconditioning by TNF-α (Lecour *et al*., 2002). It was demonstrated that post-conditioning failed to protect against IRI in the hearts of TNF-α knock-out mice. Similarly, low, non-toxic levels of TNF-α have been shown to precondition cardiomyocytes against toxicity from higher concentrations of TNF-α (Cacciapaglia *et al*., 2014). These studies indicate that TNF-α can exert protective effects that are concentration dependent. In the context of DOX-induced cardiotoxicity, heart failure may be worsened when myocardial TNF-α is down regulated (Lou *et al*., 2004). Several efforts have been made to "neutralize" TNF-α in patients with heart failure, however, heart failure was worsened with anti-TNF therapy and resulted in a time- and dose-dependent increase in hospitalization and death (Mann, 2002). Since TNFR1 and TNFR2 exert opposing effects (Hamid *et al*., 2009), knocking out TNF-α not only abolishes the detrimental effects, but also the beneficial effects. It appears that endogenous TNF-α may protect against DOX-induced cytotoxicity by up-regulating mitochondrial/manganese SOD (MnSOD) (Watanabe *et al*., 1996). Xu *et al*., (2008) observed a time- and dose-dependent decrease in TNF-α production after DOX treatment, however, ghrelin reversed this observation. Although TNF-α is generally considered to be a harmful cytokine, it is also known to exert anti-apoptotic and antioxidative effects through NFκB (Xu *et al*., 2008). By activating NFκB, TNF-α induces many anti-apoptotic genes such as cellular inhibitor of apoptosis protein (cIAP1), Bcl-2 and MnSOD that strongly oppose its pro-apoptotic potential. The protective effects of ghrelin may therefore be dependent on the upregulation of anti-apoptotic and antioxidative molecules by TNF-α. Like most interventions, TNF-α may appears to exert different effects depending on the species and type of cell studied, it's concentration and the nature of its stimulus. The effects of ghrelin on TNF-α production by cardiomyocytes therefore requires further

investigation. Moreover, whether ghrelin administration leads to TNF-α-induced activation of the SAFE pathway warrants additional research.

There is over-whelming evidence to suggest that STAT3 activation is beneficial to the heart (Negoro *et al*., 2000). During acute myocardial infarction *in vivo*, treatment with a JAK2 inhibitor reduced the phosphorylation of STAT3 and induced a significant increase in the expression of caspase-3 and Bax, suggesting that this pathway plays a pivotal role in cardioprotection. In addition, infarct size is greater in STAT3 knock-out mice (Hilfiker-Kleiner *et al*., 2004) or when STAT3 is pharmacologically inhibited using AG-490 (Suleman *et al*., 2008; Hattori *et al*., 2001). In the context of DOX-induced cytotoxicity, DNA fragmentation was substantially increased in anti-STAT3 small interfering RNA (siRNA) transfected cells (Frias *et al*., 2008). Mice with cardiac-specific over-expression of STAT3 exhibit better survival rates and a reduced inhibition of contractile genes after DOX treatment (Kunisada *et al*., 2000), whereas mice with cardiac-specific knock-out of STAT3 are more susceptible to DOX-induced injury and the development of heart failure (Jacoby *et al*., 2003). Considering that STAT3 activation is critical for the cardioprotection offered by pre- and post-conditioning (Hattori *et al*., 2001), stimulating STAT3 activity is likely to be beneficial during DOX treatment.

Although ghrelin has not been shown to be involved in JAK2/STAT3 signaling in the heart after DOX treatment specifically, ghrelin has been shown to induce the phosphorylation of STAT3 in rat hippocampal neural stem cells (NSCs) (Chung *et al*., 2013). Ghrelin was also shown to up-regulate TNF-α (Xu *et al*., 2008), a known SAFE pathway activator (Lacerda *et al*., 2009), and may activate JAK2 and STAT3 via this mechanism. While ghrelin has not yet been shown to activate the SAFE pathway after DOX treatment, the crosstalk between the RISK and SAFE pathway may still allow for the activation of the SAFE pathway. There is a large body of evidence that suggests the existence of crosstalk between these two pathways. This is demonstrated by the ability of the p85 regulatory subunit of PI3K to promote STAT3 phosphorylation (Pfeffer *et al*., 1997; Suleman *et al*., 2008) and by the fact that JAK2 can phosphorylate Akt after binding to PI3K (Nguyen *et al*., 2001). Chung *et al*., (1997) also reported that ERK1/2 is responsible for the serine 727 phosphorylation of STAT3 which enhances the transcriptional activity of STAT3. Ghrelin therefore has the potential to activate the SAFE pathway through crosstalk between the SAFE and RISK pathways however, whether this occurs in the context of cardiotoxicity remains to be elucidated.

1.10 Conclusion

Despite decades of research and the development of over 200 analogs, DOX remains an integral part of chemotherapeutic regimes. Consequently, cardiotoxicity is still a pressing issue for cancer survivors. Mitochondrial dysfunction, oxidative stress, inflammation and apoptotic cell death have all been shown to play a role in the pathogenesis of DOX-induced cardiotoxicity. The consequences of these processes are cardiac cachexia, myocardial fibrosis and reduced cardiac function and contractility. It is therefore crucial to assess the mechanisms of DOX-induced cardiotoxicity and identify potential preventative strategies. Further research into the effects of ghrelin during DOX treatment will broaden our understanding of its beneficial effects. To date, the therapeutic role of ghrelin in *chronic* DOX-induced cardiotoxicity has not been demonstrated *in vivo*. Exogenous administration of ghrelin may serve as a novel therapeutic strategy for DOX-induced cardiotoxicity, as it has a broad spectrum of functions. From drug-induced heart damage and myocardial infarction, to pathological states in several other organs, it is clear that ghrelin exerts beneficial effects such as antioxidative, anti-apoptotic and anti-inflammatory activity, in every scenario. Simply put, ghrelin appears to exhibit significant cytoprotective activity regardless of the model studied, and is therefore an extremely promising peptide that is worth exploring. Indeed, the mechanisms and effects of ghrelin during chronic DOX-induced cardiotoxicity remain undefined at present as studies on this topic are limited. Since ghrelin is a naturally produced, endogenous hormone, it also has advantages over other medications that usually prove to be toxic. This therefore highlights the huge therapeutic potential that ghrelin possesses and warrants further research for its use as a cardioprotective agent for DOX-induced cardiotoxicity.

Considering the complex and life-threatening nature of cardiotoxicity, it is important to carefully study the molecular mechanisms of this condition, as well as to identify novel therapeutic interventions that are unlike the currently utilized strategies. Although cell culture is simple to perform, it does not accurately simulate the effects that are observed in human patients, and it is therefore necessary to establish clinically relevant pre-clinical animal models. However, many of the studies performed to date have employed supraphysiological concentrations of DOX or have only assessed the effects of acute cardiotoxicity, and therefore the results of such studies should be interpreted with caution. According to Herman

and Ferrans (1998), the use of smaller cumulative doses of DOX in animals adequately simulates the chronic myocardial changes that are observed in patients. Typically, the cumulative dose cited by these authors is 15 mg/kg for rats, which should be administered over a couple of weeks. The two main role players in the development of DOX-induced cardiotoxicity are believed to be oxidative stress and apoptotic cell death. Ghrelin is an endogenous peptide more commonly known for its growth-hormone-releasing and appetite-inducing effects, however, ghrelin has also been reported to possess cardioprotective abilities. This has been attributed to its anti-apoptotic, anti-fibrotic and antioxidative effects. DOX has the potential to increase survival rates and improve the quality of life of cancer patients, however, its cardiotoxic side effects drastically affect these parameters. Since the exact mechanisms that cause this condition still remain largely undefined, this study intended to elucidate the activity of the SAFE and RISK pathways *in vivo,* as they have been demonstrated to be cardioprotective in other forms of cardiovascular injury. In addition, the cardioprotective effects of ghrelin will be investigated in this scenario as a potential cardioprotective agent.

Therefore it was hypothesized that the SAFE and RISK pathways would be down-regulated after treatment with DOX and that stimulation of these pathways by ghrelin will confer protection to the heart. We have established an *in* vivo rat model of chronic cardiotoxicity which utilizes doses of DOX that are within the clinically relevant range, thus adding to the novelty of this study. This study aimed to:

i) establish a chronic *in vivo* model of DOX-induced cardiotoxicity
ii) assess the protein expression of the RISK and SAFE pathways
iii) identify the extent of DOX-induced myocardial damage with or without ghrelin treatment
iv) investigate the effects of ghrelin treatment on myocardial fibrosis, apoptosis and oxidative stress.

Chapter 2

Materials and methods

2.1 Ethical Considerations and Animal Care

All experiments were ethically approved and carried out according to the guidelines for the care and use of laboratory animals implemented at Stellenbosch University (reference number: SU-ACUD15-00038) and conformed to the accepted standards for the use of animals in research and teaching as reflected in the South African National Standards 10386: 2008. Male Sprague-Dawley rats were obtained at four weeks old (90 – 130 g) and were allowed one week to acclimatize to the animal facility. Since chronic cardiotoxicity is most commonly observed in the survivors of childhood cancers decades after their treatment is complete, this study was performed on rats that were at an equivalent age to late childhood in humans so that early adulthood was reached by the end of the protocol (Sengupta, 2013). The rats were housed in sterilized cages with controlled humidity and a 12-hour day/night cycle, at 25 °C. Standard rat chow and tap water were provided *ad libitum*.

2.2 Experimental protocol

As mentioned above, wild-type, male Sprague-Dawley rats were used in this study as they are a multipurpose rodent model and are one of the most widely used in animal research, including cardiology. Additionally, Sprague-Dawley rats are a commonly used strain in the study of DOX-induced cardiotoxicity (Taniyama & Walsh, 2002; Zhang *et al*., 2013; Teng *et al*., 2010) Finally, their docile disposition makes them calm and easy to handle. Male rats were used in order to limit the influence of hormonal status on the development of cardiotoxicity, as female rats are believed to be protected by the presence of estrogen (Moulin *et al*., 2015).

After one week of acclimatization and handling, animals were randomly divided into control (n = 7), vehicle (n = 7), ghrelin (n = 7), DOX (n = 9) and DOX + ghrelin (n = 9) groups. The ghrelin group received three injections of 100 µg/kg ghrelin (LKT Laboratories, G2869) per week, for eight weeks (rat ghrelin of 95% purity). This dosage is based on several other studies (Yang et al., 2014; Huang et al., 2009; Li et al., 2006b; Nagaya et al., 2001c), however, we only administered one injection per day, as opposed to two, to minimize animal

suffering. The DOX-treated group received 2.5 mg/kg DOX (LKT Laboratories, D5794) per week for eight weeks (Xiang et al., 2009), resulting in a cumulative dose of 20 mg/kg. This dose of DOX falls within the range of 60 - 75 mg/m^2 that is administered to humans (human equivalent dose) (Von Hoff *et al*., 1979; Desai *et al*., 2013). Animals in the DOX + ghrelin group were administered three injections of ghrelin in addition to a single injection of DOX per week for eight weeks. Vehicle-control animals received an equal volume of physiological phosphate buffered saline four times per week (to account for the maximum number of injections experienced) for eight weeks. All injections were administered via the intraperitoneal (i.p) route using a 25 gauge needle (Lasec, HLSCDN-25, Cape Town, South Africa). Control animals remained untreated for the duration of the treatment protocol. Body weight was recorded each morning prior to preparing the injections, and food consumption was measured three times per week. Food intake was measured by weighing out 500g of food per cage and then re-weighing what was not consumed. The difference between the food given and the food consumed was the amount of food consumed per cage. This was divided by the number of rats in each cage to determine the average amount of food consumed per rat. No rats died during the experimental protocol.

2.3 Working heart perfusions

One week after the last injection of DOX, the animals were euthanized one at a time and at random, using an i.p injection of 60 mg/kg sodium pentobarbitone (Euthapent, Kyron Laboratories, 130540). When the pedal reflex was no longer observed, the heart was rapidly excised by making an incision in the skin at the xyphisternum, which was extended to the lateral ends of the left and right costal margins. An incision was made through the ribs at the left and right axillary lines to create a thoracotomy (Figure 2.1). The chest wall was deflected upwards, after which the heart was removed and arrested in ice cold Krebs-Henseleit buffer (KHB: 119 mM NaCl, 24.8 mM NaHCO$_3$, 4.72 mM KCl, 1.19 mM KH$_2$PO$_4$, 0.6 mM MgSO$_4$.7H$_2$O, 0.59 mM Na$_2$SO$_4$, 2.39 mM CaCl$_2$.2H$_2$0 and 10 mM glucose). The heart was then transferred to a working heart perfusion apparatus where the aorta was cannulated, followed by retrograde perfusion of the heart with KHB equilibrated with 95% O$_2$ and 5% CO$_2$ at a perfusion pressure of 100 cm KHB. The temperature of both the perfusate and the air surrounding the heart was maintained at 37 °C. After retrograde perfusion was initiated, the pulmonary vein was cannulated, providing an opening to the left atrium. After a

stabilization period of ten minutes in the retrograde perfusion mode, the heart was switched to the working heart mode, during which the heart rate, systolic and diastolic blood pressure, aortic output and coronary flow was recorded every five minutes for 40 minutes. This protocol was based on a previously established perfusion protocol by Wergeland *et al.*, (2011). Blood pressure was measured by connecting a pressure transducer as a side branch of the aortic cannula. The transducer converts the movement of fluid across a membrane into an electric signal which is mathematically converted back to pressure using Powerlab and LabChart 5 software. Left ventricular developed pressure (LVDP) was obtained by calculating the difference between diastolic pressure and systolic pressure (systolic pressure – diastolic pressure). The rate-pressure product (RPP) was calculated by multiplying the heart rate with systolic pressure and cardiac output was calculated as the sum of the aortic output and the coronary flow. The final parameter that was measured with regards to the functional data was the total work performed by the myocardium. The total work performed by the heart can be determined using a formula by Kannengiesser et al., (1979), where the mean external power produced by the left ventricle (mWatts) is:

$$0.002222 \left(\text{Aortic Pressure} - \left((11.25)[\text{Cardiac Output}] \right) \right).$$

At the end of the perfusion protocol, the hearts were weighed, photographed and then cut into two transverse sections, from apex to base, ensuring that each half contained both atria and ventricles. One half was snap frozen in liquid nitrogen for biochemical analysis and the other half was preserved in formalin for histological analysis. Tissue samples in the liquid nitrogen were transferred into cryoboxes and stored at – 80 °C until needed.
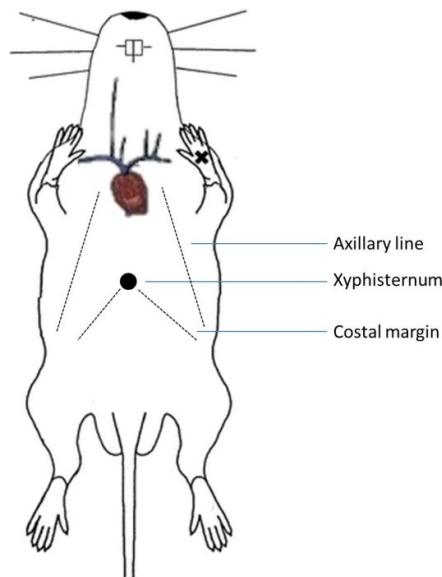
Figure 2.1: Diagram to illustrate the isolation of a rat's heart.

2.4 Blood collection

Simultaneous to the excision of the heart, blood was collected from the thoracic cavity using a 10 mL syringe and quickly placed into serum separation (Lasec, VGRV450470R, Cape Town, South Africa) and plasma (Lasec, VGRV450474R, Cape Town, South Africa) tubes. The tubes were inverted five times and then allowed to stand for ten minutes on ice. The tubes were centrifuged at 4000 RPM (1.4 x g) for ten minutes at 4 °C. After centrifugation, the serum and plasma was aliquoted into microfuge tubes at 200 µL volumes and frozen at –80 °C until further analysis.

2.4.1 Blood analysis

Serum samples from each rat were tested for various analytes using Milliplex® MAP Multiplex assays. TNF-α, ghrelin and IL-6 were measured using a rat metabolic hormone magnetic bead panel (Merck Millipore, RMHMAG-84K). cTnT, cTnI and CK-MB were measured using a rat cardiac injury magnetic bead panel (Merck Millipore, RCI1MAG-87K-03). The assay is based on the Luminex $_X$MAP® technology that makes use of fluorescent-coded magnetic beads known as MagPlex®-C microspheres. The microspheres are internally color-coded with fluorescent dyes and coated with specific capture antibodies. After an analyte in the test sample is captured by the beads, a biotinylated detection antibody is added. Streptavidin-Phycoerythrin conjugate, the reporter molecule, is used to complete the reaction.

Each microsphere is identified using the Bio-Plex® MAGPIX™ Multiplex reader (Bio-Rad, MAGPX13046706, California, USA) and the result of the bioassay on each microsphere is quantified using a fluorescent signal. The assays were carried our according to the manufacturer's instructions. Please refer to Appendix D, pages 150 and 154 for the full protocols.

2.5 Brain natriuretic peptide (BNP)

In addition to the cardiac markers of damage that were measured in the serum, B-type natriuretic peptide (BNP) was measured in heart tissue homogenates. BNP is a cardiac hormone that is released by the myocardium in response to increased filling pressure of the left ventricle during left ventricular dysfunction. BNP levels are increased even when the symptoms of heart failure are not yet apparent, and they increase even further in direct proportion to the severity of heart failure. High levels of BNP correlate with the left ventricular dysfunction associated with chemotherapy and are therefore a useful marker in assessing heart failure (Bovelli *et al*., 2010) .

The BNP 45 ELISA (Abcam, ab108816, Biocom Biotech, Pretoria) is designed for the quantitative measurement of BNP 45 in tissue extracts. Standards and test samples bind to a BNP 45 specific antibody that is pre-coated onto a 96-well plate. After the addition of a biotinylated detection antibody and a Streptavidin-Peroxidase conjugate, 3,3′,5,5′-Tetramethylbenzidine (TMB) was added to visualize the enzymatic reaction using the EL800 Universal Microplate reader (Bio-Tek Instruments Inc., Vermont, USA). The intensity of the color produced is directly proportional to the amount of BNP 45 in the samples. The concentration of BNP in each sample was normalized to the total protein concentration of each sample as determined using the Direct Detect™ system (Merck Millipore, DDHW00010-WW, Darmstadt, Germany). This system measures the absorbance of amide bonds in protein chains using infrared quantitation. Briefly, 2 µl of blank (assay buffer) and 2 µl of samples were pipetted onto the windows of the Direct Detect™ card. The card was then placed vertically inside the sampling accessory, which dries and then measures each sample as mg/mL of protein.

2.6 Histological analysis

2.6.1 Tissue processing and sectioning

Isolated cardiac tissue samples were fixed in 4% formaldehyde solution (Merck Millipore, 1.00496.5000) for a minimum of seven days. After processing through a series of dehydration steps in a tissue processor (Tissue Tek II, 4634, Sakura Finetechnical Co., Ltd, Japan), the tissue was infiltrated with Paraplast® wax (Sigma-Aldrich, A6330-4LB, Johannesburg, South Africa). Once embedded on a cassette (Lasec, PLPS191023, Cape Town, South Africa) using a tissue embedding centre (Leica EG 1160, Leica Biosystems, Germany), 5 µm thick sections were prepared using a microtome (Leica RM 2125RT, Leica Biosystems, Germany). Heart sections were placed onto glass microscope slides (Lasec, GLAS4S22M3000F, Cape Town, South Africa) and allowed to air-dry and adhere on a 20 °C heating block.

2.6.2 Hematoxylin & Eosin Staining

In order to view the overall cardiac structure and identify signs of damage, the hematoxylin & eosin (H&E) staining technique was employed. Over 100 years later, this stain is still one of the most frequently used in laboratories worldwide (Cook, 1997). H&E is based on the principle whereby cationic/basic hematoxylin binds to and stains all anionic DNA and RNA molecules blue, and is primarily employed to demonstrate nuclei. Eosin, an anionic/acidic dye, has an affinity for positively charged cytoplasmic constituents such as filaments, membranes and mitochondria and counterstains them in various shades of pink (Young *et al*., 2006; Kingsbury & Johannsen, 1935; Titford, 2009).

Prior to staining, the Mayer's Hematoxylin solution (Merck Millipore, SAAR2822001LC, Modderfontein, South Africa) was filtered, and the eosin solution (Leica Biosystems, 3801600E) was freshly prepared. The H&E staining procedure was performed using an automated staining machine (Leica ST5010 Autostainer XL, Leica Biosystems, Germany). For this stain, 5μm sections of heart were prepared as described in section 2.6.1. The slides were placed briefly into a 60 °C oven to allow the wax surrounding the tissue sections to melt. The slides were then submerged into freshly prepared reagents as indicated in the protocol found in Appendix D, page 159.

After staining, the slides were mounted using DPX mountant (Associated Chemical Enterprises, D0738NN00500) and covered with a cover slip (Lasec, GLAS2C29M2250REC, Cape Town, South Africa). The slides were left to dry thoroughly overnight. To measure the cross-sectional area of the myofibres in each section, the slides were viewed on a bright-field Nikon ECLIPSE E400 microscope fitted with a Nikon DS-Fi2 camera, and processed using a Nikon Digital Sight DS-U3 processor (Nikon®, Japan). Image processing was performed using NIS elements v4.10 software. Images were captured at 4x magnification from five randomly selected regions of interest (ROIs) in the left ventricle (Figure 2.2). Using ImageJ v1.6.0 software (Schneider *et al*., 2012), the cross-sectional area of 30 myofibres was measured in each of the five ROIs, giving a total of 150 myofibres per heart section (Gilliam *et al*., 2009; Monden *et al*., 2007). This analysis was not performed blinded.
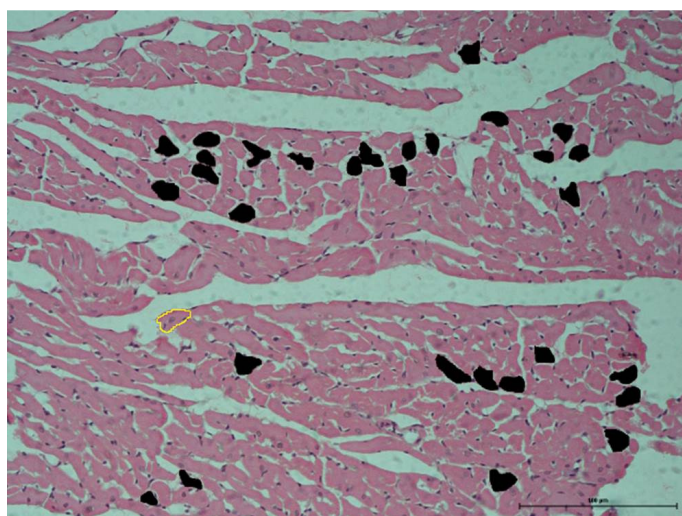
Figure 2.2: Example of the measurement of cross-sectional area in a ROI.
The border of 30 randomly selected myofibers was traced (yellow circle). Once the cross-sectional area was generated, the myofiber area was filled with a solid color to avoid duplicate measurements. This process was repeated in all five ROIs, resulting in a total of 150 myofibers measured per section. Abbreviation: ROI, region of interest.

2.6.3 Masson's Trichrome Stain

The Masson's staining technique is a 'connective tissue technique' as it is employed to demonstrate collagen deposition. As the name suggests, this stain produces three colors including black/blue-stained nuclei, green- or blue-stained collagen and red-stained cytoplasm and muscle (Young *et al*., 2006; Titford, 2009). This stain was employed for the

histological visualization of fibrosis in myocardial sections. Skin samples were used as positive control slides.

For the Masson's Trichrome stain, positively charged Histobond microscope slides were utilized (Lasec, GLAS2S13M0810401, Cape Town, South Africa). 5μm sections of heart tissue were again prepared, which were then deparaffinized and rinsed in distilled water. After incubation in hematoxylin, the slides were placed into ordinary tap water to 'blue' the sections, and then rinsed in distilled water. The slides were then stained in fuchsin Ponceau-orange G, where after they were rinsed in acetic acid water (Radchem, 600113, Illinois, USA). The slides were flushed in 5% phosphotungtic acid (Merck Millipore, 100582, Modderfontein, South Africa) solution (the mordant) and then rinsed in acetic acid water to differentiate the color tones. After staining in Light Green solution (Sigma-Aldrich, L1886, Johannesburg, South Africa), the slides were again washed in acetic acid solution. The slides were dehydrated through a series of alcohols, cleared in xylene (Merck Millipore, 1086619190, Modderfontein, South Africa) and then mounted. The same microscope and software as indicated in section 2.6.2 was used to acquire and process the images obtained. Several images of the tissue were captured at 4x magnification and stitched together to create an image of the entire section. The acquired images were analysed using ImageJ software and brightened to make each color stand out. Color thresholding was used to select the entire heart, for which a measurement was given in pixels (Figure 2.3A). The threshold slider was then adjusted to only select the red-stained myocardium and exclude the blue-stained connective tissue (Figure 2.3B). A measurement in pixels was again generated, which was subtracted from the pixel measurement of the entire heart, to give the pixels of only the blue-stained area. The blue-stained area (fibrosis) was then expressed as a percentage of the area of the entire section. Considering that this method of quantification is very subjective, a blind analysis was also performed by an independent researcher. A full protocol for this stain can be found in Appendix D, page 161.
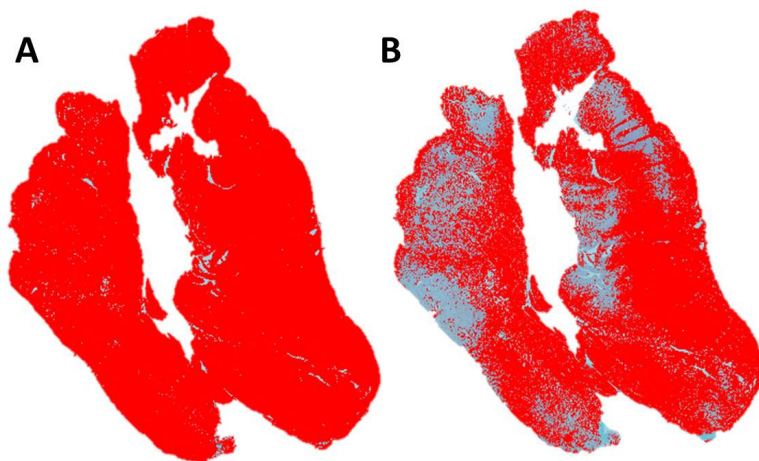
Figure 2.3: Color thresholding to measure fibrosis in histological samples.

Color thresholding was performed in order to measure the pixels of the entire heart (A) and the pixels of the red-stained myocardium (B) so that the amount of blue-stained fibrosis could be calculated. Magnification: 4x

2.6.4 Immunohistochemistry (IHC)

For the immunohistochemical stains, positively charged Histobond slides were utilized (Lasec, GLAS2S13M0810401, Cape Town, South Africa) and 5μm sections of heart tissue were again prepared. These were then deparaffinized, rinsed in distilled water and the IHC staining protocol was carried out using the Bond-Max™ Autostainer (Leica Biosystems, Germany) and the Bond™ Polymer Refine Detection kit (Leica Biosystems, DS9800). This kit is an HRP-linked antibody conjugated system for the detection of tissue-bound IgG primary antibodies. Briefly, the slides were incubated in H_2O_2 to quench endogenous peroxidase activity, followed by incubation in 1: 100 cytochrome c primary antibody (Cell Signaling Technology, 11940). After secondary binding, the 3, 3'-diaminobenzidine tetrahydrochloride hydrate (DAB) chromogen enabled visualization via a brown precipitate. Hematoxylin was used as a counterstain to visualize nuclei. In order to control for the natural peroxidase activity in the heart, negative control slides were prepared by excluding the primary antibody. Due to the time-consuming and bias nature of the grading methods of analysis, the automated digital image analysis ImageJ plugin 'IHC Profiler' was used (Varghese *et al.*, 2014). In any digital image analysis software, the pixel intensity ranges from 0 to 255, where 0 represents the darkest shade of color and 255 represents the lightest shade of color. With the assistance of pathologists, color shades were manually graded and assigned a score [high positive (3+), positive (2+), low positive (1+) and negative (0)] that correlated

with the pixel intensity. The software then calculates how many pixels fall within each category; if 60% or more of the pixels fell into a specific grading category then the image was assigned to that category (Figure 2.4). This software therefore uses color deconvolution and computerized pixel profiling to assign an automated score to the image.

Pixel Count: 40868424

Percentage contribution of High Positive: 88.9749

Percentage contribution of Positive: 0.7811

Percentage contribution of Low Positive: 2.3084

Percentage contribution of Negative: 7.9357

The score is High Positive

Figure 2.4: Pixel intensity is graded into one of four categories.
The final score is assigned to the category that contains 60% or more of the pixels.

2.7 Oxidative stress analysis

Oxidative stress is a physiological condition that arises when the balance between ROS and antioxidants is shifted. During low levels of oxidative stress, the antioxidants within a cell are able to compensate for any ROS production that may fluctuate above the norm, however, when ROS production becomes excessive, antioxidant defense mechanisms are unable to maintain the redox status of the cell, leading to DNA, protein and membrane damage (Doroshow, 1983). Three different assays were employed in this study in order to obtain a complete picture of the redox state within each treatment group. The oxygen radical absorbance capacity (ORAC) assay gives an indication of 'antioxidant power', the glutathione (GSH) assay assesses antioxidant status and the measurement conjugated dienes and thiobarbituric acid reactive substances (TBARS) are known as early and late markers of oxidative stress, respectively. The SOD activity assay gives an indication of which antioxidant may be responsible for any shifts observed in antioxidant capacity.

2.7.1 Sample preparation

For use in the ORAC, GSH, SOD and TBARS assays, tissue samples were thawed on ice, where after 100 mg of each sample was weighed out and placed into chilled microfuge tubes.

For every 100 mg of tissue, 1 mL of ice cold phosphate buffer (50 mM, pH 7.5) was added. The tissue was homogenized on ice for approximately ten seconds using a Polytron PT 2100 homogeniser (Kinematica AG, Switzerland). After homogenization, samples were sonicated at an amplitude of 10 Hz, for five to ten seconds using an Ultrasonic Liquid Processor (Misonix Incorporated, USA). The foam produced was first allowed to subside, where after the samples were centrifuged at 12 000 RPM (13.3 x g) for ten minutes at 4 °C. The supernatants were pipetted into new, chilled microfuge tubes and frozen at -80 °C until needed. To determine oxidized glutathione (GSSG) in the glutathione assay, 100 mg of each tissue was again weighed out, however for this assay 10 µL 1-methyl-2-vinyl-pyridium trifluoromethane sulfonate (M2VP) was added to the phosphate buffer prior to homogenization. The same homogenization, sonication and centrifugation steps were then followed, and the supernatant was stored at -80 °C until needed.

2.7.2 ORAC Assay (Antioxidant capacity)

To evaluate the capacity of intracellular antioxidants to overcome DOX-induced oxidative stress, and the potential ability of ghrelin to maintain or improve this capacity, the ORAC assay was used, as previously described by Ou *et al.* (2001). The assay employs the fluorophore, 'fluorescein', as the target, which becomes oxidized after the addition of the peroxyl radical 2,2'-Azobis (2-methylpropionamidine) dihydrochloride (AAPH). Antioxidants present in the test samples will prevent the oxidation of the fluorophore until the antioxidant activity becomes depleted. The samples' antioxidant capacity correlates with the fluorescence decay curve, represented as the area under the curve (AUC). 'Trolox™' (Sigma-Aldrich, 238831, Johannesburg, South Africa), a water-soluble analog of Vitamin E, is used as the standard so that the antioxidant capacity of each sample can be expressed as µmol Trolox standard equivalents per gram of tissue analysed.

The Fluoroskan Ascent™ microplate fluorometer (Thermo Fisher Scientific, Massachusetts, U.S.A.), equipped with an incubator, was set at 37 °C. All samples were first centrifuged at 14 000 RPM (16.5 x g) for ten minutes to remove turbidity, followed by deproteinization using perchloric acid (0.5M) precipitation. A fluorescein stock solution (Sigma-Aldrich, F6377, Johannesburg, South Africa) was prepared in phosphate buffer and further diluted for use in the assay. Fluorescein, test samples and AAPH (Sigma-Aldrich, 440914, Johannesburg, South Africa) were added to each well of a black 96-well plate using a

multichannel pipette. The fluorescence was read immediately, every five minutes for two hours. Fluorescence filters with an excitation wavelength of 485 nm and emission wavelength of 538 nm were used. The final ORAC values were calculated using the regression equation $y = ax^2 + bx + c$ between the Trolox concentration (μM) and the area under the curve. Refer to Appendix D, page 168 for the full protocol.

2.7.3 Conjugated Dienes

To extract and purify myocardial lipids for conjugated diene determination, frozen heart tissue was homogenized in a 1: 2 solution of chloroform and methanol. The homogenate was then centrifuged at 10 000 RPM (9.2 x g) for ten minutes at 4 °C, revealing two layers. The bottom organic chloroform layer was transferred to a new microfuge tube and allowed to evaporate overnight at 4 °C. Cyclohexane was then added to each of the dried residues. Thereafter, the samples were transferred to the wells of a 96-well plate and the absorbance was determined spectrophotometrically at 234 nm using the Multiskan® Spectrum microplate spectrophotometer (Thermo Fisher Scientific, Massachusetts, USA). The concentration of conjugated dienes was determined using the following equation:

$$\frac{A_{234S} - A_{234B}}{\varepsilon}$$

Where A_{234S}: absorbance of the sample at 234 nm

A_{234B}: absorbance of the blank at 234 nm

ξ: extinction co-efficient of 2.95 x 10^4

2.7.4 TBARS Assay

It is well known that cell death can occur as a result of lipid peroxidation, since this process induces damage in both plants and animals. Malondialdehyde (MDA) is one if the end products of this process and thus the measurement of these natural bi-products is a commonly used method of assessing oxidative damage and the level of oxidative stress (Bernheim *et al.*, 1948). TBARS is a widely used assay for assessing lipid peroxidation since MDA forms a 1:2 adduct with TBA which can be measured colorimetrically. Test samples were added to 4 mM butylated hydroxytoluene (BHT) in order to prevent oxidation during processing. 0.2 M

ortho-phosphoric acid (Merck Millipore, 1.00573.2500, Modderfontein, South Africa) and 0.11 M TBA (Sigma-Aldrich, T5500, Johannesburg, South Africa) were then added, where after the reaction mixture was boiled at 90 °C for 45 minutes, followed by immediate cooling in an ice bath. Butanol and saturated salt were added to each sample to separate the phases, where after the top phase of the samples were transferred to a 96-well plate and the absorbance was measured at 532 nm in the Multiskan® Spectrum microplate spectrophotometer (Thermo Fisher Scientific, Massachusetts, USA). The MDA concentration of the samples was then calculated using an extinction coefficient of 1.56×10^5 M/cm. Refer to Appendix D, 169 for the full protocol.

2.7.5 GSH Assay (Antioxidant status)

The ratio of reduced (GSH) and oxidized (GSSG) glutathione was determined according to the method previously described by Asensi *et al.*, (1999). Samples for GSH were diluted 100x in GSH buffer, while samples for GSSG were diluted 50x in GSH buffer. In a clear, 96-well plate, the GSH standards (Sigma-Aldrich, G4251, Johannesburg, South Africa), 1U glutathione reductase (Sigma Aldrich, G3664, Johannesburg, South Africa), 0.3 mM DTNB (Sigma-Aldrich, D21820, Johannesburg, South Africa) and samples for GSH or samples treated with M2VP (Sigma-Aldrich, 69701, Johannesburg, South Africa) for GSSG, were incubated at 25 °C for five minutes. The reaction was then initiated with 1mM NADPH (Sigma-Aldrich, N6785, Johannesburg, South Africa) and measured at 412 nm for 5 minutes at 30 second intervals in a Multiskan® Spectrum microplate spectrophotometer (Thermo Fisher Scientific, Massachusetts, USA). The concentration of total glutathione, GSH and GSSG were determined using the GSH standard (Sigma-Aldrich, G4251, Johannesburg, South Africa). Refer to Appendix D, page 170 for the full protocol.

2.7.6 SOD Activity Assay

The SOD activity assay quantifies the auto-oxidation of 6-hydroxydopamine (6-HD). Prior to this assay, the protein concentration of each sample was determined using the Direct Detect™ system described in section 2.5. 1.6 mM 6-HD (Sigma-Aldrich, H8523, Johannesburg, South Africa) was prepared in distilled water containing perchloric acid (PCA), and 0.1 mM diethylenetriaminepentaacetic acid [(DETAPAC) Sigma-Aldrich, D6518, Johannesburg, South Africa] was prepared in 50 mM phosphate buffer (pH 7.4). The samples, 6-HD and DETAPAC were added to the wells of a 96-well plate, which was then read immediately at 490 nm for four minutes, at one minute intervals using the Multiskan® Spectrum microplate

spectrophotometer (Thermo Fisher Scientific, Massachusetts, USA). The activity of SOD was determined using an equation obtained from the standard curve, where one unit of SOD is defined as the amount of the enzyme that is needed to exhibit 50% dismutation of the superoxide radical. It should be noted, however, that this assay does not differentiate between the different types of SOD enzymes.

2.8 Caspase-Glo[®]

The Caspase-Glo® Assay (Promega, G8091, Wisconsin, USA) is a luminescent assay that measures caspase-3 and -7 activities. These caspases are members of the cysteine aspartic acid-specific protease family that play important roles in the execution of apoptotic cell death. The assay makes use of a proluminescent substrate which is cleaved by active caspases to yield aminoluciferin, a substrate of luciferase, and thus enabling the production of light. Heart tissue was homogenized using the Polytron PT 2100 homogeniser (Kinematica AG, Switzerland) and 100 µg protein of each sample was used. The Caspase-Glo[®] buffer was added to the Caspase-Glo[®] substrate (as per the manufacturer's instructions) to produce the Caspase-Glo[®] reagent. This was then added in equal volumes to the lysates (i.e. 100 µl tissue lysate and 100 µl Caspase-Glo[®] reagent). The plate was mixed by gentle agitation on a belly dancer, where after it was incubated at room temperature for one hour. After incubation, the luminescent signal was measured using the GloMax[®] 96 Microplate Luminometer (Promega, Wisconsin, USA) at an excitation wavelength of 490 nm and an emission wavelength of 510 – 570 nm.

2.9 Western blot analysis

2.9.1 Preparation of cell lysates

Snap-frozen heart tissue samples were pulverized into pieces in a chilled mortar and pestle. For protein isolation, small pieces of the crushed tissue were incubated in 450 μL modified radio-immunoprecipitation (RIPA) buffer (pH 7.4) containing 50 mM Tris-HCL, 150 mM NaCl, 1% NP40 (Sigma-Aldrich, 74385, Johannesburg, South Africa), 0.25% Na-deoxycholate (Sigma-Aldrich, D6750, Johannesburg, South Africa), 1 mM EDTA (Merck Millipore, SAAR2236020EM, Modderfontein, South Africa), 1 mM NaF (Merck Millipore, 1.93270.0500, Modderfontein, South Africa), 1 mM PMSF (Sigma-Aldrich, 94382, Johannesburg, South Africa), 1mM sodium orthovanadate (Sigma-Aldrich, S6508, Johannesburg, South Africa) and a protease inhibitor cocktail (cOmplete, 11873580001,

Sigma-Aldrich, Johannesburg, South Africa). Tissue was homogenized for ten seconds in chilled microfuge tubes on ice using a Polytron PT 2100 homogeniser (Kinematica AG, Switzerland). Once the foam had subsided, the lysates were centrifuged twice at 11 000 RPM (11.2 x g) at 4 °C for 15 minutes and the supernatant was transferred into new chilled microfuge tubes. Protein concentration was determined using the Direct Detect™ system as described in section 2.5. 50 µg protein samples were prepared in Laemmli's loading buffer, boiled at 95 °C for five minutes and stored at -80 °C until needed.

2.9.2 Sodium dodecyl sulfate-polyacrylamide gel electrophoresis

Samples prepared in Laemmli's buffer were thawed on ice and then boiled again at 95 °C for five minutes. 50 μg protein of each sample was separated by 12% TGX stain-free™ FastCast™ acrylamide gels (Bio-Rad, 1610183, California, USA) for ten minutes, at 100 V, 400 mA (constant), followed by 120 V for approximately 60 minutes. The stain-free gel was activated by placing the gel directly onto the Bio-Rad UV transilluminator plate (ChemiDoc™ XRS+ system) and selecting the 'gel activation' step in the Image Lab™ software (Version 5.2.1). After activation, the proteins were transferred onto polyvinylidene fluoride (PVDF) membranes (Trans-Blot® Turbo™ ready-to-assemble mini low fluorescent PVDF transfer kit, Bio-Rad, 1707274, California, USA) using the TransBlot® Turbo™ Transfer System (Bio-Rad, California, USA) for 12 minutes at 15 V. After transfer, the stain-free blot was imaged for use in total protein normalization. Membranes were then blocked for one hour at room temperature in 3% bovine serum albumin (BSA) (phosphorylated proteins) or 5% fat free milk (total proteins) dissolved in Tris buffered saline-Tween®20 Solution (TBS-T).

After blocking, the membranes were washed three times for five minutes in TBS-T and incubated overnight at 4 °C with gentle agitation in primary antibody (1:1000) solutions dissolved in 5% BSA-TBS-T. Subsequent to primary antibody incubation, the wash step was repeated and the membranes were incubated in HRP-linked anti-rabbit or anti-mouse secondary antibody dissolved in 5% fat free milk for one hour at room temperature. Membranes were washed with TBS-T (3 x 5 minutes) and incubated with Clarity™ ECL western blotting substrate (Bio-Rad, 1705061, California, USA). The bands were detected using the ChemiDoc™ XRS+ System with the Image Lab™ Software and discrepancies in loading were corrected for by using total protein normalization (Colella *et al*., 2012; Gilda & Gomes, 2013). For proteins with double bands, the band intensity was calculated as the sum

of the two bands. For proteins with both phosphorylated and total forms, the results were expressed as the ratio of the phosphorylated protein to the total protein.

Table 2: The antibodies utilized and their respective dilutions.

PRIMARY	Company	Catalogue Number	Primary antibody dilution	Secondary Antibody	Secondary antibody dilution
P-STAT3^{Ser727}	CST	9134	1 : 1000	7074	1 :10 000
P-STAT3^{Tyr} $_{705}$	CST	9131	1 : 1000	7074	1 : 2000
T-STAT3	CST	9139	1 : 1000	7076	1 :10 000
P-Akt	CST	9271	1 : 1000	7074	1 : 2000
T-Akt	CST	9272	1 : 1000	7074	1 :10 000
P-ERK1/2	CST	4370	1 : 1000	7074	1 :10 000
T-ERK1/2	CST	4695	1 : 1000	7074	1 :10 000
Cytochrome c	CST	11940	1 : 1000	7074	1 :10 000
SOD1	CST	2770	1 : 1000	7074	1 :10 000
SOD2	CST	13141	1 : 1000	7074	1 :10 000
Cleaved PARP	CST	5625	1: 1000	7074	1: 10 000

- Abbreviations: CST; Cell Signaling Technology

2.10 Statistical analysis

All values are presented as the mean ± standard error of the mean (SEM). A one-way or two-way analysis of variance (ANOVA) was used where appropriate and a Bonferroni *post hoc* analysis was then employed to test for significance. Significance was accepted when $p <$ 0.05.

Chapter 3

Results

3.1 Ghrelin promotes increased weight gain by stimulating appetite during DOX treatment

3.1.1 Body weight

The treatment protocol was initiated in week one and terminated at the end of the eighth week, as indicated by the black arrows in the figure below. One week after the last treatment, the rats were killed for further analyses (red arrow). After approximately four weeks of DOX treatment, subjective but clinical signs of heart failure became evident, including paw and tail cyanosis, inactivity, passive behaviour and boney frame. These observations were not apparent in the DOX+ghrelin group.

 DOX suppressed the growth rate from as early as week four of the treatment protocol (Figure 3.1), however, this effect only became significant in week eight ($205.97 \pm 33.03\%$, $p < 0.05$) and week nine ($204.89 \pm 32.76\%$, $p < 0.05$) when compared to the control in week eight (393.96 ± 100.72) and week nine (397.91 ± 99.23), respectively. The weight gain between the control rats and the vehicle rats was not statistically different, whereas the weight gain of the DOX group ($204.89 \pm 32.76\%$, $p < 0.05$) was significantly lower than that of the vehicle group ($385.55 \pm 103.82\%$) after nine weeks. Weight gain was maintained in the group that received both DOX and ghrelin, as the body weight of this group did not differ from the control and the percentage change in body weight continued to increase during treatment. While weight gain in this group was higher than the DOX alone group, the results obtained were not statistically different from one another.
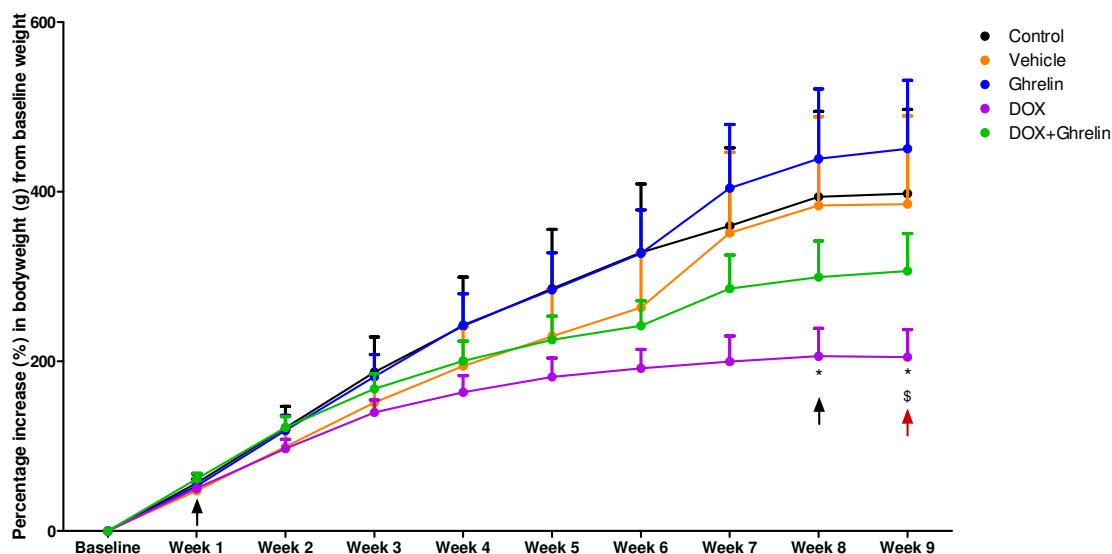
Figure 3.1: The percentage change in body weight during the treatment protocol.
Body weight was recorded and expressed as the percentage change from the baseline weight. Treatment commenced and ended at weeks one and eight (black arrows), respectively. Animals were untreated (control) or treated with physiological saline (vehicle), DOX (2.5 mg/kg/week), ghrelin alone (300 ug/kg/week) or a combination of DOX and ghrelin, for a total of eight weeks. The animals were killed in week nine (red arrow). All values are presented as mean ± SEM, *p< 0.05 vs control, $p< 0.05 vs vehicle, n = 7 – 9.

A similar result can be seen when looking at the raw body weight data (Figure 3.2). Treatment with DOX, regardless of whether ghrelin was also administered, resulted in a significantly reduced body weight from week three of the treatment protocol. Although ghrelin does not appear to increase weight gain in combination with DOX, from these results it was calculated that the DOX-treated group gained 48% less weight than the control, whereas the combination group only gained 22% less than the control. This equates to the combination group gaining 33% more weight than the DOX-alone group. In addition, the ghrelin alone group gained 13% more weight overall when compared to the control.
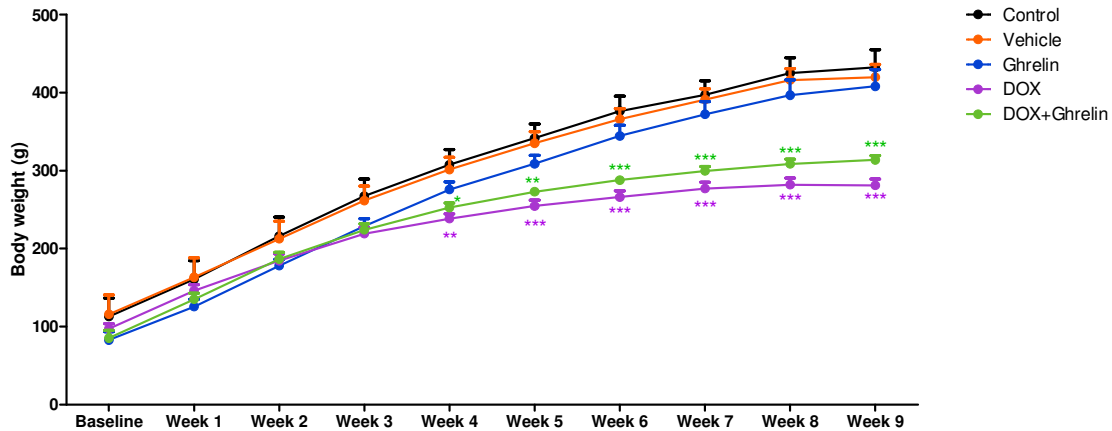
Figure 3.2: The change in body weight throughout the treatment protocol

Body weight was recorded three times per week. Animals were untreated (control) or treated with physiological saline (vehicle), DOX (2.5 mg/kg/week), ghrelin alone (300 ug/kg/week) or a combination of DOX and ghrelin, for a total of eight weeks. The animals were killed in week nine. All values are presented as mean ± SEM, *p< 0.05 vs control, **p< 0.01 vs control, ***p< 0.001 vs control, n = 7 – 9.

3.1.2 Heart weight

In addition to recording body weight, heart weight was also measured after the eight week treatment period, upon harvesting of the heart. This data was then expressed as the ratio of heart weight to body weight, however, there was no significant change in this ratio between any of the groups (Table 3). This may be due to timing, as extensive remodeling of the myocardium might not yet have taken place after eight weeks of treatment to produce detectable differences in heart size.

Table 3: Heart weight to body weight ratio.

The heart weight of each rat was expressed as a ratio to the body weight.

	CONTROL	VEHICLE	GHRELIN	DOX	DOX+ghrelin
Heart weight: body weight (AU)	0.0044 ± 0.0002	0.0043 ± 0.0003	0.0042 ± 0.0002	0.0043 ± 0.0002	0.0044 ± 0.0003

All values are presented as mean ± SEM, n = 7 – 9. Abbreviations: AU, arbitrary units.

3.1.3 Food consumption

In an effort to correlate our body weight data to how much food was consumed by each group, the average weekly food consumption was determined (Figure 3.3). Treatment with

DOX resulted in significantly reduced food intake from week six (137.45 ± 14.03 g, p< 0.05), and this was maintained throughout the duration of the study when compared to the respective controls. This result may have accounted for the reduced body weight observed in this group. A similar result was observed when the DOX group was compared to the vehicle group. Although co-administration with ghrelin modestly elevated food consumption when compared to DOX treatment alone, the results obtained were not statistically significant. However, it appears that ghrelin prevents loss of appetite by promoting food intake, as is evident from the percentage change in body weight described in section 3.1.1.
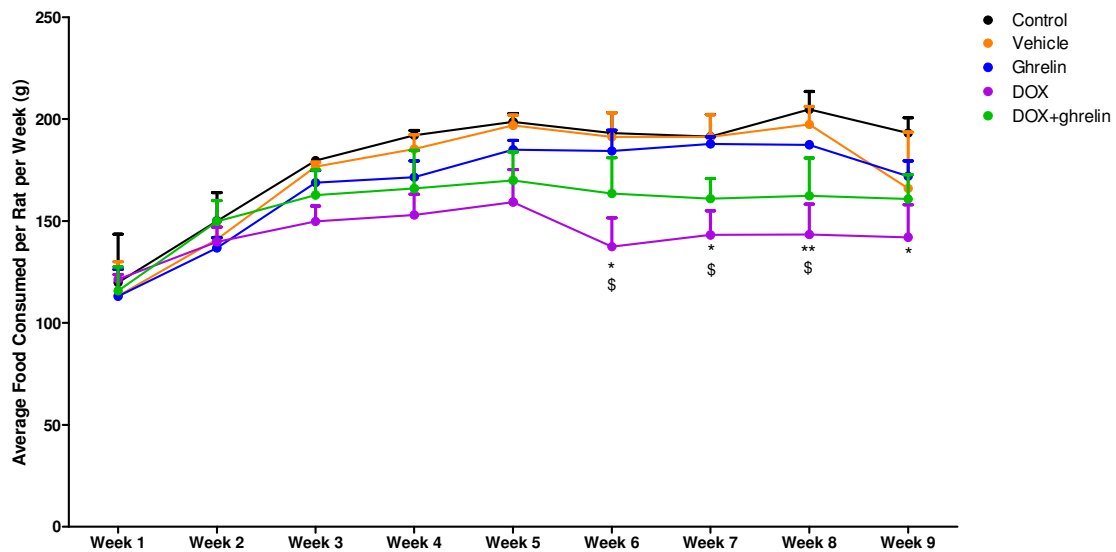
Figure 3.3: Food consumption over the treatment protocol.
Food intake was recorded three times a week throughout the eight week treatment protocol and calculated as the average food consumed per rat per week. All values are presented as mean ± SEM, *p< 0.05; **p< 0.01 vs control, $p< 0.05 vs vehicle, n = 7 – 9.

3.2 Ghrelin maintains cardiac function during DOX treatment

3.2.1 Cardiac Output, Aortic Output, Coronary Flow and Stroke Volume

It is a well-known phenomenon that DOX treatment results in cardiotoxicity which can culminate in heart failure in some individuals. However, despite chronic cardiotoxicity being the most detrimental form of this condition, very few studies have evaluated the effects of DOX in an appropriate, prolonged treatment protocol. While there is no 'accepted' definition for the term 'chronic cardiotoxicity' when referring to pre-clinical models (*in vivo*), it is extremely difficult to ascertain the dose, the duration and the frequency of the treatment regimen that induces the typical signs and symptoms of this condition. Hence we have tried to establish an *in vivo* model of chronic cardiotoxicity in order to more closely simulate clinical observations. Functional heart data was obtained by making use of working heart perfusions, where cardiac output was measured as the amount of blood pumped by the heart per minute (aortic output plus coronary flow) (Vincent, 2008). Here we demonstrate that treatment with DOX significantly reduced cardiac output (Figure 3.4) in the isolated rat heart. Cardiac function declined to a minimum at the end of the 40-minute protocol (42.30 ± 4.82 mL/minute, $p < 0.01$) when compared to the control (58.80 ± 2.78 mL/minute). While no significant changes were observed between the DOX and DOX+ghrelin groups, it is apparent from the data obtained that ghrelin, in the presence of DOX, prevents the decline in cardiac output, thus implying a protective effect.

Figure 3.4: Cardiac output (mL/minute).

After ten minutes of stabilization in the retrograde perfusion mode, heart function was assessed over a 40-minute working heart perfusion protocol. All values are presented as mean ± SEM, *p< 0.05; **p< 0.01 vs control, n = 5 – 9.

- 51 -

When looking at aortic output alone (Figure 3.5), the aortic flow rate of DOX-treated hearts was significantly reduced by the end of the perfusion protocol (25.50 ± 3.64 mL/minute, p< 0.05) when compared to the control (36.60 ± 1.47 ml/minute). Furthermore, the aortic flow rate was significantly reduced in the DOX hearts when compared to DOX+ghrelin (34.07 ± 0.97 mL/minute, p< 0.05), substantiating the protective effect of ghrelin.

Figure 3.5: Aortic flow rate (mL/minute)

After ten minutes of stabilization in the retrograde perfusion mode, heart function was assessed over a 40-minute working heart perfusion protocol. All values are presented as mean $\pm$ SEM, *p< 0.05 vs control; #p< 0.05 vs DOX+ghrelin, n = 5 – 9.

Coronary flow is the amount of blood perfusing the myocardium through the coronary arteries and was measured by the timed collection of the coronary effluent from the heart. In a similar manner to the cardiac output and aortic output results described above, DOX significantly reduced coronary flow (Figure 3.6) for the majority of the perfusion protocol, beginning at ten minutes (16.33 ± 0.73 mL/minute vs 22.60 ± 1.60 mL/minute, p< 0.05) and remaining reduced until 35 minutes (16.47 ± 1.30 mL/minute vs 22.2 ± 1.80 mL/minute, p< 0.05) when compared to the control. Even though coronary flow in the combination group was modestly reduced, the values obtained did not differ statistically from the DOX group, despite remaining above the levels of the DOX group.
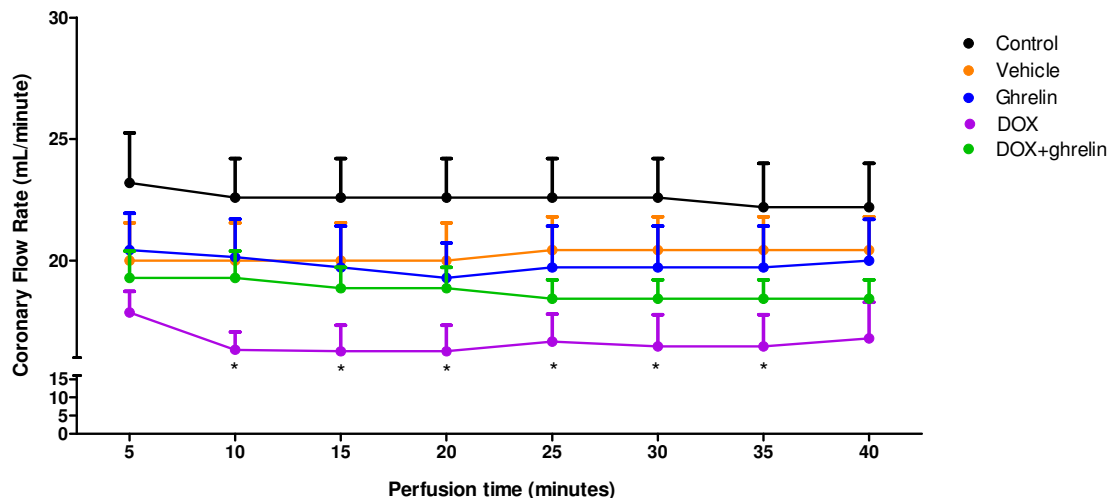
Figure 3.6: Coronary flow rate (mL/minute).

After ten minutes of stabilization in the retrograde perfusion mode, heart function was assessed over a 40-minute working heart perfusion protocol. All values are presented as mean ± SEM, *p< 0.05 vs control, n = 5 – 9.

Stroke volume is the amount of blood pumped by the left ventricle with each heartbeat and can be calculated by dividing the cardiac output by the heart rate. As indicated in Figure 3.7, DOX treatment significantly decreased the stroke volume from 30 minutes into the perfusion protocol (179.17 ± 20.93 µL/beat, p< 0.05) when compared to the control (244.09 ± 12.79 µL/beat). Stroke volume continued to decline until the end of the perfusion protocol (171.81 ± 20.61 µL/beat, p< 0.01), when compared to the control (247.55 ± 12.68 µL/beat). No significant changes were observed between the DOX and DOX+ghrelin group despite the combination group's values remaining above the DOX group's values. These results indicate that while no differences were observed with the intervention (ghrelin) in the presence of DOX, ghrelin does appear to maintain left ventricular function.
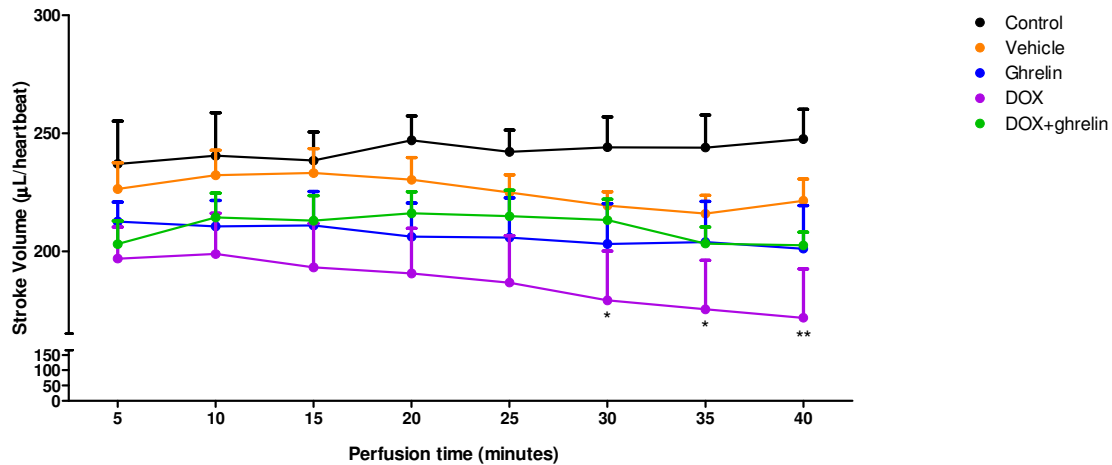
Figure 3.7: Stroke volume (µL/heartbeat).

After ten minutes of stabilization in the retrograde perfusion mode, heart function was assessed over a 40-minute working heart perfusion protocol. All values are presented as mean ± SEM, *p< 0.05; **p< 0.01 vs control, n = 5 – 9.

3.2.2 Blood pressure and Heart Rate

Although previous studies have demonstrated the effects of DOX on blood pressure (Yagmurca *et al.*, 2003), only the systolic pressure was reduced in our study (Figure 3.8A). Systolic pressure was significantly reduced at 25 minutes into the perfusion protocol (131.89 ± 4.14 mmHg, p< 0.05) when compared to the control (147.80 ± 1.66 mmHg). However, significance was lost as the perfusion protocol continued. No other differences were observed with regards to diastolic blood pressure (Figure 3.8B) and heart rate (Figure 3.8C).
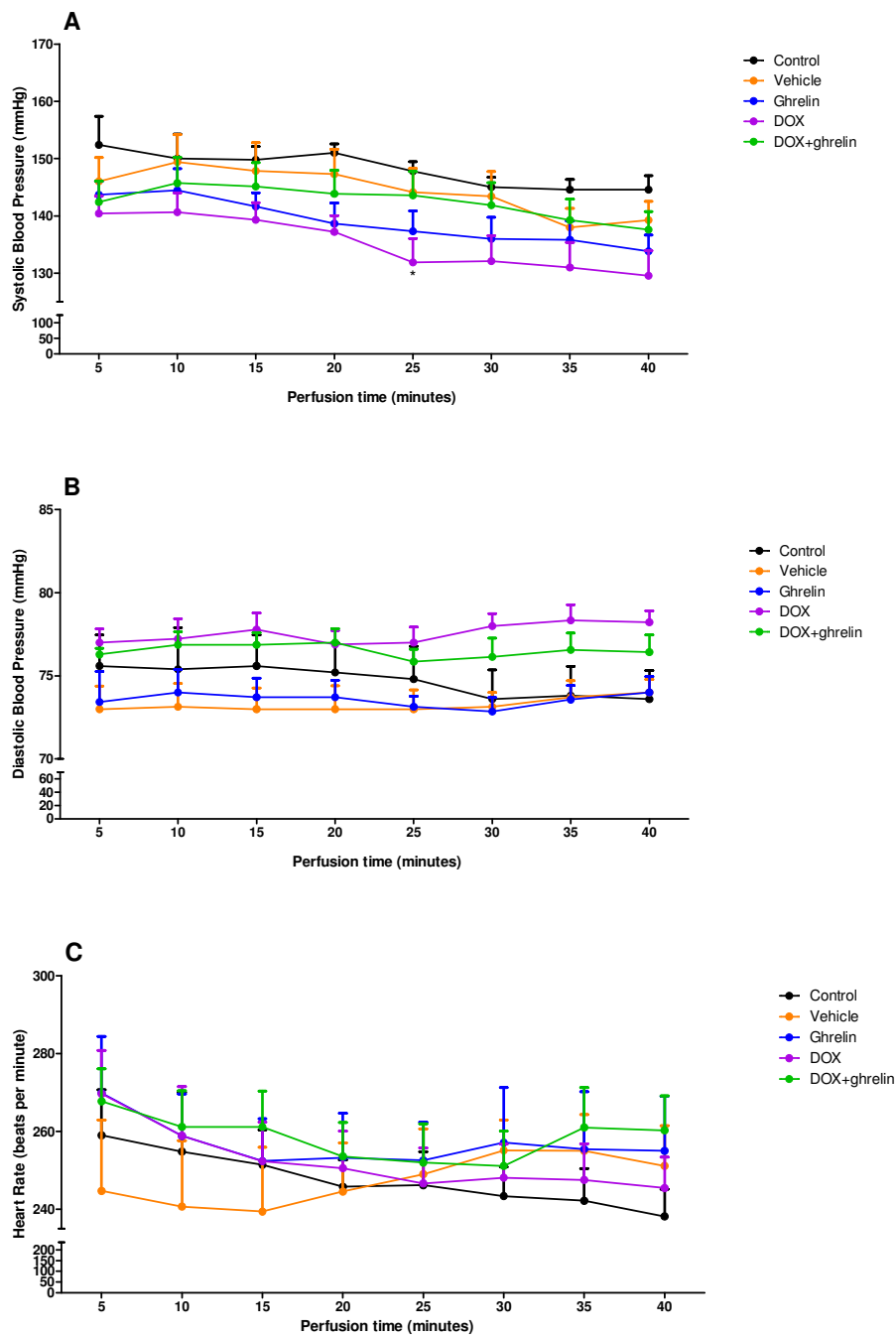
Figure 3.8: (A) Systolic blood pressure, (B) diastolic blood pressure and (C) heart rate
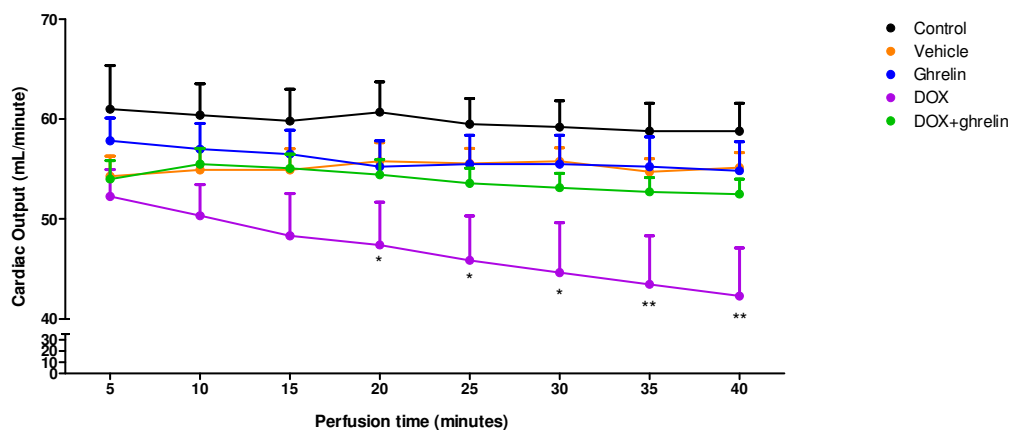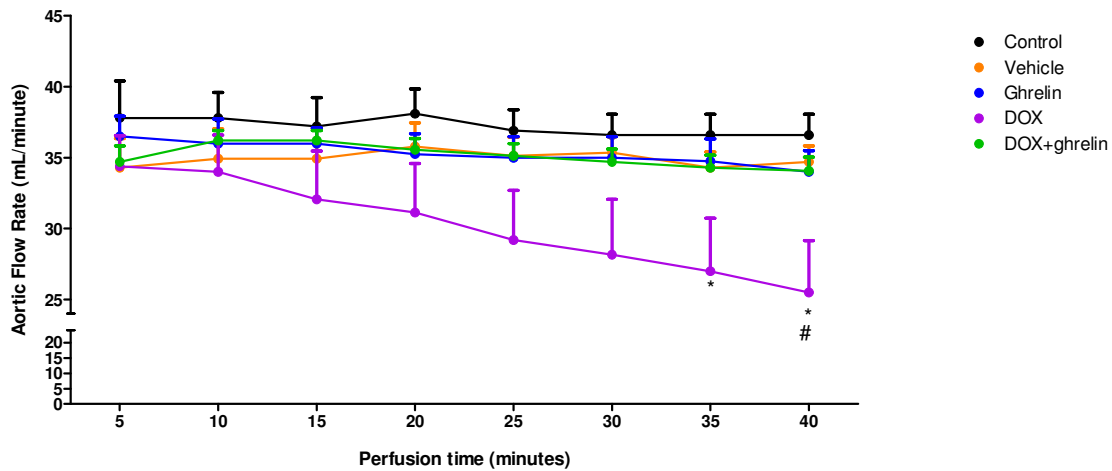After ten minutes of stabilization in the retrograde perfusion mode, heart function was assessed over a 40-minute working heart perfusion protocol. All values are presented as mean ± SEM, *p< 0.05 vs control, n = 5 – 9.

3.2.3 Left Ventricular Function

Considering that one of the signs and symptoms of chronic DOX-induced cardiotoxicity is left ventricular dysfunction (Carver *et al.*, 2007), measuring this parameter was of critical importance. As such, the performance of the left ventricle was assessed by calculating the LVDP, which is the diastolic pressure subtracted from the systolic pressure (Lecour *et al.*, 2002). From this calculation, the RPP was also measured by multiplying the LVDP by the heart rate, thereby providing an indication of both the chronotropic (changes in heart rate and rhythm) and inotropic (changes in contractile force) activity within the myocardium. These parameters essentially provide an indication of cardiac 'effort' (Aksentijevi *et al.*, 2016). As expected, LVDP (Figure 3.9A) and RPP (Figure 3.9B) were significantly reduced after DOX treatment when compared to the respective controls. The intervention group (DOX+ghrelin) produced no significant changes when compared to the DOX group, despite remaining above DOX values for both LVDP and RPP.
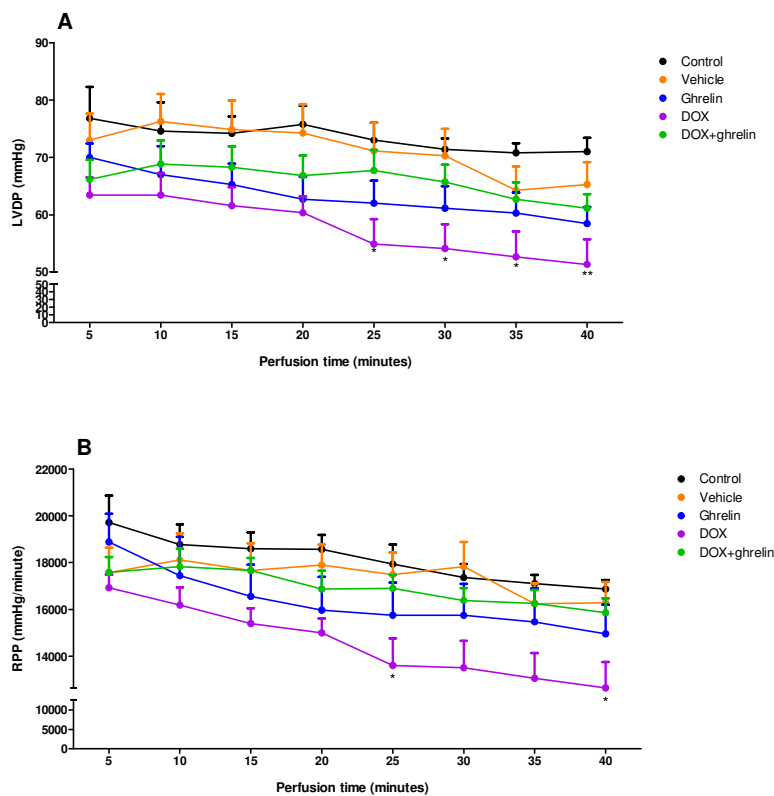
Figure 3.9: DOX treatment reduces (A) LVDP and (B) RPP.

Left ventricular performance was measured by the LVDP and the RPP. All values are presented as mean ± SEM, *p< 0.05; **p< 0.01 vs control, n = 5 – 9. Abbreviations: LVDP, left ventricular developed pressure; RPP, rate-pressure product.

3.2.4 Total work performance

Our results show that the mean external power produced by the left ventricle was significantly reduced in the DOX group for the majority of the perfusion protocol when compared to the control (Figure 3.10). The performance of the hearts that were co-treated with ghrelin resulted in no significant change when compared to the DOX treatment group. The fact that all functional data and the various parameters, both measured and calculated, follow the same trend indicates not only that the perfusion protocol was performed correctly, but that the intervention of using ghrelin in the presence of DOX was able to offer protection to the heart. Finally, it must be acknowledged that the sample size for the perfusion results is reduced because some hearts were lost upon euthanasia or during mounting on the perfusion apparatus (aortic edema, tearing of the coronary sinus, arrhythmias, ruptured atrium).
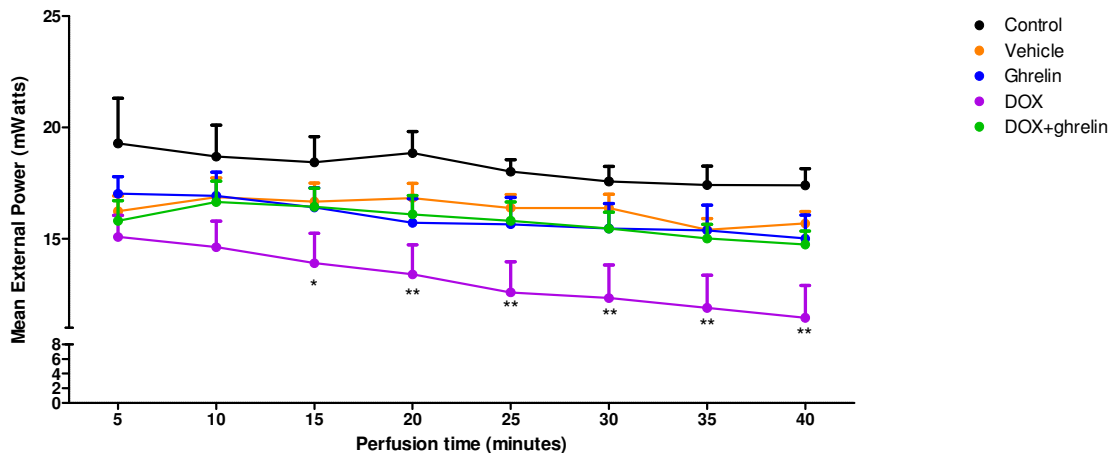
Figure 3.10: Mean external power (total work performance).

After ten minutes of stabilization in the Langendorff mode, heart function was assessed over a 40-minute working heart perfusion protocol. Cardiac function is expressed as the mean external power of the left ventricle. All values are presented as mean ± SEM, *p< 0.05; **p< 0.01 vs control, n = 5 – 9.

3.3 Blood and Tissue Analysis

3.3.1 Metabolic Parameters

As mentioned in Chapter 1, ghrelin is most well-known for its appetite-inducing effects and its levels therefore fluctuate in response to feeding and fasting. Blood was collected at the time of euthanasia, which was the light-phase for the rats. This means that the rats were sleeping and therefore in a fasted state. The serum concentration of ghrelin was measured

using a luminex-based assay. As demonstrated in Figure 3.11, ghrelin levels were significantly elevated in the group that received exogenous injections of ghrelin (42.40 ± 9.53 pg/mL, $p < 0.05$) when compared to the control (3.49 ± 1.20 pg/mL). Surprisingly, ghrelin was undetectable in the group that received DOX, suggesting that DOX may interfere with the processes that govern ghrelin production or secretion. Supporting this argument, detectable amounts of ghrelin were observed in the group that received both DOX and ghrelin treatment. It may be this increase in serum ghrelin that is accountable for the increase in body weight in this group.
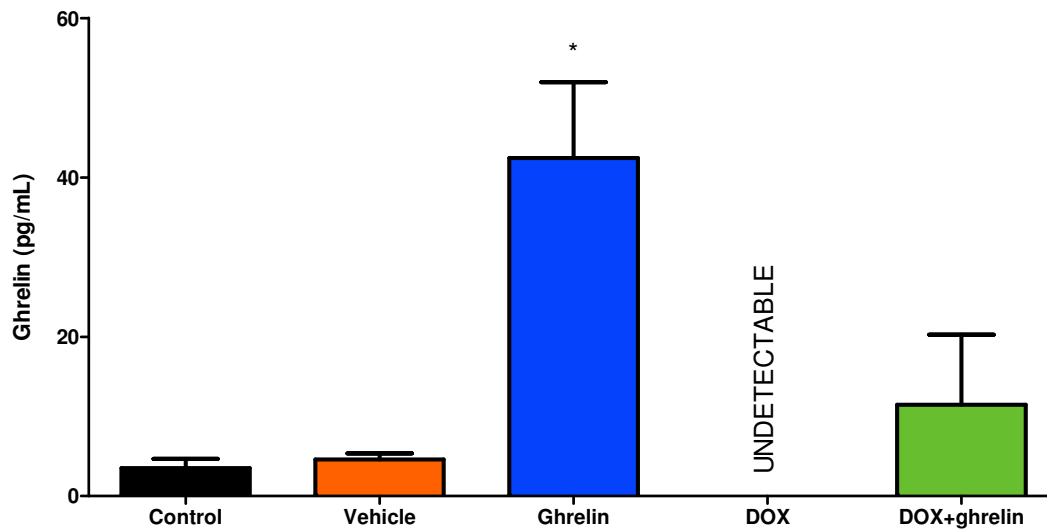
Figure 3.11: Serum ghrelin concentration (pg/mL).

One week after the last injections, blood was collected from the thoracic cavity upon euthanasia. Ghrelin was measured in the serum using a luminex-based assay. All values are presented as mean ± SEM, *$p < 0.05$ vs control, n = 7 – 9.

3.3.2 Markers of Cardiac injury.

Various well-known markers can be used to assess the extent of cardiovascular injury. In this study, the serum concentrations of cTnT, cTnI and CK-MB, and the myocardial tissue concentration of BNP were measured in order to obtain a holistic view of the sensitivity of these markers in detecting cardiotoxicity. The most significant results obtained came from the analysis of CK-MB (Figure 3.12), which was upregulated in the presence of DOX (6742 ± 664.80 pg/mL, $p < 0.01$) and in the combination group (7059 ± 608.10 pg/mL, $p < 0.001$)

when compared to the control (3884 ± 422.60 pg/mL). Other markers such as cTnI, cTnT and BNP did not yield significant differences between groups (Table 4).
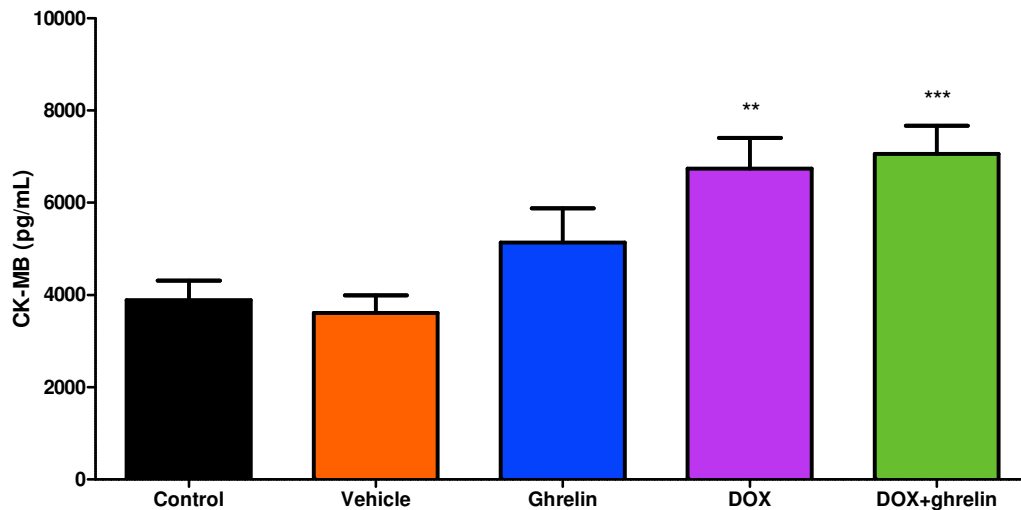
Figure 3.12: Serum CK-MB concentration (pg/mL).

The concentration of muscle creatine kinase was determined in the serum of the rats using a luminex-based assay. All values are presented as mean ± SEM, **$p < 0.01$; ***$p < 0.001$ vs control, n = 7 – 9. Abbreviations: CK-MB; creatine kinase-myocardial band.

Table 4: cTnI, cTnT and BNP.

After the eight week treatment protocol, blood was collected and heart tissue was harvested. cTnI and cTnT were measured in the serum and BNP was measured in homogenized heart tissue lysates.

	CONTROL	VEHICLE	GHRELIN	DOX	DOX+ghrelin
cTnI (pg/mL)	2420 ± 276.80	2606 ± 885.00	2200 ± 389.40	1938 ± 389.6	1410 ± 210.10
cTnT (pg/mL)	412.6 ± 83.38	498.8 ± 219.10	545 ± 180.50	413.3 ± 175.50	259.4 ± 56.71
BNP (ng/mL)	0.064 ± 0.02	0.049 ± 0.01	0.046 ± 0.03	0.061 ± 0.04	0.061 ±0.004

Abbreviations: cTnI, cardiac troponin inhibitory; cTnT, cardiac troponin tropomyosin; BNP, brain natriuretic peptide. All values are presented as mean ± SEM, n = 7 – 9.

3.4 Morphological assessment of the myocardium

3.4.1 Masson's Trichrome stain for the detection of fibrosis

The Masson's Trichrome stain was used to identify the deposition of connective tissue. Both a 4x image of the entire heart, as well as a 20x enlargement of a region of the left ventricle is shown (Figure 3.13). As indicated in the figures below, collagen was only observed in the control, vehicle and ghrelin groups when surrounding blood vessels. However, substantial blue-stained fibrosis was evident in the DOX-treated group (indicated by a closed arrowhead). Co-treatment with ghrelin resulted in a trend towards a decline in collagen deposition (indicated by an open arrowhead) when compared to the DOX group. In the DOX group, myofibrillar disorganization and fragmentation were also observed, but this was reduced in the presence of ghrelin (indicated by an asterisk).

Using color thresholding (described in section 2.6.3), the areas of blue-stained fibrosis were then quantified. No changes were observed between the control, vehicle and ghrelin groups, whereas eight weeks of DOX treatment at a cumulative dose of 20 mg/kg resulted in a significant increase in fibrosis ($40.01 \pm 3.03\%$, $p = 0.0002$) in DOX-treated hearts when compared to the control ($11.53 \pm 3.00\%$). Co-treatment with ghrelin resulted in a modest reduction in fibrosis, though this result was not significant when compared to the DOX group.
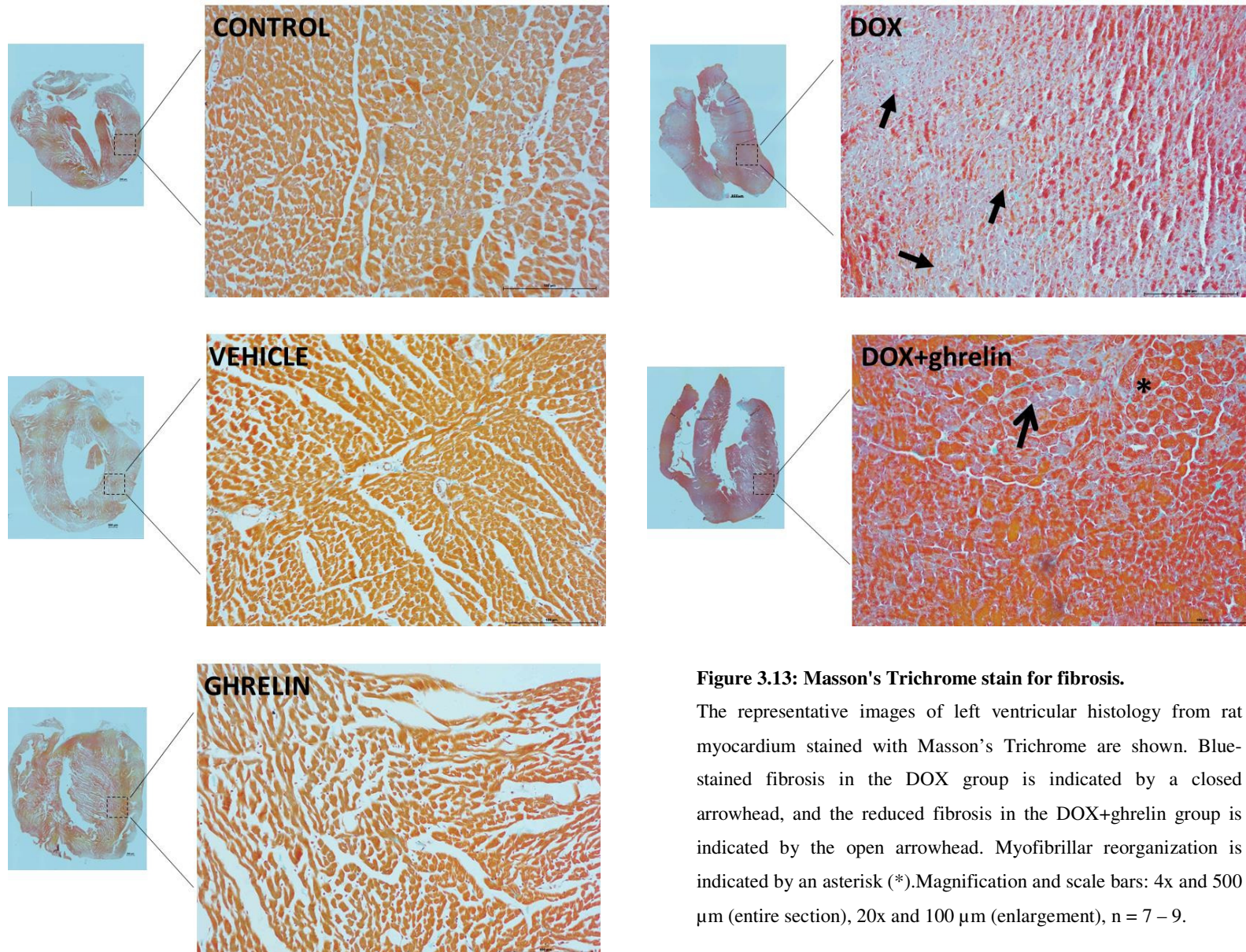
Figure 3.13: Masson's Trichrome stain for fibrosis.

The representative images of left ventricular histology from rat myocardium stained with Masson's Trichrome are shown. Blue-stained fibrosis in the DOX group is indicated by a closed arrowhead, and the reduced fibrosis in the DOX+ghrelin group is indicated by the open arrowhead. Myofibrillar reorganization is indicated by an asterisk (*).Magnification and scale bars: 4x and 500 µm (entire section), 20x and 100 µm (enlargement), n = 7 – 9.
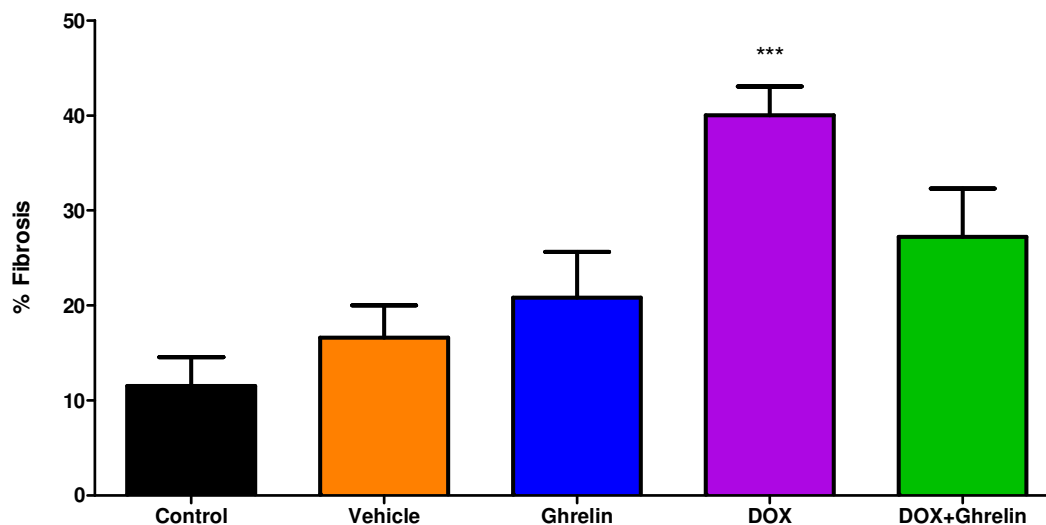
Figure 3.14: Quantification of fibrosis.

Color-thresholding was performed to quantify the formation of connective tissue in rat myocardial sections. The measurement in pixels was used to express the area of blue-stained fibrosis as a percentage of the entire heart. All values are presented as mean $\pm$ SEM, ***$p< 0.001$ vs control, n = 7 – 9.

3.4.2 Cardiomyocyte size

In an effort to assess the potential morphological changes induced by DOX and ghrelin alone or in combination, the H&E histological stain was employed. It is known that repeated administration with DOX induces histological changes to the heart in both human patients and experimental animal models, and that these changes can ultimately affect heart function. Upon the qualitative examination of the H&E slides (Figure 3.15), the control, vehicle and ghrelin-treated groups were indistinguishable from one another, showing signs of normal cardiac morphology. However, the groups treated with DOX showed signs of cytoplasmic vacuolization (asterisk), reduced myocyte size (black arrows) and myofibrillar disarray. When ghrelin was administered in combination with DOX, these affects appeared partially attenuated, however, it was difficult to determine whether ghrelin had a beneficial effect solely based on qualitative analysis.
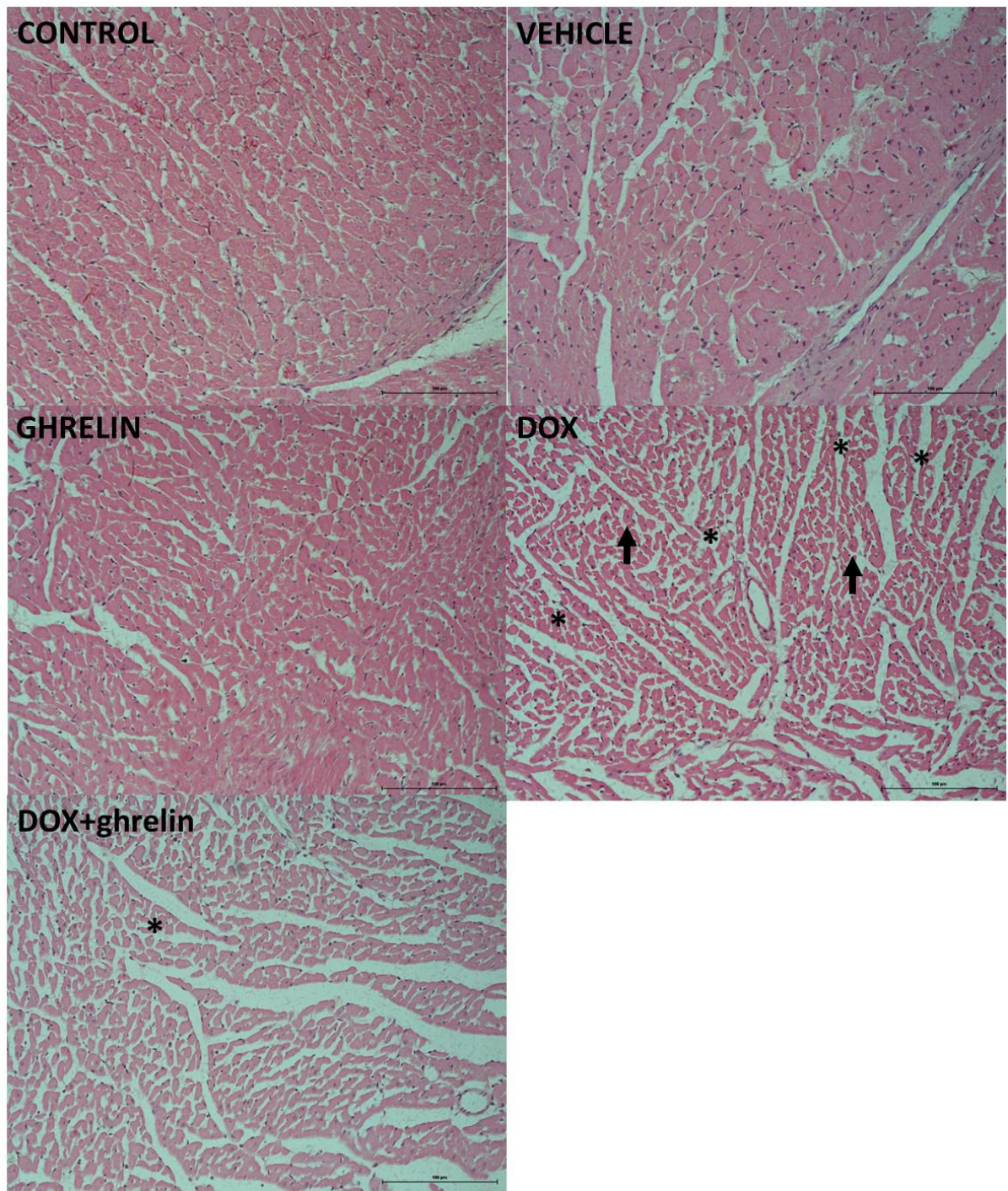
Figure 3.15: H&E analysis of cardiac morphology.

The representative images of left ventricular histology from rat myocardium stained with H&E are shown. Transverse sections were cut to show the overall morphology of the heart. DOX-treated hearts displayed signs of vacuolization (indicated by *) and reduced myofiber size (indicated by black arrows). Magnification: 20x, scale bar: 100 µm, n = 7 – 9.

To further strengthen our data and to determine the effect of ghrelin under these conditions, cardiomyocyte size (cross-sectional area) was measured. As described in the Materials and Methods (section 2.6.2, Figure 2.2), images were captured at 4x magnification from five randomly selected ROIs in the left ventricle of each heart. Then, using ImageJ, the cross-sectional area of 30 myofibres was measured in each of the five ROIs, giving a total of 150 myofibres per heart section (n = 7 – 9 sections per group). Our results indicate that DOX administration significantly reduced myocyte cross-sectional area by 8.3% (141.90 ± 2.33 μm^2, p< 0.01) when compared to the control (154.70 ± 3.27 μm^2). This result correlates with the morphological changes observed in the H&E stain, and is indicative of muscle degradation, known to be stimulated in this scenario. A modest, but insignificant increase in cross-sectional area was observed between the DOX and DOX+ghrelin group.
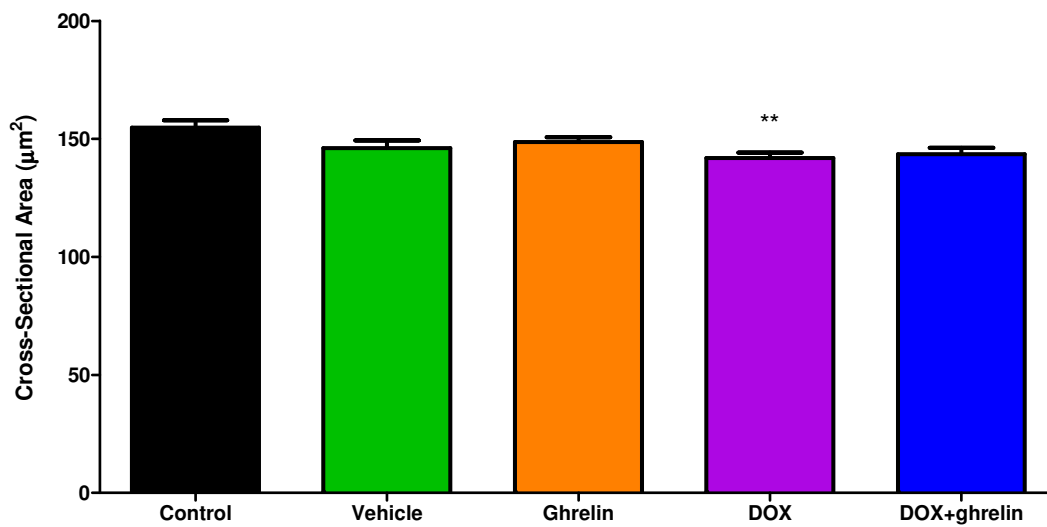
Figure 3.16: Cross-sectional area.

The cross-sectional area of 150 myofibers per section was measured. All values are presented as mean ± SEM, **p< 0.01 vs control, n = 7 – 9.

3.5 Ghrelin prevents oxidative stress

3.5.1 Lipid peroxidation

Ghrelin has previously been described to possess antioxidant properties. Therefore, considering that one of the mechanisms by which DOX induces cardiotoxicity is oxidative stress, this study aimed to evaluate the effectiveness of ghrelin against elevated levels of ROS. Lipid peroxidation is one of the main events triggered by oxidative stress and can be assessed by measuring the

levels of conjugated dienes and thiobarbituric acid reactive substances (TBARS) such as malondialdehyde (MDA). These markers, conjugated dienes and MDA, are considered as early and late indicators of lipid peroxidation, respectively.

Almost immediately after free radicals are formed, the non-conjugated double bonds that are found in membrane lipids are converted to conjugated double bonds. Figure 3.17 demonstrates that DOX significantly increased the formation of conjugated dienes (1.64 ± 0.11 µmol/gram, p = 0.0003) when compared to the control (0.55 ± 0.12 µmol/gram). This effect was attenuated in the combination group (0.86 ± 0.18 µmol/gram, p< 0.05) when compared to DOX alone.
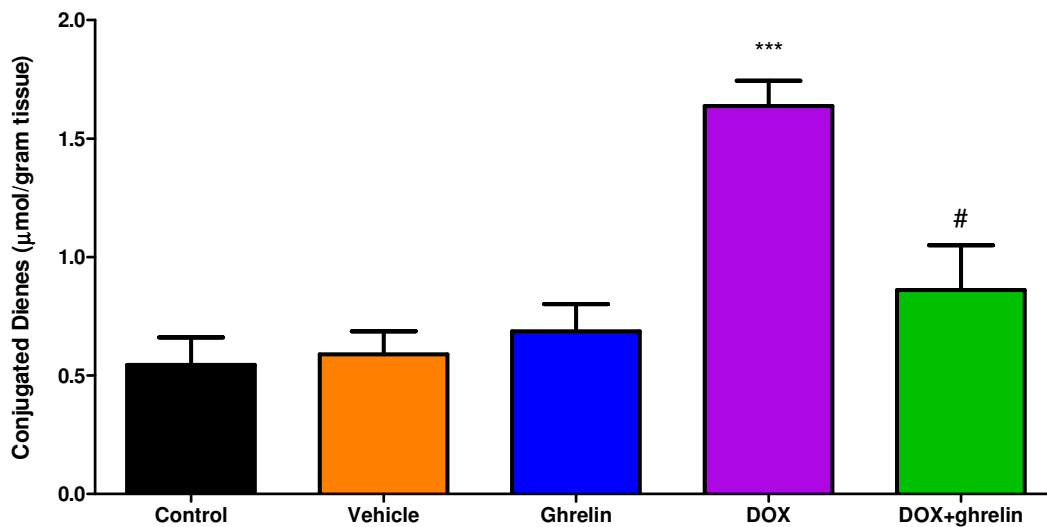
Figure 3.17: Early lipid peroxidation was assessed using measuring conjugated dienes.
Conjugated diene content was measured in myocardial tissue after eight weeks of treatment. All values are presented as mean ± SEM, ***p< 0.001 vs control; #p< 0.05 vs DOX, n = 5 – 9.

The TBARS assay measures a late marker of lipid peroxidation, MDA. However, the levels of MDA did not change in any of the treatment groups (Figure 3.18). The TBARS assay has been criticized for a lack of specificity and sensitivity, therefore HPLC has been deemed a preferred method of detection (Moselhy *et al*., 2013).
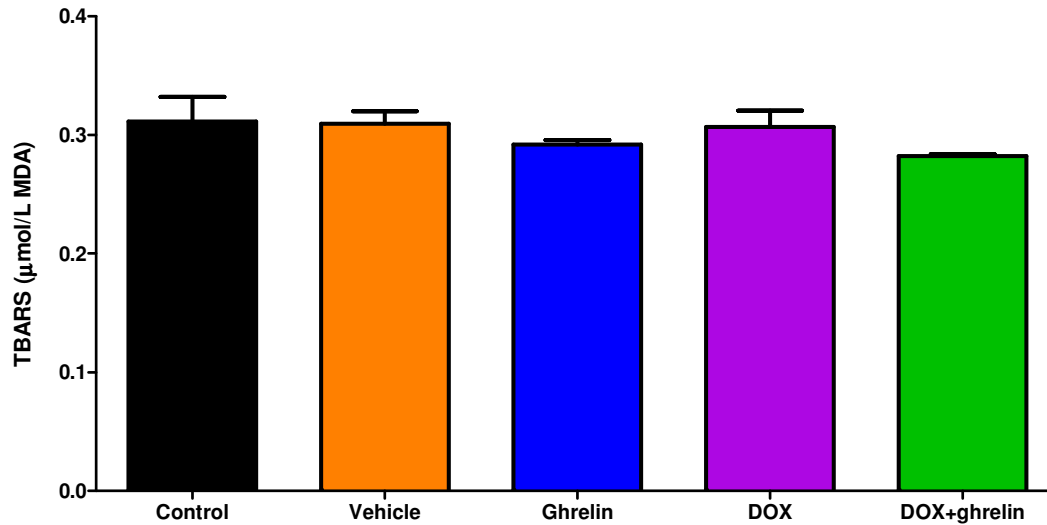
Figure 3.18: Late lipid peroxidation was assessed using the TBARS assay.

The TBARS assay measures MDA, a by-product of late lipid peroxidation. MDA was asseseds in heart tissue homogenates. All values are presented as mean ± SEM, n = 5 – 9.

3.5.2 Antioxidant capacity

Anthracycline administration is known to compromise the protective mechanisms in the heart against free radical damage (Saleem *et al*., 2014). This observation, together with the naturally low levels of antioxidants in the heart, makes the heart susceptible to oxidative stress-induced damage. Despite elevated lipid peroxidation as described in section 3.5.1, no change in antioxidant capacity, as measured by the ORAC assay, was observed in any of the treatment groups (Figure 3.19).
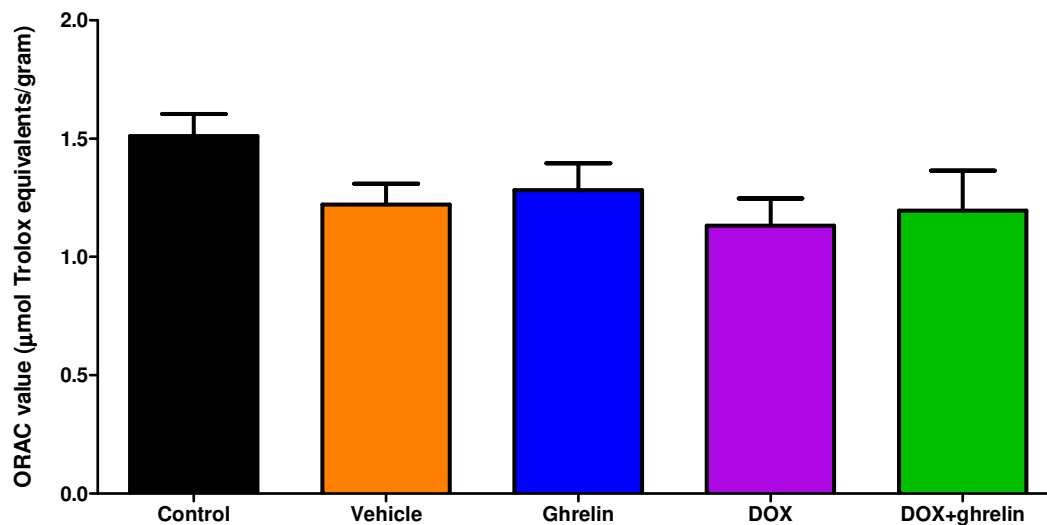
Figure 3.19: Antioxidant capacity was analysed using the ORAC assay.

The antioxidant capacity of the test samples is compared to the vitamin E analogue, Trolox, so that the ORAC value can be expressed as Trolox equivalents (μmol) per gram of tissue. All values are presented as mean ± SEM, n = 5 – 9.

This result is echoed by the SOD activity assay (Figure 3.20) and in the Western blot analysis of SOD1 (CuZn) and SOD2 (MnSOD), where no changes were observed. This may be due to the fact that the heart contains naturally low levels of antioxidants like SOD, or that the western blot analysis was not performed on mitochondrial and cytosolic fractions.
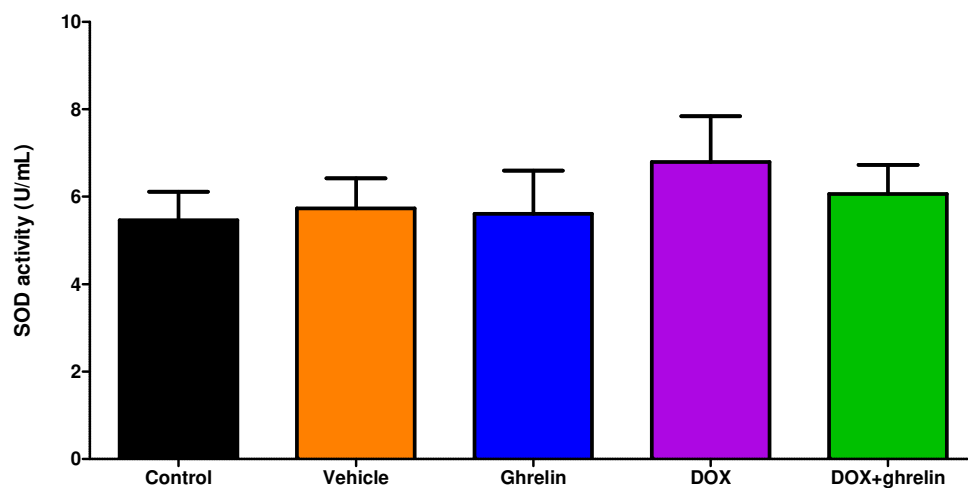
Figure 3.20: SOD activity.

SOD activity was measured in heart tissue homogenates. All values are presented as mean ± SEM, n = 5 – 9.
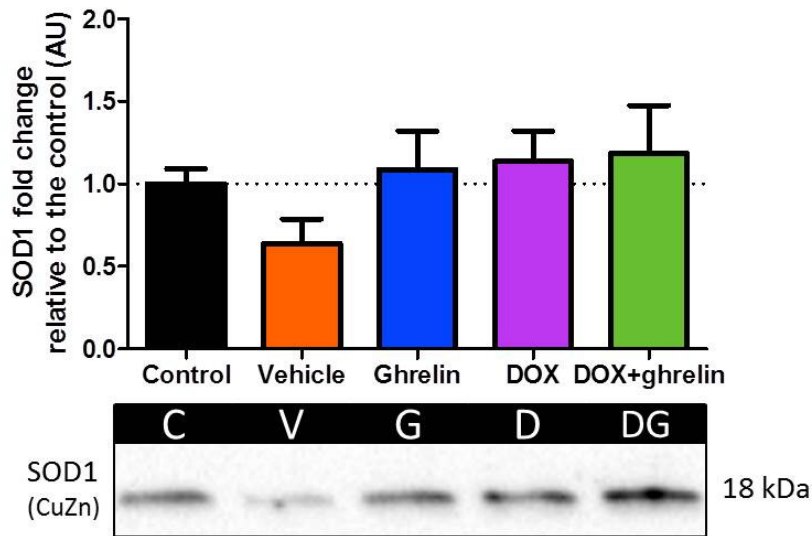
Figure 3.21: Protein expression of SOD1 (CuZn)

The lane analysis and western blots of SOD1 are shown. Protein expression was normalized to the total lane protein. The fold change relative to the control was calculated. All values are presented as mean ± SEM, n = 7 – 9. AU, arbitrary units; C, control; V, vehicle; G, ghrelin; D, DOX; DG, DOX+ghrelin.

Figure 3.22: Protein expression of SOD2 (MnSOD)

The lane analysis and western blots of SOD2 are shown. Protein expression was normalized to the total lane protein. The fold change relative to the control was calculated. All values are presented as mean ± SEM, n = 7 – 9. AU, arbitrary units; C, control; V, vehicle; G, ghrelin; D, DOX; DG, DOX+ghrelin.

3.5.3 Antioxidant status

GSH neutralizes free radicals by donating an electron, resulting in a rise in GSSG. An increase in GSSG, with the subsequent decrease in the GSH: GSSG ratio is indicative of a state of oxidative stress. While no change in GSH was observed (Table 5), treatment with DOX significantly increased GSSG levels in the DOX (605.60 ± 45.89 µmol/gram, $p< 0.001$) and DOX+ghrelin groups (477.60 ± 31.09 µmol/gram, $p< 0.05$) when compared to the control (280.30 ± 59.30 µmol/gram). However, the ratio of GSH: GSSG was only significantly reduced in the DOX group (2.10 ± 0.47 AU, $p< 0.05$) when compared to the control (9.66 ± 1.08 AU), indicating oxidative stress after DOX treatment.

Table 5: GSH, GSSG and GSH: GSSG.

	Control	Vehicle	Ghrelin	DOX	DOX+ghrelin
GSH (µmol/gram)	1526 ± 214.7	1373 ± 293.9	1308 ± 275.9	937 ± 173.3	1205 ± 219.0
GSSG (µmol/gram)	280.3 ± 59.30	384.6 ± 52.13	432.5 ± 50.52	605.6 ± 45.89***	477.6 ± 31.09*
GSH : GSSG (AU)	9.66 ± 1.08	6.64 ± 2.16	8.03 ± 2.46	2.10 ± 0.47*	3.67 ± 1.01

All values are presented as mean $\pm$ SEM, *$p< 0.05$; ***$p< 0.001$ vs control, $n = 5 – 9$.

3.6 Ghrelin reduces apoptotic cell death in the rat heart

3.6.1 Cytochrome c

In order to determine the contribution of apoptosis to DOX-induced cardiotoxicity, various markers for apoptosis were measured. Cytochrome c is released from mitochondria upon stimulation of the intrinsic apoptotic pathway. After immunohistochemical staining for cytochrome c, the immune reactivity of paraffin-embedded tissue sections was determined using the IHC Profiler plugin on Image. As described in section 2.6.4, this software grades and assigns an image a score based on the intensity of the pixels. Upon evaluating the images, it is clear that there was a strong positive reaction (arrows) for cytochrome c in the DOX treated group (Figure 3.23), indicative of apoptotic activation. This was confirmed by the digital grading software, which assigned a score of 'positive/high positive' to the DOX group. The immune reaction of cytochrome c appeared to be modestly reduced when ghrelin was administered in combination with DOX, and as such, the digitally assigned score was 'low positive'. This suggests an anti-apoptotic effect induced by ghrelin in the presence of

DOX. A negative control sample was obtained by omitting the primary antibody in order to account for the endogenous peroxidase activity within the heart.

Quantitative analysis showed a moderate increase in cytochrome c reactivity after DOX treatment (Figure 3.24), though this did not differ statistically from the control. Co-treatment with ghrelin was accompanied by a modest reduction in cytochrome c reactivity compared to DOX alone, though this was not statistically different. Finally, cytochrome c protein expression was assessed in heart tissue homogenates using western blot analysis (Figure 3.25), however, no differences between the groups were observed. This might be explained by the fact that cytochrome c is closely associated with the inner mitochondrial membrane, and these western blots were performed on tissue lysates instead of mitochondrial fractions.
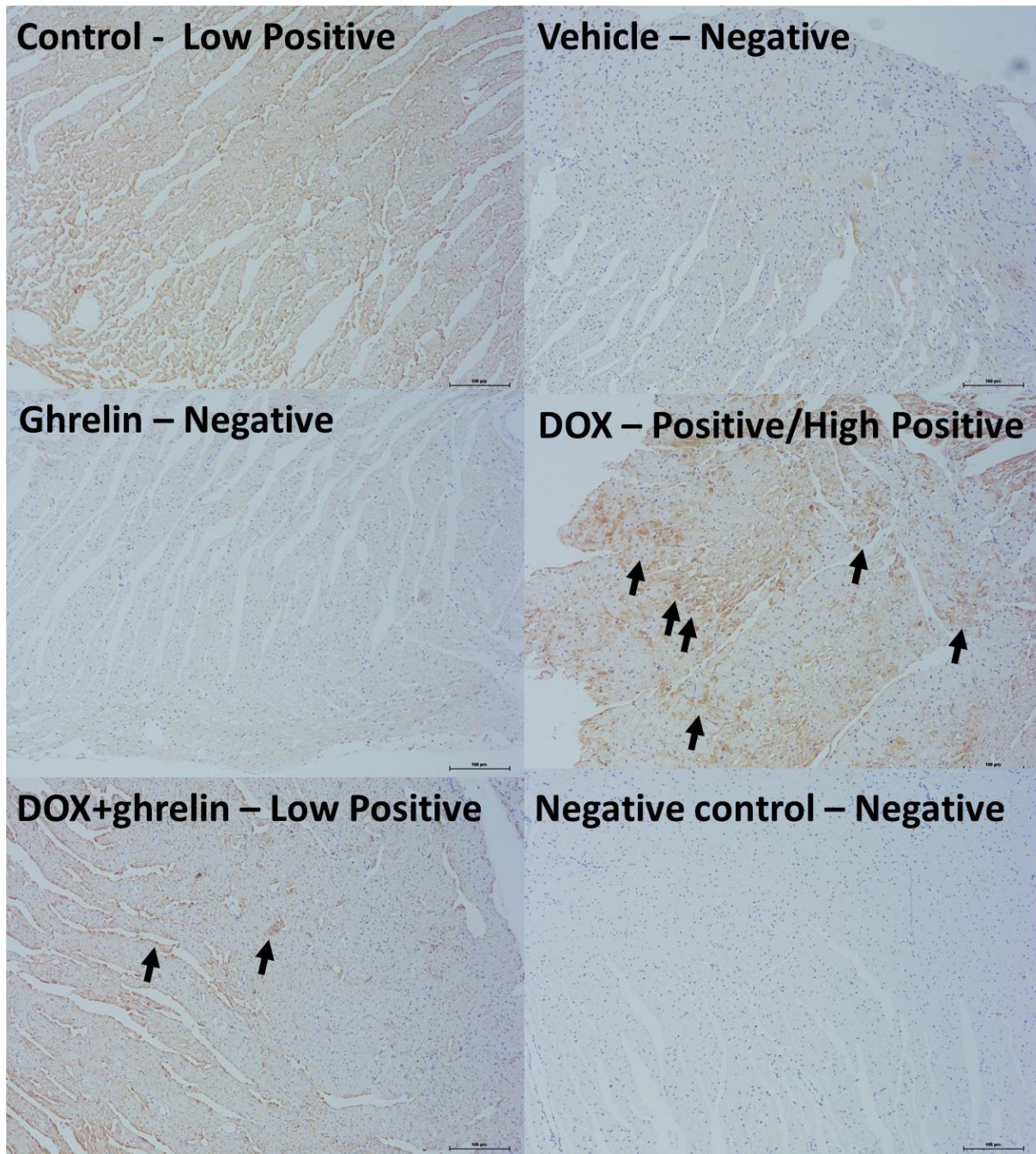
Figure 3.23: Immune reactivity of cytochrome c in heart tissue sections.

The representative images of left ventricular immunohistochemistry from rat myocardium are shown. Cytochrome c immune reactivity was scored using the IHC Profiler plugin for ImageJ. The overall score was assigned based on the pixel intensity of each image. Color shades were manually graded and assigned a score (high positive: 3+; positive: 2+; low positive: 1+; and negative: 0). Arrows indicate the brown precipitate caused by cytochrome c antibody binding. The negative control was obtained by omitting the primary antibody. Magnification: 10x, scale bar: 100 µm, n = 7 – 9. Abbreviations: IHC, immunohistochemical.
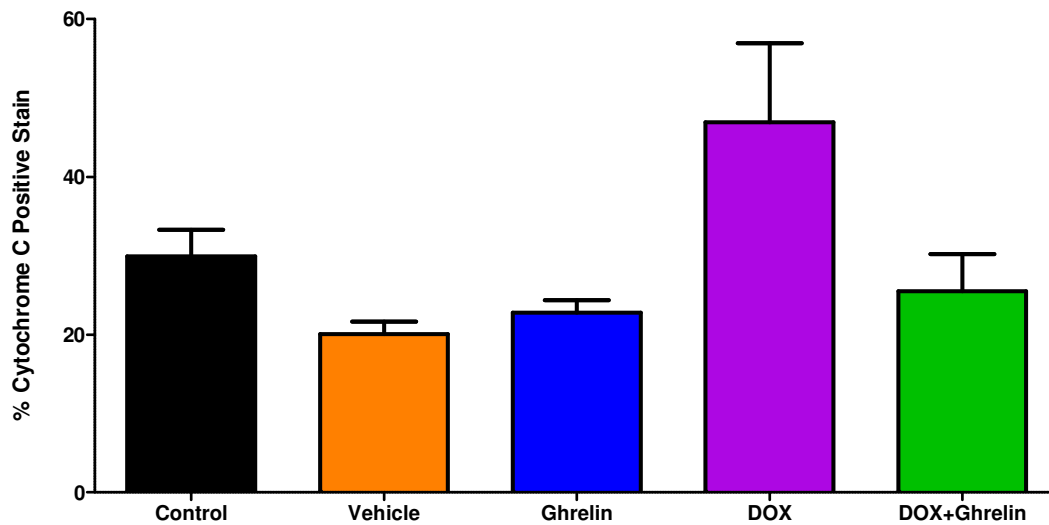
Figure 3.24: Quantification of cytochrome c immunohistochemistry.

The quantitative analysis of left ventricular immunohistochemistry from rat myocardium is shown. Cytochrome c immune reactivity was analysed using the IHC Profiler plugin for ImageJ. All values are presented as mean ± SEM, n = 7 – 9. Abbreviation: IHC, immunohistochemical.
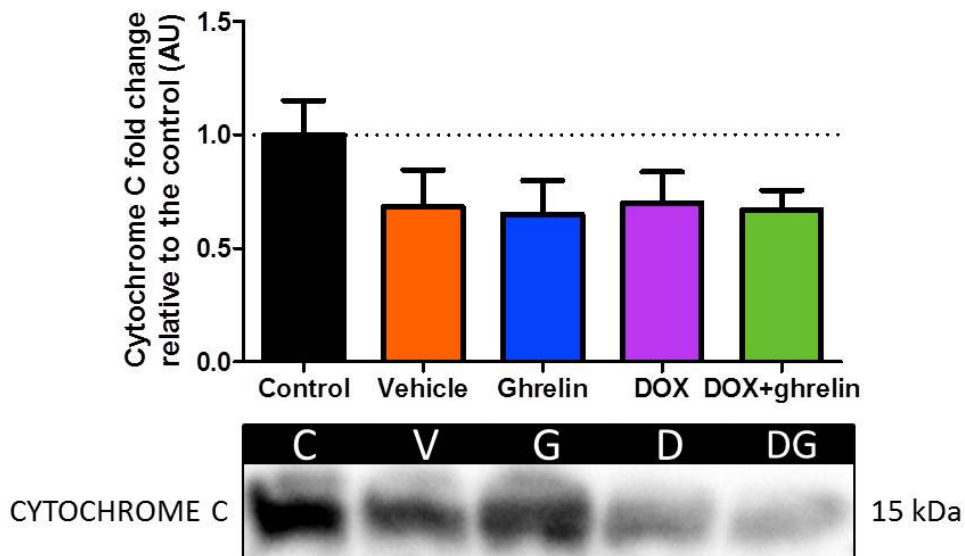
Figure 3.25: Protein expression of cytochrome c.

The lane analysis and western blots of cytochrome c are shown. Protein expression was normalized to the total lane protein. The fold change relative to the control was calculated. All values are presented as mean ± SEM, n = 7 – 9. AU, arbitrary units; C, control; V, vehicle; G, ghrelin; D, DOX; DG, DOX+ghrelin.

3.6.2 Caspase activity

Once the apoptotic pathway is activated, executioner caspases are recruited to cleave specific downstream proteins. The Caspase Glo® 3/7 assay was utilised to determine the activities of two executioner caspases that are further down the apoptotic pathway (Figure 3.26). Treatment with DOX significantly increased the activity of caspase-3 and -7 (67877 ± 15686 RLU, p< 0.0001) when compared to the control (13421 ± 1871 RLU). Co-administration of DOX and ghrelin significantly reduced caspase activity (36006 ± 3843 RLU, p< 0.05) when compared to treatment with DOX alone, confirming the anti-apoptotic activity of ghrelin.
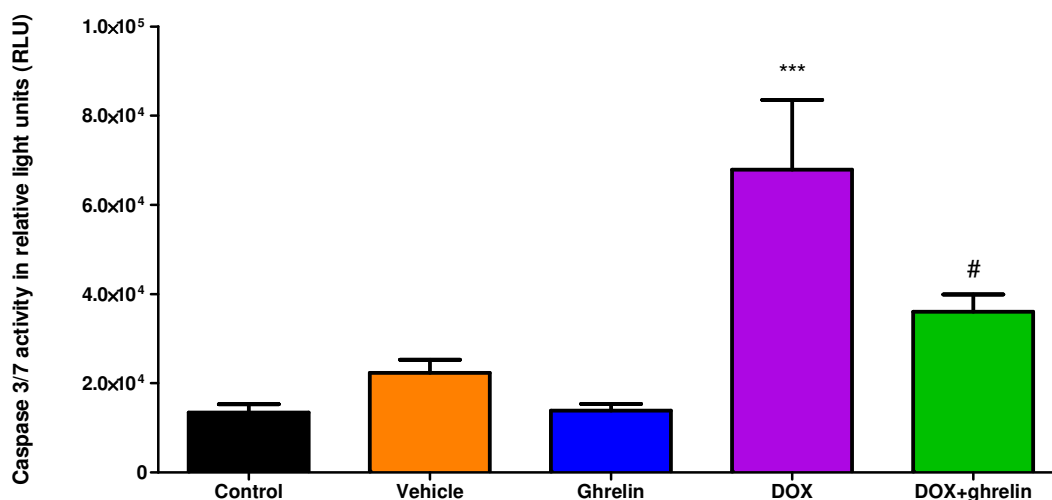
Figure 3.26: Caspase 3/7 activity.

The luminescent signal produced in this assay is directly proportional to caspase 3/7 activity. Caspase activity was determined in heart tissue homogenates. All values are presented as mean ± SEM, ***p< 0.001 vs control; #p< 0.05 vs DOX, n = 7 – 9. Abbreviations: RLU, relative light units.

3.6.3 Western blot analysis of cleaved PARP

One of the terminal events associated with apoptotic cell death is the cleavage and inactivation of PARP. Cleaved PARP is then unable to respond to and repair damaged DNA. To further validate the anti-apoptotic effects of ghrelin, the protein expression of cleaved PARP (Figure 3.27) was assessed with western blotting. Treatment with DOX significantly increased PARP cleavage (2.11 ± 0.24 fold change, p = 0.0081) when compared to the control (1.00 ± 0.09 fold change), not only indicating apoptosis, but also DNA damage. PARP cleavage was moderately reduced in the combination group, suggesting a reduction in apoptosis, although this did not differ statistically from the DOX alone group. Taken

together, our results confirm the anti-apoptotic effects of ghrelin as reported in previous studies.
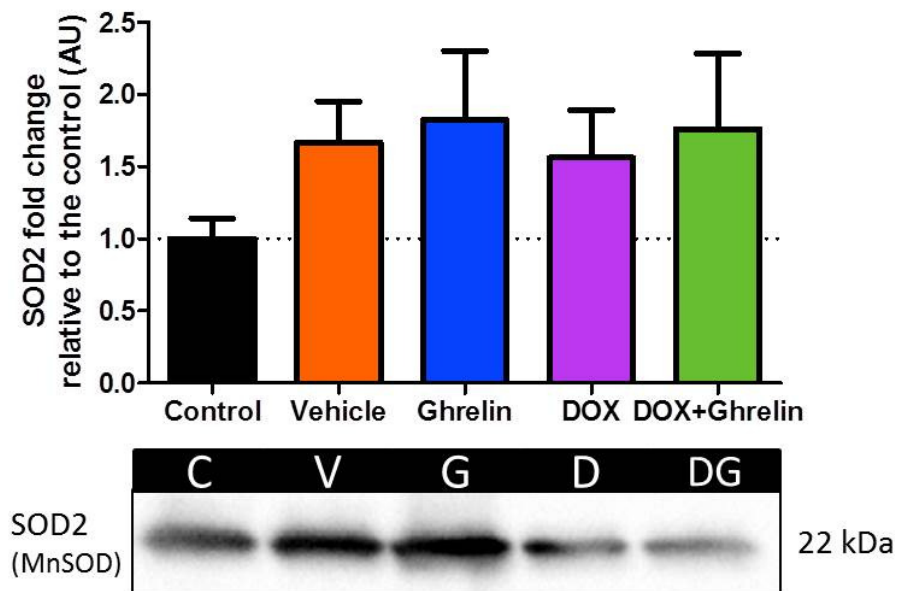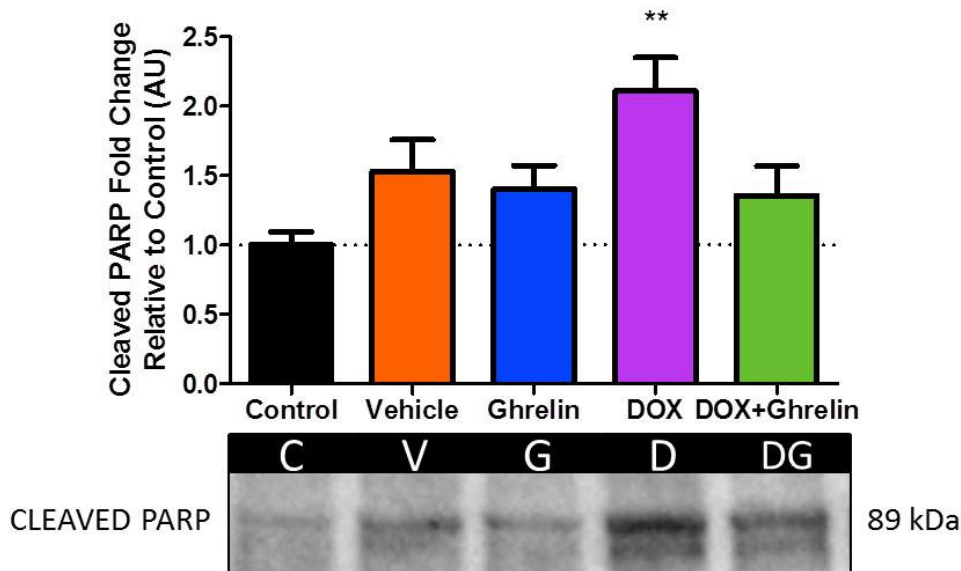

Figure 3.27: Protein expression of cleaved PARP.

The lane analysis and western blots of cleaved PARP are shown. Protein expression was normalized to the total lane protein. The fold change relative to the control was calculated. All values are presented as mean ± SEM, **$p< 0.01$ vs control, n = 7 – 9. AU, arbitrary units; C, control; V, vehicle; G, ghrelin; D, DOX; DG, DOX+ghrelin.

3.7 Ghrelin signaling does not involve the RISK pathway

3.7.1 Protein expression of ERK1/2 and Akt/PKB

Ghrelin has previously been shown to promote cellular survival by activating the pro-survival kinases, ERK1/2 and Akt/PKB (Baldanzi *et al.*, 2002). Similarly, it is ERK1/2 and Akt/PKB that prevent the apoptosis and oxidative stress during IRI. Therefore, we aimed to determine whether this pathway, the RISK pathway, was responsible for the anti-apoptotic and antioxidative effects of ghrelin during DOX treatment. Using western blot analysis, the protein expression of phosphorylated and total ERK1/2 was determined (Figure 3.28), however, there was no significant change in phospho- and total-ERK1/2 expression, or the phosphorylated to total protein ratio in any of the groups.
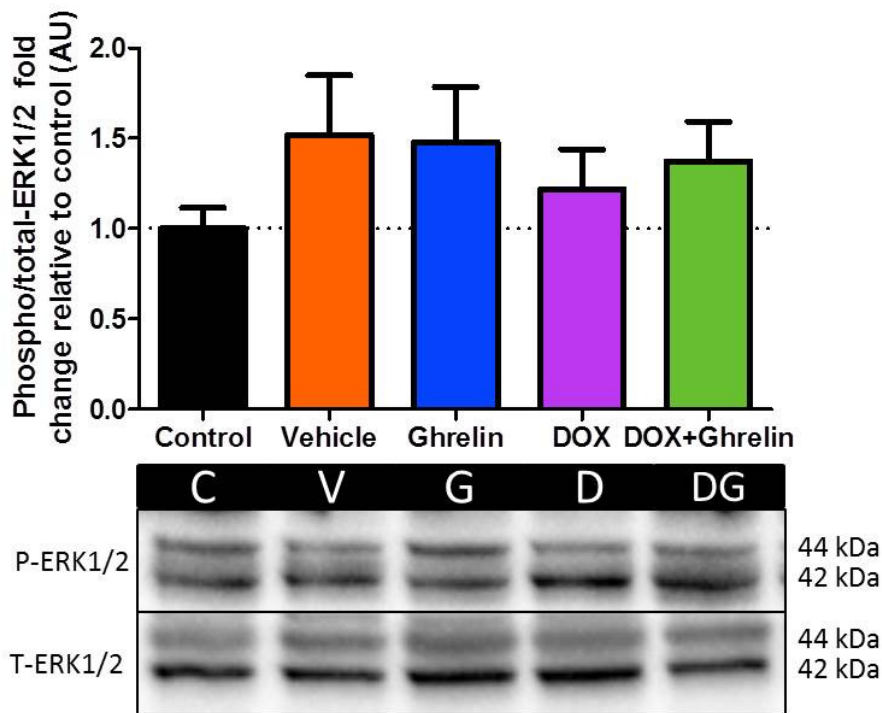
Figure 3.28: Protein expression of phosphorylated and total ERK1/2.

The lane analysis and western blots of phosphorylated and total ERK1/2 are shown. The band intensity was calculated as the sum of the 42 kDa and 44 kDa bands. Protein expression was normalized to the total lane protein, whereafter the results were expressed as the ratio of phosphorylated protein to total protein. The fold change relative to the control was calculated. All values are presented as mean ± SEM, n = 7 – 9. AU, arbitrary units; C, control; V, vehicle; G, ghrelin; D, DOX; DG, DOX+ghrelin.

Similarly to ERK1/2, there was no change in the phosphorylated or total forms of Akt in any of the treatment groups, however, there was a trend towards increased expression after treatment with DOX, although this is not significant. This data echoes the findings of our *in vitro* study (manuscript in preparation), where ERK1/2 and Akt/PKB were not expressed. These results suggest that ghrelin does not confer a protective effect via the RISK pathway, as we had initially predicted, and that a different pathway is in play.
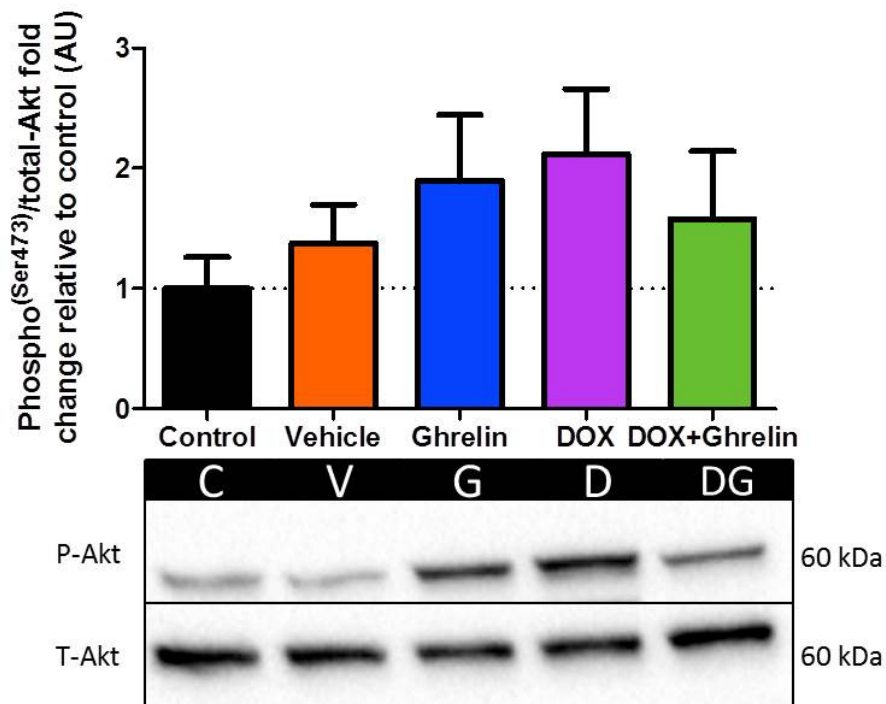
Figure 3.29: Protein expression of phosphorylated and total Akt.

The lane analysis and western blots of phosphorylated (serine 473) and total Akt are shown. Protein expression was normalized to the total lane protein, whereafter the results were expressed as the ratio of phosphorylated protein to total protein. The fold change relative to the control was calculated. All values are presented as mean ± SEM, n = 7 – 9. AU, arbitrary units; C, control; V, vehicle; G, ghrelin; D, DOX; DG, DOX+ghrelin.

3.8 Ghrelin protection involves the SAFE pathway

3.8.1 Inflammatory markers

The protein expression of TNF-α, as well as serum TNF-α, was measured not only as a marker of inflammation, but also because TNF-α is a known activator of the SAFE pathway. The SAFE pathway has also been linked to survival and thus we aimed to assess the role of ghrelin in stimulating this pathway during DOX treatment. After eight weeks of treatment, the western blot analysis of heart tissue lysates showed a significant increase in TNF-α protein expression after DOX treatment (2.77 ± 0.47 fold change, $p<0.01$) when compared to the control (1.00 ± 0.19 fold change). This suggests that treatment with DOX resulted in substantial inflammation within the heart. TNF-α expression was moderately reduced in the combination group, but this was not statistically different from the DOX group (Figure 3.30).
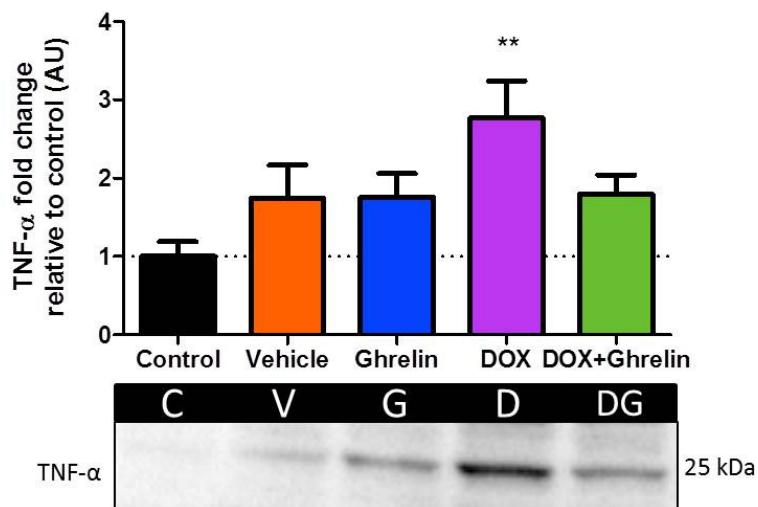
Figure 3.30: Protein expression of TNF-α.

The lane analysis and western blot of TNF-α are shown. Protein expression was normalized to the total lane protein and the fold change relative to the control was calculated. All values are presented as mean ± SEM, **p< 0.01 vs control, n = 7 – 9. AU, arbitrary units; C, control; V, vehicle; G, ghrelin; D, DOX; DG, DOX+ghrelin.

Unlike the western blot analysis of TNF-α, there were no changes in the serum concentration of TNF-α between any of the groups (Figure 3.31). This may be because the cardiomyocytes have produced the TNF-α protein but have not necessarily secreted it into the blood stream. During the processing of western blot samples, the 25 kDa transmembrane form of TNF-α is exposed, whereas TNF-α measured in the serum may not be available for antibody binding.
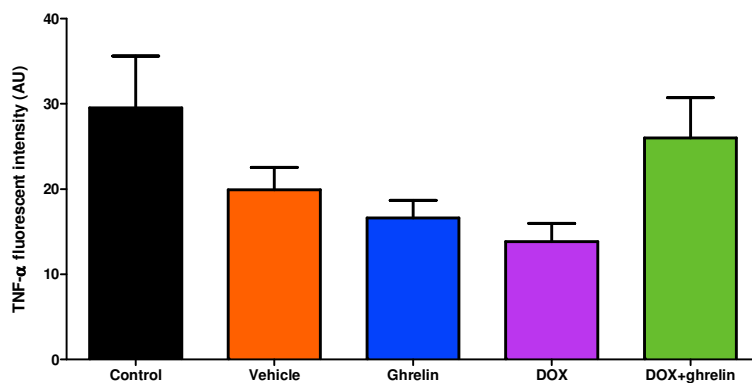
Figure 3.31: TNF-α fluorescent intensity.

The concentration of serum TNF-α is presented as the mean fluorescent intensity as extrapolation of concentration from the standard curve yielded results that were out of range. All data is presented as mean ± SEM, n = 7 – 9. AU; arbitrary units.

In addition to TNF-α, IL-6 was also measured as a marker of inflammation (Figure 3.32), however, no changes between the groups were observed. This may correlate with the serum TNF-α, suggesting that the inflammatory response had returned to baseline by the time of blood collection (one week after the last injections).
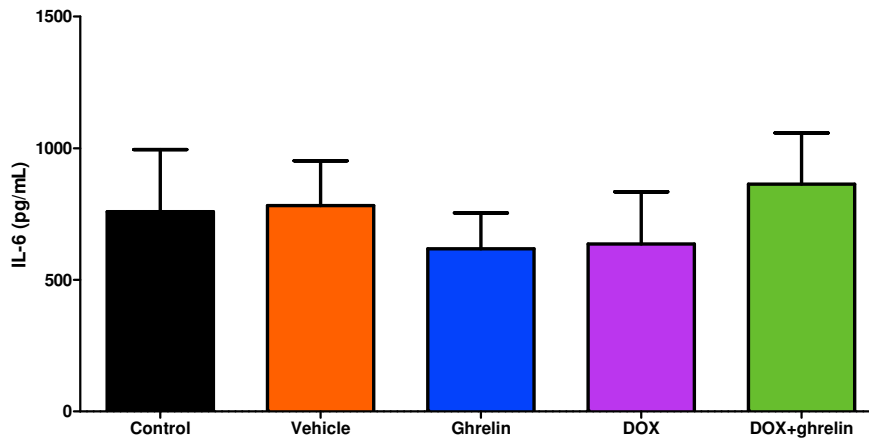
Figure 3.32: Serum concentration of IL-6.

The concentration of IL-6 was measured in rat serum after eight weeks of treatment. All data is presented as mean ± SEM, n = 7 – 9.

3.8.2 Protein expression of STAT3

To further explore the possible signaling pathways involved in ghrelin protection, we analyzed the protein expression of STAT3, since stimulation of this protein has proven to be beneficial during apoptosis and oxidative stress. Our western blot data demonstrates that serine727 phosphorylation of STAT3 was markedly reduced after DOX treatment, however, this was not significantly different from the control. Co-administration of DOX and ghrelin resulted in significantly increased STAT3 phosphorylation at this residue (6.76 ± 2.06 fold change, $p = 0.02$) when compared to DOX alone (0.27 ± 0.05 fold change). Total protein remained unchanged. Considering that the effects of TNF-α (detrimental or beneficial) are concentration dependent, we can speculate that the high levels of TNF-α observed in Figure 3.30 became detrimental. Despite high levels of TNF-α, the activation of the SAFE pathway was inhibited, possibly through the inhibition of JAK2 or by down-regulating STAT3 mRNA. In contrast, the moderately reduced levels of TNF-α following ghrelin treatment promoted a survival benefit by stimulating the SAFE pathway. Further research needs to be

performed in order to determine why the vehicle group elicited such a large response in STAT3 phosphorylation.
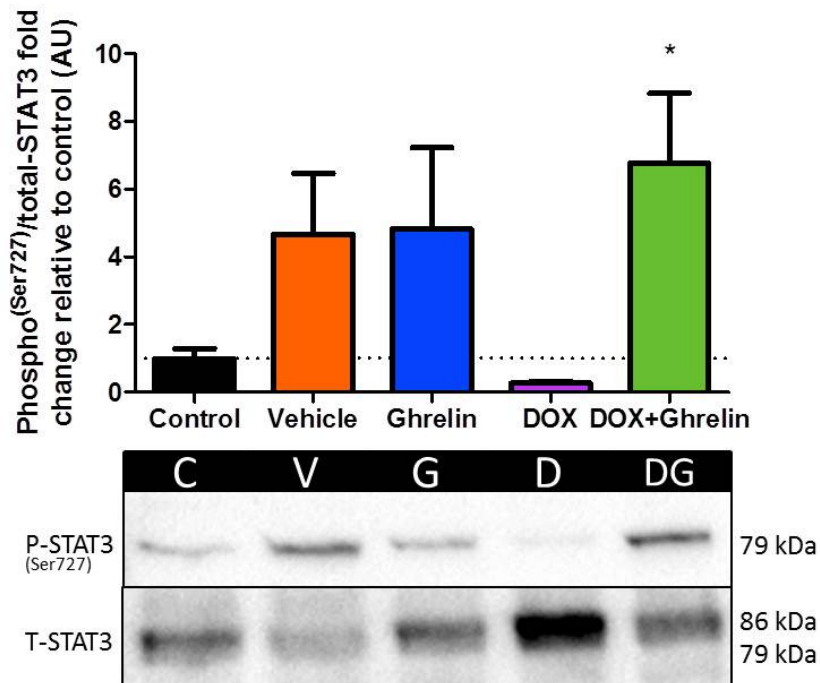
Figure 3.33: Protein expression of p-STAT3 [Serine727] and total STAT3.

The lane analysis and western blots of phosphorylated (Serine 727) and total STAT3 are shown. The band intensity was calculated as the sum of the 79 kDa and 86 kDa bands for total STAT3. Protein expression was normalized to the total lane protein, whereafter the results were expressed as the ratio of phosphorylated protein to total protein. The fold change relative to the control was calculated. Western blot analysis was performed on total protein as no fractionation was done. All values are presented as mean ± SEM, *p< 0.05, n = 7 – 9. AU, arbitrary units; C, control; V, vehicle; G, ghrelin; D, DOX; DG, DOX+ghrelin.

No changes were observed in tyrosine-phosphorylated STAT3 or total STAT3, however, a trend towards increased STAT3 phosphorylation was observed in the combination group. Although not part of the analysis of this study, JAK is responsible for the phosphorylation of STAT3 at this tyrosine residue (Kisseleva *et al*., 2002). Phosphorylation at the serine residue enhances the transcriptional activity of STAT3 (Boengler *et al*., 2008). The protein expression of p-STAT[Ser727] may therefore be upregulated to compensate for the lower expression of p-STAT[Tyr705].
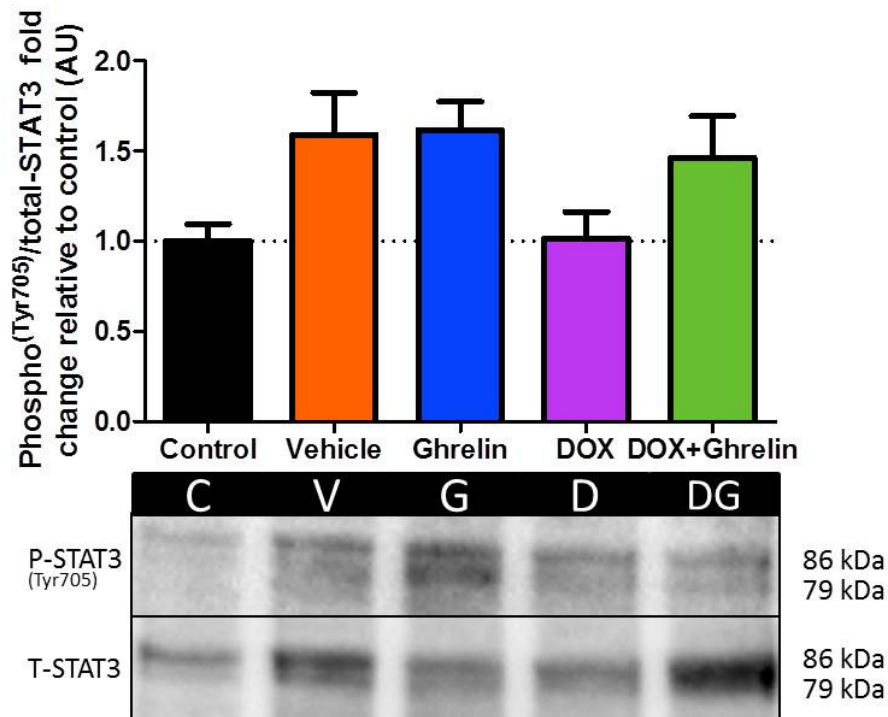
Figure 3.34: Protein expression of p-STAT3 ^Tyrosine705 and total STAT3.

The lane analysis and western blots of phosphorylated (Tyrosine 705) and total STAT3 are shown. The band intensity was calculated as the sum of the 79 kDa and 86 kDa bands. Protein expression was normalized to the total lane protein, whereafter the results were expressed as the ratio of phosphorylated protein to total protein. The fold change relative to the control was calculated. All values are presented as mean ± SEM, n = 7 – 9. AU, arbitrary units; C, control; V, vehicle; G, ghrelin; D, DOX; DG, DOX+ghrelin.

Chapter 4

Discussion

As the survival rate of cancer patients has improved due to early detection and advanced diagnostic tools, cardiovascular diseases associated with chemotherapy has now emerged as the leading cause of morbidity and mortality among cancer survivors. The major cause of cancer-associated cardiomyopathy is essentially the cardiotoxicity induced by cytotoxic drugs such as anthracyclines. Of these anthracyclines, DOX is among the most potent, leading to the development of heart failure in patients of both young and old age, and in those with pre-existing heart disease. While thousands of analogs of DOX have been produced, none have proved superior in terms of their cytotoxic action and reduced cardiotoxic side effects. Since the cytotoxic mechanisms of action of DOX have been differentiated from the cardiotoxic effects, there is hope that treatment strategies can be designed to target the adverse side effects of DOX without jeopardizing its anti-neoplastic capacity. With this in mind, this study explored the potential cardioprotective effects of ghrelin, a natural 'brain-gut' peptide with appetite-inducing effects, in a newly established *in* vivo model of chronic DOX-induced cardiotoxicity. Considering that chronic cardiotoxicity is accompanied by a very poor prognosis, it is imperative to develop chronic models of this condition in order to simulate the clinical effects more effectively. According to Doggrell and Brown (1998), the ideal animal model should **i)** mimic the human disease, **ii)** allow studies in chronic, stable conditions, **iii)** produce predictable symptoms, **iv)** meet economical, technical and ethical standards and **v)** allow for the measurement of appropriate cardiac and biochemical parameters. In the presented study, we established a rat model of chronic cardiotoxicity by injecting rats weekly with DOX for a prolonged period of time. Not only is the dose clinically relevant, but the weekly DOX schedule echoes the cumulative, dose-dependent nature of cardiotoxicity. This study aimed to simulate chronic cardiotoxicity, which is most commonly observed in the survivors of childhood cancers. Ghrelin has been documented to promote cellular protection through the activation of survival pathways like ERK1/2 and Akt/PKB. Through the activation of these pathways, ghrelin reduces oxidative stress and apoptosis in various models of heart failure. In addition, ghrelin promotes weight gain and appetite that may assist with maintaining general well-being and increasing tolerance to chemotherapy. These effects

therefore highlight a potential role for ghrelin in counteracting DOX-induced cardiotoxicity in the clinical setting.

4.1 Ghrelin induces appetite, maintains body weight and promotes general well-being

Ghrelin is most well-known for its appetite-inducing (Chang *et al*., 2005; Hiura *et al*., 2012; Akamizu & Kangawa, 2010) and growth-hormone stimulating actions (Date *et al*., 2002). This is an appealing property in the context of DOX-induced cardiotoxicity, as loss of appetite (Matsumura *et al*., 2004; Kristal *et al*., 2001) and cachexia (Ng *et al*., 1993) are commonly reported side effects during treatment with this anthracycline. We have also shown that rats treated with DOX experienced significantly slowed growth (the change in body weight over time) and decreased food intake (Figure 3.1 and Figure 3.3, respectively), whereas co-treatment with ghrelin maintained the growth rate and appetite of the rats at levels similar to the control. This data is supported by numerous other studies that reported reduced weight gain (Desai *et al*., 2013; Kihara *et al*., 2016) and food consumption (Chaudhary *et al*., 2016) during DOX treatment, and attenuation of these effects when ghrelin is administered (Wang *et al*., 2014; Neary *et al*., 2004; Hiura *et al*., 2012; Kihara *et al*., 2016). Ghrelin administration was also shown to prevent the cachexia associated with CHF in rats (Nagaya *et al*., 2001c). It would have also been interesting to measure fat pad mass, especially because DOX treatment is known to cause weight loss and ghrelin treatment increases fat storage. The reduced weight gain in the DOX treated group may have been as a result of fat loss, whereas the maintenance in weight gain in the combination group may have been due to fat gain.

In our study, food consumption was measured three times a week on the morning before injections were administered. Although it was expected that ghrelin alone would cause a potent increase in food intake, this effect was not seen in the current study. Similarly, Shintani *et al*., (2001) reported a significant increase in food intake four hours after ghrelin administration, but no difference after 24 hours. A reason for this is that food intake after a ghrelin injection occurs in under 60 minutes in rodents, which means that daily food intake measurements (every 24 hours) can easily be missed (Wren *et al*., 2000). In addition, the orexigenic effects of ghrelin are more powerful when ghrelin is administered centrally (intracerebroventricular), rather than peripherally (i.p), as in our study. Nevertheless, ghrelin appeared to maintain appetite when administered together with DOX, supporting its role as an appetite-stimulating peptide. From the stomach, ghrelin is released into the blood stream where it travels to and acts on the anterior pituitary gland after crossing the blood-brain

barrier (Kojima *et al.*, 1999; Banks *et al.*, 2002). While the exact mechanisms are still not completely understood, ghrelin administration has been shown to stimulate neurons in the arcuate nucleus, increasing the mRNA expression of NPY and AgRP, which in turn promote appetite (Shintani *et al.*, 2001). In addition to increasing appetite, ghrelin also decreases fat utilization (Tschöp *et al.*, 2000), inducing an overall increase in body weight (Strassburg *et al.*, 2008). Furthermore, the resulting positive energy balance is needed for maximizing the anabolic effects of GH. GH release, together with an increase in food intake, would contribute to the increased body weight observed in this study. Ghrelin and its receptors have also been identified in other organs of the body such as the liver, the kidneys and the pancreas. In the liver, treatment with ghrelin has been shown to reduce inflammation and oxidative stress in response to non-alcoholic fatty liver disease (Li et al., 2013). In the pancreas, studies have yielded conflicting results, with some indicating that ghrelin inhibits insulin release and others suggesting that ghrelin stimulates insulin release (Kageyama et al., 2005). In the kidney, ghrelin has been demonstrated to reduce renal injury and improve excretory function during ischemic renal failure (Vasileiou et al., 2013). Importantly, ghrelin administration does not appear to exert any adverse side effects in any of the organs.

Although other studies administered ghrelin every day, twice a day, we aimed to obtain similar results but with a less severe injection protocol, and therefore only administered ghrelin three days of a week. Ghrelin still elicited a protective effect in DOX-treated rats, but this effect may have been enhanced with an increase in ghrelin administration. Despite having a half-life of less than 60 minutes (Tolle *et al.*, 2002), we were able to detect ghrelin in rat serum from blood samples that were collected one week after the treatment protocol (Figure 3.11). It is possible that the ghrelin that was measured was naturally endogenous ghrelin, or that the exogenous ghrelin injections induced lasting effects. As expected, significantly higher ghrelin levels were measured in the serum of the ghrelin-treated group, however, what was surprising was the undetectable ghrelin levels in the DOX group. Considering that DOX-treatment was associated with reduced food intake, ghrelin levels should have been increased to signal hunger, however, the undetectable levels suggest that many of the negative side effects associated with DOX treatment may occur due to an inhibitory effect that DOX has on ghrelin. We can only speculate that DOX may damage the ghrelin-producing cells in the stomach or that DOX interferes with ghrelin once it has been secreted and is traveling to the brain. When ghrelin was administered in combination with

DOX, the level of serum ghrelin increased slightly. It is possibly this restoration of endogenous ghrelin that is responsible for its beneficial effects. Supporting our data, Beiras-Fernandez *et al*., (2010) also reported significantly reduced ghrelin expression in human hearts with CHF, further associating reduced ghrelin levels with maladaptation and the development of heart failure. In contrast to this, Nagaya *et al*., (2001b) and Xu *et al*., (2007) observed an increase in ghrelin levels in models of heart failure and concluded that ghrelin increases as a compensatory protective mechanism. This suggests that ghrelin increases to overcome the cytotoxic effects induced by DOX. These contradictory findings can be explained by the types of models studied, as ghrelin was measured in human myocardial biopsies, human plasma and in acute *in vivo* rat models of cardiotoxicity. The assay used for measuring ghrelin does have relatively good sensitivity (1 – 62 pg/mL) and its performance is measured using quality controls. However, since this is a multiplex assay that measures several different analytes, each with their own optimal conditions for measurement, we may have obtained more sensitive results if we had made use of an ELISA specifically for ghrelin.

Weight loss during chemotherapy can have a poorer outcome for the patient (Ross *et al*., 2004), therefore by promoting and maintaining appetite during DOX treatment, ghrelin preserves body weight and results in reduced morbidity, an improved quality of life and a better prognosis. In our study, DOX-treated rats began to show the clinical signs that are indicative of (but not limited to) heart failure approximately half way through the treatment protocol. In addition to weight loss, these signs included pale and cool extremities (cyanosis), passive behaviour, reduced grooming and boney frame, observations that are in agreement with Spivak *et al*., (2013). The rats that received both DOX and ghrelin did not present with these symptoms, highlighting that ghrelin is able to maintain general well-being during treatment with chemotherapy. This can possibly be attributed to the effects that are occurring on a molecular level, such as reduced cardiomyocyte apoptosis and oxidative stress.

4.2 Ghrelin improves antioxidant status during DOX treatment

Oxidative stress is believed to be one of the major contributors to the development of cardiotoxicity. The oxidative stress theory remains one of the leading hypotheses for DOX-induced cardiotoxicity because several antioxidants have proven to be successful *in vitro* and *in vivo* (Zhang *et al*., 2013; Alshabanah *et al*., 2010; Patil & Balaraman, 2011; Panchuk *et al*., 2014). However, many antioxidant therapies have failed to offer protection in the clinical setting (Ladas *et al*., 2004; Myers *et al*., 1983). In an effort to determine the antioxidant

properties of ghrelin, oxidative stress, antioxidant capacity and antioxidant status were evaluated by numerous mechanisms. As mentioned previously, DOX induces oxidative stress by producing free radicals during redox cycling and through interactions with iron. The DOX-induced increase in reactive species explains the significant conjugated diene content in the heart in the DOX-treated animals (Figure 3.17). In this scenario, ghrelin may quench free radicals through unknown mechanisms and thereby limit the oxidation of membrane lipids by these radicals, as ghrelin co-treatment significantly reduced the conjugated diene content in the heart compared to DOX alone. This is in agreement with several other studies, including studies on DOX-induced cardiotoxicity, which all reported reduced oxidative stress after ghrelin treatment (Li *et al*., 2013; Xu *et al*., 2008; Li *et al*., 2006b; Chang *et al*., 2004b), as indicated by reduced conjugated dienes and MDA. In our study however, the level of MDA measured by the TBARS assay remained unchanged (Figure 3.18). This result can be explained by the fact that MDA is a late marker of lipid peroxidation, and therefore the extent of lipid peroxidation at the time of harvesting the heart, was not severe. In obese individuals, a state associated with chronic inflammation, the low circulating ghrelin levels have been linked to increased oxidative stress (Suematsu *et al*., 2005). This may extend to cardiotoxicity, a disease characterized by similar levels of inflammation, where low ghrelin levels during DOX treatment may result in elevated oxidative stress.

The presence of cellular antioxidants protects against the damaging effects of free radicals, and according to Xu *et al*., (2008), ghrelin's antioxidative effects are induced through the upregulation of endogenous antioxidants. Our study thus evaluated the activity (Figure 3.20) and expression of SOD (Figure 3.21 and Figure 3.22) as $O_2^{\bullet-}$ is proposed to be the origin of most reactive species (Indo *et al*., 2015; McCord & Fridovich, 1969) and the oxidant produced during redox cycling of DOX. Neither the activity nor the expression of SOD1 (CuZn) and SOD2 (Mn) resulted in any significant changes in this study. While these observations are in contrast to what others have shown (Kheradmand *et al*., 2010; Xu *et al*., 2008), a likely possibility for our insignificant results is that this study did not separate the cytosolic fraction from the mitochondrial fraction where SOD1 and SOD2 are located, respectively. Although the myocardium is known to naturally express relatively low levels of this antioxidant (Doroshow *et al*., 1980), ghrelin itself might be exerting the antioxidative effect. In a similar manner, no change was observed in the antioxidant capacity results (Figure 3.19) between any of the groups. This may suggest that the free radicals produced did

not necessitate a change in the antioxidant capacity of the myocardium. Perhaps when free radicals overwhelm the antioxidant defense of the myocardium and MDA, a late marker of oxidative stress, is detected will the levels of these parameters change. In addition, the activities of other antioxidants such as GSH are not reflected in the ORAC assay.

GSH is another important antioxidant which exists in both reduced (GSH) and oxidized (GSSG) states. GSH acts as a substrate for GSH-Px1, which is involved in detoxifying reactive species in the cell. In healthy cells and tissues, approximately 90% of the total GSH pool is in the reduced form, whereas 10% exists in the oxidized form. In the reduced state, thiol groups from cysteine molecules donate reducing equivalents to ROS, resulting in an increase in GSSG (Palwankar *et al*., 2015). Therefore, an increased GSH: GSSG ratio is indicative of oxidative stress. As demonstrated in Table 5, DOX significantly increased GSSG while ghrelin, in the presence of DOX, reduced these levels. A similar effect was observed when analyzing the ratio of GSH: GSSG, indicating oxidative stress in the DOX-treated animals, although this was not significant. The myocardial GSH pool has been shown to be depleted after DOX treatment (Zhou *et al*., 2001; Zanwar *et al*., 2013). The fact that the levels of GSSG increased during DOX treatment indicates increased GSH-px1 activity, as GSH-Px1 used GSH to detoxify the ROS induced by DOX. Ghrelin, in the presence of DOX, may further increase GSH-Px1 activity in an attempt to neutralize reactive species. Ghrelin may also reduce oxidative stress by improving the antioxidant status in the cell. We can speculate that ghrelin assists in converting GSSG back into GSH by increasing the activity of GR (Dobutovic *et al*., 2014). Ghrelin therefore enhances the hearts ability to neutralize free radicals and overcome oxidative stress which, if left uncontrolled, would lead to cell death.

4.3 Ghrelin reduces myocardial injury by preventing apoptosis

It is common knowledge that oxidative stress, when in excess, can trigger apoptotic cell death. Apoptosis in the myocardium is an essential determinant of the pathogenesis of heart failure, as it results in the loss of contractile units and myofibers. In addition, the contribution of apoptosis to DOX-induced cardiotoxicity has been extensively reported (Baldanzi *et al*., 2002; Chen *et al*., 2012; Nakamura *et al*., 2000; Green & Leeuwenburgh, 2002). In agreement with these studies, we have also shown a potent increase in apoptotic cell death in the myocardium of DOX-treated rats. Considering that cardiac function has been shown to be improved once cardiomyocyte apoptosis is inhibited experimentally (Chen *et al*., 2007), inhibiting apoptosis is a potentially effective treatment strategy. Our results are testament to

this, as co-treatment with ghrelin attenuated the apoptotic cell death in the myocardium. The mitochondria are pivotal in regulating apoptosis, as they respond to signals which trigger the release of cytochrome c and the activation of the caspases. In our study, apoptosis was measured using cytochrome c (Figure 3.23 - Figure 3.25), caspase-3 and -7 activities (Figure 3.26) and cleaved PARP (Figure 3.27), indicative of the intrinsic apoptotic pathway (Childs *et al*., 2002). In all cases, DOX increased apoptosis and ghrelin attenuated it. In response to stress stimuli such as oxidative stress, cytochrome c is released from the mitochondria, triggering the intrinsic apoptotic pathway. The oxidative stress induced by DOX treatment results in DNA damage, further enhancing apoptosis. Under normal conditions, this damage is usually repaired by PARP (Cohen, 1997), however, the executioner caspases recruited during apoptosis cleave PARP, resulting in its inactivation. This explains why each of these parameters, cytochrome c, the caspases and cleaved PARP are all increased following DOX treatment. Following co-treatment with ghrelin, cytochrome c, caspase activity and PARP cleavage were reduced, indicating that ghrelin reduces mitochondrial-dependent apoptosis. It is possible that ghrelin prevents depolarization of mitochondrial membrane potential by blocking the opening of the mPTP (Chung *et al*., 2007). It has been shown that even very low levels of cardiomyocyte apoptosis (four-fold lower than observed during heart failure in humans) are sufficient to induce lethal cardiomyopathy (Wencker *et al*., 2003). This was attributed to caspase activation, which supports our own findings. The reduced apoptosis following ghrelin treatment not only improved cell survival, but also maintained cellular morphology (Wang *et al*., 2014).

4.4 Ghrelin reduces cardiomyocyte fibrosis and atrophy

Fibrosis typically involves four phases including hemostasis, inflammation, proliferation and remodeling (see Diegelmann and Evans, (2004) for full review). During hemostasis and inflammation, specific cytokines recruit macrophages and neutrophils to the site of injury, where they in turn activate resident fibroblasts. Increased collagen, produced by proliferating fibroblasts, then invades and replaces the apoptotic cardiomyocytes (Khan & Sheppard, 2006). Tissue damage and inflammation increase the production of ROS which further enhances the release of factors involved in fibrosis. Fibrosis is therefore an important part of repair, but its accumulation can result in organ dysfunction, and eventually failure. In this study, we have shown that DOX treatment causes significant fibrosis in the rat heart and that co-treatment with ghrelin appears to alleviate this effect (Figure 3.13 and Figure 3.14). This

is consistent with several studies that all reported reduced fibrosis by ghrelin in mouse models of DOX-induced cardiotoxicity (Pei *et al*., 2014; Kihara *et al*., 2016; Wang *et al*., 2014). Furthermore, ghrelin has also been shown to reduce fibrosis and collagen formation in isoproterenol-induced cardiac injury (Li *et al*., 2006) and myocardial infarction (Soeki *et al*., 2008), respectively. In these studies, fibrosis was assessed using both histological and biochemical parameters. The activation of fibroblasts occurs after exposure to profibrotic cytokines such as TNF-α and transforming growth factor beta (TGF-β) (Roberts *et al*., 1986; Ihn, 2002). In addition, TGF-β induces the expression of connective tissue growth factor (CTGF), which is responsible for enhancing the growth of fibroblasts and the secretion of extracellular matrix (Accornero *et al*., 2015). Pei *et al*., (2014) showed increased expression of CTGF in DOX-treated hearts and reduced transcription of CTGF when ghrelin was administered in combination with DOX. This may explain how ghrelin prevents the formation of fibrosis during DOX treatment.

The histological changes associated with DOX treatment consist not only of fibrosis, but also of cytoplasmic vacuolization and myofibrillar loss (Šimůnek *et al*., 2004; Gava *et al*., 2013). Such changes ultimately result in cardiac remodeling and the development of heart failure (Rahman *et al*., 1986; Lefrak *et al*., 1973). We have shown that DOX treatment significantly reduces the size of cardiomyocytes in rat hearts (Figure 3.15 and Figure 3.16), indicative of atrophy and a cachectic state. Similar findings have been reported in patients treated with Daunorubicin, with signs of atrophic muscle cells (Buja *et al*., 1973). Treatment with DOX induced vacuolization, disorganization of muscle fibers and a loss in the typical striation pattern seen in healthy heart cells, whereas treatment with ghrelin maintained cardiomyocyte size and restored organization. This has also been reported by Wang *et al*., (2014) in a mouse model of cardiotoxicity. The attenuation of cardiomyocyte atrophy by ghrelin may correlate with the increase in body weight that was observed in this group, suggesting an anti-cachectic effect. Autophagy is a well-conserved process for degrading and recycling cellular components such as organelles and proteins and as such, it can exert pro-survival and pro-death functions (Dalby *et al*., 2010). Autophagy was found to be upregulated in both mouse hearts and cell cultures following DOX treatment, and this was associated with a reduction in cardiomyocyte size (Wang *et al*., 2014). In fact, autophagy has been observed in atrophic cells and therefore plays an important role in the heart (Nishida *et al*., 2009; Vellai *et al*., 2008). Co-treatment with ghrelin significantly reduced the DOX-induced autophagy, which

resulted in an increase in the cross-sectional area of the cardiomyocytes (Wang *et al*., 2014). This excessive DOX-induced autophagy was also associated with increased apoptotic cell death, which may explain the elevated apoptosis in our own study. Ghrelin may therefore attenuate cardiomyocyte atrophy by reducing the levels of autophagy (and apoptosis) in the heart. Importantly, ghrelin alone had no effect on myocyte size of fibrosis or atrophy. Fibrosis and loss of myofibers has been shown to cause myocardial dysfunction after DOX treatment (Miyata *et al*., 2010; Chatterjee *et al*., 2010), providing a causal link between the pathohistological changes observed in our study and poor cardiac function.

4.5 Ghrelin maintains cardiac function during DOX treatment

The molecular events discussed in the preceding sections, namely cachexia, oxidative stress, apoptosis and the pathohistological changes observed, all contribute to the development of cardiac dysfunction. In the clinical setting, DOX is administered in doses of $50 - 75$ mg/m^2 on a three week cycle (Swain *et al*., 1997b). The lifetime cumulative dose is generally set to less than 500 mg/m^2 to reduce the risk of cardiomyopathies (Yi *et al*., 2006). In this study, rats were treated with a cumulative dose of 20 mg/kg, which is equivalent to the human dose of between $53.3 - 71$ mg/kg^2 (Desai *et al*., 2013). This is calculated by multiplying the animal dose by a factor that is relative to the animal's body surface area. Therefore the conditions of this study are an appropriate simulation of chronic cardiotoxicity and closely resemble the characteristics of heart failure that are observed in a clinical setting. Ghrelin is predominantly produced in the stomach, but the fact that ghrelin and its receptor are also located in the heart suggests a role for cardioprotection. Functional data is important to confirm a cardioprotective role of ghrelin and this was achieved through working heart perfusions. To the best of our knowledge, our study and the study by Hayward *et al*., (2013) are the only two that make use of the isolated working heart to study DOX-induced cardiac dysfunction. This model is important as it is a more physiologically relevant simulation of a beating heart than the Langendorff technique.

Chronic cardiotoxicity can occur decades after the completion of treatment, which means that patients may remain in an asymptomatic state for several years until events such as viral infections (Ali *et al*., 1994) act as stressors that trigger cardiotoxicity. In this study, subjecting the heart to 40 minutes of perfusion can be compared to a stressor, and our results clearly demonstrate that the DOX-treated hearts are unable to cope with this stress, resulting in a gradual decline in function (Xu *et al*., 2007; Xiong *et al*., 2006). This was observed in both

the measured (aortic output, coronary flow) and calculated (cardiac output, LVDP, RPP, total work) parameters (Figure 3.4 - Figure 3.10), confirming the presence of chronic DOX-induced cardiotoxicity. The consistent trend in dysfunction across all parameters also indicates that the perfusion technique was performed correctly. Bell *et al*., (2011) states that coronary flow for a rat should be approximately 20 mL/minute (>10, <28) and that heart rate on the perfusion apparatus should be between 250 – 320 beats per minute, which is consistent with the results we obtained. Our results also show that ghrelin preserves cardiac function during DOX treatment. Aortic flow rate was significantly improved after co-treatment with ghrelin, and the moderate improvement in the other parameters of the DOX+ghrelin group produced results similar to that of the control hearts. In line with our results, other studies have reported that ghrelin administration does not alter heart rate or blood pressure, but significantly improves coronary flow after ischemia reperfusion (Chang *et al*., 2004a), cardiac output during CHF (Nagaya *et al*., 2001c) and left ventricular function in healthy humans, isoproterenol-induced myocardial injury and DOX-treated rats (Pei *et al*., 2014; Wang *et al*., 2014; Xu *et al*., 2010; Enomoto *et al*., 2003). Although no change in heart rate or blood pressure was observed, co-administration with ghrelin still improved aortic output. This can possibly be explained by the fact that DOX has been shown to increase aortic stiffness, and ghrelin may therefore maintain the elasticity of the aorta (Jenei et al., 2013). Ghrelin has been shown to reduce apoptosis and oxidative stress, which might explain the maintained cardiac function that was observed in DOX+ghrelin group. Pei *et al*., (2014) reported that ghrelin reduced the apoptosis caused by DOX treatment and substantially improved cardiac dysfunction in a mouse model of DOX-induced cardiomyopathy. The results obtained in our study are of value because they were obtained from a chronic model, as opposed to the acute studies, however, it seems that regardless of the model used, ghrelin treatment is able to ameliorate cardiac dysfunction. Importantly, ghrelin alone did not affect the cardiac function in normal rats. Although the lack of fatty acids in the KHB may suggest that the hearts were energy starved during the perfusions, the composition of this buffer, with glucose instead of fatty acids, relies on the hearts ability to extract energy from multiple substrates (Bell et al., 2011). In addition, the relatively short perfusion protocol, and the fact that this was not a metabolic study, did not necessitate the use of fatty acids. Not only are fatty acids difficult to dissolve, but they can also result in frothing and foaming when the buffer is oxygenated. If the hearts were starved of oxygen then this would have been evident

in the control rats, but we obtained functional data with values within the recommended range.

Various factors effect cardiac output, including heart rate, contractility, preload and afterload. According to Vincent, (2008), cardiac output can be seen as analogous to riding a bicycle. The pace at which a cyclist pedals will determine the speed that the bicycle will go. If the cyclist pedals too fast for too long, he will tire and be unable to maintain his level of pedaling, but if he pedals too slowly, he will not move fast enough to cover his required distance. The same applies to the heart, where bradycardia or tachycardia results in impaired cardiac output. However, heart rate remained unchanged during DOX treatment, implying that it is not a change in heart rate that is responsible for DOX-induced cardiac dysfunction. Contractility is also a determining factor of cardiac output: the more a cyclist flexes his muscles and pushes on the pedals, the faster the bicycle will go. Too little pedal power, equated to reduced contractility of the heart, will result in reduced cardiac output, however, too much effort can result in fatigue, forcing the heart to slow down or stop. This may be the case for DOX-induced cardiotoxicity, as the decline in cardiac output is gradual and worsens over the 40-minute perfusion protocol. In addition, the total work performed by the left ventricle declined early on in the perfusion protocol, indicating that the power of the heart was reduced. DOX-induced apoptotic cell death of cardiomyocytes might explain a reduction in contractility and hence, overall cardiac function. GH and its mediating hormone, IGF-1 have been shown to promote physiological hypertrophy during CHF in rats, thereby improving cardiac function (Cittadini *et al*., 1997). Nagaya *et al*., (2004) reported a potent increase in GH release following ghrelin administration in patients with CHF. This finding may therefore explain one of the mechanisms by which ghrelin maintains cardiac function during DOX treatment. In addition, the improvement in cardiac function by ghrelin during CHF in rats has been attributed to reduced apoptosis and the production of pro-inflammatory cytokines (Huang *et al*., 2009).

Supplementary to the functional results, we also examined the levels of various markers of damage. Myocardial markers should not only assist with patient diagnosis, but also allow for the estimation of the extent of myocardial damage. We reported a significant increase in serum CK-MB in all groups treated with DOX. On the one hand, CK-MB became a marker of choice due to greater myocardial specificity (it is the isoform that is most abundant in the

heart), but on the other hand, it is released in response to both myocardial and skeletal muscle injury (Adams *et al*., 1993a). In fact, studies have shown that CK-MB released from skeletal muscle injury persists in the blood for longer periods of time (Adams *et al*., 1993b). CK-MB was measured one week after the last DOX injection in our study, so the fact that we still obtained such high levels suggests that it might be of skeletal muscle origin. The troponins are another set of useful markers of damage, as they circulate at low concentrations and increase rapidly in response to even mild cardiac injury. Therefore, their presence in the blood allows for CK-MB elevations as a result of skeletal muscle damage to be distinguished from those resulting from cardiac injury. Adams *et al*., (1993) also reported that cTnI does not appear in the blood, even when CK-MB is elevated, unless there is concomitant cardiac injury. We did not observe any changes in the troponins in the study, further indicating that the elevated CK-MB might be from DOX-induced skeletal muscle injury. However, we did not observe any changes in the ratio of gastrocnemius muscle weight to body weight (data not shown), suggesting that the elevated CK-MB may have partly arisen from the heart as well. In support of our own observations, several other studies also reported elevated CK-MB levels in response to DOX treatment (Yagmurca *et al*., 2003; Mohamed *et al*., 2004; Mitra *et al*., 2007). In most studies it is reported that CK-MB release does correlate with other evidence of myocardial injury, and the reduced cardiac function and apoptotic cell death in our study is evidence to support this. It must also be noted that the studies by Adams *et al*., focused on acute myocardial infarction and therefore these markers may be expressed differently in other forms of myocardial injury. The troponins are early markers of damage and their levels may have already returned to baseline by the time we collected blood for measurement (Dolci *et al*., 2008). These markers may be useful for predicting the development of cardiotoxicity (Cardinale *et al*., 2000; Kilickap *et al*., 2005), but offer no value when cardiotoxicity is already present. Bertinchant *et al*., (2003) reported no changes in cTnI and only observed an increase in cTnT. This can be attributed to antibody specificity and the sensitivity of the assay used. Holmgren *et al*., (2015) reported elevated cTnT levels one and two days after DOX treatment *in vitro*, but no differences beyond seven days. Furthermore, Childs *et al*., (2002) reported that cTnT was not increased even just four days after DOX treatment in rats. This observation, consistent with our findings, suggests that the troponins are released early after damage and that alternative markers should be used when assessing signs of damage during chronic cardiotoxicity.

Myocardial BNP was also unchanged in all of the treatment groups. BNP has been suggested as an early marker that *predicts* cardiac dysfunction (Skovgaard *et al*., 2014) and is present before the clinical symptoms of heart failure. BNP may therefore not be present when cardiac dysfunction is already evident, as in our study and that of Kihara *et al*., (2016). BNP is rapidly produced by the heart in response to ventricular distension (Iwanaga *et al*., 2006), however we have shown a reduction in cardiomyocyte size (as opposed to enlargement), which may further explain why there was no change in BNP. Finally, upon damage, BNP is released by the heart into the circulation (Nakao *et al*., 1990). In our study, the hearts were flushed with KHB for 40-minutes during the perfusions, and therefore any BNP in the hearts circulation may have been washed out in the effluent. Taken together, the measurement of markers such as cTnT, cTnI and BNP are useful for predicting the future development of cardiac dysfunction, but offer no value when cardiac dysfunction is already present.

4.6 Ghrelin keeps the heart 'SAFE' through STAT3 phosphorylation

In a previous study (unpublished), we reported that chronic DOX-induced cytotoxicity was associated with a reduction in ERK1/2 and Akt phosphorylation *in vitro*. This was accompanied by elevated apoptotic cell death and TNF-α production. In addition, the SAFE pathway (JAK2/STAT3) was not activated following exposure to high concentrations of DOX. It was concluded that cardiotoxicity occurs as a result of DOX-induced TNF-α production and the inhibition of protective signaling pathways. This led us in the search of a protective agent that could potentially promote survival by activating these signaling pathways. Baldanzi *et al*., (2002) showed that DOX-induced apoptosis in H9c2 cardiomyocytes was prevented by ghrelin administration through its ability to activity ERK1/2 and Akt. This prompted us to explore these effects in an *in vivo* model of chronic cardiotoxicity. Although many studies have shown that DOX reduces ERK1/2 and Akt phosphorylation (Xiang *et al*., 2009; Pei *et al*., 2014; Das *et al*., 2011) and that ghrelin promotes survival by activating these pro-survival kinases (Liang *et al*., 2013; Xiang *et al*., 2011; Pei *et al*., 2014; Yu *et al*., 2014), we did not observe any changes in the phosphorylation of ERK1/2 (Figure 3.28) and Akt (Figure 3.29) after DOX or DOX+ghrelin treatment. Our results may differ from other studies because we made use of a prolonged *in vivo* treatment protocol, as opposed to acute models or cell culture studies (Table 6).

Table 6: A summary of the studies reporting DOX-induced reduction of ERK1/2 and Akt.

Authors	Model	DOX dose	Ghrelin dose	ERK1/2 and Akt
Xiang *et al.,* (2009)	Sprague-Dawley rats	2.5 mg/kg/w/6w		↓ by DOX
Das *et al.,* (2011)	Swiss Albino rats	3 x 3 mg/kg		↓ by DOX
Yu *et al.,* (2014)	C57BL/6 mice	15 mg/kg, single	0.2 mg/kg b.i.d, 4 days	↓ by DOX ↑ by ghrelin
Pei *et al.,* (2014)	C57BL/6 mice	15 mg/kg, single	100 µg/kg b.i.d, 4 days	↓ by DOX ↑ by ghrelin
Baldanzi *et al.,* (2002)	H9c2 cardiomyocytes		1 µM, 24 hrs	↑ by ghrelin
Liang *et al.,* (2013)	MC3T3-E1 osteoblasts		10^{-11} - 10^{-9} µM, 48 hrs	↑ by ghrelin
Xiang *et al.,* (2011)	HUVECs		10^{-8} - 10^{-5} µM, 24 hrs	↑ by ghrelin

Abbreviations: w: week; b.i.d: *bis in die* (twice daily); HUVEC: human umbilical vein endothelial cells; hrs: hours.

In contrast, Li *et al.*, (2006) found no involvement of Akt during DOX-induced cardiomyopathy in mice treated with a single dose of DOX. Similarly, Lou *et al.*, (2005) observed an early, transient increase in ERK1/2 phosphorylation in rats after DOX treatment, suggesting an early adaptive response. The subsequent failure of this response was associated with heart failure. Finally, Wang *et al.*, (2014) observed no change in ERK1/2 phosphorylation after DOX treatment in mice, and no change in ERK1/2 or Akt expression in H9c2 cells when ghrelin was pre-incubated with DOX, substantiating our own results. The ERK1/2 and Akt survival kinases are associated with anti-apoptotic and antioxidative effects, so the lack of expression of these kinases might explain the poor cardiac function observed in the DOX-treated rats, however, the fact that there was improvement in cardiac function and a reduction in apoptosis and oxidative stress in the combination group suggests that other signaling pathways are in play.

Although STAT3 can be linked to skeletal muscle wasting, inflammation and cachexia, knock-out of STAT3 results in fibrosis, inflammation and the development of heart failure (Jacoby et al., 2003). In the heart, STAT3 has been implicated in inflammation, apoptosis, cell death and cell survival (Hilfiker-Kleiner *et al*., 2004; Fukada *et al*., 1996). Ourselves and others have reported the inhibition of STAT3 phosphorylation by DOX treatment (Mitra *et al*., 2007) and a significant increase in expression when ghrelin is administered. Considering the survival benefits that are associated with STAT3 activation, this reduction in expression after DOX treatment may be a possible explanation for the side effects of DOX. STAT3 knock-out mice are more sensitive to the fibrosis and oxidative stress associated with aging, and display higher levels of apoptosis after DOX treatment (Jacoby *et al*., 2003). This substantiates our own findings where DOX treatment was accompanied by fibrosis, oxidative stress and apoptosis. In the presence of ghrelin, STAT3 phosphorylation was increased and a concomitant reduction in fibrosis, oxidative stress and apoptosis was observed. Kunisada *et al*., (2000) reported enhanced heart failure in wild-type mice treated with DOX, whereas mice over-expressing STAT3 were protected. Furthermore, STAT3 phosphorylation was found to be significantly down-regulated in the hearts of patients with dilated cardiomyopathy (Podewski, 2003), which may contribute to the development of heart failure. In our study, reduced STAT3 expression in the DOX group can be associated with the poor heart function observed, and this was improved when the phosphorylation of STAT3 was increased by ghrelin treatment. In the heart, STAT3 activation has been observed during MI and pre-conditioning, suggesting that it aids in adaptation to stress (Negoro *et al*., 2001). STAT3 also increases the transcription of anti-apoptotic proteins and decreases the transcription of pro-apoptotic proteins, supporting its role in cell survival (Bolli *et al*., 2001; Hattori *et al*., 2001). As a result, the enhanced phosphorylation of STAT3 by ghrelin may lead to an increase in survival proteins and a decrease in the proteins associated with apoptosis, including cytochrome c and the caspases. Furthermore, Tian *et al*., (2011) demonstrated that the activation of the SAFE pathway has been linked with Bcl-2 elevation (not measured in our study), which prevents the opening of the mPTP by interacting with Bax (Marie Hardwick & Soane, 2013), thereby reducing apoptosis. Therefore, the ghrelin-induced activation of STAT3 may be a potential mechanism through which ghrelin reduces apoptotic cell death. To the best of our knowledge, there are no other studies that report on the effects of ghrelin treatment on STAT3 activation. We have thus highlighted a potential signaling pathway that

is responsible for the protective effects of ghrelin. Although this pathway is linked to cell survival, one of the cytokines responsible for its activation exerts effects that are not as clearly defined.

For many years, physicians have reported that patients with CHF display similar symptoms to patients with chronic inflammation (Ferrari, 1999). Indeed, studies have indicated that increased levels of TNF-α are associated with ventricular dysfunction, dilated cardiomyopathy and heart failure (Hegewisch *et al*., 1988; Moe *et al*., 2004). We have shown that treatment with DOX is accompanied by a potent increase in TNF-α protein expression (Figure 3.30), indicating the possible activation of the extrinsic apoptotic pathway. The extrinsic apoptotic pathway is activated when ligands such as TNF-α bind to death domain-containing receptors on the cell membrane, leading to caspase activation (Dempsey *et al*., 2003). TNFR1 is an example of one of these receptors, and its activation is therefore generally associated with detrimental effects. Evidence for this is that TNFR1 expression and apoptosis were found to be significantly increased in H9c2 cells after treatment with DOX, whereas the expression of TNFR2, associated with beneficial effects, was decreased (Chiosi *et al*., 2007). Although this pathway involves different signaling proteins to the intrinsic apoptotic pathway, both pathways converge at caspase-3 and -7 and induce PARP cleavage. Therefore, the activation of this pathway might explain the significant apoptosis observed in the DOX-treated group, as indicated by caspase-3 and -7 activities and the expression of cleaved PARP. By reducing the expression of TNF-α, ghrelin may have also reduced the activation of the extrinsic apoptotic pathway. However, further research into the expression of the TNF-α receptors, as well as caspase-8 (specific to the death receptor pathway), is needed before the involvement of the extrinsic apoptotic pathway can be confirmed.

Although low levels of TNF-α have been associated with protection (Chiosi *et al*., 2007; Lecour *et al*., 2002; Mann, 2002), the parallel improvement in several parameters of this study upon reduction of TNF-α expression by ghrelin, suggests that TNF-α is detrimental in this scenario. Consistently, Huang *et al*., (2009) reported a reduction in TNF-α mRNA and protein by ghrelin, concluding that ghrelin preserves cardiac function by inhibiting an inflammatory response. This may also be the case in our study, where a reduction in TNF-α by ghrelin is associated with improved cardiac function. Further supporting a detrimental role for TNF-α is the fact that intravenous administration of ghrelin exerts beneficial effects during myocardial infarction and cardiac cachexia by inhibiting the release of cytokines

(Smith *et al*., 2005). Therefore, the improvement in cardiac function, cardiomyocyte atrophy and the increase in body weight may have occurred as a result of the ghrelin-induced reduction in TNF-α. The role of TNF-α in muscle atrophy appears to involve NFκB, the levels of which are elevated after exposure to high concentrations of TNF-α (Sishi & Engelbrecht, 2011). NFκB translocates to the nucleus where it increases the transcription of MuRF-1 and MAFbx, two ubiquitin ligases involved in the ubiquitin-proteasome pathway (UPP) for protein degradation. By reducing the expression of TNF-α, ghrelin decreases the activity of the UPP and as a result, muscle atrophy is prevented. TNF-α is an important determinant of fibrosis, as it facilitates the activation of collagen-producing fibroblasts (Khan & Sheppard, 2006). Its expression may therefore explain the increase in fibrosis that was evident in this study.

Oxidative stress increases the release of pro-inflammatory cytokines. Likewise, pro-inflammatory cytokines also increase the production of ROS (Suematsu *et al*., 2003). Over-expression of TNF-α in the mouse myocardium has been linked to the increased production of $OH^{\bullet}$ radicals (Machida *et al*., 2003). This may provide a link between the elevated protein expression of TNF-α and the substantial oxidative stress in our study. When TNF-α is inhibited, the level of aldehydes, indicative of oxidative stress, is reduced (Moe *et al*., 2004). Similarly in our study, the presence of ghrelin moderately reduced TNF-α and alleviated oxidative stress. This may correspond with ghrelin's antioxidant effects, or through an unknown mechanism by which ghrelin reduces the levels of TNF-α. It has been reported that myocytes lacking STAT3 expression exhibit higher levels of TNF-α (Jacoby *et al*., 2003). This correlates well with our study, where DOX treatment reduced the expression of STAT3, resulting in higher TNF-α levels. In contrast, ghrelin treatment promoted STAT3 phosphorylation, reduced the expression of TNF-α and subsequently induced cell survival. This lower, safer level of TNF-α may now also be promoting a survival benefit by activating the SAFE pathway (Lecour *et al*., 2002; Lacerda *et al*., 2009), whereas high levels of TNF-α for prolonged periods of time can induce apoptosis and inflammation (Lien *et al*., 2006; Sack *et al*., 2000). TNF-α activates the SAFE pathway by binding to its receptor on the cell membrane. This causes the receptor to dimerize, subsequently activating JAK. By phosphorylating the receptor, JAK creates docking sites for STAT3, allowing it to bind and also be phosphorylated by JAK. STAT3 then dimerizes and translocates to the nucleus to

increase the transcription of anti-apoptotic proteins (Boengler *et al.*, 2008). In this way, TNF-α and STAT3, induced by ghrelin, can promote cell survival during DOX treatment.

In our results, we reported increased protein expression of TNF-α but no change in the serum concentration. This may be because the TNF-α protein that was produced in response to DOX treatment was not secreted into circulation. However, it has also been shown that cytokines within the cell appear before the secreted proteins are detected (Kwak *et al.*, 2000). Alternatively, blood was collected one week after the last injections and TNF-α may have returned to basal levels in the serum. The Milliplex® MAP Multiplex kit used for TNF-α analysis may also have lacked sensitivity for measuring the TNF-α which was still in the serum. Further research is needed in order to establish the levels of TNF-α during different time points in the study, to fully elucidate how its secretion is linked to the SAFE pathway.

Chapter 5

Conclusion

DOX is a chemotherapeutic drug that has drastically improved the outcome of patients suffering from several different cancers, however, severe cardiotoxicity is a common side effect that impacts on the quality of life and survival of these patients. Although the mechanisms are still undefined almost sixty years later, oxidative stress and apoptotic cell death remain the top contenders. The chemical structure of DOX allows for the production of free radicals, resulting in a condition of oxidative stress, apoptotic cell death and ultimately heart failure. Despite effectively treating several cancers, these side effects limit the therapeutic potential of DOX. Because of its high efficacy, much research has been prompted to develop cardioprotective agents that do not interfere with the anti-neoplastic action of DOX, but many, being synthetic compounds, exhibit their own detrimental side effects. Therefore, the potential cardioprotective effects of ghrelin, an endogenous appetite-stimulating gut peptide, were assessed in the current study.

Although further correlation studies are needed, Figure 5.1A summarizes the effects induced by DOX, while Figure 5.1B indicates the potential pathways that may be influenced by ghrelin treatment to protect against cardiotoxicity. DOX treatment was accompanied by undetectable levels of ghrelin, suggesting that DOX exerts an inhibitory effect on ghrelin production, secretion or receptor binding. The absence of ghrelin may account for the deleterious effects of DOX. We have shown that treatment with DOX reduces body weight gain and appetite, whereas ghrelin attenuates these effects. Ghrelin also maintains cardiac function, which was attributed to the anti-apoptotic and antioxidant activity of ghrelin, supporting the two most widely accepted mechanisms of action of DOX. Oxidative stress, further amplified by inflammation, may be responsible for the activation of apoptosis, leading to cell death, cardiomyocyte atrophy and ultimately, cardiac dysfunction. Ghrelin prevents cardiomyocyte atrophy and reduces ventricular fibrosis, most likely through an anti-inflammatory response, as ghrelin was shown to reduce TNF-α expression. TNF-α activates fibroblasts which replace apoptotic cells with fibrotic tissue, contributing to the development of cardiac dysfunction. Although we originally hypothesized that the protective effects of ghrelin would be mediated through ERK1/2 and Akt signaling, we have shown that these pathways are not activated in this model, and that protection is instead offered by the SAFE

pathway. DOX treatment was associated with down-regulation of STAT3 which may result in enhanced sensitivity to oxidative stress, cell death and fibrosis.
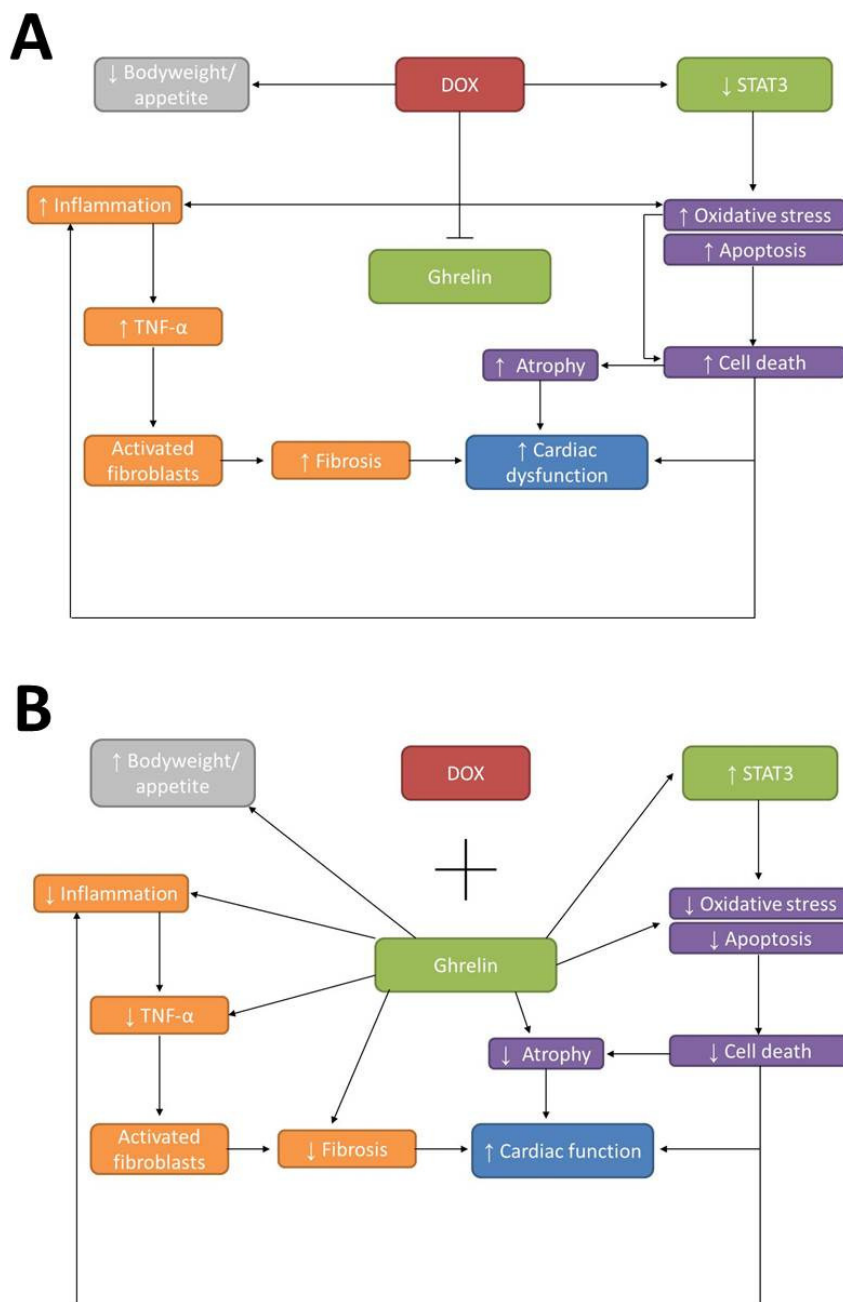
Figure 5.1: A unifying schematic of the effects of DOX treatment alone (A) and DOX+ghrelin treatment (B) in DOX-induced cardiotoxicity.

A summary of the research findings indicating the possible pathways influenced by DOX and ghrelin. Flat arrowhead: inhibits; ⟶ : leads to; ↑: increases; ↓: decreases.

Considering that the oxidative stress theory is still under debate, it is possible that the inhibition of STAT3 by DOX may be another mechanism by which cardiotoxicity develops. This is also an appealing property in terms of tumorigenesis, as cancer cell proliferation may be reduced if a pro-survival transcription factor is inhibited. STAT3 upregulates the transcription of many genes that will assist in cell survival and its stimulation by ghrelin promotes this effect, however, whether ghrelin will also promote tumorigenesis through STAT3 activation needs to be determined (Rébé et al., 2013). Although the LD_{50} of ghrelin (the dose required to kill 50% of a test sample) is not known, it is important to note that ghrelin alone did not exert any negative effects. This is an appealing property as many adjuvant therapies eventually result in toxicity. In addition, all of the ghrelin studies administered ghrelin twice a day, whereas we were able to obtain a similar effect with fewer injections, reducing animal suffering and discomfort. Future studies should consider making use of osmotic pumps in order to deliver ghrelin to the animal, as this may allow for a higher dosage to be used and possibly result in an enhanced protective effect. This study has provided a basic overview of the signaling pathways involved in the protective effects of ghrelin during chronic DOX-induced cardiotoxicity, but further research is needed to gain an in-depth understanding into the mechanisms behind ghrelin's protection.

Limitations and future directions

To the best of our knowledge, this is one of very few studies examining the chronic side effects of DOX treatment. This, together with the fact that we utilised clinically relevant doses of DOX, adds to the novelty of this study. Although this research has achieved its aims, there are still some limitations of the study that should be improved upon in the future. These include using a larger sample size so that trends can be strengthened and so that some hearts can be used for analysis and others can be used for perfusions. A reason for this is that many of the markers released by the heart into circulation might have been washed out in the effluent therefore, if we had hearts specifically for analysis of these markers, they might be detectable in the tissue. If a larger sample size is not possible, then the effluent should be collected so that these markers can be measured in the effluent using more sensitive methods such as high performance liquid chromatography. We also only measured markers in the blood one week after the end of treatment, meaning that many of these markers might already have been degraded or returned to baseline levels by the time of measurement. In future I would draw blood at various intervals throughout the treatment protocol so that a better

image can be drawn of the expression of these markers during the course of cardiotoxicity. Since CK-MB can include the damage in skeletal muscle, I would measure both CK and CK-MB so that this discrepancy can be differentiated. This will indicate the relative contribution of CK-MB to total CK. Although the markers of damage measured in this study are valuable *predictive* markers, other markers such as LDH, galectin 3 and ST-2 need to be measured to detect damage that is already present.

In the future I would fractionate tissue lysates to yield cytosolic, mitochondrial and nuclear fractions so that the localisation and measurement of proteins in these compartments is more accurate. In terms of the animal model, I would like to test the effects of ghrelin in a tumor-bearing rat model so that the effect of cancer on cardiotoxicity and the protection offered by ghrelin can be determined. It is also important to determine the effect of ghrelin on cancer growth and try to determine the best time during the course of treatment that ghrelin should be administered (before, during or after). This study was conducted on male rats, however, the effects of DOX and ghrelin on female rats should also be determined. For future studies I would suggest having a group of rats that is monitored for a longer period after the last injection, to determine when heart function begins to decline. Finally, I would like to investigate whether protection can be offered by ghrelin, but through periods of fasting, instead of injections. This would provide insight into a potential mode of 'ghrelin administration' for human subjects. We have highlighted the many cardioprotective effects of ghrelin and the possible mechanisms by which this occurs. Collectively, our data suggests that the anti-apoptotic, antioxidative and cardioprotective effects of ghrelin are mediated through STAT3 signaling. Our findings emphasize that the potential clinical implications of the cardioprotective effects of ghrelin during DOX chemotherapy are worth exploring further.

References

Accornero, F., Berlo, J.H. Van, Correll, R.N., Elrod, J.W., Sargent, M.A., York, A., Rabinowitz, J.E., Leask, A. & Molkentin, J.D. (2015). Genetic Analysis of Connective Tissue Growth Factor as an Effector of Transforming Growth Factor B Signaling and Cardiac Remodeling. *Molecular and Cellular Biology*. 35 (12). p.pp. 2154–2164.

Adams, J., Abendschein, D. & Jaffe, A. (1993a). Biochemical markers of myocardial injury. Is MB creatine kinase the choice for the 1990s? *Circulation*. 88 (2). p.pp. 750–763.

Adams, J., Bodor, G., Davila-Roman, V., Delmez, J., Apple, F., Ladenson, J. & Jaffe, A. (1993b). Cardiac troponin I. A marker with high specificity for cardiac injury. *Circulation*. 88 (1). p.pp. 101–106.

Akamizu, T. & Kangawa, K. (2010). Ghrelin for cachexia. *Journal of Cachexia, Sarcopenia and Muscle*. 1 (2). p.pp. 169–176.

Aksentijevi, D., Lewis, H.R. & Shattock, M.J. (2016). Is rate – pressure product of any use in the isolated rat heart ? Assessing cardiac 'effort' and oxygen consumption in the Langendorff-perfused heart. *Experimental Physiology*. 101 (2). p.pp. 282–294.

Alderton, P.M., Gross, J. & Green, M.D. (1992). Comparative study of doxorubicin, mitoxantrone, and epirubicin in combination with ICRF-187 (ADR-529) in a chronic cardiotoxicity animal model. *Cancer Research*. 52. p.pp. 194–201.

Alessi, D.R., James, S.R., Downes, C.P., Holmes, A.B., Gaffney, P.R., Reese, C.B. & Cohen, P. (1997). Characterization of a 3-phosphoinositide-dependent protein kinase which phosphorylates and activates protein kinase B alpha. *Current Biology*. 7 (4). p.pp. 261–269.

Ali, M., Ewer, M., Gibbs, H., Swafford, J. & Graff, K. (1994). Late Doxorubicin-Associated Cardiotoxicity in Children. *Cancer*. 74 (1). p.pp. 182–188.

Alshabanah, O.A., Hafez, M.M., Al-harbi, M.M., Hassan, Z.K., Rejaie, S.S. Al & Asiri, Y.A. (2010). Doxorubicin toxicity can be ameliorated during antioxidant L-carnitine supplementation. *Oxidative Medicine and Cellular Longevity*. 3 (6). p.pp. 428–433.

Anand, P., Kunnumakara, A., Sundaram, C., Harikumar, K., Tharakan, S., Lai, O., Sung, B. & Aggarwal, B. (2008). Cancer is a preventable disease that requires major lifestyle changes. *Pharmaceutical Research*. 25 (9). p.pp. 2097–2116.

Antman, K., Suit, H., Amato, D., Corson, J., Wood, W., Proppe, K., Harmon, D., Carey, R., Greenberger, J. & Blum, R. (1984). Preliminary results of a randomized trial of adjuvant doxorubicin for sarcomas: Lack of apparent difference between treatment groups. *Journal of Clinical Oncology*. 2 (6). p.pp. 601–608.

Arcamone, F., Franceschi, G., Penco, S. & Selva, A. (1969). Adriamycin (14-hydroxydaunomycin), a novel antitumor antibiotic. *Tetrahedron Letters*. (13). p.pp. 1007–1010.

Arola, O.J., Saraste, A., Pulkki, K., Kallajoki, M., Parvinen, M. & Voipio-Pulkki, L.M. (2000). Acute doxorubicin cardiotoxicity involves cardiomyocyte apoptosis. *Cancer*

Research. 60 (7). p.pp. 1789–1792.

Asensi, M., Sastre, J., Pallardo, F. V., Lloret, A., Lehner, M., Garcia-de-la Asuncion, J. & Viña, J. (1999a). Oxidants and Antioxidants Part A. *Methods in Enzymology*. 299. p.pp. 267–276.

Asensi, M., Sastre, J., Pallardo, F. V, Lloret, A., Lehner, M., Garcia-de-la Asuncion, J. & Viña, J. (1999b). Ratio of Reduced to Oxidized Glutathione as Indicator of Oxidative Stress Status and DNA Damage. *Methods in Enzymology*. 299 (1978). p.pp. 267–276.

Asselin, B.L., Devidas, M., Chen, L., Franco, V.I., Pullen, J., Borowitz, M.J., Hutchison, R.E., Ravindranath, Y., Armenian, S.H., Camitta, B.M. & Lipshultz, S.E. (2016). Cardioprotection and Safety of Dexrazoxane in Patients Treated for Newly Diagnosed T-Cell Acute Lymphoblastic Leukemia or Advanced-Stage Lymphoblastic Non-Hodgkin Lymphoma: A Report of the Children's Oncology Group. *Journal of Clinical Oncology*. 34 (8). p.pp. 854–62.

Bachur, N.R., Gordon, S.L. & Gee, M. V (1978). A General Mechanism for Microsomal Activation of Quinone Anticancer Agents to Free Radicals. *Cancer Research*. 38. p.pp. 1745–1750.

Baldanzi, G., Filigheddu, N., Cutrupi, S., Catapano, F., Bonissoni, S., Fubini, A., Malan, D., Baj, G., Granata, R., Broglio, F., Papotti, M., Surico, N., Bussolino, F., Isgaard, J., Deghenghi, R., Sinigaglia, F., Prat, M., Muccioli, G., Ghigo, E. & Graziani, A. (2002). Ghrelin and des-acyl ghrelin inhibit cell death in cardiomyocytes and endothelial cells through ERK1/2 and PI3-kinase/AKT. *The Journal of Biological Chemistry*. 159 (6). p.pp. 1029–1037.

Banks, W.A., Tschop, M., Robinson, S.M. & Heiman, M.L. (2002). Extent and direction of ghrelin transport across the blood-brain barrier is determined by its unique primary structure. *Journal of Pharmacology and Experimental Therapeutics*. 302 (2). p.pp. 822–827.

Barrett-Lee, P.J., Dixon, J.M., Farrell, C., Jones, A., Leonard, R., Murray, N., Palmieri, C., Plummer, C.J., Stanley, A. & Verrill, M.W. (2009). Expert opinion on the use of anthracyclines in patients with advanced breast cancer at cardiac risk. *Annals of oncology*. 20 (5). p.pp. 816–827.

Beiras-Fernandez, A., Kreth, S., Weis, F., Ledderose, C., Pöttinger, T., Dieguez, C., Beiras, A. & Reichart, B. (2010). Altered myocardial expression of ghrelin and its receptor (GHSR-1a) in patients with severe heart failure. *Peptides*. 31 (12). p.pp. 2222–2228.

Bell, R.M., Mocanu, M.M. & Yellon, D.M. (2011). Retrograde heart perfusion: The Langendorff technique of isolated heart perfusion. *Journal of Molecular and Cellular Cardiology*. 50 (6). p.pp. 940–950.

Bernheim, F., Bernheim, M.L. & Wilbur, K.M. (1948). The Reaction Between Thiobarbituric Acid and the Oxidation Products of Certain Lipides. *Journal of Biological Chemistry*. 174 (4). p.pp. 257–264.

Berridge, M.J., Lipp, P. & Bootman, M.D. (2000). The Versatility and Universality of

Calcium Signalling. *Molecular Cell Biology*. 1 (October). p.pp. 11–21.

Bersin, R.M. & Stacpoole, P.W. (1997). Dichloroacetate as metabolic therapy for myocardial ischemia and failure. *American Heart Journal*. 134. p.pp. 841–855.

Bertinchant, J.P., Polge, A., Juan, J.M., Oliva-lauraire, M.C. & Giuliani, I. (2003). Evaluation of cardiac troponin I and T levels as markers of myocardial damage in doxorubicin-induced cardiomyopathy rats, and their relationship with echocardiographic and histological findings. *Clinica Chimica Acta*. 329. p.pp. 39–51.

Blum, R. & Carter, S. (1974). Adriamycin: A New Anticancer Drug with Significant Clinical Activity. *Annals of Internal Medicine*. 80 (2). p.pp. 249–259.

Boengler, K., Hilfiker-Kleiner, D., Drexler, H., Heusch, G. & Schulz, R. (2008). The myocardial JAK/STAT pathway: from protection to failure. *Pharmacology & Therapeutics*. 120 (2). p.pp. 172–185.

Bolli, R., Dawn, B. & Xuan, Y.T. (2001). Emerging role of the JAK-STAT pathway as a mechanism of protection against ischemia/reperfusion injury. *Journal of Molecular and Cellular Cardiology*. 33 (11). p.pp. 1893–1896.

Bonadonna, G., Monfardini, S., De Lena, M., Fossati-Bellani, F. & Beretta, G. (1970). Phase I and preliminary phase II evaluation of adriamycin (NSC 123127). *Cancer Research*. 30. p.pp. 2572–2582.

Bos, J.L. (2003). Epac: a new cAMP target and new avenues in cAMP research. *Nature Reviews: Molecular Cell Biology*. 4 (9). p.pp. 733–738.

Bovelli, D., Plataniotis, G. & Roila, F. (2010). Cardiotoxicity of chemotherapeutic agents and radiotherapy-related heart disease: ESMO clinical practice guidelines. *Annals of Oncology*. 21 (Supplement 5). p.pp. 277–282.

Bowles, E., Wellman, R., Feigelson, H., Onitilo, A., Freedman, A., Delate, T., Allen, L., Nekhlyudov, L., Goddard, K., Davis, R., Habel, L., Yood, M., McCarty, C., Magid, D. & Wagner, E. (2012). Risk of heart failure in breast cancer patients after anthracycline and trastuzumab treatment: a retrospective cohort study. *Journal of the National Cancer Institute*. 104 (17). p.pp. 1293–1305.

Bradley, J.R. (2008). TNF-mediated inflammatory disease. *The Journal of Pathology*. 214 (2). p.pp. 149–160.

Bray, F. & Møller, B. (2006). Predicting the future burden of cancer. *Nature Reviews: Cancer*. 6 (1). p.pp. 63–74.

Bristow, M. (2000). Etomoxir: a new approach to treatment of chronic heart failure. *Lancet*. 356. p.pp. 1621–1622.

Bristow, M., Mason, J., Billingham, M. & Daniels, J. (1978). Doxorubicin cardiomyopathy: evaluation by phonocardiography, endomyocardial biopsy, and cardiac catheterization. *Annals of Internal Medicine*. 88 (2). p.pp. 168–175.

Buja, L., Ferrans, V., Mayer, R., Roberts, W. & Henderson, E. (1973). Cardiac ultrastructural

changes induced by Daunorubicin therapy. *Cancer*. 32. p.pp. 771–788.

Cacciapaglia, F., Salvatorelli, E., Minotti, G., Afeltra, A. & Menna, P. (2014). Low level tumor necrosis factor-alpha protects cardiomyocytes against high level tumor necrosis factor-alpha: brief insight into a beneficial paradox. *Cardiovascular Toxicology*. 14 (4). p.pp. 387–392.

Cardinale, D., Sandri, M., Martinoni, A., Borghini, E., Civelli, M., Lamantia, G., Cinieri, S., Martinelli, G., Fiorentini, C. & Cipolla, C. (2002). Myocardial injury revealed by plasma troponin I in breast cancer treated with high-dose chemotherapy. *Annals of Oncology*. 13 (5). p.pp. 710–715.

Cardinale, D., Sandri, M.T., Martinoni, A., Tricca, A., Civelli, M., Lamantia, G., Cinieri, S., Martinelli, G., Cipolla, C.M. & Fiorentini, C. (2000). Left Ventricular Dysfunction Predicted by Early Troponin I Release After High-Dose Chemotherapy. *Journal of the American College of Cardiology*. 36 (2). p.pp. 517–522.

Carvalho, F., Burgeiro, A., Garcia, R., Moreno, A., Carvalho, R. & Oliveira, P. (2014). Doxorubicin-Induced Cardiotoxicity: From Bioenergetic Failure and Cell Death to Cardiomyopathy. *Medicinal Research Reviews*. 34 (1). p.pp. 106–135.

Carver, J.R., Shapiro, C.L., Ng, A., Jacobs, L., Schwartz, C., Virgo, K.S., Hagerty, K.L., Somerfield, M.R. & Vaughn, D.J. (2007). American society of clinical oncology clinical evidence review on the ongoing care of adult cancer survivors: Cardiac and pulmonary late effects. *Journal of Clinical Oncology*. 25 (25). p.pp. 3991–4008.

Cassoni, P., Papotti, M., Ghe, C., Catapano, F., Sapino, A., Graziani, A., Deghenghi, R., Reissmann, T., Ghigo, E. & Muccioli, G. (2001). Identification, Characterization, and Biological Activity of Specific Receptors for Natural (Ghrelin) and Synthetic Growth Hormone Secretagogues and Analogs in Human Breast Carcinomas and Cell Lines. *The Journal of Clinical Endocrinology and Metabolism*. 86 (4). p.pp. 1738–1745.

Chandler, M.P., Stanley, W.C., Morita, H., Suzuki, G., Roth, B.A., Blackburn, B., Wolff, A. & Sabbah, H.N. (2002). Short-term treatment with ranolazine improves mechanical efficiency in dogs with chronic heart failure. *Circulation Research*. 91 (4). p.pp. 278–280.

Chang, C.C., Hung, C.H., Yen, C.S., Hwang, K.L. & Lin, C.Y. (2005). The relationship of plasma ghrelin level to energy regulation, feeding and left ventricular function in non-diabetic haemodialysis patients. *Nephrology Dialysis Transplantation*. 20 (10). p.pp. 2172–2177.

Chang, L., Ren, Y., Liu, X., Li, W.G., Yang, J., Geng, B., Weintraub, N.L. & Tang, C. (2004a). Protective effects of ghrelin on ischemia/reperfusion injury in the isolated rat heart. *Journal of Cardiovascular Pharmacology*. 43 (2). p.pp. 165–170.

Chang, L., Zhao, J., Li, G.-Z., Geng, B., Pan, C.-S., Qi, Y.-F. & Tang, C.-S. (2004b). Ghrelin protects myocardium from isoproterenol-induced injury in rats. *Acta Pharmacologica Sinica*. 25 (9). p.pp. 1131–1137.

Chatterjee, K., Zhang, J., Honbo, N. & Karliner, J.S. (2010). Doxorubicin cardiomyopathy.

Cardiology. 115 (2). p.pp. 155–162.

Chaudhary, D., Khatiwada, S., Sah, S.K., Tamang, M.K. & Bhattacharya, S. (2016). Effect of Doxorubicin on Histomorphology of Liver of Wistar Albino Rats. *Journal of Pharmacy and Pharmacology*. 4. p.pp. 186–190.

Chen, B., Peng, X., Pentassuglia, L., Lim, C.C. & Sawyer, D.B. (2007). Molecular and cellular mechanisms of anthracycline cardiotoxicity. *Cardiovascular Toxicology*. 7 (2). p.pp. 114–121.

Chen, H.Y., Trumbauer, M.E., Chen, A.S., Weingarth, D.T., Adams, J.R., Frazier, E.G., Shen, Z., Marsh, D.J., Feighner, S.D., Guan, X.M., Ye, Z., Nargund, R.P., Smith, R.G., Van Der Ploeg, L.H.T., Howard, A.D., Macneil, D.J. & Qian, S. (2004). Orexigenic action of peripheral ghrelin is mediated by neuropeptide Y and agouti-related protein. *Endocrinology*. 145 (6). p.pp. 2607–2612.

Chen, Y.-L., Loh, S.-H., Chen, J.-J. & Tsai, C.-S. (2012). Urotensin II prevents cardiomyocyte apoptosis induced by doxorubicin via Akt and ERK. *European Journal of Pharmacology*. 680. p.pp. 88–94.

Childs, A.C., Phaneuf, S.L., Dirks, A.J., Phillips, T. & Leeuwenburgh, C. (2002). Doxorubicin treatment in vivo causes cytochrome C release and cardiomyocyte apoptosis, as well as increased mitochondrial efficiency, superoxide dismutase activity, and Bcl-2:Bax ratio. *Cancer Research*. 62 (16). p.pp. 4592–4598.

Chin, C.T., Wang, T.Y., Li, S., Wiviott, S.D., DeLemos, J.A., Kontos, M.C., Peterson, E.D. & Roe, M.T. (2012). Comparison of the prognostic value of peak creatine kinase-mb and troponin levels among patients with acute myocardial infarction: A report from the acute coronary treatment and intervention outcomes network registry-get with the guidelines. *Clinical Cardiology*. 35 (7). p.pp. 424–429.

Chiosi, E., Spina, A., Sorrentino, A., Romano, M., Sorvillo, L., Senatore, G., D'Auria, R., Abbruzzese, A., Caraglia, M., Naviglio, S. & Illiano, G. (2007). Change in TNF-alpha receptor expression is a relevant event in doxorubicin-induced H9c2 cardiomyocyte cell death. *Journal of Interferon & Cytokine Research*. 27 (7). p.pp. 589–597.

Chopin, L., Walpole, C., Seim, I., Cunningham, P., Murray, R., Whiteside, E., Josh, P. & Herington, A. (2011). Ghrelin and cancer. *Molecular and Cellular Endocrinology*. 340 (1). p.pp. 65–69.

Chu, W.-M. (2013). Tumor necrosis factor. *Cancer Letters*. 328 (2). p.pp. 222–225.

Chung, H., Kim, E., Lee, D.H., Seo, S., Ju, S., Lee, D. & Kim, H. (2007). Ghrelin Inhibits Apoptosis in Hypothalamic Neuronal Cells during Oxygen-Glucose Deprivation. *Endocrinology*. 148 (1). p.pp. 148–159.

Chung, H., Li, E., Kim, Y., Kim, S. & Park, S. (2013). Multiple signaling pathways mediate ghrelin-induced proliferation of hippocampal neural stem cells. *Journal of Endocrinology*. 218 (1). p.pp. 49–59.

Chung, J., Uchida, E., Grammer, T.C. & Blenis, J. (1997). STAT3 serine phosphorylation by ERK-dependent and -independent pathways negatively modulates its tyrosine

phosphorylation. *Mol Cell Biol*. 17 (11). p.pp. 6508–6516.

Cittadini, A., Grossman, J.D., Napoli, R., Smith, R.J., Clark, R., Katz, S.E., Stro, H., Morgan, J.P. & Douglas, P.S. (1997). Growth Hormone Attenuates Early Left Ventricular Remodeling and Improves Cardiac Function in Rats With Large Myocardial Infarction. *Journal of Ameican College of Cardiology*. 29 (5). p.pp. 1109–1116.

Cocco, T., Cutecchia, G., Montedoro, G. & Lorusso, M. (2002). The antihypertensive drug carvedilol inhibits the activity of mitochondrial NADH-ubiquinone oxidoreductase. *Journal of Bioenergetics and Biomembranes*. 34 (4). p.pp. 251–258.

Cohen, G.M. (1997). Caspases: the executioners of apoptosis. *Biochemical Journal*. 326 (1). p.pp. 1–16.

Colella, A.D., Chegenii, N., Tea, M.N., Gibbins, I.L., Williams, K.A. & Chataway, T.K. (2012). Comparison of Stain-Free gels with traditional immunoblot loading control methodology. *Analytical Biochemistry*. 430 (2). p.pp. 108–110.

Cook, H. (1997). Tinctorial methods in histology. *Journal of Clinical Pathology*. 50. p.pp. 716–720.

Cross, T.G., Scheel-Toellner, D., Henriquez, N. V, Deacon, E., Salmon, M. & Lord, J.M. (2000). Serine/threonine protein kinases and apoptosis. *Experimental Cell Research*. 256 (1). p.pp. 34–41.

Cummings, D., Purnell, J., Frayo, S., Schmidova, K., Wisse, B. & Weigle, D. (2001). A preprandial rise in plasma ghrelin levels suggests a role in meal initiation in humans. *Diabetes*. 50. p.pp. 1714–1719.

Curran, C.F., Narang, P.K. & Reynolds, R.D. (1991). Toxicity profile of dexrazoxane (Zinecard, ICRF-187, ADR-529, NSC-169780), a modulator of doxorubicin cardiotoxicity. *Cancer Treatment Reviews*. 18 (4). p.pp. 241–252.

D'Andrea, G.M. (2005). Use of antioxidants during chemotherapy and radiotherapy should be avoided. *CA Cancer Journal for Clinicians*. 55 (5). p.pp. 319–321.

Dalby, K., Tekedereli, I., Lopez-berestein, G., Ozpolat, B., Dalby, K., Tekedereli, I., Lopez-berestein, G., Ozpolat, B., Dalby, K.N., Tekedereli, I., Lopez-berestein, G. & Ozpolat, B. (2010). Targeting the pro-death and pro-survival functions of autophagy as novel therapeutic strategies in cancer. *Autophagy*. 6 (3). p.pp. 322–329.

Das, J., Ghosh, J., Manna, P. & Sil, P.C. (2011). Taurine suppresses doxorubicin-triggered oxidative stress and cardiac apoptosis in rat via up-regulation of PI3-K/Akt and inhibition of p53, p38-JNK. *Biochemical Pharmacology*. 81 (7). p.pp. 891–909.

Date, Y., Kojima, M., Hosoda, H., Sawaguchi, A., D, T.D.Y. & Medicine, I. (2000). Ghrelin, a Novel Growth Hormone-Releasing Acylated Peptide, Is Synthesized in a Distinct Endocrine Cell Type in the Gastrointestinal Tracts of Rats and Humans. *Endocrinology*. 141 (11). p.pp. 4255–4261.

Date, Y., Murakami, N., Toshinai, K., Matsukura, S., Niijima, A., Matsuo, H., Kangawa, K. & Nakazato, M. (2002). The role of the gastric afferent vagal nerve in Ghrelin-induced

feeding and growth hormone secretion in rats. *Gastroenterology*. 123 (4). p.pp. 1120–1128.

Demant, E. & Jensen, P. (1983). Destruction of phospholipids and respiratory-chain activity in pig-heart submitochondrial particles induced by an Adriamycin-Iron complex. *European Journal of Biochemistry*. 132. p.pp. 551–556.

Dempsey, P.W., Doyle, S.E., He, J.Q. & Cheng, G. (2003). The signaling adaptors and pathways activated by TNF superfamily. *Cytokine & Growth Factor Reviews*. 14. p.pp. 193–209.

Desai, V.G., Herman, E.H., Moland, C.L., Branham, W.S., Lewis, S.M., Davis, K.J., George, N.I., Lee, T., Kerr, S. & Fuscoe, J.C. (2013). Development of doxorubicin-induced chronic cardiotoxicity in the B6C3F1 mouse model. *Toxicology and Applied Pharmacology*. 266 (1). p.pp. 109–121.

Diegelmann, R. & Evans, M. (2004). Wound healing: an overview of acute, fibrotic and delayed healing. *Frontiers in Bioscience*. 9. p.pp. 283–289.

Dixit, V., Schaffer, E., Pyle, R., Collins, G., Sakthivel, S., Palaniappan, R., Lillard, J. & Taub, D. (2004). Ghrelin inhibits leptin- and activation-induced proinflammatory cytokine expression by human monocytes and T cells. *Journal of Clinical Investigation*. 114 (1). p.pp. 57–66.

Dobutovic, B., Sudar, E., Tepavcevic, S., Djordjevic, J. & Djordjevic, A. (2014). Effects of ghrelin on protein expression of antioxidative enzymes and iNOS in the rat liver. *Experimental Research*. 10 (4). p.pp. 806–816.

Doggrell, S. & Brown, L. (1998). Rat models of hypertension, cardiac hypertrophy and failure. *Cardiovascular Research*. 39. p.pp. 89–105.

Dolci, A., Dominici, R., Cardinale, D., Sandri, M.T. & Panteghini, M. (2008). Biochemical markers for prediction of chemotherapy-induced cardiotoxicity. *American Journal of Clinical Pathology*. 130 (5). p.pp. 688–695.

Doroshow, J.H. (1983). Effect of anthracycline antibiotics on oxygen radical formation in rat heart. *Cancer research*. 43 (2). p.pp. 460–472.

Doroshow, J.H., Locker, G.Y., Ifrim, I. & Myers, C.E. (1981). Prevention of Doxorubicin cardiac toxicity in the mouse by N-acetylcysteine. *Journal of Clinical Investigation*. 68 (4). p.pp. 1053–1064.

Doroshow, J.H., Locker, G.Y. & Myers, C.E. (1980). Enzymatic defenses of the mouse heart against reactive oxygen metabolites: alterations produced by doxorubicin. *The Journal of Clinical Investigation*. 65 (1). p.pp. 128–135.

El-Mehy, A., Mansour, F., El-Fattah, N., El-Safty, F.A. & El-Fiky, M.M. (2008). Histological And Immunohistochemical Study On The Effect Of Doxorubicin On The Heart Of Adult Albino Rat And The Possible Protective Role Of An Antioxidant. *Menoufiya Medical Journal*. 21 (1). p.pp. 91–108.

Enomoto, M., Nagaya, N., Uematsu, M., Okumura, H., Nakagawa, E., Ono, F., Hosoda, H.,

Oya, H., Kojima, M., Kanmatsuse, K. & Kangawa, K. (2003). Cardiovascular and hormonal effects of subcutaneous administration of ghrelin, a novel growth hormone-releasing peptide, in healthy humans. *Clinical Science*. 105 (4). p.pp. 431–435.

Eter, E., Tuwaijiri, A., Hagar, H. & Arafa, M. (2007). In vivo and in vitro antioxidant activity of ghrelin: Attenuation of gastric ischemic injury in the rat. *Journal of Gastroenterology and Hepatology*. 22 (11). p.pp. 1791–1799.

Ewer, M.S. & Ewer, S.M. (2010). Cardiotoxicity of anticancer treatments: what the cardiologist needs to know. *Nature Reviews Cardiology*. 7 (10). p.pp. 564–575.

Fearon, K., Strasser, F., Anker, S.D., Bosaeus, I., Bruera, E., Fainsinger, R.L., Jatoi, A., Loprinzi, C., MacDonald, N., Mantovani, G., Davis, M., Muscaritoli, M., Ottery, F., Radbruch, L., Ravasco, P., Walsh, D., Wilcock, A., Kaasa, S. & Baracos, V.E. (2011). Definition and classification of cancer cachexia: An international consensus. *The Lancet Oncology*. 12 (5). p.pp. 489–495.

Ferrari, R. (1999). The role of TNF in cardiovascular disease. *Pharmacological research*. 40 (2). p.pp. 97–105.

Filigheddu, N., Fubini, A., Baldanzi, G., Cutrupi, S., Ghè, C., Catapano, F., Broglio, F., Bosia, A., Papotti, M., Muccioli, G., Ghigo, E., Deghenghi, R. & Graziani, A. (2001). Hexarelin protects H9c2 cardiomyocytes from Doxorubicin-induced cell death. *Endocrine*. 14 (1). p.pp. 113–119.

Fouladiun, M., Körner, U., Bosaeus, I., Daneryd, P., Hyltander, A. & Lundholm, K.G. (2005). Body composition and time course changes in regional distribution of fat and lean tissue in unselected cancer patients on palliative care - Correlations with food intake, metabolism, exercise capacity, and hormones. *Cancer*. 103 (10). p.pp. 2189–2198.

Frias, M.A., Somers, S., Gerber-Wicht, C., Opie, L.H., Lecour, S. & Lang, U. (2008). The PGE2-Stat3 interaction in doxorubicin-induced myocardial apoptosis. *Cardiovascular research*. 80 (1). p.pp. 69–77.

Fukada, T., Hibi, M., Yamanaka, Y., Takahashi-Tezuka, M., Fujitani, Y., Yamaguchi, T., Nakajima, K. & Hirano, T. (1996). Two signals are necessary for cell proliferation induced by a cytokine receptor gp130: involvement of STAT3 in anti-apoptosis. *Immunity*. 5 (5). p.pp. 449–460.

Fukazawa, R., Miller, T.A., Kuramochi, Y., Frantz, S., Kim, Y.-D., Marchionni, M.A., Kelly, R.A. & Sawyer, D.B. (2003). Neuregulin-1 protects ventricular myocytes from anthracycline-induced apoptosis via erbB4-dependent activation of PI3-kinase/Akt. *Journal of Molecular and Cellular Cardiology*. 35 (12). p.pp. 1473–1479.

Fülster, S., Tacke, M., Sandek, A., Ebner, N., Tschöpe, C., Doehner, W., Anker, S.D. & Von Haehling, S. (2013). Muscle wasting in patients with chronic heart failure: Results from the studies investigating co-morbidities aggravating heart failure (SICA-HF). *European Heart Journal*. 34 (7). p.pp. 512–519.

García, E. & Korbonits, M. (2006). Ghrelin and cardiovascular health. *Current Opinion in*

Pharmacology. 6. p.pp. 142–147.

Gava, F.N., Zacché, E., Ortiz, E.M.G., Champion, T., Bandarra, M.B., Vasconcelos, R.O., Barbosa, J.C. & Camacho, A.A. (2013). Doxorubicin induced dilated cardiomyopathy in a rabbit model: An update. *Research in Veterinary Science*. 94. p.pp. 115–121.

Gianni, L., Herman, E.H., Lipshultz, S.E., Minotti, G., Sarvazyan, N. & Sawyer, D.B. (2008). Anthracycline cardiotoxicity: from bench to bedside. *Journal of Clinical Oncology: Official Journal of the American Society of Clinical Oncology*. 26 (22). p.pp. 3777–3784.

Gilda, J.E. & Gomes, A. V. (2013). Stain-Free total protein staining is a superior loading control to b-actin for Western blots. *Analytical Biochemistry*. 440 (2). p.pp. 186–188.

Gilliam, L.A.A., Moylan, J.S., Patterson, E.W., Smith, J.D., Wilson, A.S., Rabbani, Z. & Reid, M.B. (2012). Doxorubicin acts via mitochondrial ROS to stimulate catabolism in C2C12 myotubes. *American Journal of Physiology: Cell Physiology*. 302 (1). p.pp. C195–C202.

Gilliam, L., Ferreira, L.F., Bruton, J.D., Moylan, J.S., Westerblad, H., St Clair, D.K. & Reid, M.B. (2009). Doxorubicin acts through tumor necrosis factor receptor subtype 1 to cause dysfunction of murine skeletal muscle. *Journal of Applied Physiology*. 107 (6). p.pp. 1935–1942.

Gnanapavan, S., Kola, B., Bustin, S., Morris, D., McGee, P., Fairclough, P., Bhattacharya, S., Carpenter, R., Grossman, A. & Korbonits, M. (2002). The tissue distribution of the mRNA of ghrelin and subtypes of its receptor, GHS-R, in humans. *The Journal of Clinical Endocrinology and Metabolism*. 87 (6). p.pp. 2988–2991.

Goodman, J. & Hochstein, P. (1977). Generation of free radicals and lipid peroxidation by redox cycling of Adriamycin and Daunomycin. *Biochemical and Biophysical Research Communications*. 77 (2). p.pp. 797–803.

Goormaghtigh, E., Chatelain, P., Caspers, J. & Ruysschaert, J.M. (1980). Evidence of a specific complex between adriamycin derivatives and cardiolipin: possible role in cardiotoxicity. *Biochemical Pharmacology*. 29 (1). p.pp. 3003–3010.

Granata, R., Isgaard, J., Alloatti, G. & Ghigo, E. (2011). Cardiovascular actions of the ghrelin gene-derived peptides and growth hormone-releasing hormone. *Experimental Biology and Medicine*. 236. p.pp. 505–514.

Granata, R., Settanni, F., Biancone, L., Trovato, L., Nano, R., Bertuzzi, F., Destefanis, S., Annunziata, M., Martinetti, M., Catapano, F., Ghe, C., Isgaard, J., Papotti, M., Ghigo, E. & Muccioli, G. (2007). Acylated and unacylated ghrelin promote proliferation and inhibit apoptosis of pancreatic B-cells and human islets: Involvement of 3',5'-cyclic adenosine monophosphate/protein kinase A, extracellular signal-regulated kinase 1/2, and phosphatidyl inositol. *Endocrinology*. 148 (2). p.pp. 512–529.

Green, P. & Leeuwenburgh, C. (2002). Mitochondrial Dysfunction is an Early Indicator of Doxorubicin-induced Apoptosis. *Biochimica et Biophysica Acta*. 62146. p.pp. 1–5.

Gustafsson, Å.B., Gottlieb, R.A. & Got, R. (2003). Mechanisms of apoptosis in the heart.

Journal of Clinical Immunology. 23 (6). p.pp. 447–459.

Guthrie, D. & Gibson, A.L. (1977). Doxorubicin cardiotoxicity: possible role of digoxin in its prevention. *British Medical Journal*. 2 (6100). p.pp. 1447–1449.

Hamid, T., Gu, Y., Ortines, R. V, Bhattacharya, C., Wang, G., Xuan, Y.-T. & Prabhu, S.D. (2009). Divergent tumor necrosis factor receptor-related remodeling responses in heart failure: role of nuclear factor-kappaB and inflammatory activation. *Circulation*. 119 (10). p.pp. 1386–1397.

Hasinoff, B.B., Schnabl, K.L., Marusak, R. a, Patel, D. & Huebner, E. (2003). Dexrazoxane (ICRF-187) protects cardiac myocytes against doxorubicin by preventing damage to mitochondria. *Cardiovascular Toxicology*. 3 (2). p.pp. 89–99.

Hattori, R., Maulik, N., Otani, H., Zhu, L., Cordis, G., Engelman, R.M., Siddiqui, M. a & Das, D.K. (2001). Role of STAT3 in ischemic preconditioning. *Journal of Molecular and Cellular Cardiology*. 33 (11). p.pp. 1929–1936.

Hausenloy, D.J. (2009). Signalling pathways in ischaemic postconditioning. *Thromb Haemost*. 101 (4). p.pp. 626–634.

Hausenloy, D.J. & Yellon, D.M. (2004). New directions for protecting the heart against ischaemia-reperfusion injury: targeting the Reperfusion Injury Salvage Kinase (RISK)-pathway. *Cardiovascular Research*. 61 (3). p.pp. 448–460.

Hayward, R., Hydock, D., Gibson, N., Greufe, S., Bredahl, E. & Parry, T. (2013). Tissue retention of doxorubicin and its effects on cardiac, smooth, and skeletal muscle function. *Journal of Physiology and Biochemistry*. 69 (2). p.pp. 177–187.

Hearse, D., Humphrey, S. & Chain, E. (1973). Abrupt reoxygenation of the anoxic potassium-arrested perfused rat heart: a study of myocardial enzyme release. *Journal of Molecular and Cellular Cardiology*. 5. p.pp. 395–407.

Hegewisch, S., Weh, H. & Hossfeld, D. (1988). TNF-induced cardiomyopathy. *The Lancet*. 335. p.pp. 294–295.

Vander Heide, R.S. & L'Ecuyer, T.J. (2007). Molecular basis of anthracycline- induced cardiotoxicity. *Heart Metab*. 35. p.pp. 1–4.

Hemmings, B.A. & Restuccia, D.F. (2012). PI3K-PKB / Akt Pathway. *Perspectives in Biology*. 4. p.pp. 1–4.

Herman, E.H., Ferraris, V.J., Myers, C.E. & Van Vleet, J.F. (1985). Comparison of the Effectiveness of +-1,2-Bis(3,5-dioxopiperazinyl-1-yl)propane (ICRF-187) and N-Acetylcysteine in Preventing Chronic Doxorubicin Cardiotoxicity in Beagles. *Cancer Research*. 45 (1). p.pp. 276–281.

Hilfiker-Kleiner, D., Hilfiker, A., Fuchs, M., Kaminski, K., Schaefer, A., Schieffer, B., Hillmer, A., Schmiedl, A., Ding, Z., Podewski, E., Podewski, E., Poli, V., Schneider, M.D., Schulz, R., Park, J.-K., Wollert, K.C. & Drexler, H. (2004). Signal transducer and activator of transcription 3 is required for myocardial capillary growth, control of interstitial matrix deposition, and heart protection from ischemic injury. *Circulation*

Research. 95 (2). p.pp. 187–195.

Hiura, Y., Takiguchi, S., Yamamoto, K., Takahashi, T., Kurokawa, Y., Yamasaki, M., Nakajima, K., Miyata, H., Fujiwara, Y., Mori, M., Kangawa, K. & Doki, Y. (2012). Effects of ghrelin administration during chemotherapy with advanced esophageal cancer patients. *Cancer*. 118 (19). p.pp. 4785–4794.

Vanden Hoek, T.L., Shao, Z., Li, C., Schumacker, P.T. & Becker, L.B. (1997). Mitochondrial electron transport can become a significant source of oxidative injury in cardiomyocytes. *Journal of molecular and cellular cardiology*. 29 (9). p.pp. 2441–50.

Von Hoff, D.D., Layard, M.W., Basa, P., Davis, H.L., Von Hoff, A.L., Rozencweig, M. & Muggia, F.M. (1979). Risk factors for Doxorubicin-induced congestive heart failure. *Annals of Internal Medicine*. 91 (5). p.pp. 710–717.

Holmgren, G., Synnergren, J., Bogestål, Y., Améen, C., Åkesson, K., Holmgren, S., Lindahl, A. & Sartipy, P. (2015). Identification of novel biomarkers for doxorubicin-induced toxicity in human cardiomyocytes derived from pluripotent stem cells. *Toxicology*. 328. p.pp. 102–111.

Hsu, H., Xiong, J. & Goeddel, D. (1995). The TNF receptor 1 associated protein TRADD signals cell death and NF kappa B activation. *Cell*. 81. p.pp. 495–504.

Huang, C.X., Yuan, M.J., Huang, H., Wu, G., Liu, Y., Yu, S.B., Li, H.T. & Wang, T. (2009). Ghrelin inhibits post-infarct myocardial remodeling and improves cardiac function through anti-inflammation effect. *Peptides*. 30 (12). p.pp. 2286–2291.

Hudson, M.M., Ness, K.K., Gurney, J.G., Mulrooney, D.A., Krull, K.R., Green, D.M., Armstrong, G.T., Nottage, K.A., Jones, K.E. & Sklar, C.A. (2013). Clinical Ascertainment of Health Outcomes Among Adults Treated for Childhood Cancer. *JAMA*. 309 (22). p.pp. 2371–2381.

Iglesias, M.J., Piñeiro, R., Blanco, M., Gallego, R., Diéguez, C., Gualillo, O., González-Juanatey, J.R. & Lago, F. (2004). Growth hormone releasing peptide (ghrelin) is synthesized and secreted by cardiomyocytes. *Cardiovascular Research*. 62 (3). p.pp. 481–488.

Ihn, H. (2002). Pathogenesis of fibrosis: role of TGF-B and CTGF. *Current Opinion in Pharmacology*. 14. p.pp. 681–685.

Indo, H.P., Yen, H.C., Nakanishi, I., Matsumoto, K., Tamura, M., Nagano, Y., Matsui, H., Gusev, O., Cornette, R., Okuda, T., Minamiyama, Y., Ichikawa, H., Suenaga, S., Oki, M. & Sato, T. (2015). A mitochondrial superoxide theory for oxidative stress diseases and aging. *Journal of Clinical Biochemistry and Nutrition*. 56 (1). p.pp. 1–7.

Insel, P.A., Zhang, L., Murray, F., Yokouchi, H. & Zambon, A.C. (2012). Cyclic AMP is both a pro-apoptotic and anti-apoptotic second messenger. *Acta Physiologica*. 204 (2). p.pp. 277–287.

Iwanaga, Y., Nishi, I., Furuichi, S., Noguchi, T., Sase, K., Kihara, Y., Goto, Y. & Nonogi, H. (2006). B-Type Natriuretic Peptide Strongly Reflects Diastolic Wall Stress in Patients With Chronic Heart Failure. *Journal of the American College of Cardiolog*. 47 (4). p.pp.

742–748.

Jacoby, J.J., Kalinowski, A., Liu, M., Zhang, S.S., Gao, Q., Chai, G., Ji, L., Iwamoto, Y., Li, E., Schneider, M., Russell, K.S., Jacoby, J.J. & Kalinowskit, A. (2003). Cardiomyocyte-restricted knockout of STAT3 results in higher sensitivity to inflammation, cardiac fibrosis and heart failure with advanced age. *Proceedings of the National Academy of Sciences of the United States of America*. 100 (22). p.pp. 12929–12934.

Jeffery, P.L., Murray, R.E., Yeh, A.H., Mcnamara, J.F., Duncan, R.P. & Francis, G.D. (2005). Expression and function of the ghrelin axis, including a novel preproghrelin isoform, in human breast cancer tissues and cell lines. *Endocrine-Related Cancer*. 12. p.pp. 839–850.

Jemal, A., Bray, F., Forman, D., O'Brien, M., Ferlay, J., Center, M. & Parkin, D.M. (2012). Cancer burden in Africa and opportunities for prevention. *Cancer*. 118 (18). p.pp. 4372–4384.

Jenei, Z., Bárdi, E., Magyar, M.T., Horváth, Á., Paragh, G. & Kiss, C. (2013). Anthracycline causes impaired vascular endothelial function and aortic stiffness in long term survivors of childhood cancer. *Pathology and Oncology Research*. 19 (3). p.pp. 375–383.

Jeyaseelan, R., Poizat, C., Wu, H. & Kedes, L. (1997). Molecular Mechanisms of Doxorubicin-induced Cardiomyopathy. *The Journal of Biological Chemistry*. 272 (9). p.pp. 5828–5832.

Jiang, X., Jiang, H., Shen, Z. & Wang, X. (2014). Activation of mitochondrial protease OMA1 by Bax and Bak promotes cytochrome c release during apoptosis. *Proceedings of the National Academy of Sciences of the United States of America*. 111 (41). p.pp. 14782–14787.

Kageyama, H., Funahashi, H., Hirayama, M. & Takenoya, F. (2005). Morphological analysis of ghrelin and its receptor distribution in the rat pancreas. *Regulatory Peptides*. 126. p.pp. 67–71.

Kalay, N., Basar, E., Ozdogru, I., Er, O., Cetinkaya, Y., Dogan, A., Inanc, T., Oguzhan, A., Eryol, N.K., Topsakal, R. & Ergin, A. (2006). Protective Effects of Carvedilol Against Anthracycline-Induced Cardiomyopathy. *Journal of the American College of Cardiology*. 48 (11). p.pp. 2258–2262.

Kalogeris, T., Bao, Y. & Korthuis, R.J. (2014). Mitochondrial reactive oxygen species: A double edged sword in ischemia/reperfusion vs preconditioning. *Redox Biology*. 2 (1). p.pp. 702–714.

Kalyanaraman, B., Joseph, J., Kalivendi, S., Wang, S., Konorev, E. & Kotamraju, S. (2002). Doxorubicin-induced apoptosis: implications in cardiotoxicity. *Molecular and Cellular Biochemistry*. 234 (1). p.pp. 119–124.

Kamegai, J., Tamura, H., Shimizu, T., Ishii, S., Sugihara, H. & Wakabayashi, I. (2001). Chronic Central Infusion of Ghrelin Increases Hypothalamic Neuropeptide Y and Agouti-Related Protein mRNA Levels and Body Weight in Rats. *Diabetes*. 50. p.pp. 2438–2443.

Kang, J., Chen, Y. & Epstein, P. (1996). Suppression of doxorubicin cardiotoxicity by overexpression of catalase in the heart of transgenic mice. *Journal of Biological Chemistry*. 271 (21). p.pp. 12610–12616.

Kannengiesser, G.., Opie, L.. & Van der Werff, T. (1979). Impaired Cardiac Work and Oxygen Uptake After Reperfusion of Regionally Ischaemic Myocardium. *Journal of Molecular and Cellular Cardiology*. 11. p.pp. 197–207.

Kantrowitz, N. & Bristow, M. (1984). Cardiotoxicity of antitumor agents. *Progress in Cardiovascular Diseases*. 27 (3). p.pp. 195–200.

Keizer, H.G., Pinedo, H.M., Schuurhuis, G.J. & Joenje, H. (1990). Doxorubicin (Adriamycin): A criticial review of free radical-dependent mechanisms of cytotoxicity. *Pharmacology & Therapeutics*. 47. p.pp. 219–231.

Kerr, J., Wyllie, A. & Currie, A. (1972). Apoptosis: A basic biological phenomenon with wide-ranging implications in tissue kinetics. *British Journal of Cancer*. 26. p.pp. 239–257.

Khan, R. & Sheppard, R. (2006). Fibrosis in heart disease: understanding the role of transforming growth factor- b 1 in cardiomyopathy, valvular disease and arrhythmia. *Immunology*. 118. p.pp. 10–24.

Kheradmand, A., Alirezaei, M. & Birjandi, M. (2010). Ghrelin promotes antioxidant enzyme activity and reduces lipid peroxidation in the rat ovary. *Regulatory Peptides*. 162 (1–3). p.pp. 84–89.

Kihara, M., Kaiya, H., Win, Z.P., Kitajima, Y. & Nishikawa, M. (2016). Protective Effect of Dietary Ghrelin-Containing Salmon Stomach Extract on Mortality and Cardiotoxicity in Doxorubicin-Induced Mouse Model of Heart Failure. *Journal of Food Science*. 0 (0). p.pp. H1–H8.

Kilickap, S., Barista, I., Akgul, E., Aytemir, K., Aksoyek, S., Aksoy, S., Celik, I., Kes, S. & Tekuzman, G. (2005). cTnT can be a useful marker for early detection of anthracycline cardiotoxicity. *Annals of Oncology*. 16. p.pp. 798–804.

Kingsbury, B. & Johannsen, O. (1935). *Histological Technique*. Wiley.

Kishimoto, I., Tokudome, T., Hosoda, H., Miyazato, M. & Kangawa, K. (2012). Ghrelin and cardiovascular diseases. *Journal of Cardiology*. 59 (1). p.pp. 8–13.

Kisseleva, T., Bhattacharya, S., Braunstein, J. & Schindler, C.W. (2002). Signaling through the JAK/STAT pathway, recent advances and future challenges. *Gene*. 285. p.pp. 1–24.

Kiu, H. & Nicholson, S.E. (2012). Biology and significance of the JAK/STAT signalling pathways. *Growth Factors*. 30 (2). p.pp. 88–106.

Kojima, M., Hosoda, H., Date, Y., Nakazato, M., Matsuo, H. & Kangawa, K. (1999). Ghrelin is a growth-hormone-releasing acylated peptide from stomach. *Nature*. 402 (6762). p.pp. 656–660.

Kojima, M., Hosoda, H., Matsuo, H. & Kangawa, K. (2001). Ghrelin: discovery of the

natural endogenous ligand for the growth hormone secretagogue receptor. *Trends in Endocrinology and Metabolism*. 12 (3). p.pp. 118–122.

Kojima, M. & Kangawa, K. (2005). Ghrelin: structure and function. *Physiology Reviews*. 85. p.pp. 295–522.

Kristal, O., Lana, S.E., Ogilvie, G.K., Rand, W.M., Cotter, S.M. & Moore, a S. (2001). Single agent chemotherapy with doxorubicin for feline lymphoma: a retrospective study of 19 cases. *Journal of Veterinary Internal Medicine / American College of Veterinary Internal Medicine*. 15 (2). p.pp. 125–130.

Kubota, T., McTiernan, C.F., Frye, C.S., Demetris, A.J. & Feldman, A.M. (1997). Cardiac-specific overexpression of tumor necrosis factor-alpha causes lethal myocarditis in transgenic mice. *Journal of Cardiac Failure*. 3 (2). p.p. 117–124.

Kui, L., Weiwei, Z., Ling, L., Daikun, H., Guoming, Z., Linuo, Z. & Renming, H. (2009). Ghrelin inhibits apoptosis induced by high glucose and sodium palmitate in adult rat cardiomyocytes through the PI3K-Akt signaling pathway. *Regulatory Peptides*. 155 (1–3). p.pp. 62–69.

Kumral, A., Giris, M., Soluk-Tekkesin, M., Olgac, V., Dogru-Abbasoglu, S., Turkoglu, U. & Uysal, M. (2016). Beneficial effects of carnosine and carnosine plus vitamin E treatments on doxorubicin-induced oxidative stress and cardiac, hepatic, and renal toxicity in rats. *Human and Experimental Toxicology*. 35 (6). p.pp. 635–643.

Kunisada, K., Negoro, S., Tone, E., Funamoto, M., Osugi, T., Yamada, S., Okabe, M., Kishimoto, T. & Yamauchi-Takihara, K. (2000). Signal transducer and activator of transcription 3 in the heart transduces not only a hypertrophic signal but a protective signal against doxorubicin-induced cardiomyopathy. *Proceedings of the National Academy of Sciences of the United States of America*. 97 (1). p.pp. 315–319.

Kwak, D.J., Augustine, N.H., Borges, W.G., Joyner, J.L., Green, W.F. & Hill, H.R. (2000). Intracellular and Extracellular Cytokine Production by Human Mixed Mononuclear Cells in Response to Group B Streptococci. *Infection and Immunity*. 68 (1). p.pp. 320–327.

Lacerda, L., Somers, S., Opie, L.H. & Lecour, S. (2009). Ischaemic postconditioning protects against reperfusion injury via the SAFE pathway. *Cardiovascular Research*. 84 (2). p.pp. 201–208.

Ladas, E.J., Jacobson, J.S., Kennedy, D.D., Teel, K., Fleischauer, A. & Kelly, K.M. (2004). Antioxidants and Cancer Therapy : A Systematic Review. *Journal of Clinical Oncology*. 22 (3). p.pp. 517–528.

Lall, S., Balthasar, N., Carmignac, D., Magoulas, C., Sesay, A., Houston, P., Mathers, K. & Robinson, I. (2004). Physiological studies of transgenic mice overexpressing growth hormone (GH) secretagogue receptor 1A in GH-releasing hormone neurons. *Endocrinology*. 145 (4). p.pp. 1602–1611.

Lear, P. V., Iglesias, M.J., Feijóo-Bandín, S., Rodríguez-Penas, D., Mosquera-Leal, A., García-Rúa, V., Gualillo, O., Ghè, C., Arnoletti, E., Muccioli, G., Diéguez, C.,

González-Juanatey, J.R. & Lago, F. (2010). Des-acyl ghrelin has specific binding sites and different metabolic effects from ghrelin in cardiomyocytes. *Endocrinology*. 151 (7). p.pp. 3286–3298.

Lebrecht, D., Geist, A., Ketelsen, U.-P., Haberstroh, J., Setzer, B. & Walker, U.A. (2007). Dexrazoxane prevents doxorubicin-induced long-term cardiotoxicity and protects myocardial mitochondria from genetic and functional lesions in rats. *British Journal of Pharmacology*. 151 (6). p.pp. 771–778.

Lecour, S. (2009a). Activation of the protective Survivor Activating Factor Enhancement (SAFE) pathway against reperfusion injury: Does it go beyond the RISK pathway? *Journal of Molecular and Cellular Cardiology*. 47 (1). p.pp. 32–40.

Lecour, S. (2009b). Multiple protective pathways against reperfusion injury: a SAFE path without Aktion? *Journal of Molecular and Cellular Cardiology*. 46 (5). p.pp. 607–609.

Lecour, S., Smith, R.M., Woodward, B., Opie, L.H., Rochette, L. & Sack, M.N. (2002). Identification of a novel role for sphingolipid signaling in TNF alpha and ischemic preconditioning mediated cardioprotection. *Journal of molecular and cellular cardiology*. 34 (5). p.pp. 509–518.

Ledderose, C., Kreth, S. & Beiras-Fernandez, A. (2011). Ghrelin, a novel peptide hormone in the regulation of energy balance and cardiovascular function. *Recent Patents on Endocrine, Metabolic & Immune Drug Discovery*. 5 (1). p.pp. 1–6.

Lefrak, E.A., Piťha, J., Rosenheim, S. & Gottlieb, J.A. (1973). A clinicopathologic analysis of Adriamycin cardiotoxicity. *Cancer*. 32. p.pp. 302–314.

Van Der Lely, A.J., Tschöp, M., Heiman, M.L. & Ghigo, E. (2004). Biological, physiological, pathophysiological, and pharmacological aspects of ghrelin. *Endocrine Reviews*. 25. p.pp. 426–457.

Li, L., Takemura, G., Li, Y., Miyata, S., Esaki, M., Okada, H., Kanamori, H., Khai, N.C., Maruyama, R., Ogino, A., Minatoguchi, S., Fujiwara, T. & Fujiwara, H. (2006a). Preventive effect of erythropoietin on cardiac dysfunction in doxorubicin-induced cardiomyopathy. *Circulation*. 113 (4). p.pp. 535–543.

Li, L., Zhang, L.K., Pang, Y.Z., Pan, C.S., Qi, Y.F., Chen, L., Wang, X., Tang, C.S. & Zhang, J. (2006b). Cardioprotective effects of ghrelin and des-octanoyl ghrelin on myocardial injury induced by isoproterenol in rats. *Acta Pharmacologica Sinica*. 27 (5). p.pp. 527–535.

Li, W.G., Gavrila, D., Liu, X., Wang, L., Gunnlaugsson, S., Stoll, L.L., McCormick, M.L., Sigmund, C.D., Tang, C. & Weintraub, N.L. (2004). Ghrelin Inhibits Proinflammatory Responses and Nuclear Factor-kB Activation in Human Endothelial Cells. *Circulation*. 109 (18). p.pp. 2221–2226.

Li, Y., Hai, J., Li, L., Chen, X., Peng, H., Cao, M. & Zhang, Q. (2013). Administration of ghrelin improves inflammation, oxidative stress, and apoptosis during and after non-alcoholic fatty liver disease development. *Endocrine*. 43 (2). p.pp. 376–386.

Liang, Q.H., Liu, Y., Wu, S.S., Cui, R.R., Yuan, L.Q. & Liao, E.Y. (2013). Ghrelin inhibits

the apoptosis of MC3T3-E1 cells through ERK and AKT signaling pathway. *Toxicology and Applied Pharmacology*. 272 (3). p.pp. 591–597.

Lien, Y.C., Lin, S.M., Nithipongvanitch, R., Oberley, T.D., Noel, T., Zhao, Q., Daosukho, C. & St Clair, D.K. (2006). Tumor necrosis factor receptor deficiency exacerbated Adriamycin-induced cardiomyocytes apoptosis: an insight into the Fas connection. *Molecular Cancer Therapeutics*. 5 (2). p.pp. 261–269.

Lipshultz, S.E., Alvarez, J.A. & Scully, R.E. (2008). Anthracycline associated cardiotoxicity in survivors of childhood cancer. *Heart*. 94 (4). p.pp. 525–533.

Lipshultz, S.E., Minotti, G., Carver, J. & Franco, V.I. (2015). An Invitation from the Editors of Cardio-Oncology. *Cardio-Oncology*. 1 (2). p.pp. 1–4.

Lipshultz, S.E., Rifai, N., Dalton, V.M., Levy, D.E., Silverman, L.B., Lipsitz, S.R., Colan, S.D., Asselin, B.L., Barr, R.D. & Clavell, L.A. (2004). The effect of dexrazoxane on myocardial injury in doxorubicin-treated children with acute lymphoblastic leukemia. *New England Journal of Medicine*. 351 (2). p.pp. 145–153.

Lopaschuk, G.D., Ussher, J.R., Folmes, C.D.L., Jaswal, J.S. & STANLEY, W.C. (2010). Myocardial Fatty Acid Metabolism in Health and Disease. *Physiological Reviews*. 90 (1). p.pp. 207–258.

Lopez, I., Mak, E.C., Ding, J., Hamm, H.E. & Lomasney, J.W. (2001). A Novel Bifunctional Phospholipase C That Is Regulated by Ga12 and Stimulates the Ras/Mitogen-activated Protein Kinase Pathway. *Journal of Biological Chemistry*. 276 (4). p.pp. 2758–2765.

Lou, H., Danelisen, I. & Singal, P.K. (2005). Involvement of mitogen-activated protein kinases in adriamycin-induced cardiomyopathy. *American Journal of Physiology Heart Circulatory Physiology*. 288 (4). p.pp. H1925–H1930.

Machida, Y., Kubota, T., Kawamura, N., Funakoshi, H., Ide, T., Utsumi, H., Li, Y.U.N.Y.O.U., Feldman, A.M., Tsutsui, H., Shimokawa, H., Takeshita, A., Kubota, T., Kawamura, N., Funakoshi, H., Ide, T., Utsumi, H., Li, Y., Feldman, A.M., Tsutsui, H. & Takeshita, A. (2003). Overexpression of tumor necrosis factor-a increases production of hydroxyl radical in murine myocardium. *American Journal of Physiology Heart Circulatory Physiology*. 284. p.pp. 449–455.

Mann, D.L. (2002). Inflammatory mediators and the failing heart: past, present, and the foreseeable Future. *Circulation Research*. 91 (11). p.pp. 988–998.

Mao, Y., Tokudome, T., Otani, K., Kishimoto, I., Miyazato, M. & Kangawa, K. (2013). Excessive sympathoactivation and deteriorated heart function after myocardial infarction in male ghrelin knockout mice. *Endocrinology*. 154 (5). p.pp. 1854–1863.

Marcus, F.I., McKenna, W.J., Sherrill, D., Basso, C., Bauce, B., Bluemke, D.A., Calkins, H., Corrado, D., Cox, M.G.P.J., Daubert, J.P., Fontaine, G., Gear, K., Hauer, R., Nava, A., Picard, M.H., Protonotarios, N., Saffitz, J.E., Sanborn, D.M.Y., Steinberg, J.S., Tandri, H., Thiene, G., Towbin, J.A., Tsatsopoulou, A., Wichter, T. & Zareba, W. (2010). Diagnosis of arrhythmogenic right ventricular cardiomyopathy/dysplasia. *European Heart Journal*. 31 (7). p.pp. 806–814.

Marie Hardwick, J. & Soane, L. (2013). Multiple functions of BCL-2 family proteins. *Cold Spring Harbor Perspectives in Biology*. 5 (2). p.pp. 1–22.

Matsumura, Y., Hamaguchi, T., Ura, T., Muro, K., Yamada, Y., Shimada, Y., Shirao, K., Okusaka, T., Ueno, H., Ikeda, M. & Watanabe, N. (2004). Phase I clinical trial and pharmacokinetic evaluation of NK911, a micelle-encapsulated doxorubicin. *British Journal of Cancer*. 91 (10). p.pp. 1775–1781.

McCord, J. & Fridovich, I. (1969). The utility of superoxide dismutase in studying free radical reactions. *The Journal of Biological Chemistry*. 244 (22). p.pp. 6056–6063.

Mimnaugh, E.G., Siddik, Z.H., Drew, R., Sikic, B.I. & Gram, T.E. (1979). The effects of α-tocopherol on the toxicity, disposition, and metabolism of adriamycin in mice. *Toxicology and Applied Pharmacology*. 49 (1). p.pp. 119–126.

Minotti, G., Menna, P., Salvatorelli, E., Cairo, G. & Gianni, L. (2004). Anthracyclines: molecular advances and pharmacologic developments in antitumor activity and cardiotoxicity. *Pharmacological Reviews*. 56 (2). p.pp. 185–229.

Mitra, M.S., Donthamsetty, S., White, B., Latendresse, J.R. & Mehendale, H.M. (2007). Mechanism of protection of moderately diet restricted rats against doxorubicin-induced acute cardiotoxicity. *Toxicology and Applied Pharmacology*. 225 (1). p.pp. 90–101.

Miyata, S., Takemura, G., Kosai, K.-I., Takahashi, T., Esaki, M., Li, L., Kanamori, H., Maruyama, R., Goto, K., Tsujimoto, A., Takeyama, T., Kawaguchi, T., Ohno, T., Nishigaki, K., Fujiwara, T., Fujiwara, H. & Minatoguchi, S. (2010). Anti-Fas gene therapy prevents doxorubicin-induced acute cardiotoxicity through mechanisms independent of apoptosis. *The American Journal of Pathology*. 176 (2). p.pp. 687–98.

Moe, G.W., Marin-garcia, J., Konig, A., Goldenthal, M., Lu, X., Feng, Q., Gordon, W., Marin-garcia, J., Konig, A., Lu, X. & Feng, Q. (2004). In vivo TNF-a inhibition ameliorates cardiac mitochondrial dysfunction, oxidative stress, and apoptosis in experimental heart failure. *American Journal of Physiology Heart Circulatory Physiology*. 287. p.pp. 1813–1820.

Mohamed, H.E., Asker, M.E., Ali, S.I. & Fattah, T.M. (2004). Protection against Doxorubicin cardiomyopathy in rats: role of phosphodiesterase inhibitors type 4. *Journal of Pharmacy and Pharmacology*. 56 (6). p.pp. 757–768.

Monden, Y., Kubota, T., Inoue, T., Tsutsumi, T., Kawano, S., Ide, T., Tsutsui, H. & Sunagawa, K. (2007). Tumor necrosis factor-a is toxic via receptor 1 and protective via receptor 2 in a murine model of myocardial infarction. *American Journal of Physiology Heart Circulatory Physiology*. 293. p.pp. 743–753.

Montaigne, D., Hurt, C. & Neviere, R. (2012). Mitochondria death/survival signaling pathways in cardiotoxicity induced by anthracyclines and anticancer-targeted therapies. *Biochemistry Research International*. 2012. p.pp. 1–12.

Monzel, J. V., Budde, T., Meyer zu Schwabedissen, H.E., Schwebe, M., Bien-Möller, S., Lütjohann, D., Kroemer, H.K., Jedlitschky, G. & Grube, M. (2017). Doxorubicin enhances oxysterol levels resulting in a LXR-mediated upregulation of cardiac

cholesterol transporters. *Biochemical Pharmacology*. 144. p.pp. 108–119.

Mootha, V.K., Arai, A.E. & Balaban, R.S. (1997). Maximum oxidative phosphorylation capacity of the mammalian heart. *The American Journal of Physiology*. 272 (2 Pt 2). p.pp. 769–775.

Moselhy, H.F., Reid, R.G., Yousef, S. & Boyle, S.P. (2013). A specific, accurate, and sensitive measure of total plasma malondialdehyde by HPLC. *Journal of Lipid Research*. 54 (3). p.pp. 852–858.

Moulin, M., Piquereau, J., Mateo, P., Fortin, D., Rucker-Martin, C., Gressette, M., Lefebvre, F., Gresikova, M., Solgadi, A., Veksler, V., Garnier, A. & Ventura-Clapier, R. (2015). Sexual dimorphism of Doxorubicin-mediated cardiotoxicity: potential role of energy metabolism remodeling. *Circulation: Heart Failure*. 8. p.pp. 98–108.

Mousseaux, D., Le Gallic, L., Ryan, J., Oiry, C., Gagne, D., Fehrentz, J.A., Galleyrand, J.C. & Martinez, J. (2006). Regulation of ERK1/2 activity by ghrelin-activated growth hormone secretagogue receptor 1A involves a PLC/PKCe pathway. *British Journal of Pharmacology*. 148. p.pp. 350–365.

Mulrooney, D.A., Armstrong, G.T., Huang, S., Ness, K.K., Ehrhardt, M.J., Joshi, V.M., Plana, J.C., Soliman, E.Z., Green, D.M., Srivastava, D., Santucci, A., Krasin, M.J., Robison, L.L. & Hudson, M.M. (2016). Cardiac Outcomes in Adult Survivors of Childhood Cancer Exposed to Cardiotoxic Therapy. *Annals of Internal Medicine*. 164. p.pp. 93–101.

Murry, C.E., Jennings, R.B. & Reimer, K. a. (1986). Preconditioning with ischemia: a delay of lethal cell injury in ischemic myocardium. *Circulation*. 74 (5). p.pp. 1124–1136.

Myers, C., Bonow, R., Palmeri, S., Jenkins, J., Corden, B., Locker, G., Doroshow, J. & Epstein, S. (1983). A randomized controlled trial assessing the prevention of doxorubicin cardiomyopathy by N-acetylcysteine. *Seminars in Oncology*. 10. p.p. 53—55.

Myers, C.E., McGuire, W.P., Liss, R.H., Ifrim, I., Grotzinger, K. & Young, R.C. (1977). Adriamycin: the role of lipid peroxidation in cardiac toxicity and tumor response. *Science (New York, N.Y.)*. 197 (4299). p.pp. 165–167.

Nagaya, N. & Kangawa, K. (2003). Ghrelin, a novel growth hormone-releasing peptide, in the treatment of chronic heart failure. *Regulatory Peptides*. 114. p.pp. 71–77.

Nagaya, N., Kojima, M., Uematsu, M., Yamagishi, M., Hosoda, H., Oya, H., Hayashi, Y. & Kangawa, K. (2001a). Hemodynamic and hormonal effects of human ghrelin in healthy volunteers. *American Journal of Physiology: Regulatory, Integrative and Comparative Physiology*. 280 (5). p.pp. R1483–R1487.

Nagaya, N., Moriya, J., Yasumura, Y., Uematsu, M., Ono, F., Shimizu, W., Ueno, K., Kitakaze, M., Miyatake, K. & Kangawa, K. (2004). Effects of Ghrelin administration on left ventricular function, exercise capacity, and muscle wasting in patients with chronic heart failure. *Circulation*. 110. p.pp. 3674–3679.

Nagaya, N., Uematsu, M., Kojima, M., Date, Y., Nakazato, M., Okumura, H., Hosoda, H.,

Shimizu, W., Yamagishi, M., Oya, H., Koh, H., Yutani, C. & Kangawa, K. (2001b). Elevated circulating level of ghrelin in cachexia associated with chronic heart failure: relationships between ghrelin and anabolic/catabolic factors. *Circulation*. 104 (17). p.pp. 2034–2038.

Nagaya, N., Uematsu, M., Kojima, M., Ikeda, Y., Yoshihara, F., Shimizu, W., Hosoda, H., Hirota, Y., Ishida, H., Mori, H. & Kangawa, K. (2001c). Chronic administration of ghrelin improves left ventricular dysfunction and attenuates development of cardiac cachexia in rats with heart failure. *Circulation*. 104 (12). p.pp. 1430–1435.

Nakamura, T., Ueda, Y., Juan, Y., Katsuda, S., Takahashi, H. & Koh, E. (2000). Fas-mediated apoptosis in Adriamycin-induced cardiomyopathy in rats: in vivo study. *Circulation*. 102 (5). p.pp. 572–578.

Nakao, K., Itoh, H., Kambayashi, Y., Hosoda, K., Saito, Y., Yamada, T., Mukoyama, M., Arai, H., Shirakami, G., Suga, S., Jougasaki, M., Ogawa, Y., Inouye, K. & Imura, H. (1990). Rat Brain Natriuretic Peptide. *Hypertension*. 15. p.pp. 774–779.

Nanzer, A.M., Khalaf, S., Mozid, A.M., Fowkes, R.C., Patel, M. V., Burrin, J.M., Grossman, A.B. & Korbonits, M. (2004). Ghrelin exerts a proliferative effect on a rat pituitary somatotroph cell line via the mitogen-activated protein kinase pathway. *European Journal of Endocrinology*. 151 (2). p.pp. 233–240.

Neary, N.M., Small, C.J., Wren, A.M., Lee, J.L., Druce, M.R., Palmieri, C., Frost, G.S., Ghatei, M.A., Coombes, R.C. & Bloom, S.R. (2004). Ghrelin increases energy intake in cancer patients with impaired appetite: Acute, randomized, placebo-controlled trial. *Journal of Clinical Endocrinology and Metabolism*. 89 (6). p.pp. 2832–2836.

Negoro, S., Kunisada, K., Tone, E., Funamoto, M., Oh, H., Kishimoto, T. & Yamauchi-Takihara, K. (2000). Activation of JAK/STAT pathway transduces cytoprotective signal in rat acute myocardial infarction. *Cardiovascular Research*. 47. p.pp. 797–805.

Negoro, S., Oh, H., Tone, E., Kunisada, K., Fujio, Y., Walsh, K., Kishimoto, T. & Yamauchi-Takihara, K. (2001). Glycoprotein 130 regulates cardiac myocyte survival in doxorubicin-induced apoptosis through phosphatidylinositol 3-kinase/Akt phosphorylation and Bcl-xL/caspase-3 interaction. *Circulation*. 103. p.pp. 555–561.

Ng, B., Wolf, R., Weksler, B., Brennan, M. & Burt, M. (1993). Growth Hormone Administration Preserves Lean Body Mass in Sarcoma-bearing Rats Treated with Doxorubicin. *Cancer Research*. 53 (22). p.pp. 5483–5486.

Nguyen, M., Ho, J., Beattie, B. & Barber, D. (2001). TEL-JAK2 mediates constitutive activation of the phosphatidylinositol 3' kinase/protein kinase B signaling pathway. *Journal of Biological Chemistry*. 276 (35). p.pp. 32704–32713.

Nishida, K., Kyoi, S., Yamaguchi, O., Sadoshima, J. & Otsu, K. (2009). The role of autophagy in the heart. *Cell Death and Differentiation*. 16. p.pp. 31–38.

Olsen, E.G.J. (1975). Pathological recognition of cardiomyopathy. *Postgraduate Medical Journal*. 51. p.pp. 277–281.

Olson, R.D., Boerth, R.C., Gerber, J.G. & Nies, A.S. (1981). Mechanism of adriamycin

cardiotoxicity: evidence for oxidative stress. *Life Sciences*. 29 (14). p.pp. 1393–1401.

Olson, R.D. & Mushlin, P.S. (1990). Doxorubicin cardiotoxicity: analysis of prevailing hypotheses. *Faseb J*. 4 (13) p.pp. 3076–3086.

Orbetzova, M. (2012). Appetite Regulatory Peptides and Insulin Resistance. In: *Insulin Resistance*. InTech, pp. 89–136.

Ou, B., Hampsch-Woodill, M. & Prior, R.L. (2001). Development and validation of an improved Oxygen Radical Absorbance Capacity assay using fluorescein as the fluorescent probe. *Journal of Agricultural and Food Chemistry*. 49 (10). p.pp. 4619–4626.

Palwankar, P., Rana, M., Arora, K. & Deepthy, C. (2015). Evaluation of non-surgical therapy on glutathione levels in chronic periodontitis. *European Journal of Dentistry*. 9 (3). p.pp. 415–422.

Panchuk, R., Skorokhyd, N., Chumak, V., Lehka, L., Omelyanchik, S., Gurinovich, V., Moiseenok, A., Heffeter, P., Berger, W. & Stoika, R. (2014). Specific antioxidant compounds differentially modulate cytotoxic activity of doxorubicin and cisplatin: in vitro and in vivo study. *Croatian Medical Journal*. 55. p.pp. 206–217.

Patil, L. & Balaraman, R. (2011). Effect of Green Tea Extract on Doxorubicin Induced Cardiovascular Abnormalities: Antioxidant Action. *Iranian Journal of Pharmaceutical Research*. 10 (1). p.pp. 89–96.

Pei, X.M., Yung, B.Y., Yip, S.P., Chan, L.W., Wong, C.S., Ying, M. & Siu, P.M. (2015). Protective effects of desacyl ghrelin on diabetic cardiomyopathy. *Acta Diabetologica*. 52 (2). p.pp. 293–306.

Pei, X.M., Yung, B.Y., Yip, S.P., Ying, M., Benzie, I.F. & Siu, P.M. (2014). Desacyl ghrelin prevents doxorubicin-induced myocardial fibrosis and apoptosis via the GHSR-independent pathway. *American Journal of Physiology: Endocrinology and Metabolism*. 306 (59). p.pp. E311–E323.

Pereira, G.G.C., Silva, A.M., Diogo, C. V, Carvalho, F.S., Monteiro, P., Oliveiraalo, P.J., Pereira, C., Silva, A.M., Diogo, C. V, Carvalho, F.S., Monteiro, P. & Oliveira, P.J. (2011). Drug-induced Cardiac Mitochondrial Toxicity and Protection: From Doxorubicin to Carvedilol. *Current Pharmaceutical Design*. 17 (20). p.pp. 2113–2129.

Perry, J., Shin, D., Getzoff, E. & Tainer, J. (2010). The structural biochemistry of the superoxide dismutatses. *Biochimica et Biophysica Acta*. 1802 (2). p.pp. 245–262.

Pfeffer, L.M., Mullersman, J.E., Pfeffer, S.R., Murti, A., Shi, W. & Yang, C. (1997). STAT3 as an Adapter to Couple Phosphatidylinositol 3-Kinase to the IFNAR1 Chain of the Type I Interferon Receptor. *Science*. 276 (5317). p.pp. 1418–1420.

Podewski, E.K. (2003). Alterations in janus kinase (JAK)-signal transducers and activators of transcription (STAT) signaling in patients with end-stage dilated cardiomyopathy. *Circulation*. 107 (6). p.pp. 798–802.

Popovic, V., Miljic, D., Micic, D., Damjanovic, S., Arvat, E., Ghigo, E., Dieguez, C. &

Casanueva, F.F. (2003). Ghrelin main action on the regulation of growth hormone release is exerted at hypothalamic level. *Journal of Clinical Endocrinology and Metabolism*. 88 (7). p.pp. 3450–3453.

Quiles, J., Huertas, J., Battino, M. & Ramirez-Tortosa, M. (2002). Antioxidant nutrients and adriamycin toxicity. *Toxicology*. 180 (1). p.pp. 79–95.

Rahman, a., Carmichael, D., Harris, M. & Roh, J.K. (1986). Comparative pharmacokinetics of free doxorubicin and doxorubicin entrapped in cardiolipin liposomes. *Cancer Research*. 46. p.pp. 2295–2299.

Rajagopalan, S., Politi, P.M., Sinha, B.K. & Myers, C.E. (1988). Adriamycin-induced Free Radical Formation in the Perfused Rat Heart: Implications for Cardiotoxicity. *Cancer Research*. 48. p.pp. 4766–4769.

Ravi, B., Kumar, C.A. & Thejomoorthy, M. (2013). Effect of Doxorubicin in Rat and Protective Role of Selected Antioxidants Vitamin A and E. *Bulletin of Pure and Applied Sciences*. 32 (2). p.pp. 61–68.

Rébé, C., Végran, F., Berger, H., Ghiringhelli, F., Georges, C., Leclerc, F., Médecine, F. De & Bourgogne, U. De (2013). STAT3 activation. A key factor in tumor immunoescape. *JAK-STAT*. 2 (1). p.pp. 1–10.

Roberts, A.B., Sporn, M.B., Assoian, R.K., Smith, J.M., Roche, N.S., Wakefield, L.M., Heine, U.I., Liotra, L.A., Falangat, V., Kehrl, J.H. & Faucit, A.S. (1986). Transforming growth factor type B: Rapid induction of fibrosis and angiogenesis in vivo and stimulation of collagen formation in vitro. *Proceedings of the National Academy of Sciences of the United States of America*. 83. p.pp. 4167–4171.

Ross, P.J., Ashley, S., Norton, A., Priest, K., Waters, J.S., Eisen, T., Smith, I.E. & O'Brien, M.E.R. (2004). Do patients with weight loss have a worse outcome when undergoing chemotherapy for lung cancers? *British Journal of Cancer*. 90 (10). p.pp. 1905–1911.

Rossi, F., Castelli, A., Bianco, M.J., Bertone, C., Brama, M. & Santiemma, V. (2009). Ghrelin inhibits contraction and proliferation of human aortic smooth muscle cells by cAMP/PKA pathway activation. *Atherosclerosis*. 203 (1). p.pp. 97–104.

Rottbauer, W., Greten, T., Muller-Bardorff, M., Remppis, A., Zehelein, J., Grunig, E. & Katus, H.A. (1996). Troponin T: a diagnostic marker for myocardial infarction and minor cardiac cell damage. *European Heart Journal*. 17. p.pp. 3–8.

Sacco, G., Bigioni, M., Evangelista, S., Goso, C., Manzini, S. & Maggi, C.A. (2001). Cardioprotective effects of zofenopril, a new angiotensin-converting enzyme inhibitor, on doxorubicin-induced cardiotoxicity in the rat. *European Journal of Pharmacology*. 414 (1). p.pp. 71–78.

Sack, M.N., Smith, R.M. & Opie, L.H. (2000). Tumor necrosis factor in myocardial hypertrophy and ischaemia — an anti-apoptotic perspective. *Cardiovascular Research*. 45 (3). p.pp. 688–695.

Saleem, M.T.S., Chetty, M.C. & Kavimani, S. (2014). Antioxidants and tumor necrosis factor alpha-inhibiting activity of sesame oil against doxorubicin-induced cardiotoxicity.

Therapeutic Advances in Cardiovascular Disease. 8 (4). p.pp. 3–11.

Scandalios, J.G. (1993). Oxygen Stress and Superoxide Dismutases. *Plant physiology*. 101 (1). p.pp. 7–12.

Schlame, M., Rua, D. & Greenberg, M.L. (2000). The biosynthesis and functional role of cardiolipin. *Progress in Lipid Research*. 39. p.pp. 257–288.

Schneider, C., Rasband, W.S. & Eliceiri, K.W. (2012). NIH Image to ImageJ: 25 years of image analysis. *Nature Methods*. 9 (7). p.pp. 671–675.

Scully, R.E. & Lipshultz, S.E. (2007). Anthracycline cardiotoxicity in long-term survivors of childhood cancer. *Cardiovascular Toxicology*. 7 (2). p.pp. 122–128.

Sengupta, P. (2013). The laboratory rat: relating its age with human's. *International Journal of Preventive Medicine*. 4 (6). p.pp. 624–630.

Sharov, V.G., Todor, A. V., Silverman, N., Goldstein, S. & Sabbah, H.N. (2000). Abnormal Mitochondrial Respiration in Failed Human Myocardium. *Journal of Molecular and Cellular Cardiology*. 32 (12). p.pp. 2361–2367.

Shimpo, K., Nagatsu, T., Yamada, K., Sato, T., Niimi, H., Shamoto, M., Takeuchi, T., Umezawa, H. & Fujita, K. (1991). Ascorbic acid and adriamycin toxicity. *American Journal of Clinical Nutrition*. 54. p.p. 1298S–1301S.

Shintani, M., Ogawa, Y., Ebihara, K., Aizawa-abe, M., Miyanaga, F., Takaya, K., Hayashi, T., Inoue, G., Hosoda, K., Kojima, M., Kangawa, K. & Nakao, K. (2001). Ghrelin, an Endogenous Growth Hormone Secretagogue, Is a Novel Orexigenic Peptide That Antagonizes Leptin Action Through the Activation of Hypothalamic Neuropeptide Y / Y1 Receptor Pathway. *Diabetes*. 50 (29). p.pp. 227–232.

Šimůnek, T., Klimtova, I., Kaplanova, J., Mazurova, Y., Adamcova, M., Štěrba, M., Hrdina, R. & Geršl, V. (2004). Rabbit model for in vivo study of anthracycline-induced heart failure and for the evaluation of protective agents. *The European Journal of Heart Failure*. 6. p.pp. 377–387.

Singal, P.K., Iliskovic, N., Li, T. & Kumar, D. (1997). Adriamycin cardiomyopathy: pathophysiology and prevention. *The FASEB Journal*. 11 (12). p.pp. 931–936.

Sinha, B.K. (1989). Free radicals in anticancer drug pharmacology. *Chemico-biological Interactions*. 69 (4). p.pp. 293–317.

Sisakian, H. (2014). Cardiomyopathies: Evolution of pathogenesis concepts and potential for new therapies. *World Journal of Cardiology*. 6 (6). p.p. 478.

Sishi, B.J.N. & Engelbrecht, A. (2011). Cytokine Tumor necrosis factor alpha (TNF-a) inactivates the PI3-kinase/PKB pathway and induces atrophy and apoptosis in L6 myotubes. *Cytokine*. 54 (2). p.pp. 173–184.

Siveski-Iliskovic, N., Kaul, N. & Singal, P.K. (1994). Probucol promotes endogenous antioxidants and provides protection against adriamycin-induced cardiomyopathy in rats. *Circulation*. 89 (6). p.pp. 2829–2835.

Skovgaard, D., Hasbak, P. & Kjaer, A. (2014). BNP Predicts Chemotherapy-Related Cardiotoxicity and Death : Comparison with Gated Equilibrium Radionuclide Ventriculography. *PLoS ONE*. 9 (5). p.p. e96736.

Smith, R.G., Jiang, H. & Sun, Y. (2005). Developments in ghrelin biology and potential clinical relevance. *Trends in Endocrinology and Metabolism*. 16 (9). p.pp. 436–442.

Smith, R.G., Van der Ploeg, L.H., Howard, A.D., Feighner, S.D., Cheng, K., Hickey, G.J., Wyvratt, M.J., Fisher, M.H., Nargund, R.P. & Patchett, A.A. (1997). Peptidomimetic regulation of growth hormone secretion. *Endocrine Reviews*. 18 (5). p.pp. 621–645.

Soeki, T., Kishimoto, I., Schwenke, D.O., Tokudome, T., Horio, T., Yoshida, M., Hosoda, H. & Kangawa, K. (2008). Ghrelin suppresses cardiac sympathetic activity and prevents early left ventricular remodeling in rats with myocardial infarction. *American Journal of Physiology: Heart and Circulatory Physiology*. 294 (1). p.pp. H426–H432.

Sonia, A., Narendra, R., Florence, A., Michel, R., Abderraouf, K., Fabienne, P. & Michel, D.W. (2009). Maurocalcine as a non toxic drug carrier overcomes doxorubicin resistance in the cancer cell line MDA-MB 231. *Pharmaceutical Research*. 6. p.pp. 1–14.

Speyer, B.J.L., Green, M.D., Zeleniuch-jacquotte, A., Wernz, J.C., Rey, M., Sanger, J., Kramer, E., Ferrans, V., Hochster, H., Meyers, M., Blum, R.H., Feit, F., Attubato, M., Burrows, W. & Muggia, F.M. (1992). ICRF-187 Permits Longer Treatment with Doxorubicin in Women with Breast Cancer. *Journal of Clinical Oncology*. 10 (1). p.pp. 117–127.

Spivak, M., Bubnov, R., Yemets, I., Lazarenko, L., Timoshok, N., Vorobieva, A., Mohnatyy, S., Ulberg, Z., Reznichenko, L., Grusina, T., Zhovnir, V. & Zholobak, N. (2013). Doxorubicin dose for congestive heart failure modeling and the use of general ultrasound equipment for evaluation in rats. Longitudinal in vivo study. *Medical Ultrasonography*. 15 (1). p.pp. 23–28.

Srdjenovic, B., Milic-Torres, V., Grujic, N., Stankov, K., Djordjevic, A. & Vasovic, V. (2010). Antioxidant properties of fullerenol C60(OH)24 in rat kidneys, testes, and lungs treated with doxorubicin. *Toxicology Mechanisms and Methods*. 20 (6). p.pp. 298–305.

Strassburg, S., Anker, S.D., Castaneda, T.R., Burget, L., Perez-Tilve, D., Pfluger, P.T., Nogueiras, R., Halem, H., Dong, J.Z., Culler, M.D., Datta, R. & Tschop, M.H. (2008). Long-term effects of ghrelin and ghrelin receptor agonists on energy balance in rats. *American Journal of Physiology: Endocrinology and Metabolism*. 295 (1). p.pp. E78-84.

Suematsu, M., Katsuki, A., Sumida, Y., Gabazza, E.C., Murashima, S., Matsumoto, K., Kitagawa, N., Akatsuka, H., Hori, Y., Nakatani, K., Togashi, K., Yano, Y. & Adachi, Y. (2005). Decreased circulating levels of active ghrelin are associated with increased oxidative stress in obese subjects. *European Journal of Endocrinology*. 153 (3). p.pp. 403–407.

Suematsu, N., Tsutsui, H., Wen, J., Kang, D., Ikeuchi, M., Ide, T., Hayashidani, S., Shiomi, T., Kubota, T., Hamasaki, N. & Takeshita, A. (2003). Oxidative stress mediates tumor necrosis factor-a-induced mitochondrial DNA damage and dysfunction in cardiac

myocytes. *Circulation*. 107. p.pp. 1418–1423.

Sugden, P.H. & Clerk, A. (1998). 'Stress-Responsive' Mitogen-Activated Protein Kinases (c-Jun N-Terminal Kinases and p38 Mitogen-Activated Protein Kinases) in the Myocardium. *Circulation Research*. 83 (4). p.pp. 345–352.

Suleman, N., Somers, S., Smith, R., Opie, L.H. & Lecour, S.C. (2008). Dual activation of STAT-3 and Akt is required during the trigger phase of ischaemic preconditioning. *Cardiovascular Research*. 79 (1). p.pp. 127–133.

Suzuki, H., Matsuzaki, J. & Hibi, T. (2011). Ghrelin and oxidative stress in gastrointestinal tract. *Journal of Clinical Biochemistry and Nutrition*. 48 (2). p.pp. 122–125.

Swain, B.S.M., Whaley, F.S., Gerber, M.C., Weisberg, S., York, M., Spicer, D., Jones, S.E., Wadler, S., Desai, A., Vogel, C., Speyer, J., Mittelman, A., Reddy, S., Pendergrass, K., Velez-garcia, E., Ewer, M.S., Bianchine, J.R. & Gams, R.A. (1997a). Cardioprotection With Dexrazoxane for Doxorubicin- Containing Therapy in Advanced Breast Cancer. *Journal of Clinical Oncology*. 15 (4). p.pp. 1318–1332.

Swain, S.M., Whaley, F.S. & Ewer, M.S. (2003). Congestive heart failure in patients treated with doxorubicin: a retrospective analysis of three trials. *Cancer*. 97 (11). p.pp. 2869–2879.

Swain, S.M., Whaley, F.S., Gerber, M.C., Weisberg, S., York, M., Spicer, D., Jones, S.E., Wadler, S., Desai, A., Vogel, C., Speyer, J., Mittelman, A., Reddy, S., Pendergrass, K., Velez-Garcia, E., Ewer, M.S., Bianchine, J.R. & Gams, R.A. (1997b). Cardioprotection with dexrazoxane for doxorubicin-containing therapy in advanced breast cancer. *Journal of Clinical Oncology* . 15 (4). p.pp. 1318–1332.

Tajima, M., Weinberg, E.O., Bartunek, J., Jin, H., Yang, R., Paoni, N.F. & Lorell, B.H. (1999). Treatment with Growth Hormone Enhances Contractile Reserve and Intracellular Calcium Transients From Rats With Postinfarction Heart Failure. *Circulation*. 99. p.pp. 127–134.

Takemura, G. & Fujiwara, H. (2006). Morphological aspects of apoptosis in heart diseases. *Journal of Cellular and Molecular Medicine*. 10 (1). p.pp. 56–75.

Taniyama, Y. & Walsh, K. (2002). Elevated myocardial Akt signaling ameliorates doxorubicin-induced congestive heart failure and promotes heart growth. *Journal of Molecular and Cellular Cardiology*. 34 (10). p.pp. 1241–1247.

Teng, L.L., Shao, L., Zhao, Y.T., Yu, X., Zhang, D.F. & Zhang, H. (2010). The beneficial effect of n-3 polyunsaturated fatty acids on doxorubicin-induced chronic heart failure in rats. *The Journal of International Medical Research*. 38 (3). p.pp. 940–948.

Thomas, C. & Aust, S. (1986). Release of Iron from Ferritin by Cardiotoxic Anthracycline Antibiotics. *Archives of Biochemistry and Biophysics*. 248 (2). p.pp. 684–689.

Thomas, X., Le, Q.H. & Fiere, D. (2002). Anthracycline-related toxicity requiring cardiac transplantation in long-term disease-free survivors with acute promyelocytic leukemia. *Annals of Hematology*. 81 (9). p.pp. 504–507.

Tian, Y., Zhang, W., Xia, D., Modi, P., Liang, D. & Wei, M. (2011). Postconditioning inhibits myocardial apoptosis during prolonged reperfusion via a JAK2-STAT3- Bcl-2 pathway. *Journal of Biomedical Science*. 18 (1). p.pp. 1–8.

Titford, M. (2009). Progress in the development of microscopical techniques for diagnostic pathology. *The Journal of Histotechnology*. 32 (1). p.pp. 9–19.

Tokarska-Schlattner, M., Zaugg, M., Zuppinger, C., Wallimann, T. & Schlattner, U. (2006). New insights into doxorubicin-induced cardiotoxicity: The critical role of cellular energetics. *Journal of Molecular and Cellular Cardiology*. 41 (3). p.pp. 389–405.

Tolle, V., Bassant, M.H., Zizzari, P., Poindessous-Jazat, F., Tomasetto, C., Epelbaum, J. & Bluet-Pajot, M.T. (2002). Ultradian rhythmicity of ghrelin secretion in relation with gh, feeding behavior, and sleep-wake patterns in rats. *Endocrinology*. 143 (4). p.pp. 1353–1361.

Tong, J., Dave, N., Mugundu, G.M., Davis, H.W., Gaylinn, B.D., Thorner, M.O., Tschöp, M.H., D'Alessio, D. & Desai, P.B. (2013). The pharmacokinetics of acyl, des-acyl, and total ghrelin in healthy human subjects. *European Journal of Endocrinology*. 168 (6). p.pp. 821–828.

Toro-Salazar, O.H., Gillan, E., Ferranti, J., Orsey, A., Rubin, K., Upadhyay, S., Mazur, W. & Hor, K.N. (2015). Effect of myocardial dysfunction in cardiac morbidity and all cause mortality in childhood cancer subjects treated with anthracycline therapy. *Cardio-Oncology*. 1 (1). p.pp. 1–9.

Torre-Amione, G., Kapadia, S., Lee, J., Durand, J.B., Bies, R.D., Young, J.B. & Mann, D.L. (1996). Tumor necrosis factor-alpha and tumor necrosis factor receptors in the failing human heart. *Circulation*. 93 (4). p.pp. 704–711.

Tschöp, M., Smiley, D.L. & Heiman, M.L. (2000). Ghrelin induces adiposity in rodents. *Nature*. 407 (6806). p.pp. 908–913.

Tukenova, M., Guibout, C., Oberlin, O., Doyon, F., Mousannif, A., Haddy, N., Guérin, S., Pacquement, H., Aouba, A., Hawkins, M., Winter, D., Bourhis, J., Lefkopoulos, D., Diallo, I. & De Vathaire, F. (2010). Role of cancer treatment in long-term overall and cardiovascular mortality after childhood cancer. *Journal of Clinical Oncology*. 28 (8). p.pp. 1308–1315.

Ueno, M., Kakinuma, Y., Yuhki, K., Murakoshi, N., Iemitsu, M., Miyauchi, T. & Yamaguchi, I. (2006). Doxorubicin induces apoptosis by activation of caspase-3 in cultured cardiomyocytes in vitro and rat cardiac ventricles in vivo. *Journal of Pharmacological Sciences*. 101. p.pp. 151–158.

Valko, M., Leibfritz, D., Moncol, J., Cronin, M.T.D., Mazur, M. & Telser, J. (2007). Free radicals and antioxidants in normal physiological functions and human disease. *The International Journal of Biochemistry & Cell Biology*. 39 (1). p.pp. 44–84.

Vandenabeele, P., Declercq, W., Beyaert, R. & Fiers, W. (1995). Two tumour necrosis factor receptors: structure and function. *Trends in Cell Biology*. 5 (10). p.pp. 392–399.

Varghese, F., Bukhari, A.B., Malhotra, R. & De, A. (2014). IHC profiler: An open source

plugin for the quantitative evaluation and automated scoring of immunohistochemistry images of human tissue samples. *PLoS ONE*. 9 (5). p.p. e96801.

Vasileiou, I., Patsouras, D., Patsouris, E. & Theocharis, S. (2013). Ghrelin and toxicity: recent findings and future challenges. *Journal of applied toxicology*. 33 (4). p.pp. 238–245.

Vellai, T., Bicsák, B., Tóth, M.L., Takács-vellai, K., Kovács, L., Vellai, T., Bicsák, B., Tóth, M.L., Takács-vellai, K. & Kovács, A.L. (2008). Regulation of cell growth by autophagy. *Autophagy*. 4 (4). p.pp. 507–509.

Vincent, J.-L. (2008). Understanding cardiac biomarkers. *Critical Care*. 12 (174). p.pp. 12–14.

Wakasugi, S., Fischman, A.J., Babich, J.W., Callahan, R.J., Elmaleh, D.R., Wilkinson, R. & Strauss, H.W. (1993). Myocardial substrate utilization and left ventricular function in adriamycin cardiomyopathy. *Journal of Nuclear Medicine*. 34 (9). p.pp. 1529–1535.

Wallace, T.W., Abdullah, S.M., Drazner, M.H., Das, S.R., Khera, A., Mcguire, D.K., Wians, F., Sabatine, M.S., Morrow, D.A. & Lemos, J.A. De (2006). Prevalence and Determinants of Troponin T Elevation in the General Population. *Circulation*. 113. p.pp. 1958–1965.

Wang, X., Wang, X.-L., Chen, H.-L., Wu, D., Chen, J.-X., Wang, X.-X., Li, R.-L., He, J.-H., Mo, L., Cen, X., Wei, Y.-Q. & Jiang, W. (2014). Ghrelin inhibits doxorubicin cardiotoxicity by inhibiting excessive autophagy through AMPK and p38-MAPK. *Biochemical Pharmacology*. 88 (3). p.pp. 334–350.

Waseem, T., Duxbury, M., Ito, H., Ashley, S.W. & Robinson, M.K. (2008). Exogenous ghrelin modulates release of pro-inflammatory and anti-inflammatory cytokines in LPS-stimulated macrophages through distinct signaling pathways. *Surgery*. 143 (3). p.pp. 334–342.

Weiss, R. (1992). The Anthracyclines: Will We Ever Find a Better Doxorubicin? *Seminars in Oncology*. 19 (6). p.pp. 670–686.

Wencker, D., Chandra, M., Nguyen, K., Miao, W., Garantziotis, S., Factor, S.M., Shirani, J., Armstrong, R.C. & Kitsis, R.N. (2003). A mechanistic role for cardiac myocyte apoptosis in heart failure. *Journal of Clinical Investigation*. 111 (10). p.pp. 1497–1504.

Wergeland, A., Bester, D.J., Sishi, B.J.N., Engelbrecht, A.M., Jonassen, A.K. & Rooyen, J. Van (2011). Dietary red palm oil protects the heart against the cytotoxic effects of anthracycline. *Cell Biochemistry and Function*. 29. p.pp. 356–364.

Willis, M.S., Homeister, J.W. & Stone, J.R. (2014). *Cellular and Molecular Pathobiology of Cardiovascular Disease*.

Wren, A., Small, C., Ward, H., Murphy, K., Dakin, C., Taheri, S., Kennedy, A., Roberts, G., Morgan, D., Ghatei, M. & Bloom, S. (2000). The Novel Hypothalamic Peptide Ghrelin Stimulates Food Intake and Growth Hormone Secretion. *Endocrinology*. 141 (11). p.pp. 4325–4328.

Wu, S., Ko, Y.-S., Ming-Sheng Teng, Ko, Y.-L., Hsu, L.-A., Hsueh, C., Chou, Y.-Y., Liew, C.-C. & Lee, Y.-S. (2002). Adriamycin-induced cardiomyocyte and endothelial cell apoptosis: In vitro and in vivo studies. *Journal of Molecular and Cellular Cardiology*. 34 (12). p.pp. 1595–1607.

Xia, P., Liu, Y. & Cheng, Z. (2016). Signaling Pathways in Cardiac Myocyte Apoptosis. *BioMed Research International*. 2016. p.pp. 1–22.

Xiang, P., Deng, H.Y., Li, K., Huang, G.-Y., Chen, Y., Tu, L., Ng, P.C., Pong, N.H., Zhao, H. & Zhang, L. (2009). Dexrazoxane protects against doxorubicin-induced cardiomyopathy: upregulation of Akt and Erk phosphorylation in a rat model. *Cancer Chemotherapy and Pharmacology*. 63 (2). p.pp. 343–349.

Xiang, Y., Li, Q., Li, M., Wang, W., Cui, C. & Zhang, J. (2011). Ghrelin inhibits AGEs-induced apoptosis in human endothelial cells involving ERK1/2 and PI3K/Akt pathways. *Cell Biochemistry and Function*. 29 (2). p.pp. 149–155.

Xiong, Y., Liu, X., Lee, C.P., Chua, B.H.L. & Ho, Y.S. (2006). Attenuation of doxorubicin-induced contractile and mitochondrial dysfunction in mouse heart by cellular glutathione peroxidase. *Free Radical Biology and Medicine*. 41 (1). p.pp. 46–55.

Xu, J.P., Wang, H.X., Wang, W., Zhang, L.K. & Tang, C.S. (2010). Ghrelin improves disturbed myocardial energy metabolism in rats with heart failure induced by isoproterenol. *Journal of Peptide Science*. 16 (8). p.pp. 392–402.

Xu, Z., Lin, S., Wu, W., Tan, H., Wang, Z., Cheng, C., Lu, L. & Zhang, X. (2008). Ghrelin prevents doxorubicin-induced cardiotoxicity through TNF-alpha/NF-κB pathways and mitochondrial protective mechanisms. *Toxicology*. 247 (2). p.pp. 133–138.

Xu, Z., Wu, W., Zhang, X. & Liu, G. (2007). Endogenous ghrelin increases in adriamycin-induced heart failure rats. *Journal of Endocrinology Investigation*. 30. p.pp. 117–125.

Yagmurca, M., Fadillioglu, E., Erdogan, H., Ucar, M., Sogut, S. & Irmak, M.K. (2003). Erdosteine prevents doxorubicin-induced cardiotoxicity in rats. *Pharmacological Research*. 48 (4). p.pp. 377–382.

Yang, C., Liu, Z., Liu, K. & Yang, P. (2014). Mechanisms of ghrelin anti-heart failure: Inhibition of Ang II-induced cardiomyocyte apoptosis by down-regulating AT1R expression. *PLoS ONE*. 9 (1). p.pp. 1–9.

Yi, X., Bekeredjian, R., DeFilippis, N.J., Siddiquee, Z., Fernandez, E. & Shohet, R. V (2006). Transcriptional analysis of doxorubicin-induced cardiotoxicity. *American Journal of Physiology. Heart and Circulatory Physiology*. 290 (3). p.pp. H1098–H1102.

Young, B., Lowe, J., Stevens, A. & Heath, J. (2006). *Wheater's Functional Histology*. Fifth Edit. I. Ozols (ed.). Elsevier.

Yu, A.P., Pei, X.M., Sin, T.K., Yip, S.P., Yung, B.Y., Chan, L.W., Wong, C.S. & Siu, P.M. (2014). Acylated and unacylated ghrelin inhibit doxorubicin-induced apoptosis in skeletal muscle. *Acta Physiologica*. 211 (1). p.pp. 201–213.

Yue, T.-L., Wang, C., Gu, J.-L., Ma, X.-L., Kumar, S., Lee, J.C., Feuerstein, G.Z., Thomas,

H., Maleeff, B. & Ohlstein, E.H. (2000). Inhibition of extracellular signal-regulated kinase enhances ischemia/reoxygenation-induced apoptosis in cultured cardiac myocytes and exaggerates reperfusion injury in isolated perfused heart. *Circulation Research*. 86 (6). p.pp. 692–699.

Zanwar, A.A., Hegde, M. V & Bodhankar, S.L. (2013). Protective role of concomitant administration of flax lignan concentrate and omega-3-fatty acid on myocardial damage in doxorubicin-induced cardiotoxicity. *Food Science and Human Wellness*. 2 (1). p.pp. 29–38.

Zhang, G., Yin, X., Qi, Y., Pendyala, L., Chen, J., Hou, D. & Tang, C. (2010). Ghrelin and cardiovascular diseases. *Journal of Cardiology*. 6. p.pp. 62–70.

Zhang, Q., Huang, W.D., Lv, X.Y. & Yang, Y.M. (2011). Ghrelin protects H9c2 cells from hydrogen peroxide-induced apoptosis through NF-kB and mitochondria-mediated signaling. *European Journal of Pharmacology*. 654 (2). p.pp. 142–149.

Zhang, Y.-W., Shi, J., Li, Y.-J. & Wei, L. (2009). Cardiomyocyte death in doxorubicin-induced cardiotoxicity. *Archivum Immunologiae et Therapiae Experimentalis*. 57 (6). p.pp. 435–445.

Zhang, Y., Li, L., Xiang, C., Ma, Z., Ma, T. & Zhu, S. (2013). Protective effect of melatonin against Adriamycin-induced cardiotoxicity. *Experimental and Therapeutic Medicine*. 5 (5). p.pp. 1496–1500.

Zhang, Y., Ying, B., Shi, L., Fan, H., Yang, D., Xu, D., Wei, Y., Hu, X., Zhang, Y., Zhang, X., Wang, T., Liu, D., Dou, L., Chen, G., Jiang, F. & Wen, F. (2007). Ghrelin inhibit cell apoptosis in pancreatic B cell line HIT-T15 via mitogen-activated protein kinase/phosphoinositide 3-kinase pathways. *Toxicology*. 237 (1–3). p.pp. 194–202.

Zhao, Z.-Q., Corvera, J.S., Halkos, M.E., Kerendi, F., Wang, N.-P., Guyton, R.A. & Vinten-Johansen, J. (2003). Inhibition of myocardial injury by ischemic postconditioning during reperfusion: comparison with ischemic preconditioning. *American Journal of Physiology: Heart and Circulatory Physiology*. 285 (2). p.pp. H579-5788.

Zhou, H., Li, X.M., Meinkoth, J. & Pittman, R.N. (2000). Akt regulates cell survival and apoptosis at a postmitochondrial level. *Journal of Cell Biology*. 151 (3). p.pp. 483–494.

Zhou, S., Palmeira, C.M. & Wallace, K.B. (2001). Doxorubicin-induced persistent oxidative stress to cardiac myocytes. *Toxicology letters*. 121 (3). p.pp. 151–157.

Zhu, W., Zou, Y., Aikawa, R., Harada, K., Kudoh, S., Uozumi, H., Hayashi, D., Gu, Y., Yamazaki, T., Nagai, R., Yazaki, Y. & Komuro, I. (1999). MAPK superfamily plays an important role in Daunomycin-induced apoptosis of cardiac myocytes. *Circulation*. 100 (20). p.pp. 2100–2107.

Zweier, J.L. (1988). Measurement of superoxide-derived free radicals in the reperfused heart. *The Journal of Biological Chemistry*. 263 (3). p.pp. 1353–1357.

Zweier, J.L. (1984). Reduction of O2 by Iron-Adriamycin. *The Journal of Biological Chemistry*. 259 (10). p.pp. 6056–6059.

Appendix A

In vitro analysis of the effect of ghrelin on cancer cell proliferation

Introduction

Oncologists are often asked by their patients if there is anything they can supplement with to reduce the toxic side effects associated with their chemotherapy, without interfering with the anti-neoplastic effects of the treatment. While there is extensive evidence that demonstrates how antioxidants and vitamins protect non-cancer cells against chemotherapy (Srdjenovic *et al*., 2010; Patil & Balaraman, 2011; D'Andrea, 2005; Ladas *et al*., 2004), it is crucial to determine whether cancer cells are also being protected. If this is the case then the effectiveness of chemotherapy would be reduced. The results of studies have been conflicting, with some stating that antioxidants are selectively protective to normal cells but cytotoxic to cancer cells, and others reporting enhanced survival of cancer cells. Since our study investigated the potential cardioprotective effects of ghrelin during DOX treatment, we felt it necessary to evaluate the effect of ghrelin on cancer cell proliferation.

Materials and Methods

MDA MB 231 cells (estrogen receptor negative, aggressive metastatic breast adenocarcinoma) and MCF7 cells (estrogen receptor positive, non-metastatic adenocarcinoma, responds to chemotherapy) were cultured and then treated daily with either 0.2 µM DOX (LKT Laboratories, D5794), 1 µM ghrelin (LKT Laboratories, G2869) or a combination of the two for a period of 120 hours. This treatment protocol was based on our previously established *in* vitro model of DOX-induced cytotoxicity. One day after the last treatment, cell viability, which was used as an indication of proliferation, was determined using the 3-[4, 5-dimethylthiazol-2-yl]-2, 5-diphenyl tetrazolium bromide (MTT) assay. MTT (Sigma-Aldrich, M2128, Johannesburg, South Africa) was prepared as a 0.01 g/mL solution in sterile phosphate buffered saline (PBS) at room temperature, and after a two hour incubation period at 37 °C, the supernatant was carefully discarded and an isopropanol (1%)/triton (0.1%) solution was added. Following a short agitation period, absorbance was determined at 540 nm using the EL800 Universal Microplate reader (Bio-Tek Instruments Inc., Vermont, USA). Cell viability was expressed as the percentage of treated cells relative to the untreated (control) cells.

Results

As indicated in Figure A0.1, ghrelin alone significantly reduced the cell viability of MDA MB 231 cells (86.23 ± 2.85%, p< 0.05) when compared to the control (100 ± 4.87), as did DOX (39.66 ± 1.72%, p< 0.001) and DOX+ghrelin (63.69 ± 1.89%, p< 0.001). Interestingly, the viability of the cells that received both treatments (DOX+ghrelin) was significantly increased when compared to the DOX alone, albeit remaining lower than the control.
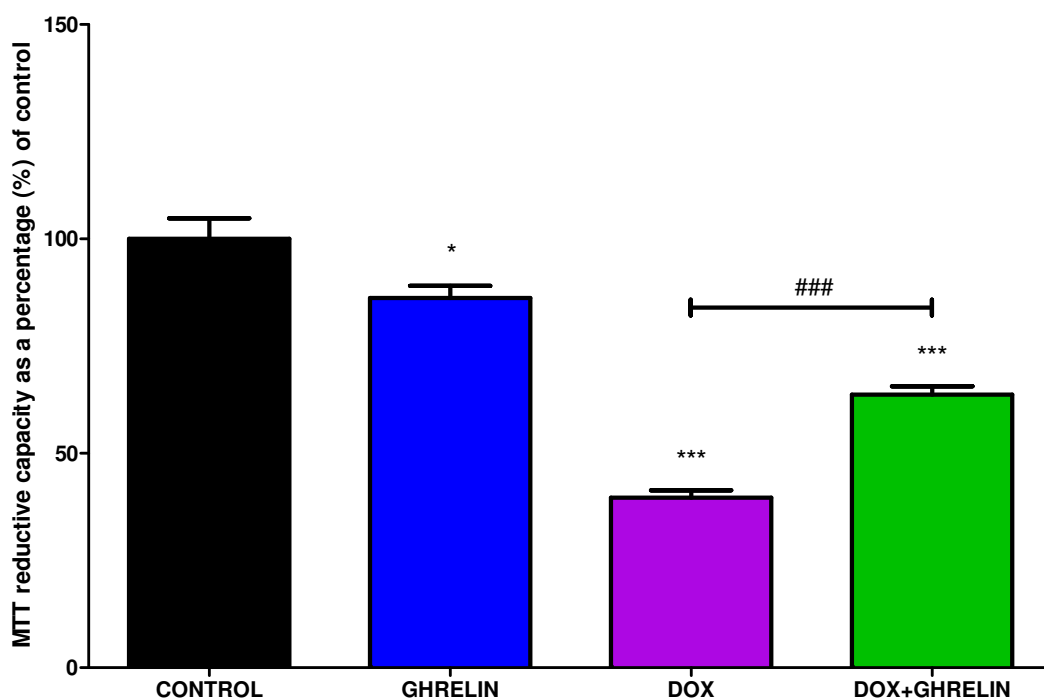
Figure A0.1: MTT reductive capacity of MDA MB 231 cells

MDA MB 231 cells were treated daily for five days with ghrelin, DOX or DOX+ghrelin. The cell viability was quantified by the cells ability to reduce MTT. All values are expressed as a percentage of the control (100%) and presented as mean ± SEM. *p< 0.05 versus control, ***p< 0.001 versus control, ###p< 0.001 versus DOX, n = 4.

In contrast to the MDA MB 231 cells, ghrelin alone had no effect on cell viability in the MCF7 cells (Figure A0.2), whereas DOX (35.06 ± 6.38%, p< 0.001) and DOX+ghrelin (34.81 ± 4.92%, p< 0.01) significantly reduced cell viability compared to the control (100 ± 11.05%). These results therefore suggest that the cytotoxic effect of ghrelin is dependent on the type and nature of the cancer cells.

- 133 -
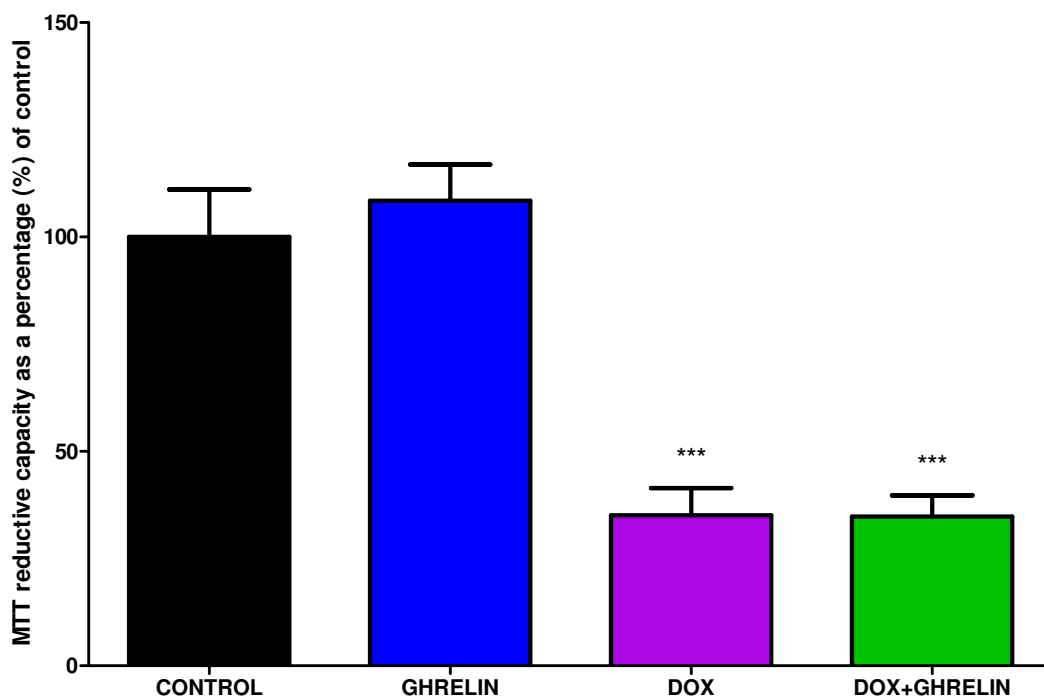
Figure A0.2: MTT reductive capacity of MCF7 cells

MCF7 cells were treated daily for five days with ghrelin, DOX or DOX+ghrelin. The cell viability was quantified by the cells ability to reduce MTT. All values are expressed as a percentage of the control (100%) and presented as mean ± SEM., ***p< 0.001 versus control, n = 4.

Discussion and Conclusion

There is no need to reiterate that an adjuvant therapy cannot be tested on humans when it is based solely on positive results from cell culture studies, as even reductions of only a few percent in the efficacy of a chemotherapeutic agent such as DOX may still lead to substantial morbidity and mortality. Like our own observations, the results of studies on ghrelin and cancer have proven to be controversial. While some studies report that ghrelin stimulates cancer cell proliferation, others have indicated that it may inhibit proliferation (see Chopin *et al*., 2011 for a full review).These discrepancies can be attributed to the fact that different concentrations of ghrelin were used, and different end-points were measured.

We have shown that in MDA MB 231 cells, ghrelin alone reduced cell proliferation, but when combined with DOX, the cell proliferation was increased. This finding is peculiar because ghrelin alone appears to be cytotoxic to cancer cells, but in the presence of a more cytotoxic agent, DOX, ghrelin promotes cell survival. This also suggests that ghrelin interferes

with the ability of DOX to kill this cancer cell line. This cell line is fairly resistant to DOX (Sonia *et al*., 2009), so it is possible that ghrelin provides a boost that promotes resistance. It is not the result we were hoping for but it still provides vital information about the safety of ghrelin supplementation during cancer. In contrast, ghrelin in combination with DOX significantly reduced the proliferation of the MCF7 cells, which is a cell line that responds well to chemotherapy. In this cell line, ghrelin may enhance the cytotoxic action of DOX whilst simultaneously protecting the non-cancerous cells. While Cassoni *et al*., (2001) demonstrated that 1 µM ghrelin (alone) decreased the cell number of MCF7 cells after 96 hours of treatment, Jeffery *et al*., (2005) reported that ghrelin stimulated proliferation in MDA MB 231 cells but had no effect on MCF7 cells. Although there is huge potential for ghrelin as a cardioprotective agent, there is also evidence to suggest that ghrelin should be used with caution during cancer treatment. With the above in mind, further research is required to determine the timing of ghrelin administration (pre-treatment or post-treatment, allowing DOX to be used alone) and the effects thereof. The fact that there is a latency period between the cessation of treatment and the onset of cardiotoxicity may indicate that the anti-neoplastic activity of DOX can be uncoupled from the toxic effects observed in the myocardium by administering a cardioprotective post-treatment regimen. However, if ghrelin alone is exerting an inhibitory effect or no effect on cancer cells, then ghrelin can be administered together with DOX to protect the non-cancerous cells. Although this study performed a single experiment in the context of cancer, we would have liked to continue and expand our experimental methods, however, this was beyond the scope of the current study.

Appendix B

Permissions/Copyright

- **Figure 1: The chemical structure of DOX**

<u>**Author:**</u> Carvalho *et al.*, (2014)

JOHN WILEY AND SONS LICENSE
TERMS AND CONDITIONS
Jul 05, 2017

This Agreement between Miss. Toni Goldswain ("You") and John Wiley and Sons ("John Wiley and Sons") consists of your license details and the terms and conditions provided by John Wiley and Sons and Copyright Clearance Center.

License Number	4142540582720
License date	Jul 05, 2017
Licensed Content Publisher	John Wiley and Sons
Licensed Content Publication	Medicinal Research Reviews
Licensed Content Title	Doxorubicin-Induced Cardiotoxicity: From Bioenergetic Failure and Cell Death to Cardiomyopathy
Licensed Content Author	Filipa S. Carvalho,Ana Burgeiro,Rita Garcia,António J. Moreno,Rui A. Carvalho,Paulo J. Oliveira
Licensed Content Date	Mar 11, 2013
Licensed Content Pages	30
Type of use	Dissertation/Thesis
Requestor type	University/Academic
Format	Print and electronic
Portion	Figure/table
Number of figures/tables	1
Original Wiley figure/table number(s)	Figure 2
Will you be translating?	No
Title of your thesis / dissertation	Ghrelin: a multifunctional hunger hormone that 'satisfies' several conditions associated with Doxorubicin-induced cardiotoxicity
Expected completion date	Dec 2017
Expected size (number of pages)	200
Requestor Location	Miss. Toni Goldswain Physiological Sciences Stellenbosch university Stellenbosch, Western Cape 7600 South Africa Attn: Miss. Toni Goldswain
Publisher Tax ID	EU826007151
Billing Type	Invoice
Billing Address	Miss. Toni Goldswain Physiological Sciences Stellenbosch university

Stellenbosch, South Africa 7600
Attn: Miss. Toni Goldswain

Total   0.00 USD

Terms and Conditions

TERMS AND CONDITIONS

This copyrighted material is owned by or exclusively licensed to John Wiley & Sons, Inc. or one of its group companies (each a"Wiley Company") or handled on behalf of a society with which a Wiley Company has exclusive publishing rights in relation to a particular work (collectively "WILEY"). By clicking "accept" in connection with completing this licensing transaction, you agree that the following terms and conditions apply to this transaction (along with the billing and payment terms and conditions established by the Copyright Clearance Center Inc., ("CCC's Billing and Payment terms and conditions"), at the time that you opened your RightsLink account (these are available at any time at http://myaccount.copyright.com).

Terms and Conditions

- The materials you have requested permission to reproduce or reuse (the "Wiley Materials") are protected by copyright.

- You are hereby granted a personal, non-exclusive, non-sub licensable (on a stand-alone basis), non-transferable, worldwide, limited license to reproduce the Wiley Materials for the purpose specified in the licensing process. This license, **and any CONTENT (PDF or image file) purchased as part of your order,** is for a one-time use only and limited to any maximum distribution number specified in the license. The first instance of republication or reuse granted by this license must be completed within two years of the date of the grant of this license (although copies prepared before the end date may be distributed thereafter). The Wiley Materials shall not be used in any other manner or for any other purpose, beyond what is granted in the license. Permission is granted subject to an appropriate acknowledgement given to the author, title of the material/book/journal and the publisher. You shall also duplicate the copyright notice that appears in the Wiley publication in your use of the Wiley Material. Permission is also granted on the understanding that nowhere in the text is a previously published source acknowledged for all or part of this Wiley Material. Any third party content is expressly excluded from this permission.

- With respect to the Wiley Materials, all rights are reserved. Except as expressly granted by the terms of the license, no part of the Wiley Materials may be copied, modified, adapted (except for minor reformatting required by the new Publication), translated, reproduced, transferred or distributed, in any form or by any means, and no derivative works may be made based on the Wiley Materials without the prior permission of the respective copyright owner.**For STM Signatory Publishers clearing permission under the terms of the STM Permissions Guidelines only, the terms of the license are extended to include subsequent editions and for editions in other languages, provided such editions are for the work as a whole in situ and does not involve the separate exploitation of the permitted figures or extracts,** You may not alter, remove or suppress in any manner any copyright, trademark or other notices displayed by the Wiley Materials. You may not license, rent, sell, loan, lease, pledge, offer as security, transfer or assign the Wiley Materials on a stand-alone basis, or any of the rights granted to you hereunder to any other person.

- The Wiley Materials and all of the intellectual property rights therein shall at all times remain the exclusive property of John Wiley & Sons Inc, the Wiley Companies, or their respective licensors, and your interest therein is only that of having possession of and the right to reproduce the Wiley Materials pursuant to Section 2 herein during the continuance of this Agreement. You agree that you own no right, title or interest in or to the Wiley Materials or any of the intellectual property rights therein. You shall have no rights hereunder other than the license as provided for above in Section 2. No right, license or interest to any trademark, trade name, service mark or other branding ("Marks") of WILEY or its licensors is granted hereunder, and you agree that you shall not assert any such right, license or interest with respect thereto

- NEITHER WILEY NOR ITS LICENSORS MAKES ANY WARRANTY OR REPRESENTATION OF ANY KIND TO YOU OR ANY THIRD PARTY, EXPRESS, IMPLIED OR STATUTORY, WITH RESPECT TO THE MATERIALS OR THE ACCURACY OF ANY INFORMATION CONTAINED IN THE MATERIALS, INCLUDING, WITHOUT LIMITATION, ANY IMPLIED WARRANTY OF MERCHANTABILITY, ACCURACY, SATISFACTORY QUALITY, FITNESS FOR A PARTICULAR PURPOSE, USABILITY,

INTEGRATION OR NON-INFRINGEMENT AND ALL SUCH WARRANTIES ARE HEREBY EXCLUDED BY WILEY AND ITS LICENSORS AND WAIVED BY YOU.

- WILEY shall have the right to terminate this Agreement immediately upon breach of this Agreement by you.

- You shall indemnify, defend and hold harmless WILEY, its Licensors and their respective directors, officers, agents and employees, from and against any actual or threatened claims, demands, causes of action or proceedings arising from any breach of this Agreement by you.

- IN NO EVENT SHALL WILEY OR ITS LICENSORS BE LIABLE TO YOU OR ANY OTHER PARTY OR ANY OTHER PERSON OR ENTITY FOR ANY SPECIAL, CONSEQUENTIAL, INCIDENTAL, INDIRECT, EXEMPLARY OR PUNITIVE DAMAGES, HOWEVER CAUSED, ARISING OUT OF OR IN CONNECTION WITH THE DOWNLOADING, PROVISIONING, VIEWING OR USE OF THE MATERIALS REGARDLESS OF THE FORM OF ACTION, WHETHER FOR BREACH OF CONTRACT, BREACH OF WARRANTY, TORT, NEGLIGENCE, INFRINGEMENT OR OTHERWISE (INCLUDING, WITHOUT LIMITATION, DAMAGES BASED ON LOSS OF PROFITS, DATA, FILES, USE, BUSINESS OPPORTUNITY OR CLAIMS OF THIRD PARTIES), AND WHETHER OR NOT THE PARTY HAS BEEN ADVISED OF THE POSSIBILITY OF SUCH DAMAGES. THIS LIMITATION SHALL APPLY NOTWITHSTANDING ANY FAILURE OF ESSENTIAL PURPOSE OF ANY LIMITED REMEDY PROVIDED HEREIN.

- Should any provision of this Agreement be held by a court of competent jurisdiction to be illegal, invalid, or unenforceable, that provision shall be deemed amended to achieve as nearly as possible the same economic effect as the original provision, and the legality, validity and enforceability of the remaining provisions of this Agreement shall not be affected or impaired thereby.

- The failure of either party to enforce any term or condition of this Agreement shall not constitute a waiver of either party's right to enforce each and every term and condition of this Agreement. No breach under this agreement shall be deemed waived or excused by either party unless such waiver or consent is in writing signed by the party granting such waiver or consent. The waiver by or consent of a party to a breach of any provision of this Agreement shall not operate or be construed as a waiver of or consent to any other or subsequent breach by such other party.

- This Agreement may not be assigned (including by operation of law or otherwise) by you without WILEY's prior written consent.

- Any fee required for this permission shall be non-refundable after thirty (30) days from receipt by the CCC.

- These terms and conditions together with CCC's Billing and Payment terms and conditions (which are incorporated herein) form the entire agreement between you and WILEY concerning this licensing transaction and (in the absence of fraud) supersedes all prior agreements and representations of the parties, oral or written. This Agreement may not be amended except in writing signed by both parties. This Agreement shall be binding upon and inure to the benefit of the parties' successors, legal representatives, and authorized assigns.

- In the event of any conflict between your obligations established by these terms and conditions and those established by CCC's Billing and Payment terms and conditions, these terms and conditions shall prevail.

- WILEY expressly reserves all rights not specifically granted in the combination of (i) the license details provided by you and accepted in the course of this licensing transaction, (ii) these terms and conditions and (iii) CCC's Billing and Payment terms and conditions.

- This Agreement will be void if the Type of Use, Format, Circulation, or Requestor Type was misrepresented during the licensing process.

- This Agreement shall be governed by and construed in accordance with the laws of the State of New York, USA, without regards to such state's conflict of law rules. Any legal action, suit or proceeding arising out of or relating to these Terms and Conditions or the breach thereof shall be instituted in a court of competent jurisdiction in New York County in the State of New York in the United States of America and each party hereby consents and submits to the personal jurisdiction of such court, waives any objection to venue in such court and consents to service of process by registered or certified mail, return receipt requested, at the last

- **Figure 2: Cumulative risk of developing DOX-induced heart failure**

<u>Author:</u> Barrett-Lee *et al.*, (2009)

Institution name	
Title of your work	Ghrelin: a multifunctional hunger hormone that 'satisfies' several conditions associated with Doxorubicin-induced cardiotoxicity
Publisher of your work	n/a
Expected publication date	Dec 2017
Permissions cost	0.00 USD
Value added tax	0.00 USD
Total	0.00 USD
Requestor Location	Miss. Toni Goldswain Physiological Sciences Stellenbosch university Stellenbosch, Western Cape 7600 South Africa Attn: Miss. Toni Goldswain
Publisher Tax ID	GB125506730
Billing Type	Invoice
Billing Address	Miss. Toni Goldswain Physiological Sciences Stellenbosch university Stellenbosch, South Africa 7600 Attn: Miss. Toni Goldswain
Total	0.00 USD
Terms and Conditions	

STANDARD TERMS AND CONDITIONS FOR REPRODUCTION OF MATERIAL FROM AN OXFORD UNIVERSITY PRESS JOURNAL

1. Use of the material is restricted to the type of use specified in your order details.

2. This permission covers the use of the material in the English language in the following territory: world. If you have requested additional permission to translate this material, the terms and conditions of this reuse will be set out in clause 12.

3. This permission is limited to the particular use authorized in (1) above and does not allow you to sanction its use elsewhere in any other format other than specified above, nor does it apply to quotations, images, artistic works etc that have been reproduced from other sources which may be part of the material to be used.

4. No alteration, omission or addition is made to the material without our written consent. Permission must be re-cleared with Oxford University Press if/when you decide to reprint.

5. The following credit line appears wherever the material is used: author, title, journal, year, volume, issue number, pagination, by permission of Oxford University Press or the sponsoring society if the journal is a society journal. Where a journal is being published on behalf of a learned society, the details of that society must be included in the credit line.

6. For the reproduction of a full article from an Oxford University Press journal for whatever purpose, the corresponding author of the material concerned should be informed of the proposed use. Contact details for the corresponding authors of all Oxford University Press journal contact can be found alongside either the abstract or full text of the article concerned, accessible from www.oxfordjournals.org Should there be a problem clearing these rights, please contact journals.permissions@oup.com

7. If the credit line or acknowledgement in our publication indicates that any of the figures, images or photos was reproduced, drawn or modified from an earlier source it will be necessary for you to clear this permission with the original publisher as well. If this permission has not been obtained, please note that this material cannot be included in your publication/photocopies.

8. While you may exercise the rights licensed immediately upon issuance of the license at the end of the licensing process for the transaction, provided that you have disclosed complete and accurate details of your proposed use, no license is finally effective unless and until full payment is received from you (either by Oxford University Press or by Copyright Clearance Center (CCC)) as provided in CCC's Billing and Payment terms and conditions. If full payment is not received on a timely basis, then any license preliminarily granted shall be deemed automatically revoked and shall be void as if never granted. Further, in the event that you breach any of these terms and conditions or any of CCC's Billing and Payment terms and conditions, the license is automatically revoked and shall be void as if never granted. Use of materials as described in a revoked license, as well as any use of the materials beyond the scope of an unrevoked license, may constitute copyright infringement and Oxford University Press reserves the right to take any and all action to protect its copyright in the materials.

9. This license is personal to you and may not be sublicensed, assigned or transferred by you to any other person without Oxford University Press's written permission.

10. Oxford University Press reserves all rights not specifically granted in the combination of (i) the license details provided by you and accepted in the course of this licensing transaction, (ii) these terms and conditions and (iii) CCC's Billing and Payment terms and conditions.

11. You hereby indemnify and agree to hold harmless Oxford University Press and CCC, and their respective officers, directors, employs and agents, from and against any and all claims arising out of your use of the licensed material other than as specifically authorized pursuant to this license.

- **Figure 3: The process of redox cycling**

Author: Tokarska-Schlattner *et al*., (2006)

ELSEVIER LICENSE
TERMS AND CONDITIONS
Jul 05, 2017

This Agreement between Miss. Toni Goldswain ("You") and Elsevier ("Elsevier") consists of your license details and the terms and conditions provided by Elsevier and Copyright Clearance Center.

License Number	4142521353091
License date	Jul 05, 2017
Licensed Content Publisher	Elsevier
Licensed Content Publication	Journal of Molecular and Cellular Cardiology
Licensed Content Title	New insights into doxorubicin-induced cardiotoxicity: The critical role of cellular energetics
Licensed Content Author	Malgorzata Tokarska-Schlattner,Michael Zaugg,Christian Zuppinger,Theo Wallimann,Uwe Schlattner
Licensed Content Date	Sep 1, 2006
Licensed Content Volume	41
Licensed Content Issue	3
Licensed Content Pages	17
Start Page	389
End Page	405
Type of Use	reuse in a thesis/dissertation
Portion	figures/tables/illustrations
Number of figures/tables/illustrations	1
Format	electronic
Are you the author of this	No

Elsevier article?	
Will you be translating?	No
Order reference number	
Original figure numbers	Figure 2
Title of your thesis/dissertation	Ghrelin: a multifunctional hunger hormone that 'satisfies' several conditions associated with Doxorubicin-induced cardiotoxicity
Expected completion date	Dec 2017
Estimated size (number of pages)	200
Elsevier VAT number	GB 494 6272 12
Requestor Location	Miss. Toni Goldswain Physiological Sciences Stellenbosch university Stellenbosch, Western Cape 7600 South Africa Attn: Miss. Toni Goldswain
Publisher Tax ID	ZA 4110266048
Total	0.00 USD
Terms and Conditions	

INTRODUCTION

1. The publisher for this copyrighted material is Elsevier. By clicking "accept" in connection with completing this licensing transaction, you agree that the following terms and conditions apply to this transaction (along with the Billing and Payment terms and conditions established by Copyright Clearance Center, Inc. ("CCC"), at the time that you opened your Rightslink account and that are available at any time at http://myaccount.copyright.com).

GENERAL TERMS

2. Elsevier hereby grants you permission to reproduce the aforementioned material subject to the terms and conditions indicated.

3. Acknowledgement: If any part of the material to be used (for example, figures) has appeared in our publication with credit or acknowledgement to another source, permission must also be sought from that source. If such permission is not obtained then that material may not be included in your publication/copies. Suitable acknowledgement to the source must be made, either as a footnote or in a reference list at the end of your publication, as follows:

"Reprinted from Publication title, Vol /edition number, Author(s), Title of article / title of chapter, Pages No., Copyright (Year), with permission from Elsevier [OR APPLICABLE SOCIETY COPYRIGHT OWNER]." Also Lancet special credit - "Reprinted from The Lancet, Vol. number, Author(s), Title of article, Pages No., Copyright (Year), with permission from Elsevier."

4. Reproduction of this material is confined to the purpose and/or media for which permission is hereby given.

5. Altering/Modifying Material: Not Permitted. However figures and illustrations may be altered/adapted minimally to serve your work. Any other abbreviations, additions, deletions and/or any other alterations shall be made only with prior written authorization of Elsevier Ltd. (Please contact Elsevier at permissions@elsevier.com). No modifications can be made to any Lancet figures/tables and they must be reproduced in full.

6. If the permission fee for the requested use of our material is waived in this instance, please be advised that your future requests for Elsevier materials may attract a fee.

7. Reservation of Rights: Publisher reserves all rights not specifically granted in the combination of (i) the license details provided by you and accepted in the course of this licensing transaction, (ii) these terms and conditions and (iii) CCC's Billing and Payment terms and conditions.

8. License Contingent Upon Payment: While you may exercise the rights licensed immediately upon issuance of the

license at the end of the licensing process for the transaction, provided that you have disclosed complete and accurate details of your proposed use, no license is finally effective unless and until full payment is received from you (either by publisher or by CCC) as provided in CCC's Billing and Payment terms and conditions. If full payment is not received on a timely basis, then any license preliminarily granted shall be deemed automatically revoked and shall be void as if never granted. Further, in the event that you breach any of these terms and conditions or any of CCC's Billing and Payment terms and conditions, the license is automatically revoked and shall be void as if never granted. Use of materials as described in a revoked license, as well as any use of the materials beyond the scope of an unrevoked license, may constitute copyright infringement and publisher reserves the right to take any and all action to protect its copyright in the materials.

9. Warranties: Publisher makes no representations or warranties with respect to the licensed material.

10. Indemnity: You hereby indemnify and agree to hold harmless publisher and CCC, and their respective officers, directors, employees and agents, from and against any and all claims arising out of your use of the licensed material other than as specifically authorized pursuant to this license.

11. No Transfer of License: This license is personal to you and may not be sublicensed, assigned, or transferred by you to any other person without publisher's written permission.

12. No Amendment Except in Writing: This license may not be amended except in a writing signed by both parties (or, in the case of publisher, by CCC on publisher's behalf).

13. Objection to Contrary Terms: Publisher hereby objects to any terms contained in any purchase order, acknowledgment, check endorsement or other writing prepared by you, which terms are inconsistent with these terms and conditions or CCC's Billing and Payment terms and conditions. These terms and conditions, together with CCC's Billing and Payment terms and conditions (which are incorporated herein), comprise the entire agreement between you and publisher (and CCC) concerning this licensing transaction. In the event of any conflict between your obligations established by these terms and conditions and those established by CCC's Billing and Payment terms and conditions, these terms and conditions shall control.

14. Revocation: Elsevier or Copyright Clearance Center may deny the permissions described in this License at their sole discretion, for any reason or no reason, with a full refund payable to you. Notice of such denial will be made using the contact information provided by you. Failure to receive such notice will not alter or invalidate the denial. In no event will Elsevier or Copyright Clearance Center be responsible or liable for any costs, expenses or damage incurred by you as a result of a denial of your permission request, other than a refund of the amount(s) paid by you to Elsevier and/or Copyright Clearance Center for denied permissions.

LIMITED LICENSE

The following terms and conditions apply only to specific license types:

15. **Translation**: This permission is granted for non-exclusive world **English** rights only unless your license was granted for translation rights. If you licensed translation rights you may only translate this content into the languages you requested. A professional translator must perform all translations and reproduce the content word for word preserving the integrity of the article.

16. **Posting licensed content on any Website**: The following terms and conditions apply as follows: Licensing material from an Elsevier journal: All content posted to the web site must maintain the copyright information line on the bottom of each image; A hyper-text must be included to the Homepage of the journal from which you are licensing at http://www.sciencedirect.com/science/journal/xxxxx or the Elsevier homepage for books at http://www.elsevier.com; Central Storage: This license does not include permission for a scanned version of the material to be stored in a central repository such as that provided by Heron/XanEdu.

Licensing material from an Elsevier book: A hyper-text link must be included to the Elsevier homepage at http://www.elsevier.com . All content posted to the web site must maintain the copyright information line on the bottom of each image.

Posting licensed content on Electronic reserve: In addition to the above the following clauses are applicable: The web site must be password-protected and made available only to bona fide students registered on a relevant course. This

- 143 -

permission is granted for 1 year only. You may obtain a new license for future website posting.

17. **For journal authors:** the following clauses are applicable in addition to the above:

Preprints:

A preprint is an author's own write-up of research results and analysis, it has not been peer-reviewed, nor has it had any other value added to it by a publisher (such as formatting, copyright, technical enhancement etc.).

Authors can share their preprints anywhere at any time. Preprints should not be added to or enhanced in any way in order to appear more like, or to substitute for, the final versions of articles however authors can update their preprints on arXiv or RePEc with their Accepted Author Manuscript (see below).

If accepted for publication, we encourage authors to link from the preprint to their formal publication via its DOI. Millions of researchers have access to the formal publications on ScienceDirect, and so links will help users to find, access, cite and use the best available version. Please note that Cell Press, The Lancet and some society-owned have different preprint policies. Information on these policies is available on the journal homepage.

Accepted Author Manuscripts: An accepted author manuscript is the manuscript of an article that has been accepted for publication and which typically includes author-incorporated changes suggested during submission, peer review and editor-author communications.

Authors can share their accepted author manuscript:

- immediately
    - via their non-commercial person homepage or blog
    - by updating a preprint in arXiv or RePEc with the accepted manuscript
    - via their research institute or institutional repository for internal institutional uses or as part of an invitation-only research collaboration work-group
    - directly by providing copies to their students or to research collaborators for their personal use
    - for private scholarly sharing as part of an invitation-only work group on commercial sites with which Elsevier has an agreement
- After the embargo period
    - via non-commercial hosting platforms such as their institutional repository
    - via commercial sites with which Elsevier has an agreement

In all cases accepted manuscripts should:

- link to the formal publication via its DOI
- bear a CC-BY-NC-ND license - this is easy to do
- if aggregated with other manuscripts, for example in a repository or other site, be shared in alignment with our hosting policy not be added to or enhanced in any way to appear more like, or to substitute for, the published journal article.

Published journal article (JPA): A published journal article (PJA) is the definitive final record of published research that appears or will appear in the journal and embodies all value-adding publishing activities including peer review co-ordination, copy-editing, formatting, (if relevant) pagination and online enrichment.

Policies for sharing publishing journal articles differ for subscription and gold open access articles:

<u>**Subscription Articles:**</u> If you are an author, please share a link to your article rather than the full-text. Millions of researchers have access to the formal publications on ScienceDirect, and so links will help your users to find, access, cite, and use the best available version.

Theses and dissertations which contain embedded PJAs as part of the formal submission can be posted publicly by the awarding institution with DOI links back to the formal publications on ScienceDirect.

If you are affiliated with a library that subscribes to ScienceDirect you have additional private sharing rights for others'

research accessed under that agreement. This includes use for classroom teaching and internal training at the institution (including use in course packs and courseware programs), and inclusion of the article for grant funding purposes.

Gold Open Access Articles: May be shared according to the author-selected end-user license and should contain a CrossMark logo, the end user license, and a DOI link to the formal publication on ScienceDirect.

Please refer to Elsevier's posting policy for further information.

18. **For book authors** the following clauses are applicable in addition to the above: Authors are permitted to place a brief summary of their work online only. You are not allowed to download and post the published electronic version of your chapter, nor may you scan the printed edition to create an electronic version. **Posting to a repository:** Authors are permitted to post a summary of their chapter only in their institution's repository.

19. **Thesis/Dissertation**: If your license is for use in a thesis/dissertation your thesis may be submitted to your institution in either print or electronic form. Should your thesis be published commercially, please reapply for permission. These requirements include permission for the Library and Archives of Canada to supply single copies, on demand, of the complete thesis and include permission for Proquest/UMI to supply single copies, on demand, of the complete thesis. Should your thesis be published commercially, please reapply for permission. Theses and dissertations which contain embedded PJAs as part of the formal submission can be posted publicly by the awarding institution with DOI links back to the formal publications on ScienceDirect.

Elsevier Open Access Terms and Conditions

You can publish open access with Elsevier in hundreds of open access journals or in nearly 2000 established subscription journals that support open access publishing. Permitted third party re-use of these open access articles is defined by the author's choice of Creative Commons user license. See our open access license policy for more information.

Terms & Conditions applicable to all Open Access articles published with Elsevier:

Any reuse of the article must not represent the author as endorsing the adaptation of the article nor should the article be modified in such a way as to damage the author's honour or reputation. If any changes have been made, such changes must be clearly indicated.

The author(s) must be appropriately credited and we ask that you include the end user license and a DOI link to the formal publication on ScienceDirect.

If any part of the material to be used (for example, figures) has appeared in our publication with credit or acknowledgement to another source it is the responsibility of the user to ensure their reuse complies with the terms and conditions determined by the rights holder.

Additional Terms & Conditions applicable to each Creative Commons user license:

CC BY: The CC-BY license allows users to copy, to create extracts, abstracts and new works from the Article, to alter and revise the Article and to make commercial use of the Article (including reuse and/or resale of the Article by commercial entities), provided the user gives appropriate credit (with a link to the formal publication through the relevant DOI), provides a link to the license, indicates if changes were made and the licensor is not represented as endorsing the use made of the work. The full details of the license are available at http://creativecommons.org/licenses/by/4.0.

CC BY NC SA: The CC BY-NC-SA license allows users to copy, to create extracts, abstracts and new works from the Article, to alter and revise the Article, provided this is not done for commercial purposes, and that the user gives appropriate credit (with a link to the formal publication through the relevant DOI), provides a link to the license, indicates if changes were made and the licensor is not represented as endorsing the use made of the work. Further, any new works must be made available on the same conditions. The full details of the license are available at http://creativecommons.org/licenses/by-nc-sa/4.0.

CC BY NC ND: The CC BY-NC-ND license allows users to copy and distribute the Article, provided this is not done for commercial purposes and further does not permit distribution of the Article if it is changed or edited in any way, and provided the user gives appropriate credit (with a link to the formal publication through the relevant DOI), provides a link to the license, and that the licensor is not represented as endorsing the use made of the work. The full details of the license are available at http://creativecommons.org/licenses/by-nc-nd/4.0. Any commercial reuse of Open Access articles

- **Figure 4: The pathways involved in free radical scavenging**

<u>Author:</u> own art work

- **Figure 5: A summary of the known biological actions of ghrelin**

<u>Author:</u> own art work

- **Figure 6: Structure of acyl-ghrelin (left) and des-acyl ghrelin (right)**

<u>Author:</u> Orbetzova, (2012)

"Dear Toni,

My name is Ivan Šuljić and I am writing you from InTech's Publishing Ethics and Legal Affairs Department.

You may freely use figure in your publication as long as you cite the source chapter of the original figure, and include the following notice in the figure caption:

© 2012 Orbetzova M. Published in [short citation] under CC BY 3.0 license. Available from: http://dx.doi.org/10.5772/50977
If you need any other help feel free to contact me.

Kind regards,

Ivan"

--
Ivan Šuljić
Publishing Ethics and Legal Affairs
_____

InTech - open science | open minds
Email: suljic@intechopen.com
Website: www.intechopen.com
Phone: +385 51 688 977
Fax: +385 51 686 166

- **Figure 7: Ghrelin regulates energy balance and appetite by at least two mechanisms**

Author: own art work

- **Figure 8: The Intrinsic Apoptotic Pathway**

Author: own art work

- **Figure 9: The Potential Signaling Pathways Induced by Ghrelin**

Author: own art work

Appendix C

Animal Ethics

UNIVERSITEIT·STELLENBOSCH·UNIVERSITY
jou kennisvennoot • your knowledge partner

Approved with Stipulations

Date: 29-Apr-2016

PI Name: Goldswain, Toni T

Protocol #: SU-ACUD15-00038

Title: Investigating the role of the RISK and SAFE pathways, through ghrelin stimulation, in an in vivo rat model of chronic Doxorubicin-induced cardiotoxicity.

Dear Toni Goldswain, the Response to Modifications submission was reviewed on 26-Apr-2016 by Research Ethics Committee: Animal Care and Use via committee review procedures and was approved on condition that the following stipulations are adhered to:

1. South African Veterinary Council authorisation for Dr Bester is not addressed in the response to modification. Sodium Pentobarbital is a scheduled substance, the committee recommend a suitable person be responsible for euthanasia using this substance. By suitable, referring to a person registered with SAVC or alternatively authorised by SAVC to do this procedure.

Applicants are reminded that they are expected to comply with accepted standards for the use of animals in research and teaching as reflected in the South African National Standards 10386: 2008. The SANS 10386: 2008 document is available on the Division for Research Developments website www.sun.ac.za/research.

As provided for in the Veterinary and Para-Veterinary Professions Act, 1982. It is the principal investigator's responsibility to ensure that all study participants are registered with or have been authorised by the South African Veterinary Council (SAVC) to perform the procedures on animals, or will be performing the procedures under the direct and continuous supervision of a SAVC-registered veterinary professional or SAVC-registered para-veterinary professional, who are acting within the scope of practice for their profession.

Please remember to use your protocol number, SU-ACUD15-00038 on any documents or correspondence with the REC: ACU concerning your research protocol.

Any event not consistent with routine expected outcomes that results in any unexpected animal welfare issue (death, disease, or prolonged distress) or human health risks (zoonotic disease or exposure, injuries) must be reported to the committee, by creating an Adverse Event submission within the system.

If you have any questions or need further help, please contact the REC: ACU secretariat at WABEUKES@SUN.AC.ZA or 0218089003.

Sincerely,

Winston Beukes

REC: ACU Secretariat

Appendix D

Detailed Protocols

Protocol 1: Milliplex® MAP Kit (Rat Cardiac Injury Magnetic Bead Panel 1)

<u>STORAGE CONDITIONS UPON RECEIPT</u>

Recommended storage for kit components is 2 - 8°C.

Avoid multiple (>2) freeze/thaw cycles.

DO NOT FREEZE Antibody-Immobilized Beads, Detection Antibody, and

Streptavidin-Phycoerythrin

Reagents Supplied	Catalog Number	Volume	Quantity
Rat Cardiac Injury Panel 1 Standard	RCI1-8087-1	Lyophilized	1 vial
Rat Cardiac Injury Panel 1 Quality Controls 1 and 2	RCI1-6087-1	Lyophilized	1 vial each
Serum Matrix Note: Contains 0.08% Sodium Azide	LHPT-SM	Lyophilized	1 vial
Set of one 96-Well Plate with 2 sealers	-----------	-----------	1 plate 2 sealers
Assay Buffer	L-AB	30 mL	1 bottle
10X Wash Buffer Note: Contains 0.05% Proclin	L-WB	60 mL	1 bottle
Rat Cardiac Injury Panel 1 Detection Antibodies	RCI1-1087-1	3.2 mL	1 bottle
Streptavidin-Phycoerythrin	L-SAPE4	3.2 mL	1 bottle
Mixing Bottle	-----------	-----------	1 bottle

Bead/Analyte Name	Luminex Magnetic Bead Region	Customizable 7 Analytes (20X concentration, 200 μL) Available Cat. #
Anti-Rat Cardiac Troponin I Bead	22	RTRPNTI-MAG
Anti-Rat Cardiac Troponin T Bead	25	RTRPNT-MAG
Anti-Rat CKM Bead	39	RCKM-MAG

PREPARATION:

A. Dilute serum samples 1: 5 by adding 15 µL of each sample to 60 µL assay buffer.

B. Preparation of Antibody-Immobilized Beads

For individual vials of beads, sonicate each antibody-bead vial for 30 seconds; vortex for 1 minute. Add 150 μL from each antibody-bead vial to the Mixing Bottle and bring final volume to 3.0 mL with Assay Buffer. Vortex the mixed beads well. Unused portion may be stored at 2-8°C for up to one month. (Note: Due to the composition of magnetic beads, you may notice a slight color in the bead solution. This does not affect the performance of the beads or the kit). Example: When using 3 antibody-immobilized beads, add 150 μL from each of the 3 bead vials to the Mixing Bottle. Then add 2.55 mL Assay Buffer.

C. Preparation of Quality Controls

Before use, reconstitute Quality Control 1 and Quality Control 2 with 250 μL deionized water. Invert the vial several times to mix and vortex. Allow the vial to sit for 5-10 minutes. Unused portion may be stored at -20°C for up to one month.

D. Preparation of Wash Buffer

Bring the 10X Wash Buffer to room temperature and mix to bring all salts into solution. Dilute 60 mL of 10X Wash Buffer with 540 mL deionized water. Store the unused portion at 2-8°C for up to one month.

E. Preparation of Serum Matrix

Add 1 mL deionized water to the bottle containing lyophilized Serum Matrix. Mix well. Allow at least 5 minutes for complete reconstitution. Dilute reconstituted Serum Matrix 1:15 by adding 60 μL of reconstituted Serum Matrix to 885 μL of assay buffer. Discard leftover diluted Serum Matrix, leftover undiluted Serum Matrix should be stored at -20°C for up to one month.

F. Preparation of Rat Cardiac Injury Panel 1 Standard

Prior to use, reconstitute the Rat Cardiac Injury Panel 1 Standard with 250 μL deionized water. Refer to table below for analyte concentrations. Invert the vial several times to mix. Vortex the vial for 10 seconds. Allow the vial to sit for 5-10 minutes. This will be used as Standard 7; the unused portion may be stored at -20°C for up to one month.

G. Preparation of Working Standards

Label 6 polypropylene microfuge tubes Standard 1 through Standard 6. Add 200 μL of Assay Buffer to each of the 6 tubes. Prepare serial dilutions by adding 100 μL of the reconstituted standard to the Standard 6 tube, mix well and transfer 100 μL of Standard 6 to the Standard 5 tube, mix well and transfer 100 μL of Standard 5 to the Standard 4 tube, mix well and transfer 100 μL of Standard 4 to the Standard 3 tube, mix well and transfer 100 μL of Standard 3 to the Standard 2 tube, mix well and transfer 100 μL of Standard 2 to the Standard 1 tube and mix well. The 0 pg/mL standard (Background) will be Assay Buffer.

Preparation of Standards Standard	MYL3 (pg/mL)	CKM (pg/mL)	FABP3, TIMP-1 (pg/mL)	Cardiac Troponin T, Follistatin-like 1 (pg/mL)	Cardiac Troponin I (pg/mL)
Standard 1	4	21	41	82	123
Standard 2	12	62	123	247	370
Standard 3	37	185	370	741	1,111
Standard 4	111	556	1,111	2,222	3,333

Standard 5	333	1,667	3,333	6,667	10,000
Standard 6	1,000	5,000	10,000	20,000	30,000
Standard 7	3,000	15,000	30,000	60,000	90,000

IMMUNOASSAY PROCEDURE

1. Allow all reagents to warm to room temperature (20-25°C) before use in the assay.

2. Diagram the placement of Standards 0 (Background), Standard 1 through 7, Controls 1 and 2, and Samples on Well Map Worksheet in a vertical configuration. It is recommended to run the assay in duplicate.

3. Add 200 μL of wash buffer into each well of the plate to pre-wet the wells.

4. Decant wash buffer and remove the residual amount from all wells by inverting the plate and tapping it smartly onto absorbent towels several times.

5. Add 25 μL of each Standard or Control into the appropriate wells. Assay buffer should be used for 0 pg/mL standard (Background).

6. Add 25 μL of assay buffer to the sample wells.

7. Add 25 μL of appropriate matrix solution to the background, standards, and control wells. When assaying serum or plasma, use the serum matrix.

8. Add 25 μL of Sample (diluted) into the appropriate wells.

9. Vortex Mixing Bottle and add 25 μL of the Mixed Beads to each well. (Note: During addition of Beads, shake bead bottle intermittently to avoid settling.)

10. Seal the plate with a plate sealer. Wrap the plate with foil and incubate with agitation (550 rpm) on a plate shaker overnight (16-18 hours) at 2-8°C.

11. Gently remove well contents and wash plate 3 times using the Bio-Rad Bio-Plex Pro™ wash station.

12. Add 25 μL of Detection Antibodies into each well.

13. Seal, cover with foil and incubate with agitation on a plate shaker (600 rpm) for 1 hour at room temperature (20-25°C). **DO NOT ASPIRATE AFTER INCUBATION. TAKE NOTE OF TIME ON COMPUTER.**

14. Add 25 μL Streptavidin-Phycoerythrin to each well containing the 25 μL of Detection Antibodies.

15. Seal, cover with foil and incubate with agitation on a plate shaker for 30 minutes at room temperature (20-25°C). **TAKE NOTE OF TIME ON A COMPUTER.**

16. Gently remove well contents and wash plate 3 times

17. Add 150 μL of Drive Fluid (EMD Millipore, MPXDF-4PK) to all wells. Resuspend the beads on a plate shaker for 5 minutes.

18. Run plate on MAGPIX® with xPONENT® software.

19. Save and analyze the Median Fluorescent Intensity (MFI) data using a 5-parameter logistic or spline curve-fitting method for calculating analyte concentrations in samples. (Note: For diluted samples, final sample concentrations should be multiplied by the dilution factor. For samples diluted as per protocol instructions, multiply by 5.

Protocol 2: Milliplex® MAP Kit (Rat Metabolic Hormone Magnetic Bead Panel)

Reagents Supplied	Catalog Number	Volume	Quantity
Rat Metabolic Hormone Standard	RMH-8084	lyophilized	1 vial
Rat Metabolic Hormone Quality Controls 1 and 2	RMH-6084	lyophilized	2 vials
Set of one 96-Well black Plate with 2 sealers	-----------	-----------	1 plate 2 sealers
Assay Buffer	LE-ABGLP	30 mL	1 bottle
Serum Matrix	LRGT-SM	1 mL	1 bottle
Bead Diluent	LE-BD	3.5 mL	1 bottle
10X Wash Buffer Note: Contains 0.05% Proclin	L-WB	60 mL	1 bottle
Rat Metabolic	RMH-1084	5.5 mL	1 bottle

Hormone Detection Antibodies			
Streptavidin-Phycoerythrin	L-SAPE12	5.5 mL	1 bottle
Mixing Bottle	-----------	-----------	1 bottle

Bead/Analyte Name	Luminex Magnetic Bead Region	Cat. #
Anti-Ghrelin Beads	20	HGRLN-MAG
Anti-Glucagon Beads	33	HGLU-MAG
Anti-IL-6 Beads	35	RIL6-MAG
Anti-Insulin Beads	37	RMINS-MAG
Anti-Leptin Beads	38	RMLPTN-MAG
Anti-TNFα Beads	65	RMTNFA-MAG

PREPARATION

A. Centrifuge samples at 3000xg for five minutes prior to assay setup.

DO NOT DILUTE

B. Preparation of Antibody-Immobilized Beads

Sonicate each antibody-bead vial for 30 seconds; vortex for 1 minute. Add 150 μL from each antibody bead vial to the Mixing Bottle and bring final volume to 3.0 mL with Bead Diluent. Vortex the mixed beads well. Unused portion may be stored at 2-8°C for up to one month. (Note: Due to the composition of magnetic beads, you may notice a slight color in the bead solution. This does not affect the performance of the beads or the kit.)

C. Preparation of Quality Controls

Before use, reconstitute Quality Control 1 and Quality Control 2 with 250 μL deionized water. Invert the vial several times to mix and vortex. Allow the vial to sit for 5-10 minutes, vortex and then transfer the controls to appropriately labeled

polypropylene microfuge tubes. Unused portion may be stored at -20°C for up to one month.

D. Preparation of Wash Buffer

Bring the 10X Wash Buffer to room temperature and mix to bring all salts into solution. Dilute 60 mL of 10X Wash Buffer with 540 mL deionized water. Store unused portion at 2-8°C for up to one month.

E. Preparation of Serum Matrix

Add 1.0 mL deionized water to the bottle containing lyophilized Serum Matrix. Mix well. Allow at least 10 minutes for complete reconstitution. Leftover reconstituted Serum Matrix can be stored at -20°C for up to one month.

F. Preparation of Rat Metabolic Hormone Standard

Prior to use, reconstitute the Rat Metabolic Hormone Standard with 250 μL deionized Water. Invert the vial several times to mix. Vortex the vial for 10 seconds. Allow the vial to sit for 5-10 minutes, vortex and then transfer the standard to appropriately labeled polypropylene microfuge tube. This will be used as Standard 7.

G. Preparation of Working Standards

Label 6 polypropylene microfuge tubes tubes "Standard 6," "Standard 5," "Standard 4," "Standard 3," "Standard 2," and "Standard 1." Add 200 μL Assay Buffer to each of the six tubes. Perform 3 times serial dilutions by adding 100 μL of the "Standard 7" to the "Standard 6" tube, mix well and transfer 100 μL of the "Standard 6" to the "Standard 5" tube, mix well and transfer 100 μL of the "Standard 5" to "Standard 4" tube, mix well and transfer 100 μL of the "Standard 4" to the "Standard 3" tube, mix well and transfer 100 μL of the "Standard 3" to the "Standard 2" tube, mix well and transfer 100 μL of the "Standard 2" to the "Standard 1" tube. The 0 Standard (background) will be assay buffer.

Standard Tube #	Ghrelin (pg/ml)	Glucagon, TNFα (pg/ml)	IL-6, Insulin, Leptin, (pg/ml)
1	6.9	14	69
2	21	41	206

3	62	124	617
4	185	370	1,852
5	556	1,111	5,556
6	1,667	3,333	16,667
7	5,000	10,000	50,000

IMMUNOASSAY PROCEDURE

1. Allow all reagents to warm to room temperature (20-25°C) before use in the assay.

2. Diagram the placement of Standards [0 (Background), 1, 2, 3, 4, 5, 6, and 7], Controls 1 and 2, and Samples on Well Map Worksheet in a vertical configuration. It is recommended to run the assay in duplicate.

3. Add 200 μL of Assay Buffer into each well of the plate to pre-wet the well.

4. Decant Assay Buffer and remove the residual amount from all wells by inverting the plate and tapping it smartly onto absorbent towels several times.

5. Add 25 μL of appropriate matrix solution to the background, standards, and control wells. When assaying serum or plasma, use the Serum Matrix provided in the kit.

6. Add 25 μL of Assay Buffer to the background (0 pg/ml standard) and sample wells.

7. Add 25 μL of each Standard or Control into the appropriate wells.

8. Add 25 μL of sample into the appropriate wells.

9. Vortex Mixing Bottle and add 25 μL of the Mixed to each well. (Note: During addition of Beads, shake bead bottle intermittently to avoid settling.)

10. Seal the plate with a plate sealer. Wrap the plate with foil and incubate with agitation on a plate shaker overnight (18-20 hours) at 4°C.

11. The next day, allow reagents and assay plate to come to room temperature. Gently remove well contents and wash plate 3 times

12. Add 50 μL of Detection Antibodies into each well. 11. Seal, cover with foil and incubate with agitation on a plate shaker for 30 minutes at room temperature (20-25°C). **DO NOT ASPIRATE AFTER INCUBATION.**

13. Add 50 μL Streptavidin-Phycoerythrin to each well containing the 50 μL of Detection Antibodies.

14. Seal, cover with foil and incubate with agitation on a plate shaker for 30 minutes at room temperature (20-25°C).

15. Gently remove well contents and wash plate 3 times

16. Add 100 μL of Drive Fluid to all wells. Resuspend the beads on a plate shaker for 5 minutes.

17. Run plate on MAGPIX® with xPONENT software.

18. Save and analyze the Median Fluorescent Intensity (MFI) data using a 5-parameter logistic or spline curve-fitting method for calculating analyte concentrations in samples.

Protocol 3: Tissue processing and sectioning

Processing:

- Prepare various concentrations of alcohol (70%, 96%, 99.9%) and xylene in 1L Schott bottles
- Pour the solutions into the jars of the tissue processor
- Place formalin-fixed tissues into a cassette in the correct orientation.
- Close the lid and label with a pencil.
- On the tissue processor, switch the dial to "manual" to allow the rotor with basket hook to move to position 1
- Move circular dial to "start" position (arrow).
- Place the closed casettes into the basket.
- Turn the dial to "auto" to check that upon dipping, all casettes are fully submerged (if not, rearrange)
- Return switch to auto and allow the processing cycle to take place.
- Processing will proceed in the following sequence:

Step	Solution	Time (minutes)	Temperature (°C)
1	10% formalin	30	Room temperature

2	70% ethanol	30	Room temperature
3	96% ethanol	30	Room temperature
4	96% ethanol	30	Room temperature
5	99.9% ethanol	30	Room temperature
6	99.9% ethanol	30	Room temperature
7	99.9% ethanol	30	Room temperature
8	Xylene	30	Room temperature
9	Xylene	30	Room temperature
10	Paraffin	60	60
11	Paraffin	60	60
12	Paraffin	60	60

- When the tissue has been processed, remove the casettes from the basket and pour the solutions back into the Schott bottles using a funnel.
- Relabel new cassettes.
- Fill the top compartment of the Leica tissue embedding station with wax (do not cover hole).
- Place the piece of tissue into a warm metal embedding mould, in the correct orientation
- Break the lid of the new cassette off and put the basket of the cassette on top of the sample/mould.
- Fill the basket of the cassette with wax and leave to set for one hour on a cooling block.
- Once it is set, the embedding mold can be removed to yield a tissue block.

Sectioning:

- Place tissue blocks into the freezer two hours prior to sectioning.
- The tissue block was first trimmed until the tissue started to appear, and then sectioned into uniform 5 µm sections using a microtome.
- Carefully lift the sectioned 'ribbons' using a paint brush and place on top of a microscope slide.
- Partially rehydrate using a 50% alcohol solution

- Gently place the sections onto the surface of a warm floatation bath (40 °C) to flatten and unravel them.
- Pick up the sections onto a clean, labelled microscope slide and allow them to dry thoroughly on a 20 °C heating block.

  *During sectioning, it is important that the blade of the microtome does not become blunt.

Protocol 4: H&E Stain

- *Mayer's hematoxylin:* commercially available Mayer's Hematoxylin (Merck Millipore, SAAR2822001LC) was filtered through Whatman's number 2 filter paper before each stain and placed into the correct position of the automated staining machine. Stock was stored at room temperature.
- *Eosin:* commercially available alcoholic Eosin (Leica Biosystems, 3801600E) was further diluted (5% in 95% ethanol) and placed in the correct position of the automated staining machine. Stock was stored at room temperature.
- *Xylene (clearing agent):* commercially available xylene (Merck, 1086619190) was stored at room temperature and used when required.
- *Ethanol:* stored at room temperature and used for the dehydration steps in the automated staining apparatus.

1. Section heart tissue and allow sections to adhere to microscope slides
2. Prior to sectioning, place the slides into an oven to allow the wax surrounding the tissue to melt.
3. Load the slides into the 'holders' of the Leica Auto Stainer XL
4. Press 'start' and then immediately press 'pause' to indicate that there are additional slides to load. After two minutes, the first 'rack' will move to the second jar, allowing a new rack to be placed into the first jar. Repeat this process until all four racks are submerged in reagents, followed by 'start'.

Step	Solution	Time (minutes)
1	Xylene	5
2	Xylene	5
3	Ethanol (99%)	2
4	Ethanol (99%)	2
5	Ethanol (96%)	2
6	Ethanol (70%)	2
7	Tap water	2
8	Mayer's Hematoxylin	8
9	Running water	5
10	Eosin (0.1%)	4
11	Running water	1
12	Ethanol (70%)	0.5
13	Ethanol (96%)	0.5
14	Ethanol (96%)	0.5
15	Ethanol (99%)	0.5
16	Xylene	1

5. Mount using DPX mountant, and allow the slides to dry for 48 hours.

Protocol 5: Masson's staining reagents

- *Mayer's hematoxylin:* commercially available Mayer's Hematoxylin (Merck Millipore, SAAR2822001LC) was filtered through Whatman's number 2 filter paper before each. Stock was stored at room temperature.

- *Acetic acid water:* add 2 mL glacial acetic acid (Radchem, 600113) to 1000 mL distilled water

- *Masson's Fuchsin Ponceau-Orange G:* prepare a stock solution by adding 2 g Ponceau (2R) de xylidine (Sigma-Aldrich, P2395), 1 g acid fuchsin (Sigma-Aldrich, F8129) and 2 g Orange G (Sigma-Aldrich, 861286) to 300 mL 0.2% acetic acid water. Then prepare a working solution by combining 10 mL of the stock solution with 90 mL 0.2% acetic acid water.

- *Light Green Solution:* add 0.1 g Light Green to 100 mL 0.2% acetic acid water

- *Phosphotungstic acid solution:* add 5 g phosphotungstic acid to 100 mL distilled water

- *Xylene (clearing agent):* commercially available xylene (Merck, 1086619190) was stored at room temperature and used when required.

Briefly warm the slides in an oven to melt surrounding wax.

Perform the Masson's Trichrome stain in the follow sequence:

Step	Reagent	Time required
1	Xylene	5 minutes
2	Xylene	5 minutes
3	99% alcohol	5 minutes
4	99% alcohol	5 minutes
5	96% alcohol	5 minutes
6	96% alcohol	5 minutes

7	96% alcohol	5 minutes
8	70% alcohol	5 minutes
9	Running tap water	5 minutes
10	Rinse in distilled water	10 seconds
11	Hematoxylin	5 minutes
12	Running tap water until blue	5 minutes
13	Rinse in distilled water	10 seconds
14	Fuchsin Ponceau Orange	20 minutes
15	Acetic acid water	10 seconds
16	Phosphotungstic acid	5 minutes
17	Acetic acid water	1 minutes
18	Light Green solution	20 minutes
19	Acetic acid water	5 minutes
20	70% alcohol	5 dips
21	96% alcohol	5 dips
22	96% alcohol	5 dips
23	96% alcohol	5 dips
24	99% alcohol	5 dips
25	99% alcohol	5 dips
26	Xylene	1 minute

27	Xylene	At least 5 minutes

Lastly, mount with DPX mounting medium.

Protocol 6: Immunohistochemistry

Leica Bond Max Autostainer

Step	Solution	Incubation Time (minutes)	Temperature
1	Peroxide block	5	Ambient
2	Bond wash solution	0	Ambient
3	Bond wash solution	0	Ambient
4	Bond wash solution	0	Ambient
5	Primary antibody	15	Ambient
6	Bond wash solution	0	Ambient
7	Bond wash solution	0	Ambient
8	Bond wash solution	0	Ambient
9	Post primary	8	Ambient
10	Bond wash solution	2	Ambient
11	Bond wash solution	2	Ambient
12	Bond wash solution	2	Ambient
13	Poly-HRP IgG	8	Ambient
14	Bond wash solution	2	Ambient
15	Bond wash solution	2	Ambient
16	Deionized water	0	Ambient
17	Deionized water	0	Ambient

18	Mixed DAB Refine	10	Ambient
19	Deionized water	0	Ambient
20	Deionized water	0	Ambient
21	Deionized water	0	Ambient
22	Hematoxylin	5	Ambient
23	Deionized water	0	Ambient
24	Deionized water	0	Ambient
25	Deionized water	0	Ambient

Protocol 7: Western blotting

Protein extraction

- Work on ice at all times to prevent protein degradation
- Thaw lysates and homogenise on ice in 450 µL RIPA buffer
- Rinse the tip of the homogeniser between each sample.
- Allow the foam to settle for at least one hour
- Centrifuge the lysates at 11 000 RPM (11.2 x g) for 2 x 15 minutes, at 4 °C, transferring to new microfuge tubes after each centrifugation

Protein determination using the Direct Detect® Infrared Spectrometer

- Switch on the laptop and infrared spectrometer to allow the machine to warm upand calibrate the level of humidity.
- Initiate the Direct Detect program, select 'operator', click to select 'proteins' and 'lipids' (if applicable), choose correct buffer for standard curve. Choose 'extended drying cycle'.
- Apply 2 µL of sample solution (position 2-4) and sample buffer blank (position 1) on the card.

- Insert the card vertically into the slot in the top of the sampling accessory. The card notch should face towards the center of the instrument (align arrows on card and instrument).
- The instrument dries samples, then measures each spot.
- After the first measurement, select 'use previous blank'

Preparation of assembly and gels

- Clean glass plates with 70% alcohol and place into casting frames
- Clean rubber with 70% alcohol to remove any debris
- Place the frames with rubber gaskets into casting stands and firmly clip into place.
- Check for leaks with distilled water, then discard water
- Make up the separating gel (% determined by size of proteins or FastCast kit)
- Using a Pasteur pipette, pour the separating gel between the glass plates, to the top of the green door - avoid making bubbles by pipetting into the corner of the plate
- Pour a layer of iso-butanol onto the gel (if pouring own gel) to prevent oxidation and to ensure a straight line (otherwise make stacking gel).
- Allow the gel to set (± 30 minutes)
- Wash off the iso-butanol using distilled water
- Prepare the 4% stacking gel
- Using a Pasteur pipette, pour the stacking gel onto the top on the separating gel
- Immediately insert the appropriate comb (10- or 15-well)
- Allow to set for +-30 minutes.
- Denature samples by boiling at 95 °C for 5 minutes
- Centrifuge samples briefly.
- Carefully remove combs from the set gel.
- Place gels into the U-shaped adaptor.
- Place the apparatus into a tank and add running buffer into the middle compartment until it overflows into the wells

Loading samples

- Pipette 5 µL BLUeye Prestained protein ladder into the first well of the gel
- Pipette samples in the rest of the wells using a new tip for each one.

- Once all samples are loaded, pour running buffer into the outer compartments
- Place a lid onto the tank and ensure the electrodes are correctly orientated – red to red and black to black
- Run samples for 10 minutes at 400 mA and 100 V (constant)
- Then run samples at 400 mA, 120 V for about 50 minutes

Membrane transfer

- Place the ready-to-assemble transfer stacks into transfer buffer to equilibrate.
- Place PVDF membrane into methanol, and then into transfer buffer to equlillibrate.
- Place the transfer stack onto a cassette, followed by the membrane.
- Roll out any air bubbles
- Carefully place the gel on top of the membrane.
- Again roll out any bubbles
- Place the top transfer stack on top of the gel
- Roll out any bubbles
- Put the lid back on and lock into place.
- Set the transfer for 7 – 12 minutes.
- Once the transfer is complete, put the membrane into methanol, then allow to dry, then wet in methanol, and lastly place into TBS-T for a short rinse.
- Finally, place into blocking solution

Antibodies

- Wash the membrane 3 x 3 minutes with TBS-T
- Make up the primary antibody solution in a 50 mL falcon tube and roll the membrane inside the tube
- Rotate in a 4 °C fridge overnight.
- The next day, wash 3 x 3 minutes with TBS-T.
- Make up secondary antibody solution in a 50 mL falcon tube and roll the membrane inside the tube
- Leave on roller for 1 hour at room temperature

Exposure

- Wash membrane 3x 3 minutes with TBS-T
- Prepare a 1:1 solution of ECL substrate (must be room temperature)
- Evenly pipette the ECL over the membrane
- Expose in the ChemiDoc until desired bands appear.

Stripping membranes

- Wash membrane for 5 minutes in distilled water
- Wash for 5 minutes in NaOH
- Wash for 5 minutes in distilled water.

OR

- Wash membrane in stripping buffer for 2 x 5 minutes
- Wash for 2 x 10 minutes in distilled water
- Block in milk solution

Protocol 8: ORAC Assay

Use BLACK fluorescence plates
Do not use the first two columns (1, 2) and the last column of plate (12) – inaccurate read
The assay runs at 37 °C so no need for ice
Switch on the plate reader and Fluoroskan 30 minutes before starting:

Fanie's profile
Fluoroskan
Open session
ORAC
Open
General tab, layout – check plate layout
Measure tab
Excitation – 485 nm
Emission – 538 nm

Phosphate buffer 75 mM, pH 7.4:
Weigh 1.035g sodium di-hydrogen orthophosphate-1-hydrate in 100 mL ddH$_2$O and mix until dissolved.
Weigh 1.335g di-sodium hydrogen orthophosphate dehydrate (Merck, 5822880EM) in 100 mL ddH$_2$O and mix until dissolved.
Mix 18 mL of 1st solution with 82 mL 2nd solution
Check pH – adjust with phosphate buffer to pH 7.4
Store at 4 °C

Fluorescein Stock: Sigma #F6377
Dissolve 0.0225g in 50 mL phosphate buffer (made above)
Store at 4 °C in a brown bottle (can be reused for one year)

Fluorescein Working Solution:
Take 10 µL of the stock and add it to 2 mL phosphate buffer (into an epi)
Take 240 µL of this and dilute in 15 mL phosphate buffer (into a 15 mL falcon)

Peroxyl radical: Sigma #440914 25 mg/mL
Weigh 150 mg of AAPH into a 15 mL falcon tube
Only add 6 mL phosphate buffer later on

Trolox (standard): 250 µM stock   Sigma #238831
Weigh 0.00312 g and add 50 mL phosphate buffer
Mix until dissolved
Should give an absorbance of 0.670 at 289nm

Procedure:
Spin down samples at 14 000 RPM for ten minutes – they must not be turbid
Deproteinize with perchloric acid at a 1: 1 ratio
Add 6 mL phosphate buffer to the AAPH weighed earlier, mix well.

Put in water bath at 37 °C

Label 6 epi's A – F

Prepare standards as follows:

	Concentration (uM)	Trolox stock (uL)	Phosphate buffer (uL)	Well
1	0	0	750	A3-5
2	83	125	625	A6-8
3	167	250	500	A9-11
4	250	375	375	A3-5
5	333	500	250	B6-8
6	417	625	125	B9-11

- Add 12 µL standards to each well
- Add 12 µL of samples per well, in triplicate
- Add 138 µL of fluorescein working solution to each well using a multichannel
- Add 50 µL of the AAPH solution to each well using a multichannel (AT the plate reader)
- Put the plate into the plate reader
- Read for 2 hours

Protocol 9: TBARS Assay

Before you start:

Set waterbath to 90 °C (fill it to 80%)

Use 2 mL epi's and punch holes in their lids

- Put 50 µL of sample into an epi.
- Add 6.25 µL of BHT dissolved in 100% ethanol (to give a concentration of 4mM) to each sample
- Add 50 µL ortho-phosphoric acid (0.2M)***** to each sample
- Vortex
- Add 6.25 µL TBA reagent to each sample (concentration of 0.11M in 0.1M NaOH)******
- Vortex
- Heat at 90 °C for 45 minutes (be strict with time and degrees for each repeat)
- Place samples in an ice bath for 2 minutes (or until needed)
- Transfer to wells, use butanol as the blank and read $A_{532} – A_{572}$

*14.6M stock of O-Phosphoric acid, therefore:

$C_1V_1 = C_2V_2$

$(14.6M)(V_1) = (0.2M)(50mL)$ (made 50mL for bulk)

V_1 = 684.93 uL in 50 mL water

$$**n = \frac{m}{MR} \ldots\ldots m = MR \ x \ n \qquad\qquad C = \frac{n}{V} \ldots\ldots n = CV \qquad\qquad therefore \ m(g) =$$

MR x C x V
g = M_R x C x V
= 144.15 x 0.11M x 0.05L
= 0.792g in 50 mL 0.1M NaOH

EQUATIONS:

Ɛ = 1.54 x 10^5

Inter-assay CV = <8%

C = A/ Ɛ

Protocol 10: GLUTATHIONE ASSAY

(Asensi *et al*., 1999a)

Reagents:

Buffer A (500 mM NaPO$_4$, 1mM EDTA, pH 7.5)

NADPH (1mM, 0.83 mg/mL) in buffer A (add 12 mL directly to vial)* NADPH, disodium salt, Cat nr. N6785 (10 vials) Sigma

M2VP (30 mM in 0.1 M HCL)   measures GSSG Cat nr. 69701 (100mg) Sigma

DTNB (0.3 mM (0.12 mg/mL) in buffer A)

Standard solution (GSH - 3 µM) (GSSG – (1.5 µM), in buffer A

Glutathione reductase (16 µL in 984 µL buffer = 1 mL)   x5 for one plate) Cat nr. G3664 (500 Units) Sigma

Procedure:

To a test run to check whether samples need to be diluted. The curve needs to be steeper than the blank, but less steep than the higher standard.

Prepare standards as follows:

	Blank	1	2	3	4	5
GSH (µL)	0	167	333	500	667	833
Buffer A (µL)	1000	833	667	500	333	167

- Add 50 µL standards/samples to the wells of a 96-well plate
- Add 50 µL of the DTNB using a multichannel
- Add 50 µL of the glutathione reductase using a multichannel
- Mix briefly and incubate for 5 minutes at 25 °C in a preheated BioTek plate reader
- Add 50 µL NADPH to each well as quickly as possible (30 seconds max)
- Measure absorbance at 412 nm every 30 seconds for 3 minutes
- Use linear slope of the standards to calculate concentration of samples

*10 mg per vial

10 mg/x mL = 0.83 mg/1mL

X = 12 mL

NADPH + glutathione reductase → GSSG → GSH

GSH binds to DTNB → yellow

Protocol 11: SOD activity assay

Prepare 50 mM $NaPO_4$ SOD buffer, without Triton-X-100, at pH 7.4

Prepare 1.6 mM 6-hydroxydopamine by adding 50 µL perchloric acid to 10 mL distilled water. Then add 4 mg of 6-HD to 1- mL of the solution made above. Wrap in foil, store on ice and use as soon as possible.

Prepare 0.1 mM DETAPAC by adding 0.4 mg to 10 mL SOD assay buffer. Store at -20 °C.

Prepare different dilutions of test samples.

Add 12 µL of each sample in triplicate to a 96-well plate.

Then add 15 µL 6-HD to each well.

At the plate reader, add 170 µL DETAPAC

Then record the auto-oxidation at 490 nm for four minutes, at one minute intervals.

Protocol 12: Conjugated Dienes

- o Weigh 100 mg tissue
- o Add 100 ul chloroform + 200 ul methanol
- o Homogenise for 2 mins
- o Then add 100 ul chloroform
- o Homogenise for 30 seconds
- o Add 100 ul dH$_2$O
- o Homogenise for 30 seconds
- o Centrifuge at 10 000 rpm for 10 mins
    - ▪ Should be 2 layers – chloroform layer = bottom
- o Transfer bottom layer to new eppie [RECORD AMOUNT]
- o Add 100 ul NaCl until suspended properly
- o Leave open eppies in 4°C walk-in fridge [~ 2 days / weekend]
    - ▪ Freeze what is left in eppie
- Once all eppies are dry, add 700 ul cyclohexane into each eppie
- The add 150 ul of each eppie into each well on plate
- (Blanks = 150 ul cyclohexane)

Protocol 13: BNP ELISA

Equilibrate all kit components to room temperature

Preparation of Reagents and Samples:

- Diluent (10x)
  Prepare a 1x diluent solution by mixing 30 mL diluent with 270 mL distilled water.

- Wash buffer (20x)
  Prepare 1x wash buffer by mixing 30 ml buffer with 570 mL distilled water

- Biotinylated detector antibody (50x)
  Dilute 105.6 uL detector antibody with 5174.4 uL diluent.

- SP Conjugate (100x)
  Prepare 1x SP conjugate by adding 80 uL to 7920 uL diluent

- Prepare the standards by resuspending the powder in the vial (8 ng) in 8000 uL diluent to give 1 ng/mL. This is standard 1. Allow it to sit for 10 minutes with gentle agitation.

- Label tubes 2 – 7 and pipette 120 uL of diluent into each one. Then pipette 120 uL standard 1 into tube 2. Mix thoroughly. Then pipette 120 uL tube 2 into tube 3 – repeat until tube 6. Tube 7 serves as the blank (diluent).

- Homogenise samples in 0.1M PBS containing 1% Triton-X-100. Centrifuge at 14 000 x g for 20 minutes at 4 °C. Measure the protein concentration in the supernatant, then assay.

1. Add 50 uL of each standard and sample into the 96-well plate, in duplicate. Seal and incubate for two hours.
2. Wash five times with wash buffer
3. Add 50 uL biotinylated detector antibody to each well. Cover the plate and incubate for two hours.
4. Wash the plate five times
5. Add 50 uL SP conjugate to each well and incubate for 30 minutes. Set up the plate reader during this time
6. Wash the plate five times
7. Add 50 uL chromogen substrate and incubate for about ten minutes. Tap to mix.
8. Add 50 uL STOP solution to each well and read the plate immediately at 450 nm.

Appendix E

Preparation of Reagents

Protocol 1: DOX preparation (2.5 mg/kg):

Resuspend 50 mg DOX in 12.5 mL sterile saline to give a stock of 4 mg/mL = 4 µg/µL
Vortex thoroughly.

Example:

Animal weight: 118.1 g

→ 118.1 g x 2.5 µg/g

→ 295.25 µg DOX

> Animal dose = 2.5 mg/kg
>
> = 2.5 µg/g

Stock = 4 µg/ µL

→ $\frac{4\ µg}{1\ µL} = \frac{295.25\ µg}{X}$

x = 73.8125 µL DOX stock (4 µg/ µL) in 200 µL saline (200 uL is the injection volume)

BUT… multiply by 2 to account for bubbles and wastage

→ 73.8125 x 2 = 147.625 µL DOX in 252.375 µL saline.

Vortex thoroughly.

Inject 200 µL.

Protocol 2: Ghrelin preparation

Resuspend 5 mg ghrelin in 5 mL sterile saline to give a stock solution of 1 mg/mL = 1 µg/µL
Vortex thoroughly.

Example:

Animal weight: 118.1 g

→ 118.1 g x 0.1 µg/g

→ 11.81 µg ghrelin

> Animal dose = 100 µg/kg
>
> = 0.1 µg/g

Stock = 1 µg/ µL

→ $\frac{1\ µg}{1\ µL} = \frac{11.81\ µg}{X}$

x = 11.81 µL ghrelin stock (1 µg/ µL) in 200 µL saline (200 uL is the injection volume)

… multiply by 2 to account for bubbles and wastage

→ 11.81 x 2 = 23.62 µL ghrelin in 376.38 µL saline.

Vortex thoroughly.

Inject 200 µL.

Protocol 3: Krebs Henseleit Buffer

- Stock 1
    - 279 g NaCl in 2 L distilled water
    - M_R: 58.44, Radchem, S1327B
- Stock 2
    - 83.6 g NaHCO$_3$ in 2 L distilled water
    - M_R: 84.01, Merck, K45372729428
- Stock 3:
    - 17.6 g KCL
    - M_R: 74.56, Kimix,
    - 8.10 g KH$_2$PO$_4$
    - M_R: 136.09, Saarchem, 5043600EM
- Stock 4:
    - 7.4 g MgSO$_4$.7H$_2$O
    - M_R: 246.48, Saarchem, SAAR4124000EM
    - 4.2 g Na$_2$SO$_4$
    - M_R: 142.04, Saarchem, 5825260EM
- Additives:
    - 1.76 g CaCl$_2$.2H$_2$O (M_R: 147.02, Saarchem, SAAR1524820EM)
    - 9 g glucose anhydrous (M_R: 180.16, Radchem)

Buffer:

1. 250 mL stock 1
2. 250 mL stock 2
3. 100 mL stock 3
4. 100 mL stock 4

5. Fill up with distilled water to approximately 3 L

6. Add 1.76 g CaCl2.2H2O to a small amount of water

7. Mix well to avoid crystalisation

8. Add to the buffer and mix well

9. Mix 9g glucose to the buffer while mixing vigorously.

10. Top up to 5 L mark.

Protocol 4: Phosphate Buffered Saline 1X (PBS)

Dissolve the following in 1L of distilled water:

16 g NaCl

0.4 g KCl

2.88 g Na_2HPO_4

0.48 g KH_2PO_4

- Adjust the pH to 7.4

- Fill up to the 2L mark with distilled water

- Autoclave

Protocol 5: 95% alcohol (1L)

- Dilute 950 mL 100% ethanol in 50 mL distilled water

Protocol 6: 90% alcohol (1L)

- Dilute 900 mL 100% ethanol in 100 mL distilled water

Protocol 7: 70% alcohol (1L)

- Dilute 700 mL 100% ethanol in 300 mL distilled water

Protocol 8: RIPA Buffer (100 mL)

- Prepare 50 mM Tris-HCl: add 790 mg Tris to 75 mL distilled water. Add 900 mg NaCl and stir. Adjust pH to 7.4 using HCl. Pour the prepared Tris-HCl into a 100 mL beaker.

- Add the following in the same order that they appear:

	Volume (mL)	Final Concentration
NP-40	10	1%
Na-deoxycholate	2.5	0.25%
EDTA	1	1 mM
Phenylmethylsulponyl Fluoride (PMSF)	1	1 mM
Leupeptin	1 (µL)	1 µg/mL
SBTI-1	80 (µL)	4 µg/mL
Benzamidine	100 (µL)	1 mM
Na$_3$VO$_4$	1	1 mM
NaF	500 (µL)	1 mM

- Add 1000 µL Triton-X-1000 to the solution and fill up to the mL mark with distilled water.
- Mix thoroughly.
- Aliquot the RIPA into 1 mL microfuge tubes and store at -20 °C.

Protocol 9: Laemmli's Sample Buffer (stock)
- 3.8 mL distilled water
- 1 mL 0.5M Tris-HCl, pH 6.8
- 0.8 mL glycerol
- 1.6 mL 10% (w/v) SDS
- 0.4 mL 0.05% (w/v) Bromophenol blue

Note: For use in western blotting, make a working solution by adding 150 µL β-mercaptoethanol to 850 µL Laemmli's stock solution.

Protocol 10: 10% Sodium dodecyl sulphate (SDS)
- Weigh out 50 g SDS and add 500 mL distilled water

Protocol 11: 10X Running Buffer
- Weigh off 60.6 g Tris
- Weigh off 288 g glycine

- Add to ± 1.5L distilled water
- Add 20 g SDS
- Adjust the pH to 8.6
- Fill up to the 2L mark with distilled water.

Protocol 12: 10X TBS

- Dissolve 24.2g Tris and 80g NaCl in 600 mL distilled water.
- Adjust pH to 7.6 with HCl
- Fill up to 1L mark with distilled water.

- For use in Western Blotting, make up 1X TBS-T by thoroughly mixing 100 mL TBS in 900 mL distilled water, with 1mL Tween

Protocol 13: 10% Ammonium persulphate

- Weigh out 0.1 g APS into an microfuge tube and add 1000 µL distilled water

Protocol 14: Tris pH 8.8

- Weigh out 68.1 g Tris (1.124M) and 1.5 g SDS (0.3%) and place into a beaker
- Add 400 mL distilled water, mix and then adjust pH to 8.8 using HCl
- Make the final volume up to 500 mL

Protocol 15: Tris pH 6.8

- Weigh out 30.3 g (0.5M) Tris and 2 g SDS (0.4%) and place into a beaker
- Add 400 mL distilled water, mix and adjust pH to 6.8 with HCl
- Make final volume up to 500 mL

Protocol 16: Tris pH 6.7

- Weigh out 6.057 g Tris (100 mM) and place in a beaker
- Add 400 mL distilled water, mix and adjust the pH to 6.7 using HCl
- Make final volume up to 500 mL

Protocol 17: Acrylamide Resolving Gels (makes enough for 2 gels)

Gel Constituent	6%	8%	10%	12%	15%
dH₂O	5.88 mL	7.84 mL	9.8 mL	11.76 mL	14.70 mL
30% Acrylamide	3 mL	4 mL	5 mL	6 mL	7.5 mL
1.5M Tris-HCl, pH 8.8	3 mL	4 mL	5 mL	6 mL	7.5 mL
20% w/v SDS	60 µL	80 µL	100 µL	120 µL	150 µL
10% w/v APS	60 µL	80 µL	100 µL	120 µL	150 µL
TEMED (last!!)	24 µL	32 µL	40 µL	48 µL	60 µL

Protocol 18: 4% Acrylamide Stacking Gel (makes enough for 2 gels)

Gel Constituent	
dH₂O	7.5 mL
30% Acrylamide	1.5 mL
0.5M Tris-HCl, pH 6.8	3 mL
20% w/v SDS	60 µL
10% w/v APS	80 µL
TEMED (last!!)	40 µL

Protocol 19: Milk blocking solution

- Measure out 5 mL fat-free milk and add 95 mL of TBS-T
- Mix well on a magnetic stirrer
- This is enough for one membrane

Protocol 20: Primary (1°) Antibody

- Pipette 5 µL of the primary antibody into a falcon tube containing 5 mL TBS-T.
- Prepare just before use

Protocol 21: Secondary (2°) Antibody

- Pipette 0.5 µL secondary antibody into a falcon tube containing 5 mL TBS-T.

Protocol 22: Stripping Buffer

- 7.5 g glycine
- 0.5 g SDS
- 5 mL Tween

- Dissolve in +- 300 mL distilled water

- Adjust pH to 2.2

- Fill up to the 500 mL mark with dH_2O

Protocol 23: 50 mM phosphate buffer (Na_2HPO_4) with 1 mM EDTA

m (g) = C x V x M_R
m (g) = 50 x 10^{-3} x 0.1L x 141.96
m (g) = 0.7098g Na_2HPO_4 in 100 mL distilled water

m (g) = C x V x M_R
m (g) = 1 x 10^{-3} x 0.1L x 292.24
m (g) = 0.029g EDTA in 100 mL distilled water
Add 0.7098g Na_2HPO_4 and 0.029g EDTA to approximately 50 mL distilled water. Adjust the pH to 7.5. Mix thoroughly and then fill up the volume to 100 mL.

Protocol 24: M2VP

Prepare 0.1M HCL by adding 4.91 mL of 32% HCL to 500 mL distilled water.

Add 100 mg M2VP to 12.5 mL 0.1M HCL.

Appendix F

Reagents

Reagents	Catalogue #	Company
2-Propanol	UN1219	Merck
32% Hydrochloric acid	UN1789	Merck
2,2'-Azobis (2-methylpropionamidine) dihydrochloride (AAPH)	440914	Sigma-Aldrich
Absolute alcohol	32221	Riedel deHaën
Acrylamide	UN3426	Merck
Acrylamide	A3699	Sigma-Aldrich
Ammonium Persulphate (APS)	UN1444	Merck
Antibiotic antimycotic (AA)	15240-062	Gibco
Bovine Serum Albumin	A4503	Sigma-Aldrich
Bromophenol Blue	32400A	UnivAR
Caspase Glo 3/7	G8091	Promega
Coomassie Brilliant Blue G	27815	Fluka
D-(+)-Glucose	G7021	Sigma-Aldrich
Di-sodium hydrogen orthophosphate dehydrate	5822880EM	Merck
Doxorubicin	D1515	Sigma-Aldrich
DTNB	D21820	Sigma-Aldrich
Dulbecco's Modified Eagles Medium (DMEM)	D5796	Sigma-Aldrich
Fetal Bovine Serum	10270-106	Invitrogen Gibco
Fluorescein sodium salt	F6377	Sigma-Aldrich
Glutathione standard	G4251	Sigma-Aldrich
Glutathione reductase (GR)	G3664	Sigma-Aldrich
Glycerol	G5516	UnivAR
Glycine	G8898	Sigma-Aldrich
Horse Serum	S9133	Biochrom
Iso-butanol	UN1212	Merck
LDH Cytoxicity Kit	G1780	Promega
Malondialdehyde	805797	Merck

Methanol	UN1250	Merck
Mouse Quantikine TNF-α ELISA Kit	MTA00B	R&D Systems
MTT (Thiazolyl Blue Tetrazolium Bromide	M2128	Sigma-Aldrich
M2VP	69701	Sigma-Aldrich
NADPH disodium salt	N6785	Sigma-Aldrich
Ortho-phosphoric acid	UN1805	Merck
PenStrep	15140-122	Invitrogen Gibco
Pierce® ECL Western Blotting Substrate	32106	Thermo Scientific
Ponceau S Solution	P7170	Sigma-Aldrich
Rat Quantikine TNFα ELISA Kit	RTA00	R&D Systems
Sodium Dodecyl Sulphate (SDS)	L3771	Sigma-Aldrich
Thiobarbituric acid	T5500	Sigma-Aldrich
TEMED	T9281	Sigma-Aldrich
TNF-α	400-14	PeproTech Inc.
Trolox	238831	Sigma-Aldrich
Triton-X-100	BB306324	BDH
Trizma-Base	93304	Fluka
Trypsin EDTA	25200-012	Invitrogen Gibco
Tween®20	P1379	Sigma-Aldrich
β-Mercaptoethanol	M3148	Sigma-Aldrich

Appendix G

Turnitin Report

Thesis PhD

ORIGINALITY REPORT

19%	15%	12%	4%
SIMILARITY INDEX	INTERNET SOURCES	PUBLICATIONS	STUDENT PAPERS

PRIMARY SOURCES

1	ir1.sun.ac.za Internet Source	6%
2	Submitted to University of Stellenbosch, South Africa Student Paper	<1%
3	www.ncbi.nlm.nih.gov Internet Source	<1%
4	atvb.ahajournals.org Internet Source	<1%
5	Central Functions of the Ghrelin Receptor, 2014. Publication	<1%
6	orca.cf.ac.uk Internet Source	<1%
7	journals.lww.com Internet Source	<1%
8	scholar.sun.ac.za Internet Source	<1%